STUDIES ON THE EFFECT OF INCORPORATION OF SOME SELECTED IMPURITIES ON THE GROWTH AND PROPERTIES OF DIAMOND FILMS

Thesis Submitted to the

UNIVERSITY OF PUNE

for the Degree of

DOCTOR OF PHILOSOPHY

in

PHYSICS

by

DNYANESHWAR VASANT MUSALE

Physical and Materials Chemistry Division
National Chemical Laboratory
Pune 411 008, India.

January 2001

CERTIFICATE

CERTIFIED that the work incorporated in the thesis "**STUDIES ON THE EFFECT OF INCORPORATION OF SOME SELECTED IMPURITIES ON THE GROWTH AND PROPERTIES OF DIAMOND FILMS"** submitted by **Mr. Dnyaneshwar Vasant Musale** was carried out by the candidate under my supervision. Such material as has been obtained from other sources has been duly acknowledged in the thesis.

Date: **(Dr. S. T. Kshirsagar)**

Place: Pune **Research Guide**

LIST OF PUBLICATIONS OF THE CANDIDATE DURING THE COURSE OF THE PRESENT RESEARCH WORK

1. Effect of coupling of radio-frequency plasma on the growth of diamond films in a hot filament reactor.
   M. P. Pai, **D. V. Musale**, S. T. Kshirsagar, A. Mitra, and S. R. Sainkar
   Thin Solid Films 322 (1998) 167.

2. Low-pressure chemical vapour deposition of diamond films in a radio-frequency-plasma-assisted hot-filament reactor.
   M. P. Pai, **D. V. Musale**, and S. T. Kshirsagar
   Diam. Relat. Mater. 7 (1998) 1526.

3. Enhancement of nucleation and growth of diamond films using In-Sn-O buffer layer on Si substrate.
   D. V. Musale, M. P. Pai, S. R. Sainkar, and S. T. Kshirsagar
   Materials Letters 39 (1999) 86.

4. Synthesis of highly conductive Boron doped p-type hydrogenated microcrystalline Silicon (mc-Si:H) by hot-wire CVD technique.
   S. R. Jadkar, J. V. Sali, M. G. Takwale, **D. V. Musale**, and S. T. Kshirsagar
   Solar Energy Materials and Solar Cells 64 (2000) 333.

5. Stuctural, Electrical and Optical properties of undoped and phosphorous doped microcrystalline silicon prepared by prepared by hot - wire CVD technique.
   S. R. Jadkar, J. V. Sali, M. G. Takwale, **D. V. Musale**, and S. T. Kshirsagar
   1st International conference on Hot-Wire CVD process, Nov. 14-17,2000, Kanazawa, Japan, P177.

6. Role of hydrogen dilution and phosphorous doping on Structural, Electrical and Optical properties of microcrystalline silicon prepared by hot-wire CVD technique.
   S. R. Jadkar, J. V. Sali, M. G. Takwale, **D. V. Musale**, and S. T. Kshirsagar
   Thin Solid Films, In Press (2000).

7. Raman, Photoluminescence and Morphological studies of Si-doped diamond films grown by HF-CVD technique.
   D. V. Musale, M. P. Pai, S. R. Sainkar and S. T. Kshirsagar
   Communicated.

8. Effect of *in situ* incorporation of nitrogen on the growth and properties of HF-CVD diamond films.

D. V. Musale, M. P. Pai, N. R. Pawaskar and S. T. Kshirsagar
Communicated.

9. Effect of ion implantation of impurities on the properties of HF-CVD diamond films.
D. V. Musale, J. Prabhjyot Pal and S. T. Kshirsagar
Communicated.

10. The effect of substrate temperature on the hot-wire CVD deposited hydrogenated amorphous silicon (a-Si:H).
S. R. Jadkar, J. V. Sali, M. G. Takwale, **D. V. Musale** and S. T. Kshirsagar
Communicated.

11. Influence of Silane flow on Structural, Optical and Electrical properties of a-Si:H thin films deposited by hot-wire chemical vapour deposition technique.
S. R. Jadkar, J. V. Sali, M. G. Takwale, **D. V. Musale** and S. T. Kshirsagar, Communicated.

CONTENTS

CHAPTER 1

INTRODUCTION: DIAMOND THIN FILMS

This chapter gives introduction to diamond thin films and highlights their possible innovative applications which are simply not feasible by using diamond bulk crystals. Then it presents the state of the art production of these films by various techniques and reviews briefly the present knowledge on the mechanism of chemical vapour deposition technique. Then it focusses its attention to the various problems encountered in obtaining high nucleation densities and growth rates as well as the incorporation of possible defects and impurities particularly in relation to production of device quality films. Subsequently, it brings about the objectives and motivation for undertaking the present work.

1.1 Historical Background

In the last quarter century, due to increase in demand for high performance materials required for various industrial applications, there has been growing interest in research and development in the field of high-tech ceramic materials. In fact, worldwide efforts are now focused on to analytically characterize various ceramic materials found in nature, to optimize the methods of synthesis of these materials in the laboratory and to simultaneously look for their special industrial applications. One of these ceramic materials that tops the present research interest is the diamond in thin film form [1]. As the diamond displays very extraordinary combination of its extreme physical and chemical properties compared to other materials, it has attracted large technological and scientific interest over the past several years for its wide range of applications [2-7].

The most fascinating property of well-faceted and highly polished diamonds used in ornaments and decorative fixtures by ancient people was its glittering appearance which attracted most humans to acquire them at any cost. In fact, historically, diamonds were known to mankind as the precious gems found in nature and several centuries ago, the skills for cutting and polishing this super hard material were developed. The rarity of this naturally found stone elevated its cost to very high levels, but nevertheless, it enthused the scientific and industrious minds to investigate what the diamonds are composed of and how to manufacture them artificially.

Scientifically, first clue came from Sir Isaac Newton, who studied the refraction of light through diamond and proposed that diamonds were of organic origin [8]. More authentic evidence was then obtained by French chemist L. Lavaisier in 1772 from the analysis of the diamond combustion products which behaved as if they were composed solely of carbon dioxide. In 1797, the English chemist Smithson Tennant studied the combustion of mixture of equal amounts of salt-peter and diamond in three different closed chambers and found that the solid remains of each combustion had the same amount of carbon. This was the first systematic step towards the revealing of the composition of diamond as organic species that were very close to the elemental carbon. Naturally, fascinating ideas for transformation of similar carbon species into diamond started getting roots in the field of science and technology. During the eighteenth century, attempts were made to transform carbon into diamond [8] which only

indicated the need for understanding the chemical phases of carbon which exists in various forms. Diamond and graphite were the known crystalline forms of carbon which drastically differed in their properties.

With the development of modern thermodynamics, J. W. Gibbs theoretically showed that graphite could turn into diamond if the thermodynamic potential of diamond was less than that of graphite [9]. This provided a basis to establish the conditions of temperature and pressure needed to transform the carbon into the stable form of diamond. The first report on the phase diagram of carbon was proposed in 1939 by P. W. Bridgman of Harvard University [9]. This report stressed the need for high temperature and high pressure conditions under which carbon could exist in molten state and diamond crystals could be grown from this melt. Bridgman subsequently developed the high temperature and high pressure (HPHT) apparatus for growth of crystals of several materials for which he was awarded Nobel Prize in 1946. But his attempts to grow diamond crystals by this apparatus were unsuccessful. The successful synthesis of diamond from graphite was carried out subsequently by a group of scientists at Allemanna Svenska Elektriska in Sweden in 1953 and at General Electric in US in 1954 [1]. Thus in the late 1950s, a "New Diamond Technology" was born. The applications of these diamond crystals were limited to a specific field, particularly abrasive products. However, HPHT technique proved to be very expensive and required special expertise for production of diamond while the realization of diamond semiconductor devices and coatings remained out of reach.

It was therefore more natural to inquire whether diamonds could be grown at substantially low pressure and low temperature conditions which may be convenient for economical production. The detailed studies on the thermodynamics of the formation of diamond suggested that diamond could be nucleated and grown at low pressure and low temperature (LPLT) in an ambient of supersaturated carbon vapour [10]. The phase diagram (shown in Fig. 1.1) indicated that there is a favorable region of pressures less than the atmospheric pressure and temperature of about 800^0C to 1000^0C, where diamond formation is possible in a non-equilibrium condition. In this region, the diamond, being a higher energy phase, is said to be metastable with respect to graphite and hence under these LPLT condition, either of them can nucleate and grow simultaneously [4].

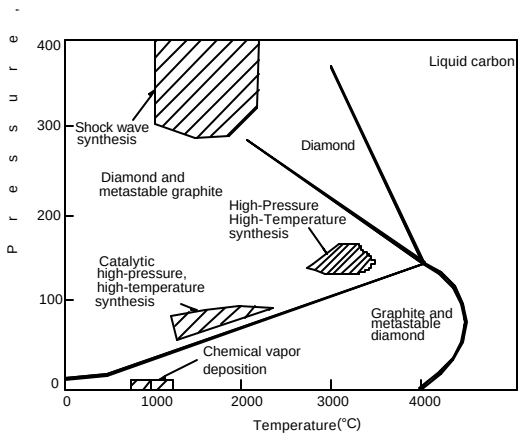

Fig. 1.1 Phase Diagram of Carbon

The first pioneering successful attempt to grow diamond particles from a organic species which may be obtained by decomposition of hydrocarbon gases under LPLT condition were made by Eversole of Union Carbide Corp. Similar work was then carried out independently by Deryagin and Fedoseev of the USSR [10]. This marked the beginning of the new technology called "CVD Diamond Technology". The possibility of the enhancement of nucleation density and growth rate of diamond particles in presence of atomic hydrogen during the hydrocarbon pyrolysis was then demonstrated in the later part of 1970s by the Soviet group of scientists led by Prof. Derjaguin. They were also successful in depositing diamond particles on non-diamond substrates [11]. More systematic and detailed analysis of nucleation and growth mechanism of diamond particles was then reported by Angus and his co-workers in US and the group of scientists from National Institute of Research in Inorganic Materials (NIRIM) in Japan [1]. The latter group was successful in growing diamond particles forming what may be called as polycrystalline coating or thin film deposition on a variety of non-diamond substrates by low pressure chemical vapour deposition (LP-CVD) techniques involving various agencies for decomposition of hydrocarbon source gases. This gave rise to "Diamond Film Technology".

These discoveries triggered tremendous world wide research interest in CVD diamond technology driven by both scientific curiosity and technological exploitation for diverse applications. Therefore the last decade and a half has seen an explosive growth in the synthesis of diamond coatings/films by a variety of deposition techniques involving LP-CVD processes.

This chapter summarizes briefly the diamond chemistry and the overall technological development of the subject.

1.2 Diamond: An Important Allotrope of Carbon

Carbon is the most interesting element having valancy of four and placement at the sixth position in Group IV of the periodic table and found everywhere in nature either in purely elemental or compound forms called hydrocarbons. Under the suitable hybridization condition, the four valence electrons can form single, double or triple bonds with electrons of other carbon atoms or even atoms of different elements leading to a variety of compounds with different structures and a wide range of properties [12]. Depending upon structural and bonding configurations, carbon is found in nature in different phases called "allotropic forms" (as shown in Table 1.1).

Table 1.1 Classification of various forms of carbon according to bonding and crystal structure

Carbon	Amorphous carbons and hydrocarbons	Graphite	Diamond-like carbons and diamond-like hydrocarbons	Diamond
C-C Bonding:				
sp^1	-------- sp^1/sp^2 ---------	sp^2	------- sp^3/sp^2 --------	sp^3
	0% 100%		0% 100%	
Crystal Structure:				
Amorphous		2-D Crystalline	Amorphous, micro-crystalline, poly-crystalline	Single crystals

The most common allotrope is graphite in which the carbon atoms are bonded by using the sp^2 hybridized atomic orbitals. It can be viewed as the stack of layers of sp^2 bonded six-member aromatic rings lying in flat planes which are held together by weaker p bonds in the z-direction

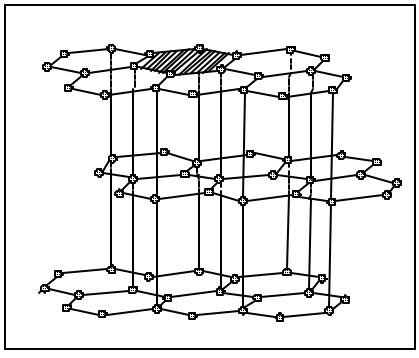

formed by using the P_z orbitals (as shown in Fig. 1.2).

Fig. 1.2 Crystal Structure of Graphite

This gives anisotropy to graphite properties. Each plane is staggered from the planes above and below resulting in AB AB AB... sequence. In plane, carbon atoms form strong sigma bonds with the nearest neighbor spacing of 1.42 Å while the p bonds between the sheets are 3.35 Å long. The π bonds are so weak that even a small force can break them and the sp^2-bonded sheets can easily slide over each other resulting in the solid state lubricant property of graphite. The lattice constant in the basal plane of graphite is 6.707 Å.

The other important and the most precious allotrope of carbon is diamond. It is formed by tetrahedrally bonded carbon atoms by using sp^3 hybridized atomic orbitals. Basic structure of diamond is cubic and is well-known as "Diamond Cubic Lattice". It consists of two interpenetrating face centered cubic (FCC) lattices, one with basis at (0,0,0) and the other with the basis at (1/4,1/4,1/4). In a diamond unit cell, there are eight sp^3-bonded carbon atoms. Each carbon atom is coordinated to four other carbon atoms via covalent sigma bonds emanating from sp^3 hybrid atomic orbitals. The lattice constant of diamond structure is 3.56 Å and the bond length is 1.54 Å. The cubic structure of diamond is as shown in Fig.1.3. The only

weakness in this structure lies in the octahedral planes where diamond crystal can be

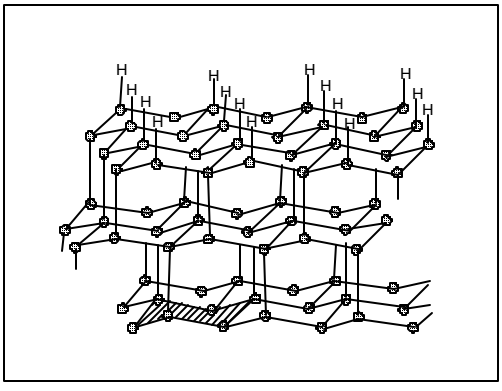

cleaved with relative ease. This property

Fig. 1.3(a) Crystal Structure of Diamond

Fig. 1.3(b) Face-centered Cubic Structure of the Diamond Crystal

of diamond structure is fully employed by jewelers for production of highly faceted diamonds for use in ornaments.

The natural diamond consists of approximately 99% carbon-12 and 1% the isotope carbon-13. The natural diamonds are found in coal mines where high pressure and high temperature conditions are provided by the earth's crust. The colours of natural diamond crystals can vary from white transparent to pink, yellow, green and blue depending on the

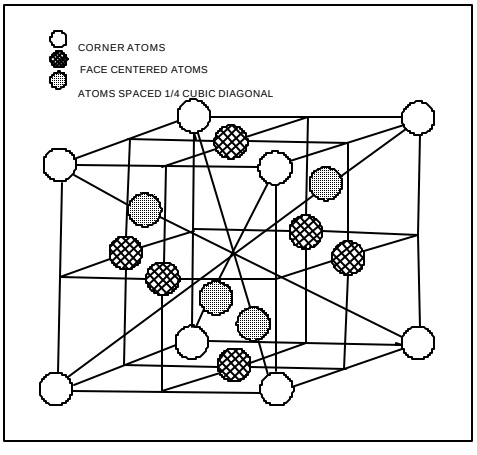

impurities present in the crystal. They are classified into four main types depending upon their optical absorption and luminescence spectra which result from the impurities present in the

structure [1,4]. They are type IA, IB, IIA and IIB. Type I has large amounts of nitrogen included. If the nitrogen is aggregated, it is type IA and if the nitrogen is dispersed, it is type IB. Type II is virtually free of nitrogen. If it is highly insulating and has no detectable boron, it is type IIA and if its boron content exceeds the nitrogen, it is type IIB. In general, these impurities are picked up during growth from the surrounding environment.

The other forms of carbon are Lonsdaleite (the hexagonal crystalline structure formed of sp^3 hybridized carbon atoms), fullerene (a closed cage molecule formed by combinations of sp^2 and sp^3 hybridized carbon atoms), microcrystalline carbon and amorphous carbon. Microcrystalline carbon is the poorly synthesized artifact of diamond where the atomic structure of the particles have some long range order resulting primarily in sp^3 bonding but with sp^2 bonding near the crystalline grain boundaries. When the particle size decreases, the structure becomes amorphous with mixed bonding having large share in sp^3 symmetry and remaining share in sp^2 bonded carbon atoms.

These different allotropic forms can be distinguished from each other by using their Raman (vibrational) spectra which display different signatures, characteristic of each allotrope [12a]. The 1580 cm^{-1} Raman signature indicates presence of graphite crystallites while 1332 cm^{-1} represents diamond crystallites. When particles become smaller in size, these signatures shift to lower frequencies, e.g. to 1500 cm^{-1} of sp^2 bonded carbon atoms in polycrystalline graphite, and to 1140 cm^{-1} in sp^3 bonded carbon atoms in microcrystalline diamond. The 1355 cm^{-1} signature, in general, results from grain boundary disordered sp^2 bonded carbon atoms.

1.3 Applications and Future Prospects of Diamond Films

Diamond in its bulk as well as thin film form offers the opportunity not only to improve the operating performance of many existing technological systems but also to develop a wide variety of new devices in the semiconductor, electronic, optical, computer and mechanical industries [13-15]. Because of the unique combination of the extreme properties possessed by diamond, it offers almost ideally suited solid state material choice for semiconductor device applications which involve extreme temperature and environmental conditions [16,17]. The possibility of depositing diamond coatings onto non-diamond substrates at extremely low

pressures and moderate temperatures has enhanced the prospects of these coatings for newer and newer applications. Possible applications range from wear resistant coatings to active semiconducting devices and from X-ray windows to new types of displays. Table (1.2) summarizes the most important properties of diamond in comparison with currently used competing materials and its possible application fields [18,19]. The initial realization of diamond application was based on certain properties such as extreme hardness and the best thermal conductivity. But recently the unique combination of its properties , e.g. electron emission combined with high resistance to electricity, has caught the attention of the technological world.

Due to its extreme hardness, diamond is being used for cutting and drilling purpose for long time. The diamond coating synthesis methods have introduced the concept of applying diamond coating to the edge of a non-diamond tool. The cutting performance of the diamond coated tool is observed to improve by several orders of magnitude. Diamond thin films produced by chemical vapour deposition show promise as a new heat-dissipating material for electronic applications. Attempts to use diamond as a heat-sink material in high-power electronic and opto-electronic devices began in 1960s. These devices produce large amounts of heat over a small area, thereby creating a tremendous heat flux. In order to cool these devices efficiently, it is necessary to spread the narrow heat flux by inserting a layer of high thermal conductivity between the device and the cooling system. Initially, these devices used type II A natural diamond or HPHT synthetic diamonds, having high cost as well as size limitations [20-22]. The availability of CVD diamond plates with thermal conductivities around 20 W cm-1 K at room temperature [23,24**]** has promoted the efforts to use CVD diamond for thermal management applications such as submounts for integrated circuits, heat-spreaders for high power laser diodes or even as a substrate material for multichip modules [25**]**. Particularly, due to the small size of the laser diodes, the heat needs to be spread before it can be efficiently transported away by conventional cooling techniques. If CVD diamond is used as heatspreader material, the thermal resistance can be reduced by 50% [26]. The cooling of high-power semiconducting laser diodes by diamond heatspreaders has been first commercially applied by AT & T for laser diodes used in undersea optical cables [27]

Diamond is transparent to electromagnetic radiation of a wide range of wavelengths from the infrared to the ultraviolet region as well as to X-rays. Due to its high

transparency, radiation hardness and mechanical sturdiness, diamond is an ideal choice as an optical window material, especially for high-power infrared lasers (CO_2 laser at

Table 1.2 The extreme properties of diamond compared to some currently used competing materials and the possible fields of applications.

Properties of Diamond		Comparison with Competitors	Possible Applications
Vickers' Hardness [kg/mm^2]	12x10^3-15x10^3	hardest material known	drill bits, polishing material, cutting tools, sintered or brazed diamond compacts, wear resistant coatings on windows and bearings
Coefficient of Friction	0.1 (in air)	very low in air (higher if kept clean under vacuum)	
Young's modulus [N/m^2]	1.2x10^{12}	twice the modulus of alumina; highest mechanical strength	stiff membranes for lithography masks, lightweight coatings for audio devices
Sound propagation velocity [km/s]	18.2	1.6x the velocity in alumina	
Chemical Inertness	Inert	at room temp. resistant to all acids, bases and solvents	coatings for reactor vessels
Range of high transmittance [μm]	0.22-2.5 and > 6	In the infrared frequency region, orders of magnitude lower than other material	UV-Vis-IR windows and coatings, microwave windows, optical filters, optical wave guides
Refractive index (RI)	2.41	1.6x the RI for silica	
Band Gap [eV]	5.45	1.1 for Si 1.43 for GaAs 3.0 for β-SiC	high power electronics, high frequency-semiconducting devices, hot thermistors, hot-transistors, lasers, detectors
Electron / hole mobility [cm^2/Vs]	1900/1600	1500/600 for Si 8500/400 for GaAs	
Dielectric Constant	5.5	11 for Si 12.5 for GaAs	
Thermal Conductivity [W/cmK]	20	value for type IIa natural diamond at room temp. is 4x the value of Cu or Ag	insulating heat sinks for electronic devices
Thermal expansion coeff. [1/K]	0.8 x 10^{-6}	value at room temp. close to that of silica (0.57 x	thermally stable substrates e.g. for X-ray lithography

		10^{-6})	masks
Luminescence [μm]	430	blue luminescence scarce (β-SiC works)	blue LEDs, displays

10.6 μm), X-ray sources etc. A systematic evaluation of the properties such as infrared absorption, elastic properties, mechanical strength and thermal properties has been carried out to reveal that CVD diamond has orders of magnitude of advantages in infrared applications in adverse environments as compared to other materials [28-30]. With the realization of the epitaxial/oriented, large area and excellent quality free-standing diamond films, the possibility of commercial use of diamond windows has come quite close to reality.

Antireflection coatings of diamond would have considerable advantages. Silicon and GaAs solar cells coated with diamond film would exhibit greater efficiency because of reduction of reflective losses, while at the same time the cells would be resistant to degradation from the environment. Also, a number of prototype electronic devices have been reported using impurity doped CVD diamond. Some of the devices reported in the literature are: schottky diodes[31], diamond surface channel FET[32], p-i-n solar cells[33], thermistors [34], field emission arrays [35], surface - acoustics- wave (SAW) devices for high-frequency applications and telecommunications [36], etc.

CVD diamond films have already made their impact on the grinding and cutting tools business. CVD diamond heat sinks are also ready for immediate introduction into the market. As for optical window applications, diamond windows and membranes are on the stands in several industrial laboratories and the tests , most likely for in-house applications in other products, are already yielding promising results. Electrical and electro-optical applications are not that close to the market yet. Boron doping leads to a p-type diamond semiconductor and prototype high-temperature Schottky diodes operating above 550^0C (current silicon devices die above 120^0C) have been demonstrated at Pennsylvania State University, USA [19]. The luminescence light emitted by undoped CVD diamond is most intense in the blue region at ~ 445 nm. Emission from boron doped diamond crystals appears in the green part of the visible spectrum. Adding nitrogen to the CVD diamond results in an additional orange luminescence band. The intensities of these bands are far from being sufficient for an LED, but the possibility of a existence of a new type of light emitter is there. The vast variety of possible products justifies the tremendous efforts being put in this exciting field. The field is expanding

very rapidly and hence a market forecast given by the Japanese "New Diamond Forum" with its more than 100 industrial member companies [37] is worth while for perusal and is shown in Fig. 1.4 which illustrates the high potential of vapour grown diamond. In fact, a multi-billion dollar market is predicted for the year 2010.

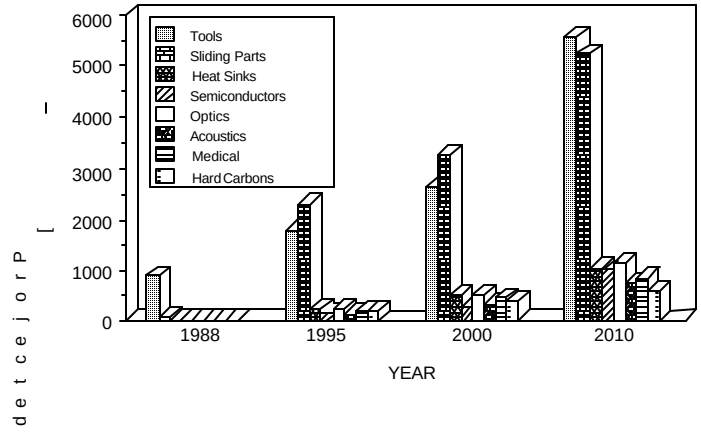

Fig. 1.4 Projected Japanese Sales of "New Diamond" Products

(The data are based on a market survey by the Japanese "New Diamond Forum".)

1.4 Synthesis of Diamond

Natural diamond is found in deep below the earth's crust where high pressure - high temperature (HPHT) conditions are possible. Initially the same route was suggested for synthesis of diamond in the laboratory. This route involves subjecting of graphite to high pressure and high temperature (the conditions at which diamond is thermodynamically stable phase) in the presence of a molten metal like iron, nickel, cobalt or tantalum which act as a solvent for carbon and a catalyst as well [38]. This route has also been used for making gem quality diamond stones of different colors [39]. Another early method for diamond synthesis was shock wave technique [1]. In this process, pressure of several million psi and temperature of 1000^0C are used to grow diamond. This method was first used by DeCarli and Jamieson in 1961 to produce diamond by developing the pressure of the order of 300,000 atmosphere (4.5 million psi) using explosive charge for a millionth of a second by shock wave in graphite

[40,41]. Although this method can produce sufficient quality of diamond crystallites for mechanical and thermal applications, the process is very expensive. Also the main drawback of this method is that, if the pressure drops down to normal much more rapidly, then the diamond again converts back to graphite.

It is during the last two decades only that several research groups have successfully synthesized diamond coatings by low pressure-low temperature (LPLT) routes. This route involves low pressure deposition of diamond from the vapour phase. Being economically feasible, this route is being followed by a large number of research groups all over the world. Most of the LPLT synthesis techniques used by them fall in the category of chemical vapour deposition (CVD).

1.5 Status of LP-CVD of Diamond Films

In a CVD process, the reactant gases are allowed to pass through energetic zones where they decompose into reactive species. These species are transported by forced flow or diffusion and/or convection throughout the reactor and eventually on reaching to the substrate surface, either get condensed directly or transformed into condensable species via the chemical reactions at the substrate and ultimately result in the production of required material in the thin film form. In the CVD of diamond films, the source gas contains a carbon-bearing species such as hydrocarbon, alcohol, carbon monoxide or carbon dioxide and the molecules of these carbon species are activated either by high temperature and/or electric discharge (plasma). These activated gas molecules decompose into reactive species which diffuse towards the substrate surface via collision processes. Upon reaching to substrate, these reactive carbon-bearing species get transformed into diamond particulates forming the sites for nucleation. The driving force for this transport of carbon-bearing species comes from the temperature gradient or even by the gas flow/blowing processes. For the conversion of carbon-bearing species into diamond particulates at the substrate surface, it is essential that the substrate is predisposed to nucleation and growth of diamond from the vapour phase. Since the diamond is formed by covalent bonding via sp^3 hybridized orbitals of depositing carbon-species, the substrate or the environment near the substrate surface needs to be favorable for the formation of sp^3 bonds and should suppress the formation of other bonds and hybridization.

In CVD technique, the energetic zone centre can be created by the application of heat, electric discharge or plasma source. Depending upon the type of excitation source, these techniques are categorized in different types. In early 1970s, J. C. Angus suggested that the simultaneous production of atomic hydrogen (H^0) during hydrocarbon pyrolysis can enhance the deposition of diamond. This suggestion was tested by Soviet Researchers who generated H^0 by dissociation of H_2 using an electric discharge or a hot filament ($T > 1800^0C$). This deliberate addition of H^0 during diamond CVD enabled: a) dramatic increase in the diamond deposition rate to ~ 1μm/hr, b) suppression of graphite formation and, c) the nucleation and growth of diamond on non-diamond substrate. During last two decades, these CVD techniques have found industrial applications in fabrication technologies ranging from semiconductor devices [42,43] to cutting tools [44] and optical fibers [45] and from diamonds [46,47] to high temperature superconductors [48] and ferroelectrics [49]. The different CVD techniques used for diamond deposition and their working principles are discussed briefly in the following paragraphs.

1.5.1 Microwave (MW) Plasma Enhanced LP-CVD

Microwave plasma enhanced CVD was demonstrated to grow polycrystalline diamond films on non-diamond substrates by a research group at Japan's National Institute for Research in Inorganic Materials (NIRIM) [50]. In this method, the microwave plasma is used to activate the gas mixture to produce carbon-bearing species as well as atomic hydrogen (H^0). The microwave frequency oscillates electrons and collisions of these energetic electrons with gas atoms and molecules generate high ionization fractions. Microwave plasmas are typically described as having "hot" electrons and "cool" ions and neutrals and the excitation of H_2 by microwave plasma generates superequilibrium concentrations of atomic hydrogen which is useful for enhanced nucleation and growth rates.

The general schematic diagram of the microwave reactor is shown in the Fig.1.5 [51]. In this method, microwaves (2.45 GHz) generated by a magnetron are introduced from the top of the reactor by a rectangular metal waveguide. The waves are then picked up by an antenna and are emitted centro-symmetrically into the circular waveguide that contains the evacuated bell jar.

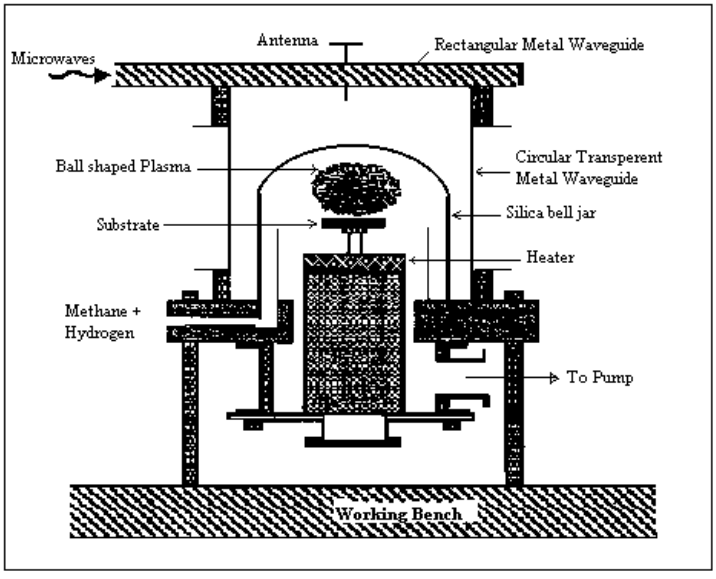

Fig. 1.5 The Schematic Diagram of a Microwave Plasma-Enhanced LP-CVD Reactor

The plasma is generated at the point of highest electrical field strength inside the bell jar. Its shape, size and also its stability are dependent on the deposition conditions, the plasma power, the pressure and the gas composition. If correct conditions are chosen, a ball-shaped, stable plasma is formed in the center of the bell jar, far away from the reactor walls. In this method, typical deposition pressure is between 1 and 400 torr and the substrate temperature is between 400^0C and 1000^0C. The substrate can be heated by the plasma alone or with a separate heating source. The heated substrate is kept below a plasma ball and the activated gas radicals are condensed on it.

By using this method, contamination-free, uniform and reasonably good quality diamond films can be obtained. But the growth rate achieved by this method is very low (~0.1 - 1.0 μm/hr). Also, the uniform films can not be grown over a large area. Moreover, this method involves very expensive equipments, hence it is not economically feasible foe industrial production.

1.5.2 Direct Current (DC) Plasma Enhanced LP-CVD

In 1951, H. Konig and G. Helwig [52] reported the deposition of hydrocarbon films from a DC plasma excited benzene molecules. This technique was further modified to produce an arc discharge between the two electrodes. This process was developed by Kurihara and co-workers [53] at Fujitusu Laboratories and was entitled as DC Plasma Jet process (DIA-JET). Due to the pressure gradients and high gas flows, the DC plasma arc thus formed expands into a reactor vessel, where a substrate is mounted onto a water-cooled stage [54,55]. Inside the plasma arc, both heavy ions and molecules as well as free electrons are at the same high temperature. Temperatures of more than 5000^0C can easily be reached in such a plasma and practically all molecules injected in such a hot zone are decomposed into atoms or even ionized, depending on the energy supplied to the arc. When the substrate material is sufficiently cooled, it withstands the relatively harsh environment of a plasma jet and higher deposition rates have been achieved. The schematic diagram of this technique [56] is shown in the Fig. 1.6.

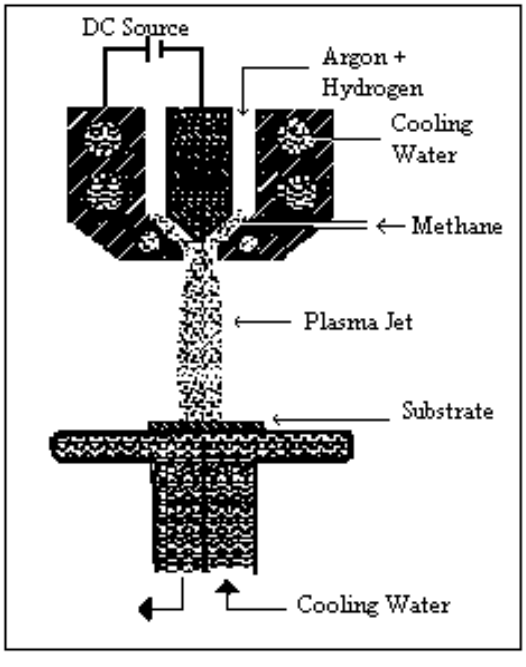

Fig. 1.6 Schematic Diagram of a DC Plasma-Enhanced LP-CVD

It uses a gas injection nozzle composed of a rod cathode concentric with a tube anode. Gases pass between the cathode and anode and are sprayed out from an orifice in the

anode. The gas mixture used is CH_4 + H_2 with a carrier gas (Ar or He) and the total pressure is between 30 and 300 torr. As the DC arc is sustained by 80-150 V and 10-50 A, the substrate must be water cooled to maintain a proper substrate temperature (500^0C -1200^0C).

By using this method, extremely high deposition rates (~ 80 μm/hr) can be achieved. But the major disadvantages of this approach are the relatively small deposition area, non-uniformity in terms of the thickness as well as the graphitic contaminations at the periphery of the diamond deposit. In addition, the experimental set-up can be quite sophisticated and expensive and the stabilization of both the plasma generation and the deposition conditions, specifically the temperature needs considerable efforts. For some applications where bulk diamond is needed, e.g. heat sink, this approach can be the method of choice.

1.5.3 Radio-Frequency (RF) Plasma Enhanced LP-CVD

Generally, radio-frequency power can be used to produce plasma when applied either to a capacitively coupled parallel plate reactor or by induction through induction coil coupled to the reactor. These two methods are schematically shown in the following Fig. 1.7 [57].

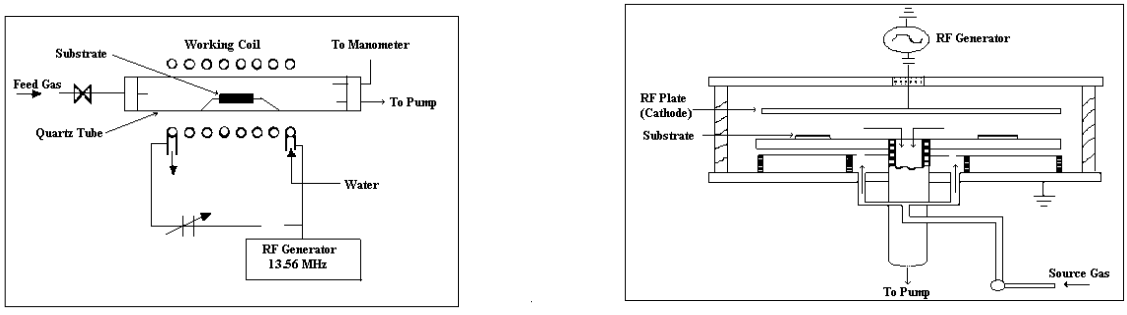

(a) **(b)**

Fig. 1.7 The Schematic Diagram of-

(a) an inductively coupled and,

(b) parallel plate, capacitively coupled RF Plasma-Enhanced LP-CVD Reactor

Typically, RF plasma enhanced CVD employs a frequency of 13.56 MHz. The advantage with RF plasmas is that they can be easily generated over much larger area than MW plasma. To maximize plasma stability, an impedance matching network is connected between the RF

generator and the electrode assembly in order to match the plasma load to that of the RF power supply. Since ion bombardment from the plasma can destroy the sp^3 bonded nuclei to stabilize as sp^2 bonded nuclei, capacitively coupled RF plasmas produces mainly hydrocarbon films with superhard properties which are termed as diamond-like coatings [46,58]. Wood et al.[59] have reported the synthesis of diamond films by parallel plate, capacitively coupled RF plasma reactor.

From the equipment point of view, RF-PA-CVD is the most suitable method for scaling up and industrialization of diamond deposition. But this method suffers from low growth rates, film contamination and poor crystalline quality.

1.5.4 Hot Filament (HF) LP-CVD

This technique comes under the category of thermal CVD. Because of its simplicity, comparatively low capital and operating cost, hot filament assisted CVD has become popular in industry where it is imperative to minimize cost per gram of synthetic diamond. A typical schematic diagram of a hot filament reactor used to grow diamond films is

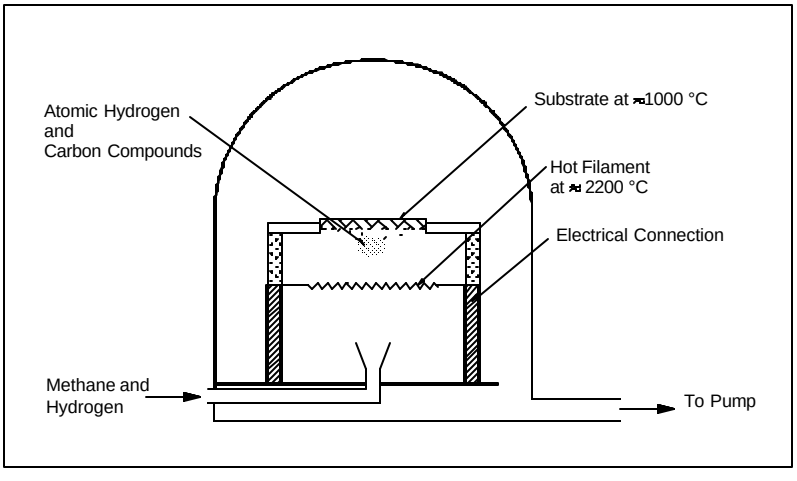

shown in Fig. 1.8.

Fig. 1.8 The Schematic Diagram of a Hot Filament LP-CVD Reactor

The elementary principle of this method was first published by Matsumoto et al. [60] In this method, the gaseous starting materials (e.g. for diamond synthesis, a mixture of hydrogen and

methane in the ratio ~ 100:2 is used) are guided to a hot filament maintained at ~ 2200^0C. Refractory metals like tungsten, tantalum, and rhenium have been used as filament materials. At pressures of 10 to 100 torr that are commonly used, the hot filament transforms the input hydrocarbon (e.g. CH_4) into acetylenic species, methyl radicals and other hydrocarbons stable at high temperature, and H_2 decomposes into atomic hydrogen (H^0). The H^0 and high-temperature hydrocarbons then diffuse from the filament to the surface of the substrate which is mounted at a distance of 5mm to 10mm from the filament. The temperature gradient between the filament and substrate provides the driving force for the diffusion of these species [61]. The substrate is heated by either the hot filament or a separate heater to 800^0C - 1000^0C resulting in the deposition of polycrystalline diamond film. This type of process is usually termed as hot to cold transport because the hot gas passing through the filament deposits on a much colder substrate.

This method has been successfully used to coat areas of more than 100 cm^2. According to the requirement of the deposition area, the shape and size of the filament can be changed. The important drawback of this method involves non-homogeneous film formation as it depends upon the shape and size of the filament. It also suffers from contamination of the growing film due to evaporation of wire materials. However, because of its simplicity, economical feasibility and up-scaling potential, it is the technique of choice for the deposition on cutting tools and wear parts.

1.5.5 Combustion Flame CVD

Another important thermal CVD method for diamond synthesis is combustion flame method . The experimental set-up of this method is as shown in Fig. 1.9 [18]. In this method, a gaseous mixture of oxygen and acetylene is used as starting material. A flame is produced from the mixture of these two gases in atmospheric pressure. This flame has three regions [62,63], viz.:

1) The inner core that bounds the O_2-C_2H_2 flame front.
2) The acetylene feather zone where the excess acetylene burns with the oxygen that diffuses into the flame from the surrounding air.

3) The outer flame where the CO and H_2 produced in the inner zone and the feather zone are burnt to produce CO_2 and H_2O.

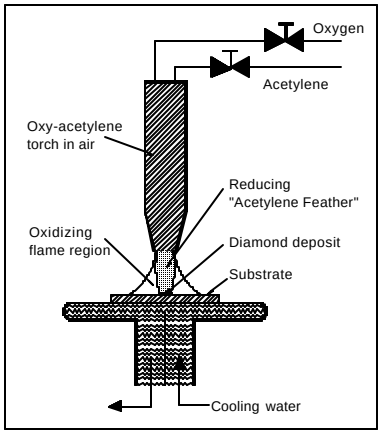

Fig. 1.9 The Schematic Diagram of an Oxy-acetylene Combustion Flame CVD Method

The growth of diamond is observed when the substrate is in the feather zone. Synthesis of diamond by combustion flame CVD was first reported by Hirose et al.[64] An advantage of this method is that diamond films can be grown in the open atmosphere. For the high quality diamond coatings over large areas, combustion flame technique is a good choice. The main disadvantage of this method is the requirement of high substrate temperature (> 1000^0C) which causes the limitations on the substrates. This method also suffers from the poor uniformity of the film.

1.6 Present Knowledge on the Mechanism of Chemical Vapour Deposition of Diamond

As discussed in the earlier section, there are numerous low pressure chemical vapour deposition techniques which have been used for production of diamond coatings and free standing polycrystalline diamond plates. Some understanding about the nucleation and growth processes involved in the synthesis is also achieved and various models have been proposed on the basis of thermodynamic and chemical kinetic considerations. Fig. 1.10 represents a generalized schematic of the growth process and

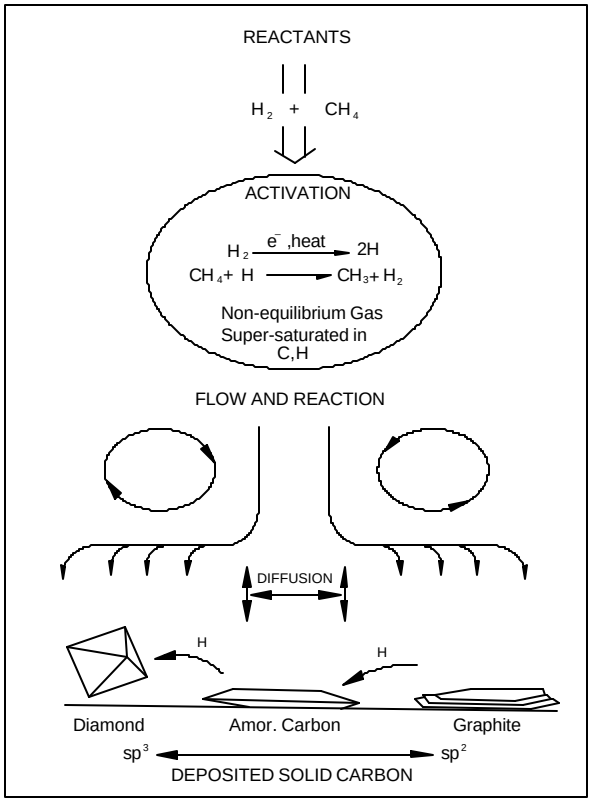

Fig. 1.10 The Schematic Representation of "Diamond Deposition Process"

chemistry occurring in CVD reactor [65,66]. The CVD growth environment can thus be quite complex and varied. In typical CVD of diamond, the starting gaseous material is a mixture comprised of a small amount of hydrocarbon (usually methane) in hydrogen. In the deposition process, the reactant gases enter a high temperature or energetic region in which the gases are activated by a plasma, a hot filament, or a combustion flame front. In this region the chemical reactions are initiated where the decomposition of some gases such as CH_4, C_2H_6, H_2 etc. takes place into the reactive species. These species consist of fragmented hydrocarbon species such as CH_3, CH_2, CH, acetylene and atomic hydrogen as well as undissociated CH_4 and H_2 [67]. Subsequently part of these species diffuse towards the substrate surface through a stagnant flow or by the forced flow mechanism. The former can get set through the temperature gradient while the latter is controlled by the in-flow of the source gases. On the substrate surface, various processes occur leading to the thin film deposition of diamond film. These processes include usual bond breaking and bond formation, transport of atomic species on the substrate surface

forming the nucleation sites, and rearrangement of atomic species at the nucleation site, thereby causing the crystallite growth. These various processes depend on surface temperature, the structure of the exposed surface and the surface composition of the substrate. Under the steady state condition, an equilibrium between the supply of atomic species and absorption of these species on the substrate would set and a boundary layer may be formed between the gas zone and substrate surface. A better control over the nucleation and growth process can then be achieved by adjusting the deposition parameters at the substrate.

The actual mechanism of CVD of diamond is mainly combination of two processes, viz. nucleation and growth, which are described in brief in the following section.

Nucleation:

The growth of diamond from vapour phase begins with nucleation which is the early stage of crystal formation and has been one of the most studied topics in diamond CVD [71]. In case of homo-CVD, i.e. growth of diamond on diamond surface, the nucleation sites can be provided by the surface vacancies and broken bonds. But for the hetero-CVD, i.e. growth of diamond on non-diamond surface, the nucleation sites have to be external to the substrate surface and the process of formation of nucleus beyond a critical size and its stability are necessary. During the formation of such a critical nucleus, i.e. the size above which it is more probable that a nucleus will survive and grow rather than it will decay, the change in the system free energy must be negative [72]. Here the system includes the substrate, growing particles, and the boundary layer gas-phase reservoir of species contributing to lattice growth. Diamond nucleation during CVD has been understood to occur as a result of combination of some reactions leading to (a) suppression of formation of graphite nuclei, (b) stabilization of diamond nuclei and surfaces with respect to graphite nuclei and surfaces, and (c) preferential etching of sp^2 bonded carbon [73-75]. In order to accomplish these conditions, most current diamond CVD growth environments employ large amounts of molecular hydrogen compared to the carbon source gas which allows supersaturation of atomic hydrogen resulting from the gas activation agencies such as a hot filament or electric discharge.

Nucleation process is two step process and is mainly dependent upon substrate type, its pretreatment, and deposition process parameters. In the first step, carbon species

impinging on the substrate from the gas phase are proposed to diffuse into the bulk. The rate of carbon diffusion into the substrate depends on various factors and decreases as diffusing species form a barrier, e.g. formation of a carbide layer with a low carbon diffusion coefficient. When the substrate surface becomes relatively impervious to further carbon diffusion, the surface carbon concentration increases and eventually exceeds the level necessary for the second step of diamond nucleus stabilization. The second step of nucleation depends on the presence or absence of surface features and diamond seeds. These are plenty available for homo-CVD and nucleation appears to occur when carbon species form nucleation sites at surface flaws. For non-diamond substrates (hetero-CVD) preprocessing of the surface is necessary which may be achieved by scratching the substrate with diamond powder. On diamond-scratched substrates, diamond fragments of very small size get locked into scratches and provide the nucleation sites. The carbon species thus diffuse into the existing nucleation sites. Further diffusion of carbon and bonding of carbon species results into the formation of critical nuclei and the growth process sets in.

Growth:

By definition, growth is the process of depositing additional carbon on the substrate surface to increase the bulk dimensions. Some progress has already been made in understanding the growth mechanism of CVD diamond from hydrocarbon species dispersed in a low pressure but hydrogen rich atmosphere. Several investigations have been performed to analyze the gas-phase reactions which might occur at the gas-substrate surface interface [76,77]. It was observed that , in addition to atomic and molecular hydrogen, radical species derived from methane are most commonly known neutral and reactive gas species in the gaseous environment. In this context, Celii et al. [78] have first time reported the formation of reactive hydrocarbon species like CH_3, C_2H_2, C_2H_4 in addition to CH_4. Atomic hydrogen is a necessary chemical component of all the proposed mechanisms of diamond growth and is always observed in the analysed reactive vapor [79]. The hydrocarbon species on the growth surface may contain single (C-C), double (C=C) or triple (C≡C) bonded carbons. The atomic H rapidly attacks all but the sp^3 bonded diamond components. Thus it helps to maintain sp^3

bonding in this phase and simultaneously reduces the amount of graphitic or amorphous C which can be the part of deposits on the substrate.

Secondly, as H-C bond is stronger than the C-C bond, a monolayer of reacted atomic H bonded to the surface carbon atoms having dangling unpaired sp^3 orbital will prevent further bonding. Therefore, no diamond growth can occur, unless a bound H atom is displaced from the surface by another carbon atom or carbon containing species. Vacant sites are created on the diamond surface by the reaction between the bonded and gas phase atomic H species. Then the most probable next event is that another H will come and fill up the vacant site. However, occasionally, a C-containing species will interact with the vacant site and attach to the diamond crystallite, thereby generating diamond crystal growth [80]. Thus, the crystal growth is essentially a process replacing existing surface sites and consequently producing new ones by adatoms.

Various models have been proposed for the diamond chemical vapour deposition process from hydrocarbon species in a low pressure hydrogen atmosphere [81-83].These models reaffirm the importance of atomic hydrogen in both gaseous and surface chemical processes and suggest CH_3 and/or C_2H_2, C_2H_4 as the principal carbon deposition species. The detailed mechanisms for the incorporation of the hydrocarbon species into the growing diamond surface have also been proposed for the diamond {111}and {100} crystal surfaces [84,85].

1.7 Effect on the Nucleation and Growth of CVD Diamond Films due to Addition of Impurities to Source Gas

It has already been brought out in the preceding sections that the atomic hydrogen (H^0) plays a crucial role in removal of sp^2 bonded graphitic carbon materials and in stabilization of sp^3 bonded nuclei on the substrate surface. Moreover, hydrogen acts as an catalyst for growth of crystallites beyond their nucleation stage by passivating surface sites and replacing these sites by other carbon containing hydrocarbon species. The process of removal of sp^2 bonded material can further be enhanced by addition of small amounts of oxygen to the source gas [86,87] thereby enhancing the nucleation and growth of diamond. Similarly halogen atoms are also shown to enhance the nucleation and growth[88-90]. Bachmann et al.[18] have

suggested that irrespective of the starting molecular gas composition and the technique used for excitation of the source gases, the diamond growth by CVD process is possible as long as the C-H-O composition falls within a well defined area, called "Diamond domain" of an atomic C-H-O phase diagram (as shown in Fig.1.11). Some researchers have shown that even incorporation of small amounts of N_2 is useful for the nucleation and growth process[91]. However, many of the impurities, e.g. nitrogen, are likely to get absorbed in the diamond films and may affect the properties of thus deposited diamond films. But there are only scant reports on these studies and therefore the topic needs further investigations. On the other hand, other impurities which may dissolve in diamond at the substrate surface may interact with the diamond lattice and modify its properties.

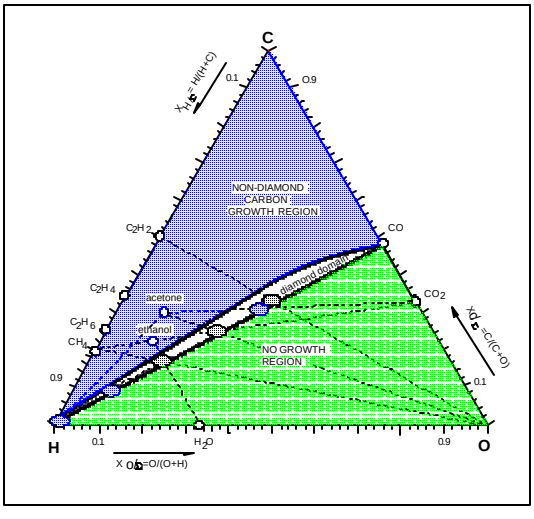

Fig. 1.11 Atomic C-H-O Phase Diagram with the "Diamond Domain"

In fact, carbon being isoelectronic with Silicon, diamond is expected to behave similar to Si in extrinsic semiconduction when doped with trivalent impurities such as Boron, Gallium or with pentavalent impurities such as Phosphorous, Nitrogen, Arsenic etc. Presently efforts are being made to dope the diamond films with proper impurities. Many of the defects in diamond are being understood to be associated with these different impurities.

Natural diamond can occur in Nitrogen and Boron mixed compositions. Boron has been identified as the suitable dopant impurity responsible for p-type behavior in these naturally occurring semiconducting diamonds[16]. From geometric and energetic considerations B appears to be the only probable element that can be substitutionally incorporated into

diamond without distorting the lattice. Recently, it has been shown that B doped polycrystalline diamond films of high room temperature conductivity can readily be prepared by the LP-CVD technique with B_2H_6 gas or related B containing solids forming the B source [92-94]. In addition to this in situ B incorporation in CVD diamond films, some experiments on B implantation have also been reported [95-97]. These results indicate that ion implantation generates large number of defects and formation of a surface layer of graphite upon annealing. Although it is possible to remove the surface layer of graphite by various chemical etching processes, the increased defect density remains to be a problem [95].

For the flexibility in device design and operation, it is of great advantage to be able to introduce shallow n-type dopants in diamond. However n-type doping has not been observed in natural or synthetic crystals. Nitrogen, a commonly occurring impurity in diamond, contributes to donor type centers with a low energy threshold for the photoconductivity at ~ 2 eV and a thermal activation energy between 1.6 eV and 1.7 eV [16]. As this level is electrically inactive at normal temperatures, this N doped diamond is unsuitable for typical semiconductor device application. Though nitrogen is considered to be critically important for modifying the surface morphology and growth kinetics [91]. Attempts to incorporate the potential n-type impurities Li and P during LP-CVD have not yet met with any clear success[98]. In addition to the in situ doping of CVD grown films, ion implantation offers an alternative technique for introduction of impurities in a more precisely controlled manner. Numerous efforts to dope diamond n-type by implanting various ions such as Li, P, As, Sb, Kr have been reported [99]. In some cases, the observed n-type activity was attributed to a residual damage. Upon annealing at high temperature, the n-type behavior was found to disappear[100,101]. As the solubility of Li and P in diamond is low, kinetic trapping under non-equilibrium conditions, e.g. during ion implantation, would be a preferred technique for introducing an excess concentration of these dopants in the diamond lattice. Phosphorus doped layers in diamond are expected to be stable due to its low diffusivity while Lithium diffuses to voids rapidly in diamond even at room temperature. Vavilov et al. [102] have reported the Li ion implantation studies. To some extent, they were successful in doping Li in diamond lattice. However, recent experiments [103,104]on Li doping studies have not produced desired results.

Besides these impurities, there are other impurities like Si, F, Cl, O which play very important and interesting role in the nucleation and growth of CVD diamond films[88-90,105-107]. Incorporation of these impurities in the diamond lattice modifies different characteristics of the film such as:

1) Quality of the film,

2) Effect on orientation , grain size and grain boundaries,

3) Growth rate of the film,

4) Proportion of sp^2 bonds to sp^3 bonds in the polycrystalline diamond film,

5) Defects and vacancies in the film, etc.

Enhancement of nucleation and growth can also be achieved by use of foreign material layer at the interface of the substrates and diamond film. There are a very few investigations in these aspects. The interlayer atoms are likely to act as catalysts and provide better nucleation density and growth rate (108,109)

1.8 Problems in CVD Technology and Motivation Behind the Present Work

From the above background, it is clear that the CVD diamond technology is an emerging technology in modern industry. The possibility of obtaining diamond in the form of polycrystalline thin films and coatings has increased its application potential by several times. However, there are several technical barriers to be overcome before applying CVD diamond to practical use. Some of these barriers are : strength of adhesion to substrate materials, control of grain size, high nucleation density, high growth rates, large area depositions etc. A thorough understanding of the mechanisms involved in nucleation and growth of polycrystalline diamond film is a key to the solutions of these problems. Diamond nucleation and growth depends upon different deposition parameters such as, the flow rate, deposition chamber pressure, methane concentration, substrate temperature, etc. In the present work, an attempt has been made to get the optimum deposition conditions for yielding most pure films having the best possible nucleation densities, high growth rates and excellent morphology (Chapter 3-Part 1). These parameters are generally considered as the measure of the quality of the diamond films.

Among all the deposition parameters, the nature of the substrate surface is found to have strong influence on the nucleation density. The diamond nucleation on perfect

surfaces, e.g. mirror polished Si wafers, is known to be extremely sluggish whereas the imperfect surfaces obtained by scratching with diamond or other similar hard particles produces high nucleation density which is useful for specific applications. However, the scratching process can be detrimental to the fabrication of diamond thin film devices on silicon substrates which are processed for electronic device packaging.

Various interlayers of foreign materials are therefore being tried to obtain better growth rates and nucleation densities. In the present study, as In and Sn are non-formers of carbide compounds and oxygen can act as an agent for etching off the graphitic (non-diamond) portions in the films, buffer layers of In-Sn-O (ITO) are employed to understand the diamond growth on scratched and unscratched silicon substrates (Chapter 3 - Part 2).

The polycrystalline diamond films grown so far by CVD technique are highly defective and therefore their properties differ in many respects from those of the perfect diamond crystals. Some of these defects may be intrinsic in nature and can be minimized by controlling the deposition conditions. But the extrinsic defects induced by / or associated with the undesired impurities diffused into the CVD films from the substrate or other sources in the deposition chamber may pose problems in their control. A small amount of such an undesired impurity may have pronounced adverse or advantageous effects on the properties and growth of the CVD films and hence systematic investigations of intentional incorporation of impurities in CVD diamond films is necessary.

The most commonly observed but unintentionally incorporated impurities in CVD diamond films are Si and N. The unintentional incorporation of Si in CVD diamond is expected to result mainly from the interface diffusion of substrate Si atoms during the nucleation and growth. The Si atoms may get incorporated non-substitutionally and hence can induce strains and stresses in the film leading to a variety of defects and vacancies in the diamond films. On the other hand, the source of N impurity is mainly the atmospheric leaks into the deposition chamber or the low purity of starting gases. At low concentrations, N may occupies the diamond lattice sites producing the substitutionally N-doped n-type semiconducting diamond films. However, for larger concentrations, N may get incorporated in cluster form producing additional changes in bonding and growth habits of the films. The studies reported so far have been performed on samples with unintentionally doped impurities and

therefore there is lack of information on behavioral aspects of these impurities in CVD films. Hence, it is felt necessary to undertake the systematic investigations on intentional doping of some selected impurities in CVD diamond films. In the present study, the impurities Si and N are intentionally incorporated in CVD diamond films and their effect on the properties and growth of the films is studied in details (Chapter 4 and Chapter 5 respectively). Fluorine is also one of the important impurities which plays important role in nucleation and growth of diamond films. It can react with atomic hydrogen to form HF forming a possible etchant for Si and sp^2 bonded carbon related species. Therefore it is expected to modify the growth characteristics and properties of diamond films (Chapter 6).

When impurities have very low diffusion velocity in the host diamond lattice, they can be incorporated using the non-equilibrium process such as ion-implantation. Using this technique, it is possible to control the concentration and depth profile of the implanted dopants. The present work presents the study of N, Li, P ion implanted diamond films and compares these results with those obtained on the films in which the impurities are incorporated in situ. The implanted films are annealed at different temperatures and the changes observed in the properties of the films are also studied. (Chapter 7).

References

1. P. K. Bachmann & R. Meisser, C & EN, 24 (May 15, 1989).
2. J. Wilks and E. Wilks, "Properties and Applications of Diamond", (Butterworth-Heinmann, Oxford, 1991).
3. J. E. Field, ed., "The properties of Natural and Synthetic Diamond" (Academic Press, London, 1992).
4. R. F. Davis, ed., "Diamond Films and Coatings", (Noyas Publications, Park Ridge, NJ, 1993).
5. A. Lettington and J. W. Steeds, eds., Thin Film Diamond (Chapman & Hall, London, 1994).
6. K. E. Spear & J. P. Dismukes, eds., Synthetic Diamond (John Wiley & Sons, New York, 1994).
7. M. A. Prelas, G. Popavici, and L. K. Bigelow, eds., Handbook of industrial

diamonds and Diamond Films (Marcel Dekker, New York, 1998).

8. A. C. Austin, The Story of Diamonds, (Gemological Institute of America, Sept. 1948).
9. Max. N. Yoder, "Synthetic Diamond - its properties and synthesis", Mat. Res. Soc. Symposium Proceedings 97 (1987) 315.
10. A. H. Deutchman & J. Partyka, "Diamond Film Deposition : a Gem of a Process", Advanced Mat. and Processes, June 89, P29.
11. B. V. Spitsyn, L. L. Bouilov & B. V. Derjaguin, J. Cryst. Growth 52 (1981) 219.
12. K. E. Spear, A. W. Phelps, W. B. White, J. Mater. Res. 5 (1990) 2277.

12a. D. S. Knight and W. B. White, J. Mater. Res., 4 (1989) 385.

13. "NEW DIAMOND", Japan Reviews in New Diamond, 1990.
14. "Diamond Deposition : Science & Technology" 1(1), Sept.1990.
15. "Diamond Deposition : Science & Technology" 2(2), April 1991.
16. A. T. Collins, E. C. Lightowler, The Properties of Diamond, in : J. E. Field (Ed.), Academic Press, San Diego (1979).
17. M. W. Geis, Proc. IEEE 79 (1991) 669.
18. P. K. Bachmann, D. Leers and D. U. Wiechert, J. DE PHYSIQUE IV, Colloque C2, Suppl. au Journal de Physique II, Vol. 1 (Sept. 1991) C2- 907.
    P. K. Bachmann, D. Leers and H. Lydtin, Diam. Relat. Meter. 1 (1991) 1.
19. P. K. Bachmann, Physics World (April 1991) 32.
20. C. B. Swan, Proc. IEEE (Letters) 55 (1967) 451.
21. D. R. Decker & A.J.Schorr, IEEE Trans. Electron Devices, Vol. ED-17 (1970) 739
22. J. C. Dyment & L. A. D'Asaro, Appl. Phys. Lett. 11 (1967) 292.

23 E. Worner, C. Wild, W. Muller-Sebert, R. Locher and P. Koidl, Diam. Relat. Mater. 5 (1996) 668.

24. J. E. Graebner, S. Jin, G. W. Kammlott, J. A. Herb and C. F, Gardinier, Appl. Phys. Lett. 60 (1992) 1576.
25. G. Lu, "Applications of Diamond Films and Related Materials", 2nd Int. Conf., (ed. A. Feldmann et al.) (1993) p. 269.
26. P. J. Boudreaux, "Applications of Diamond Films and Related Materials", 3rd Int. Conf., (ed. A. Feldmann et al.) (1995) p. 603.

27. C. T. Troy, Photon Spectra 28 (1992)28.

28. W. A. Yarbrough, N. D. Rosen, L. J. Pilione & W. D. Drawl, Proc. SPIE 1112 (1989) 176.

29. C. A. Klein, Diam. Relat. Mater. 2 (1993) 1024.

30. E. J. Coad C. S.J. Pickles,G.H. Jilbert & J. E. Field, Diam.Relat.Mater.5 (1996) 640

31. A. Vescon, I. Daumiller, P. Gluche, W. Ebert, E. Kohn, IEEE- Electron Device Lett. 18(11) (1997) 556.

32. P. Gluche, A. Aleksov, A. Vescan, W. Ebert, E. Kohn, IEEE- Electron Device Lett. 18(11) (1997) 547.

33. Lee Chang Hyun, Lim Koeng Su, Appl. Phys. Lett. 72(1) (1998) 106.

34. P. R. Chalker, C. Johnson, J. A. A. Grossley, J. Ambrose, C. F. Ayres, R. E. Harper, I. M. Buckley-Golder, K. Kobashi, Diam. Relat. Mater. 2 (1993) 1100.

35. N. A. Fox, W. N. Wang, T. J. Davis, J. W. Steeds, P. W. May, Appl. Phys. Lett. 71 (1997) 2337.

36. J. T. Glass, B.A.Fox, D. L. Dreifus & B. R. Stoner, MRS Bulletin 23(9) (1998) 49.

37. New Diamond 1990,Japanese New Diamond Forum, Ohsa Ltd.,Tokyo,Japan (1990)

38. Wentorf R. H., Jr., High Pressure Research, 4 (1974) 247.

39. M. O'Donoghue in Gemstones (Chapman & Hall, London) (1988) p176.

40. L. C. Trueb, J. Appl. Phys. 42 (1971) 503.

41. P. S. Decarli & J. C. Jamieson , Science 133 (1961) 182.

42. T. F. Kutech, Materials Science Reports 2(1) (1987) p1.

43. K. Tanaka & A. Matsuda , Materials Science Reports 2(4) (1987) p139.

44. D. G. Bhat and P. F. Woerner, J. Metals 38 (1986) p68.

45. P. K. Bachmann, P. Geittner & H. Lydtin, Technical Digest 9, Optical Fiber Communications Conference (OFC), Atlanta, GA, USA (Optical Soc. of America, Washington D. C.) (1986) p76.

46. J. C. Angus and C. Hayman, Science 241 (1988) 913.

47. K. Spear , J. Am. Ceram. Soc. 72(2) (1989) 171.

48. T. Nakamori, H. Abe,T.Kanamori & S.Shibata, Jap.J. Appl. Phys. 27(7) (1988) 1265.

49. B. S. Kwak, E. B. Boyd & A. Erbil, Appl. Phys. Lett. 53 (18) (1988) 1702.

50. S. Matsumoto, in Diamond and Diamond-like Films, (J. Dismukes, et al., eds.), Electrochem. Soc. Proc., Vol. PV 89-12 , p.50, Pennington, NJ (1989).

51. P. K. Bachmann, W. Drawl, D. Knight, R. Weimer and R. Meisser, Diamond and Diamond-like Materials, Proc. MRS Symp. Vol. EA-15, ed. Badzian et al. (1988) p. 99.

52. H. Konig and G. Helwig, Zeitschrift Fur Physik 129 (1951) 491.

53. K. Kurihara,K. Sasaki, M.Kawarada and N. Koshono, Appl. Phys.Lett. 52 (1988)437.

54. S. Matsumoto, M. Hino, & T. Kobayashi, Appl. Phys. Lett. 51(10) (1987) 737.

55. K. Suzuki, A. Sawabe and T. Inuzuka, Appl. Phys. Lett. 53(19) (1988) 1818.

56. M. N. Gardos, K. V. Ravi, in Diamond and Diamond-like Films, (J. Dismukes, et al., ed.), Electrochem. Soc. Proc., Vol. PV 89-12, p.475, Pennington, NJ (1989).

57. C. V. Deshpandey and R. F. Bunshah, J. Vac. Sci. Tech. A7(3) (1989) 2294.

58. J. C. Angus, F. A. Buck, M. Sunkara, T. F. Groth, C. C. Hayman and R. Gat, MRS Bulletin 14(10) (1989) 38.

59. P. Wood, T. Wydeven, & O. Tsuji, in Program and Abstracts of the First International Conference on the New Diamond Science and Technology , New Diamond Forum , Tokyo, Japan (1988) 100.

60. S. Matsumoto, Y. Sato, M. Kamo and N. Sekata, Jap. J. Appl. Phys. 21 (1982) L183.

61. C. H. Wu, M. A. Tamor, T. J. Potter & E. W. Kaiser, in Diamond, BN, SiC and Related Wide Bandgap Semiconductors, (J. T. Glass, R. Meisser, & N. Fujimori, eds.), Mater. Res. Soc. Proc. Vol 162, Pittsburg, PA (1990).

62. K. V. Ravi, C. A. Koch, H. S. Hu & A. Joshi , J. Mater. Res. 5 (1990) 2356.

63. R. T. Rozbicki and V. K. Sarin, Thin Solid Films 332 (1998) 87.

64. Y. Hirose & M. Mitsuizumi, New Diamond (English Ed.) 2 (1990) 27.

65. P. E. Pehrsson, F. G. Celii & J. E. Buttler, in “Diamond Films and Coatings”, Ed. R.F. Davis (Noyes Publications, Park Ridge, NJ, U. S. A.).

66. J. E. Buttler and H. Windischmann, MRS Bulletin 23(9) (1998) 22.

67. S. Veprek, J. Crystal Growth 17 (1972) 101.

68. R. Berman, The Properties of Diamond, (J. E. Field, Ed.) Academic Press, London (1979).

69. J. L. Zilko, in : Handbook of Thin-Film Deposition Processes and Techniques,(K. K. Schuegraf, ed.) Noyes Publications, Park Ridge,NJ (1988).

70. J. C. Brice, in : Properties of Gallium Arsenide, EMIS Data Reviews Series No. 2, INSPEC, London (1986).

71. H. Liu, and D. S. Dandy, in: Diamond Chemical Vapour Deposition (Noyes Publications, Park Ridge, NJ (1995).

72. J. L. Robins, Applied Surface Science 33/34 (1988) 379.

73. W. A. Yarbrough & R. Messier, Science 247 (1990) 688.

74. T. R. Antony, Vacuum 41 (4-6) (1990) 1356.

75. E. S. Machlin, J. Mat. Res. 3(5) (1988) 958.

76. J. W. Kim, Y. J. Baik, K. Y. Eun and D. N. Yoon, Thin Solid Films 212 (1992)104.

77. M. Sommer and F. W. Smith, J. Mater. Res. 5 (1990) 2433.

78. F. G. Celii, P. E. Pehrsson, H. T. Wang and J. E. Buttler, Appl. Phys. Lett. 52 (1988) 2043.

79. F. G. Celii and J. E. Buttler, Ann. Rev. Phys. Chem. 42 (1991) 643.

80. R. F. Davis, J. Crystal Growth 137 (1994) 161.

81. J. E. Buttler and F. G. Celii, Electrochem. Soc. Proc. 89 (1989) 317.

82. S. J. Harris, Appl. Phys. Lett. 56 (1990) 2298.

83. M. Frenklach & K. E. Spear, J. Mat. Res. 3(1988)133.

84. M. Tsuda, M. Nakajima and S. Oikawa, J. Am. Chem. Soc. 108(1986) 5780.

85. S. J. Harris, Appl. Phys. Lett. 56(1990) 2298 .

86. Y. J. Baik & K. Y. Eun, Thin Solid Films 214 (1992)123.

87. M. A. Tamor & M. P. Everson, J. Mater. Res. 9 (1994) 1839.

88. M. Asmann, J. Heberlein & E. Pfender, Diamond and Related Materials 8 (1999)1.

89. I. Schmidt, F. Hentschel & C. Benndorf , Diamond and Related materials 5(1996)1318.

90. E. J. Corat, V. J. Trava-airoldi, N. F. Leite, M. C. A. Nono & V. Baravauskas, J.

Materials Science 32(1997)941.

91. Z. Yu, U. Karlsson and A. Flodstrom, Thin Solid Films 342 (1999) 74.
92. K. Nishimura et al. , J. Appl. Phys. 69 (1991) 3142.
93. N. Fujimori et al. , Vacuum 36 (1986) 99.
94. J. Mort et al. , Appl. Phys. Lett. 55 (1989) 1121.
95. G. Braunstein & R. Kalish, J. Appl. Phys. 54 (1983) 2106.
96. J. R. Zeidler, Phys. Rev. B 47 (1993)2065.
97. R. Kalish, C. Uzan-Saguy, A. Samoiloff, R. Locher and P. Koidl, Appl. Phys. Lett. 64 (1994) 2532.
98. K. Okumura et al. , Appl. Phys. Lett. 57 (1990) 1907.
99. V. S. Vavilov, Radiation Eff. 37 (1978) 229.
100. V. S. Vavilov, M. I. Guseva, E. A. Konorova & V. F. Sergienko, Sov. Phys. Semicond 4 (1970) 6.
101. V. S. Vavilov, M. A. Gukasyan, E. A. Konorova & Y. V. Milyutin, Sov. Phys. Semicond 4 (1970) 6.
102. V. S. Vavilov, M. A. Gukasyan, M. I. Guseva & E. A. Konorova , Sov. Phys. Semicond 6 (1972) 741.
103. K. Okumura, J. Mort & M. Machonkin, Appl. Phys. Lett. 57(1990) 1907.
104. C. P. Jr. Beetz, B.A. Lincoln & D. R. Winn, Diamond Optics III (A. Feldman and S. Holly, ed.) 1325:241 SPIE (1990).
105. J. Ruan, W. J. Choyke, & W. D. Partlow, Appl. Phys. lett. 58 (1991) 295.
106. J Ruan, W. J. Choyke, & K. Kobashi, Appl. Phys. Lett. 62 (1993) 1379.
107. C. D. Clark, H. Kanda, I. Kiflawi, & G. Sittas, Phys. Rev. B 51 (1995) 16681.
108. D. V. Musale, M. P. Pai, S.R. Sainkar and S. T. Kshirsagar, Materials Letters 39 (1999) 86.
109. S. M. Kanetkar, A. A. Kulkarni, A. Vaidya, R. D. Vispute, S. B. Ogale, S. T. Kshirsagar and S. C. Purandare, Appl. Phys. Lett. 63 (1993) 740.

CHAPTER 2

EXPERIMENTAL TECHNIQUES USED FOR SYNTHESIS AND CHARACTERIZATION OF DIAMOND FILMS

The early part of this chapter gives brief account of the merits and demerits of the existing deposition techniques used for the deposition of diamond thin films and focusses its attention on the hot-filament chemical vapour deposition (HFCVD) technique which is used in the present study. This is then followed by the details of the HFCVD apparatus designed and developed in the course of the present work. Subsequently, it gives a brief note on the RF sputter deposition technique which is used for the production of interlayes. Remaining part of this chapter describes the various characterization techniques used in the present work.

2.1 Introduction

As described in chapter 1, different techniques have been developed for the synthesis of diamond thin films. The CVD techniques have proved to be quite reliable techniques for synthesizing diamond films having high crystalline quality and purity. However, each of the CVD techniques has its own advantages and drawbacks. Therefore, the choice of the technique depends on the specific application, e.g., for contamination-free, uniform coatings on medium size substrates, the low pressure MW-PA-CVD is probably a good choice. But it involves very expensive equipment. For bulk materials on small areas, DC-PA-CVD seems to be promising. RF-PA-CVD is the most suitable method for scaling up and industrial manufacture of diamond coatings, but it suffers from low growth rates and poor crystalline quality. For obtaining high quality diamond coatings over relatively large areas, combustion flame technique is a good choice while the poor uniformity of the film is its main disadvantage.

In cases where contamination of the film by the filament material is not a serious problem while large area deposition is major requirement, the hot filament method is advantageous. It is the most simple and economically feasible method as the shape and size of the filament can be changed according to the requirement of the deposition area. Therefore, this technique has been accepted widely for most industrial production. we have also adopted this technique for the synthesis of diamond films. The details of the system developed by us are given in section 2.2.

For some of the specific research studies reported in this work, other experimental systems were used, e.g. radio-frequency (RF) sputter deposition technique was used for depositing the ITO buffer layers on pretreated Si substrate. The details of the RF sputter deposition system are given in section 2.3

CVD diamond coatings are characterized by a number of techniques. The techniques, viz. laser Raman spectroscopy, photoluminescence spectroscopy, Scanning Electron Microscopy (SEM), X-Ray Diffraction (XRD), and Energy Dispersive Analysis of X-rays (EDAX) used in the present study are described in brief in section 2.4.

2.2 Hot- Filament Chemical Vapour Deposition (HFCVD) System

The HFCVD set-up used in the present work is schematically shown in Fig. 2.1. This set up accommodates a pair of vacuum tight water-cooled electrodes for energizing the filament, a filament holder, tungsten filament, a substrate holder, a thermocouple (Pt: Pt+13%Rd) for substrate temperature measurements and a vacuum tight gas inlet control assembly to direct the H_2 and hydrocarbon (CH_4) gas flow towards the filament. The cylindrical deposition chamber is 28 cm in height and 26 cm in diameter. There are eight teflon vacuum sealed feedthroughs at the bottom of the chamber . These feedthroughs are used for the filament holder and two thermocouples (one for the inner temperature of substrate holder and the other for the outer temperature of the substrate holder). The other two feedthroughs are used for the gas inlet and for the pressure gauge. There is one side port which is used as a view port. All the feedthroughs and ports are vacuum sealed with neoprene O-rings.

The flow rates of the precursor gases are adjusted with the help of Mass Flow Controllers (Make Unit Instruments Inc., USA, Model UFC-1100A) coupled with the Read out and Control Unit (Make Unit Instruments Inc., USA, Model No. URS - 100). The gas mixture is introduced into the chamber through a quarter inch diameter stainless steel tube . The initial evacuation of the chamber is achieved by using a rotary vacuum pump (Edwards make) with a minimum pressure level of 10^{-3} Torr. The chamber pressure measurements are carried out by connecting a Transducer Capacitance Gauge (Make MKS Instruments Inc., USA, Model No. 690A100) coupled with a Signal Conditioner Control Unit (Make MKS Instruments Inc., USA, Model No. 270).

The geometry of the tungsten filament is optimized by trying different shapes (such as U shaped, line shaped and M shaped) and sizes. The M shaped filament is found to be appropriate and is accepted for the present work as only these filaments survived for long periods of deposition time as well as permitted constant uniform distance between the filament and substrate surface. To save the filament from sagging as well as from strain due to thermal expansion, the filament was mounted on a specially designed filament holder. Fig. 2.2 shows the schematic diagram of the filament holder.

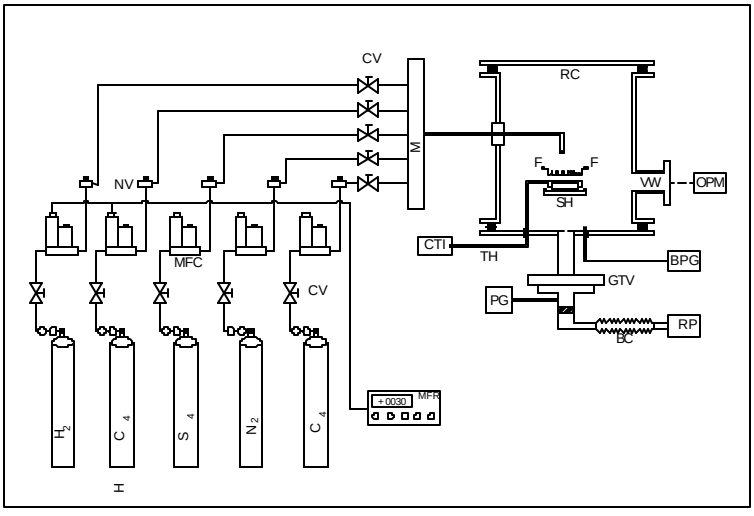

RC – Reactor
FF – Filament
SH – Substrate Holder
TH – Thermocouple
CTI – Calibrated Temp. Indicator
VW – Viewing Window
OPM – Optical Pyrometer
BPG – Barotron Pressure Guage
GTV – Gate Valve
PG – Pirani Guage
BC – Bellow Connection
RP – Rotary Pump
CV – Complete Shut-off Valve
NV – Needle Valve
MFC – Mass Flow Controller
MFR – Mass Flow Read-out

Fig. 2.1 The Schematic Diagram and Photograph of the HF-CVD System used for the deposition of the diamond films

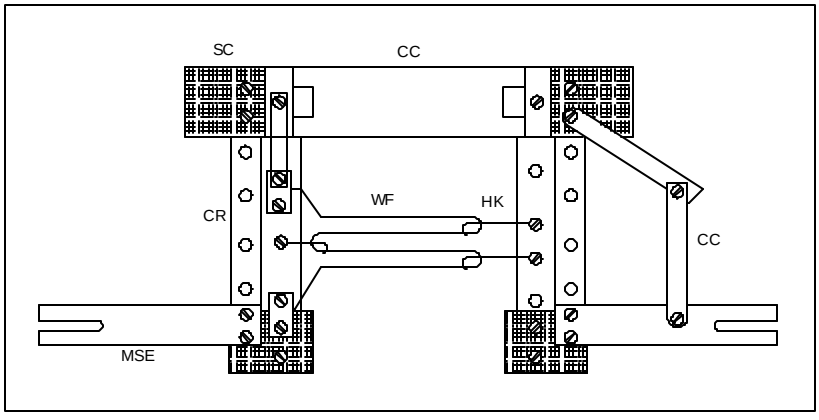

WF- Tungsten Filament, CR- Ceramic Bars, MSE- Mild Steel Electrodes
CC- Copper Conductors, SC- SS connectors, HK- Tungsten Hooks,O-S.S. Bolts.

Fig. 2.2 The Schematic Diagram of Filament Holder.

It consists of Ceramic Bars (length ~ 60 mm, Width ~ 10 mm and thickness ~ 8 mm) in which equidistant holes of diameter ~ 1/8 inch were made for receiving the SS bolts. These bolts pass through the circular hole of hooks made out of tungsten wire (750 micron gauge) . These hooks provide point supports to the tungsten filament as shown in the figure. The point support saves filament from heat loss to the SS bolts and the ceramic slabs. Moreover, these supports keep the filament in a plane parallel to the substrate surface and save the filament from sagging and breakage as well. This arrangement is very crucial as the distance between the filament and the substrate needs to be maintained constant during the deposition period. The perforated ceramic bars are tightly fitted to each other by SS connectors and the filament holder takes the shape of pi (Π) like symbol. The particular Π shape of this holder leaves open space for imaging the filament directly into the optical pyrometer for temperature measurements. More importantly, this design of the filament holder allows scale up of the deposition area for the purpose of deposition on large area substrates. For most of the present work, the M shaped filament is made using 99.99 % pure 500 μm thick tungsten wire 15 cm in length. The power supply to the filament is obtained from a Welding Transformer set, the primary coil of which is

supplied with AC 50 Hz stabilized power supply. The transformer is capable of giving current of maximum 150 Amp. at 50 volts in the secondary. The filament temperature is measured using an Optical Pyrometer (Energia EP5 224/1963r, Poland).

The design of the substrate holder with respect to the filament size and shape is very important to obtain the desired substrate temperature. The heat emitted by the filament at its peak temperature (~ 2000^0C) has been used to heat up the substrate holder and the substrate. This required design of the substrate holder to accommodate a heat sink or a heat exchanger . We have worked out this design so that no external heating or cooling be required and a constant substrate temperature could be maintained. Various materials used to fabricate the heat sink were Copper, Graphite and Ceramic so as to get the substrate temperature 750^0C, 850^0C, and 950^0C respectively. On the top of the heat sink, a circular mild steel disc is placed which served as the substrate supporter. The schematic diagram of the substrate holder

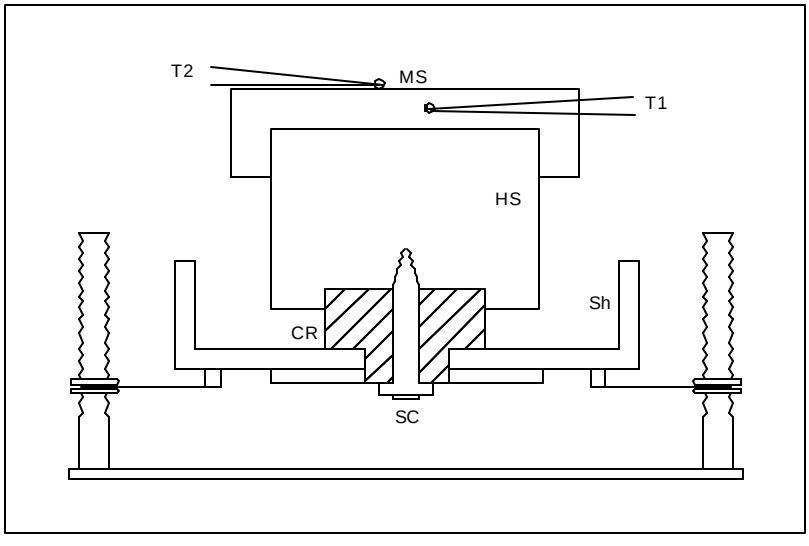

assembly is shown in figure 2.3.

MS- Mild Steel Substrate Holder, HS- Heat Sink, CR- Ceramic Spacer, Sh- SS Shield, SC- Tightening Screw, T1 & T2- Thermocouples

Fig. 2.3 Schematic Diagram of the Substrate Holder

The substrate temperature is measured with the help of a (Pt : Pt + 13% Rd) thermocouple connected to a caliberated temperature indicator (Mahindra Electroflo, India, Model No. PC538). The substrate holder was made to rest on the SS threaded rods welded to the base plate so that the substrate surface to filament distance can be adjusted without touching the fragile filament. The lock-nuts engaged on the threaded rods can be used to lock the distance between the filament and the substrate surface for any number of deposition experiments.

2.3 Radio-Frequency Sputter Deposition Technique

Sputtering has reemerged in recent years as one of the most versatile techniques which meets the demand of contemporary film technology needs. Sputtering is the controlled method of coating which involves the transport of almost any material from a source , called a target , to a substrate of almost any other material. The early process was direct current (DC) sputtering. Though it represented the simplest and most practical arrangement, DC sputtering was only useful in laying down a metallic film. It was during the last two decades that radio-frequency (RF) sputtering was developed. RF expands the uses of sputtering to non-metals. Improvements in vacuum technology have made it possible to lay down large areas of high purity film of uniform and reproducible thickness, and to utilize a single material source for hundreds of coatings.

In this process, the ejection of the source material is accomplished by the bombardment of the surface of the target with the ions accelerated by a high voltage. Particles of atomic dimensions are ejected from the target as a result of momentum transfer between incident ions and the target. The target-ejected particles traverse the vacuum chamber and subsequently deposit on a substrate as a film. The schematic diagram of the sputter deposition technique used in the present study is shown in Fig. 2.4. There are four major components required for sputtering. These parts are vacuum system to evacuate the chamber, a target, a power supply and the sputtering chamber. For evacuating the chamber , the combination of diffusion pump and rotary mechanical pump is used. The RF power supply is used to generate the plasma. The difference in mobility of electrons and heavy gas ions produces negative potential which accelerate the ions to impinge on the target. The target provides the material

which is to be deposited as a thin film onto the substrate material. The target is disc shaped and it consists of a backing plate and a layer of target material. The basic sputtering chamber generally consists of different components. These components are chamber top plate, vacuum chamber, cathode assembly, a dark space shield, shutter, substrate holder, anode and the leak valve.

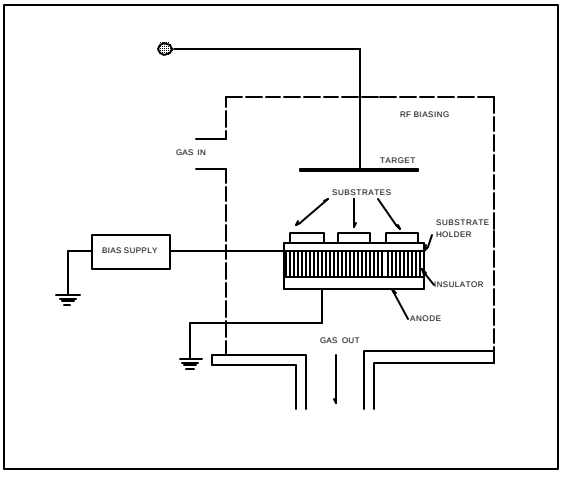

Fig. 2.4 The Schematic Diagram and Photograph of sputter depsition system

We have used this technique for the production of In-Sn-O (ITO) films to act as an intermediate oxide layer for deposition of diamond films. The model '8620 Sputtering System' manufactured by Materials Research Corporation, Orangeburg, New York, USA was employed for production of uniform, homogeneous ITO films. The sputtering gas was mainly Ar while about 5% O_2 was used to obtain stoichiometric ITO films.

2.4 CHARACTERIZATION TECHNIQUES

2.4.1 Laser Raman Spectroscopy

Raman spectroscopy is one of the many light wave scattering phenomena. The Raman effect belongs to the class of molecular scattering phenomena and it is very sensitive to the nature of chemical bonding in solids. It is based on inelastic light scattering arising from the interaction of photons with lattice vibrations (or lattice waves) which have quantized energies called phonons. The interaction of phonons with photons is through the electric charge polarization induced in the crystal by the electric field of the intense monochromatic light beam, generally obtained from a laser tuned to a single line. A lattice vibration is Raman active when the vibration changes the polarizability [1]. Thus, the coupling of such lattice vibration with light photons generates induced oscillating dipoles that may emit light which may have either same frequency as the incident beam (called elastic Rayleigh scattering) or have frequency shifted by an amount equal to the vibrational frequency of the lattice (inelastic light scattering). In other words, in the scattering process, the incident photon gives part of its energy to the lattice in the form of a phonon of energy $h\omega_p$ and emerges out with a lower energy $h\omega_s$, obeying the energy conservation equation [2],

$$h\omega_s = h\omega_1 - h\omega_p$$

This down-converted frequency shift is the Stoke's-shifted scattering. Another way of viewing this interaction is that the incident photon perturbs the electrons in the valence

band so that it gets raised to a virtual level from which the scattered radiation is emitted (see Fig. 2.5a). It is explicitly assumed here that the radiation interacts with the lattice vibrations through the intermediary of the electrons in the crystal. Thus the scattering process would involve three virtual electronic transitions accompanied by the following photon and phonon transitions: (1) the photon $h\omega_1$ is absorbed by the electrons, (2) an optic phonon $h\omega_p$ is created and (3) a photon $h\omega_s$ is emitted (see Fig.2.5b). Here it may be noted that the scattering crystal is generally in its electronic ground state, with all valence bands full and all conduction bands empty at the start of the scattering process and it also returns to its electronic ground state at the end of the event. The virtual intermediate states, of course, involve the excitations of electron-hole pairs. These sequential events over a time period are shown in Fig. 2.5a .

In case of less-than-gap photon energy, the scattered photons can be viewed in any desired direction. However, if the exciting photon has a greater-than-gap energy, the electron transition is to a real state and a much stronger excitation results with this non-penetrating radiation, the scattered photon must then be viewed only in the back-reflection geometry.

On the other hand, if the lattice of the semiconductor already has an appreciable density of phonons, the scattering process can result in the emission of a more energetic photon (see Fig. 2.5b) and obeys the energy conservation equation-

$$h\omega_s = h\omega_1 + h\omega_p$$

These up-converted frequency shifts are anti-Stokes-shifted scattering mode. Normally, the intensity of the anti-Stokes mode is much weaker than that of the Stokes component, because usually there are few phonons to be absorbed compared to the density of phonons that can be emitted, the probability for absorption being lower than the probability for emission by a factor of $\exp(h\omega_p / kT)$. This scattering is useful for investigation of temperature dependent vibrational properties of the solids.

In addition to the conservation of energy, as treated above, momentum must also be conserved in the photon-phonon collision interaction. The momentum of wave is hK, where K is the wave propagation vector and $h = h/2\pi$. The momentum of the scattered photon (hK_S), therefore, is found by vectorial construction (see Fig. 2.6a). The momentum vector of a incident photon ($K_I = 2\pi/\lambda_I \leq 10^5$ cm^{-1}) is very small compared to the range that is available to

phonons (upto $K_P = 2\pi/a \geq 10^8$ cm^{-1}, 'a' being the lattice spacing). Since the photon-phonon interaction involves two photons and one phonon, the momentum of the phonon is restricted to small values. In this range of $K_P << K_1$, the optical phonon dispersion spectrum ($\hbar\omega_p$) is practically constant in frequency and hence

Chapter 2 *Experimental techniques used.....*

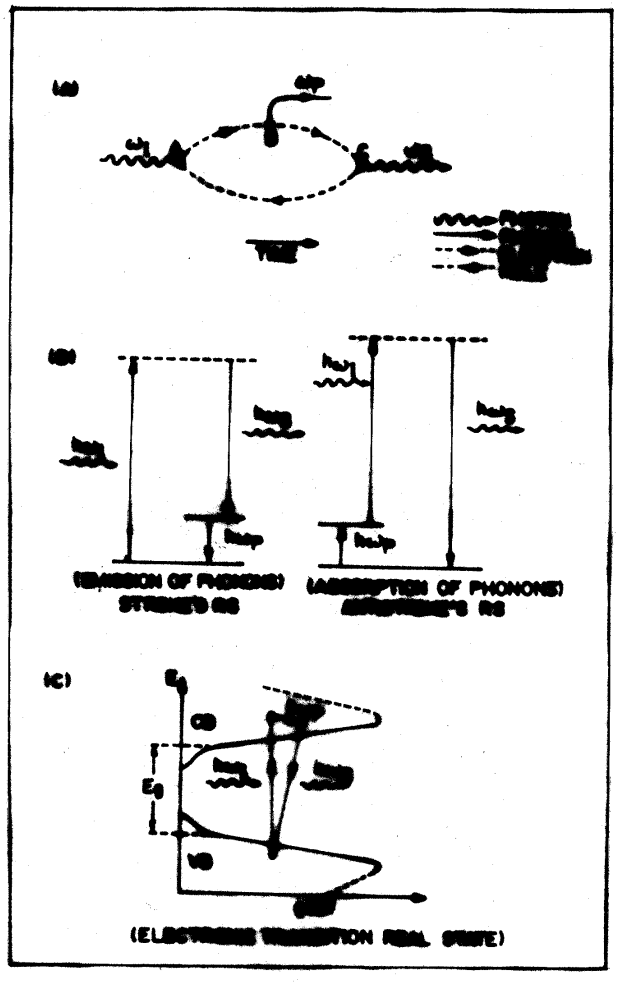

Fig. 2.5 (*A*) Representation of Raman scattering process on time axis, A - Initial state and absorption of photon (ω_I) by electron, B - Transition of the electron to virtual state and emission of phonon (ω_P), and C- Returning of electron to ground state by emission of photon (ω_S); (*B*) and (*C*) represent the electronic transitions during the Raman scattering process to virtual state and real state respectively.

the Raman scattering results in a sharp band positioned at this frequency with K_P practically equal to zero, i.e. $K_P \sim 0$ becomes the selection rule (see Fig. 2.6b).

This process of scattering with $K_P \sim 0$, is the first order Raman scattering. However, the condition of vanishingly small wave vector can also be met by combination of two phonons, such as $K_{P1} \pm K_{P2} \sim 0$, leading to what is known as second order Raman scattering. However, these processes are extremely low probable and thus produce only weak Raman scattering. Similarly more phonons can combine to produce higher order Raman scattering. Thus, the momentum conservation rule is a natural manifestation of the translation symmetry which forbids the transitions for vibrations having $K \neq 0$. The point group symmetry of crystals however places further restrictions on the phonons which may contribute to the Raman scattering [3].

Long-range ordered crystals with different symmetries have their characteristic signatures in the Raman spectrum originating from phonons at Brillouin zone center that satisfies the momentum conservation condition at $K_P \sim 0$. Moreover, when the crystallite size becomes small or the crystals are subjected to a strain, the anharmonicity of the interatomic potential increases and gives rise to coupling between the modes of vibration so that if one phonon of a particular mode is excited, it will in time decay into other mode. The anharmonic interaction broadens the Raman bands, particularly, the one phonon spectrum, as a result of the finite life time of the mode and also changes the frequency as the temperature is altered [4]. Similarly, the introduction of defects into crystals considerably modifies the properties of the modes of vibration. The defect is in fact localized at a particular lattice site at which the wave vector is not conserved. This gives rise to a local mode frequency and there will be contribution to the scattering at this frequency which may generally be superimposed as the induced scattering from all of the other phonons.

However, in the lattice networks, where there is complete loss of long-range order (amorphous solid) the momentum conservation rule becomes meaningless. As a consequence, phonons with any wave vector throughout the Brillouin zone may contribute to the Raman spectrum of the amorphous solid. Stoke's scattering amplitude (I_ω) in the first-order Raman spectrum of the intrinsic fundamental vibrations of the amorphous network is related to the amorphous vibrational (phonon) density of states (VDOS) through the approximate relation:

Chapter 2 Experimental techniques used.....

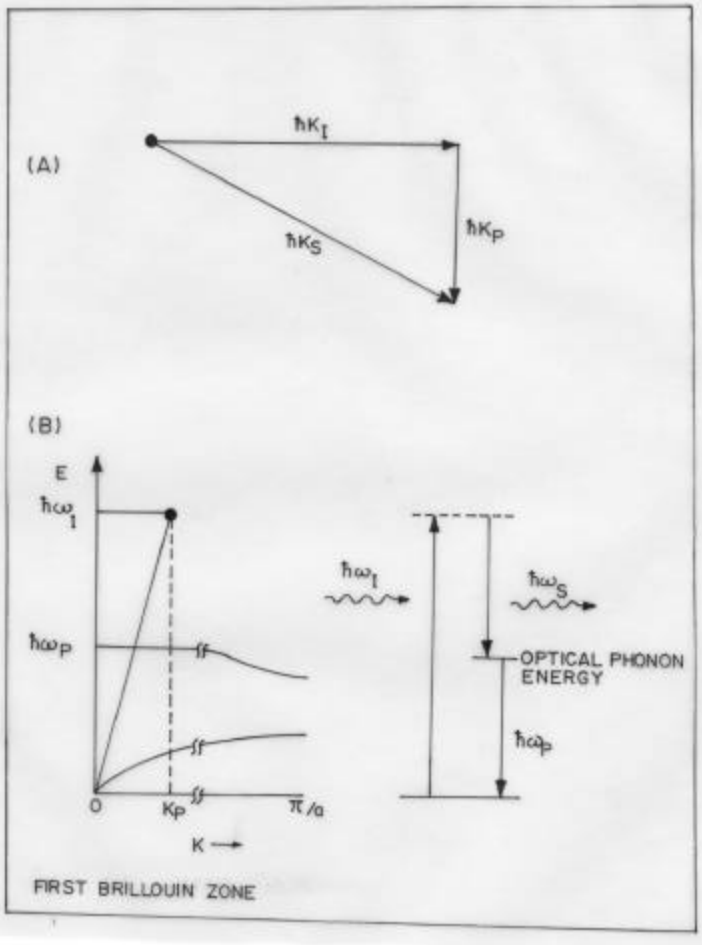

Fig. 2.6 (*A*) Vectorial representation of the momentum conservation during first order Raman scattering process; (*B*) Energy levels in the dispersion curves involved in the Stokes' Raman scattering process

$$I_\omega = C_\omega(<n+1>/\omega)\, g_\omega$$

where, C_ω is the coupling constant, n is the Bose-Einstein factor and g_ω is the phonon density of states [5]. Thus, the reduced Raman spectrum, viz. the spectrum of I_ω divided by frequency ω, would approximate the experimental measurements of the variation of amorphous VDOS and the analysis of Raman spectrum of amorphous solid reduces to comparing them with the calculated spectrum of amorphous VDOS [6].

The number of the observed Raman bands (frequencies), the intensities or half widths depend on the crystal structure and crystal states. Hence one can invariably obtain information about the crystal structure and the degree of crystallization by measuring the Raman spectrum of the materials. It can be seen from the above discussion that RS can be used as a key tool to bring out the chemistry and physics of carbon, particularly of CVD diamond films. Since it is very sensitive to the nature of chemical bonding and carbon is also capable of forming various kinds of covalent bonding, Raman spectroscopy can be used to distinguish between various types of carbon, viz., diamond, graphite, microcrystalline, and amorphous or hydrogenated carbon.

Depending on the structure and the nature of chemical bonding, every carbon phase has its characteristic signature in the Raman spectrum (Fig. 2.7) and they are described briefly in the following paragraphs.

Tetrahedrally bonded cubic diamond [7,8] **:** Diamond belongs to the face-centered cubic lattice with space group Fd3m. It is characterized by four-fold-coordinated sp^3 bonding of O_h symmetry. There are two carbon atoms in the primitive unit cell and thus a single triply degenerate first order phonon with symmetry T_{2g}. From the selection rules of factor group O_h, this mode is only Raman active. Hence, the diamond structure has no first order infrared absorption. The tetrahedrally bonded carbon atoms in diamond give rise to a single sharp line corresponding to first-order Raman scattering at 1332 cm^{-1} (as shown in Fig. 2.7a). It is the characteristic diagnostic feature for diamond.

Trigonally Bonded Hexagonal Graphite [7] **:** Graphite consists of stacked sheets with the carbons within the layers arranged in a two-dimensional network of regular hexagons. The space group of graphite is P63/mmc with four carbon atoms in the primitive hexagonal cell [9]. The first order phonons of graphite can be classified in factor group D_{6h} of space group P63/mmc. The three-fold coordinated sp^2 bonded structure of graphite

Chapter 2 *Experimental techniques used.....*

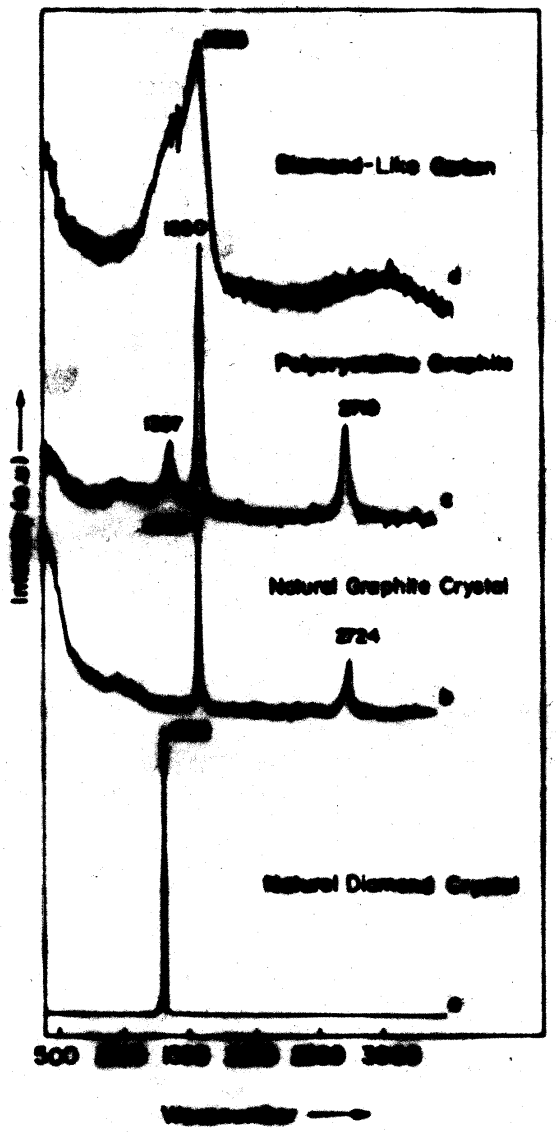

Fig. 2.7 Raman spectra of various crystalline and amorphous forms of carbon

leads to the first order Raman line at 1580 cm^{-1} that corresponds to the in-plane C-C stretching mode vibrations with E_{2g} symmetry[10,11]. This peak is mainly characteristic of large crystals of graphite.. The feature at 2710-2724 cm^{-1} is a two-phonon band taken to be 2 x 1357, the band that appears in the spectrum of polycrystalline graphite. The 1357 cm^{-1} band doesn't appear in large grain single crystals but does appear in well-crystallized graphite with small particle size. Since the Raman scattering efficiency for graphite is much greater (~50 times) than for diamond [12,13], small amounts of graphitic carbon codeposited in CVD diamond films can also be readily detected.

Raman Scattering in amorphous non-hydrogenated (a-C) and amorphous hydrogenated (a-C:H) diamond-like carbon films (mixed sp^2 and sp^3 bonded) [7,14]**:** Depending on the deposition techniques and conditions used for preparation, a-C and a-C:H films are either graphite-like consisting entirely of sp^2 bonded carbon or containing both sp^2 and sp^3 hybridized carbon and hydrogen to passivate the dangling bonds. These are therefore called "diamond-like" carbon films. The Raman spectrum of a-C is dominated by a large broad band at 1550 cm^{-1} labelled "G" band with a small shoulder at 1350 cm^{-1}, labelled "D" band. This Raman spectrum is interpreted as providing a strong evidence in favour of graphite bonding. The 1550 cm^{-1} band is close to the frequency of vibrational mode in graphite and well above the frequency of any vibrational mode possible in an sp^3 bonded lattice. The lack of features at 1332 cm^{-1} (diamond phase) can not itself be used as the evidence against sp^3 bonding as diamond has a much lower Raman scattering cross section than graphite [12,13]. The shoulder band "D" around 1350 cm^{-1} is not attributed to the sp^3 bonds, but to a disorder mode of graphite microcrystals.

Thus, if one is interested in a fast, sensitive and qualitative test of a film in terms of the bonding types, Raman spectroscopy is an excellent choice.

The schematic diagram of the Raman spectrometer arrangement used in the present study is shown in Fig. 2.8.

The spectrophotometer consists of :

1. A laser source (monochromatic radiation source)
2. Sample illumination and sample holding device set up.
3. Fore-optics for collection of Raman radiation.

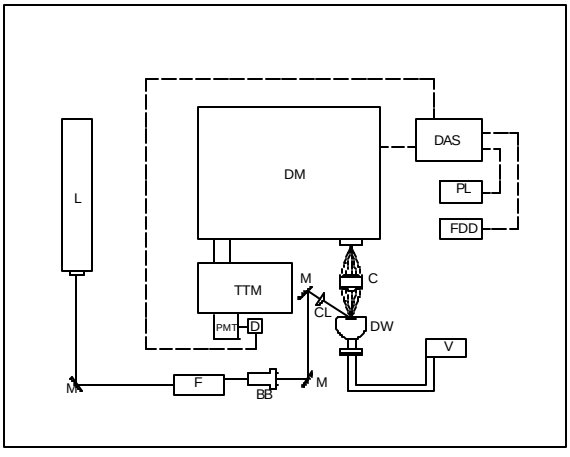

L – Laser
M – Mirror
F – Filter
BB – Beam Broader
CL – Cylindrical Lens
DW – Dewar
C – Camera Lens
DM – Double Monochromator
TTM – Third Monochromator
PMT – Photomultiplier Tube
D – Noise Discriminator
DAS – Data Acquisition System
PL – Plotter
FDD – Floppy Disk Drive

Fig. 2.8 The Schematic Diagram and Photograph of the Laser Raman Setup

4. Detector system.

The Raman scattering measurements were performed in the region 1000-1800 cm^{-1} in the backscatterering mode using the SPEX 1403 reflection grating type double spectrometer. The SPEX 1442 third monochromator, slaved in tandem to the double monochromator was used to reduce the Rayleigh light and other background effects. The data were collected in the photon counting mode using the RCA C31034 GaAs photo-multiplier detector system and SPEX DM1 DATAMATE spectrometer controller and data processor. The radiation of wavelength 514.5 nm from the Argon-ion laser (Spectra Physics model 165-B) , filtered through the SPEX lasermate, was allowed to fall on the sample in a line focus geometry (approximately 1 cm x 0.005 cm area) with the help of a cylindrical lens. The intensity of the radiation incident on the sample was ~ 300 mW. The scattered radiation was collected and focused onto the spectrometer slit using a Minolta camera lens (55 mm, f/1.2) . The polarization of the incident radiation was kept fixed in the horizontal plane. The actual positions, intensities and widths of the various Raman bands were measured after a light smoothing of the raw data by using the in-built software of the DM1 data processor. The ultimate resolution at the 250 μm wide exit slit was better than + 2 cm^{-1} .

2.4.2 Photoluminescence Spectroscopy

Luminescence is a technique widely used for studying localized states within the band gap of a semiconductors/insulators. Since the localized states can originate from incorporation of defects and impurities during growth, luminescence has also proved to be a useful characterization tool for studying the effects of deposition conditions.

Luminescence, i.e., light emission by recombination of excited states in a crystal can take place via two limiting cases [15]. In the first limiting case, excitation of crystal causes electrons from the valence band to be transferred into the conduction band and then the

recombination can occur in several stages involving defect levels. Some of these stages may involve radiation while others do not. In the present studies, we have used the excitation radiation, λ = 514.5 nm (~2.41 eV) which has the photon energy much less than the band gap of diamond (~5.5 eV) and hence the possibility of this band to band transition can be eliminated. In the second limiting case, excitation and relaxation into the ground state may occur within the defect itself, i.e. excitation and relaxation of an electron may take place within an imperfection, their interaction with the crystal lattice being restricted to the immediate vicinity. Since the energy levels involved are generally near the band edges, such transitions could be possible in our samples and all these radiative transitions involving levels less than 2.41 eV can occur. Our PL spectra possibly consist of such transitions within the imperfections.

The process of photoluminescence is better explained with the help of configuration coordinates of the imperfection and its immediate surrounding [15,16]. The electronic charge distribution of the defect atom is changed when it is excited from the ground state into an excited state. The bonding with the nearest neighbours in the lattice will therefore be influenced. The equilibrium configuration of the neighbouring ions/atoms becomes unstable and they take up new equilibrium position. The part of the excitation energy is thus transferred to the lattice. This process takes long time compared with the electronic transition, i.e. one can assume that the electronic transition occurs while the lattice configuration is still unchanged (Franck-Condon Principle).

The electronic transition back to the ground state takes place under the new lattice configuration. The ground state is not therefore reached immediately. The electronic transition is instead followed by a rearrangement of the ions into the original configuration. Since energy has thus been given twice to the lattice, the electron recombination energy is less than the excitation energy. The concept of configuration co-ordinate is often employed to describe this state of affairs. If one formally combines the changes in all lattice co-ordinates between both lattice configurations into one configuration co-ordinate, the potential energy of the system "defect electron+surrounding lattice" can be represented as in Fig. 2.9 [16]. In the ground state and the excited state, the potential energy is a quadratic function of the configuration co-ordinate, each having a minimum at the respective equilibrium configurations. The parabolic shape of the typical configuration co-ordinate suggests that the system is likely to obey the

Hook's law so that quantum mechanically, it would behave as a simple harmonic oscillator and thus the ground state and excited state shall be accompanied by vibrational energy level distribution as shown by the equidistant horizontal lines having

Chapter 2 *Experimental techniques used.....*

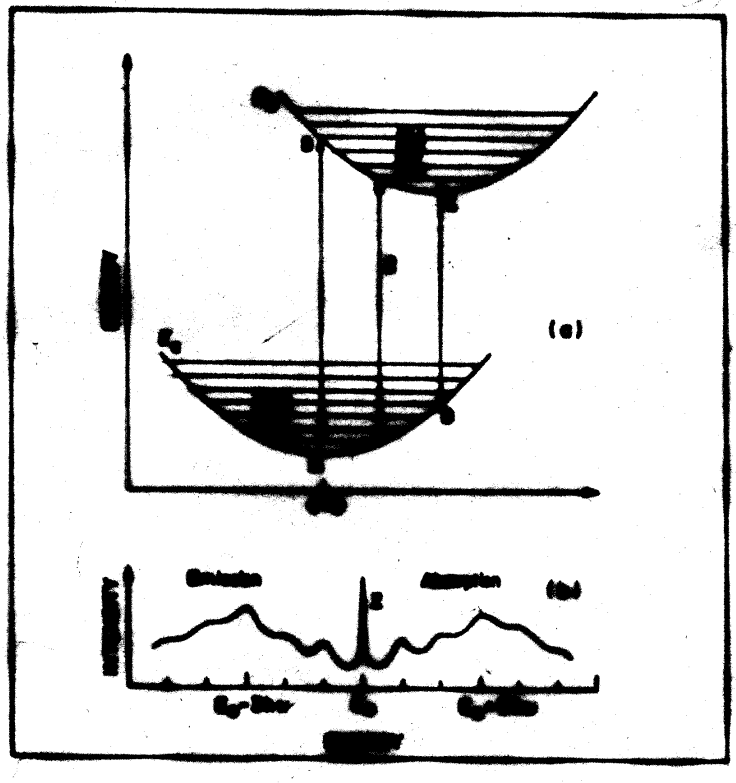

Fig. 2.9 (*a*) A configuration coordinate diagram showing the ground (E_a) and excited (E_b) electronic states with their vibrational sublevels. Z is the zero-phonon line; (*b*) The corresponding absorption and emission bands

energy in $h\nu/2$. The lowest level with m=0 would then represent the zero point energy of the system.

At T=0 K, only the vibronic (vibrational-electronic) state (m=0) is populated. In figure 4.1, the equilibrium position of the ground state occurs at A and if the center absorbs light, it is raised from the m=0 vibronic state in the groundstate to the n th vibronic excited state at B. The transition is a vertical one since it is assumed in the Franck-Condon principle that the electronic transition occurs in a time short compared with the time necessary for an ion to move appreaciably. After the center has reached the excited state, the ions of the system adjust until a new equilibrium is reached at C with energy level n=0. The energy difference between the states B & C is given off as lattice vibration. Having reached its new equilibrium position in excited state at C, the center may return to the ground state at D by the emission of a quantum of luminescent light. The center relaxes from D to A by again giving up energy to the lattice vibration. The photon energy of this 'luminescent light' is smaller than that of the absorbed photon because of the energy transferred to the lattice vibration. This stoke's shift generally depends on the extent of interaction of the center with its neighbouring/surrounding ions since this determines both the shape of the configuration co-ordinate center and their relative displacement along the co-ordinate axis.

The most probable (Franck-Condon) transition is the vertical one A→ B, with n = S, the defect can then relax to C by emission of S phonons, decay to D by emission of a photon of the luminescent light and relax back to A by emission of another S phonons. The normalized transition probability from m=0 to n th level of the excited state is given by,

$$W_{no} = S^n e^{-s}/n!$$

where, 'S' is the Huang-Rhys factor and is a measure of the electron-phonon coupling.

A very important transition occurs between the levels m=0 and n=0. This is a Zero Phonon Line (ZPL) shown as Z in figure 4.1, which is purely electronic transition. Since no phonons are involved, it is very sharp. In principle, its width is determined by the life time of the excited state, though, in practice, random strains in the crystal broadens it to values of 1 meV. Moreover, the way this transition splits under various perturbations gives valuable information about the symmetry of the defect. At high temperature or for large S, (i.e. strong electron-phonon coupling), the ZPL is weak compared to the phonon side bands. In fact, for S>6, it is usually thought to be unobservable.

The corresponding absorption band due to the phonon assisted transition occurs at higher energy than the ZPL whereas the emission band due to phonon emission occurs at lower energy. In the simple defect model, there should be mirror symmetry about the ZPL. If it is not there, non-linear electron-phonon coupling or a Jahn-Teller effect must be present [16]. This is the case for some defects in diamond.

The Huang-Rhys (H-R) factor indicates the fractional intensity of the ZPL, the magnitude of the Stoke's shift and the width of the phonon-side bands (all measured at T=0 K), i.e.

$$I_{ZPL} = I_{total} \exp(-S) \quad \text{.....} \quad \text{(I).}$$

$$E_{abs} - E_{emit} = 2Shw \quad \text{.....} \quad \text{(II).}$$

$$\Delta^2 = 5.6 (hw)^2 S \quad \text{.....} \quad \text{(III).}$$

In case of the neutral vacancy system, the values of S calculated by these equations do not match and hence it is the case of electronic degeneracy, a Jahn-Teller effect or a change in force constant [17].

The ability of a material to exhibit luminescence is associated with the presence of "activators". These activators may be impurity atoms occurring in relatively small concentrations in the host material, or a small stoichiometric excess of one of the constituents of the material. In the latter case one speaks of self activation. The presence of a certain type of impurity may also inhibit the luminescence of other centers, in which case the former are referred to as "killers" [18].

There are characteristic luminescence features associated with CVD diamond films, possibly related to various impurities introduced during deposition. There are several reports [19-22] on photoluminescence spectra excited by the same laser as that used to stimulate Raman scattering showing that almost all CVD diamond films exhibit a strong luminescence peak at ~1.68 eV. This line is very close to the GR1 line at 1.674 eV common in natural diamond attributed to neutral vacancies [23-25]. The relative intensities and even position of the PL lines can vary with the deposition conditions and the structural quality of the films.

The PL measurements in the present work were carried out by employing the same Raman spectrometer described in the previous section. The excitation was carried out by

the usual 514.5 nm laser line and the PL character was confirmed by additional excitation by 488 nm laser line.

2.4.3 Scanning Electron Microscopy (SEM) [26]:

The technological progress has been strongly influenced by the creation of new materials and further improvement of the existing material. It is important to know and understand the microstructure while developing and using a new material. The scanning electron microscope (SEM) is the most suited instrument for this purpose and is one of the powerful techniques for the study of thin film surface topography. It is very powerful instrument having very high magnification and resolving power and great depth of focus. In this technique, a very fine probe of electrons with energies upto 40 keV is focused at the surface of the specimen and scanned across it in a raster. The electrons are obtained by thermionic emission from a tungsten filament, accelerated by applying a voltage and focused into a fine beam through an arrangement of magnetic lenses. The impact of electrons with the surface causes a number of phenomena. As far as SEM is concerned , two phenomena are the most important , viz. emission of secondary electrons with energies of a few tens of eV and backscattering of electrons from the probe beam. The intensity of emission of the secondary as well as the backscattered electrons is highly sensitive to the angle of incidence between the probe beam and the surface , i.e. to the topography of the surface. The current which is supplied to the scanning system are made to pass through deflection coils of a cathode ray tube (CRT) to produce a similar but larger image of substrate surface on the viewing screen in a synchronous fashion. Generally, the image is recorded photographically.

The magnification produced by SEM is the ratio between the dimensions of the final image display and the field scanned on the specimen. Changes in magnification are achieved by altering the extent of scan on the specimen. Typically the magnification range is x20 to x100 000. The resolving power of an SEM is directly related with the probe diameter. Typically, the smallest attainable probe size is ~ 4 nm . However, the practical resolution in secondary and backscattered images is generally poorer than the probe diameter would suggest. This is because the electron beam penetrates and diffuses sideways in the specimen leading to secondary emission from a wider area than that actually illuminated by the probe.

A scanning electron micrograph is essentially a true reproduction of the surface features of the sample, Thus, it can be used to study the surface topography. In the case of CVD diamond, the SEM is generally used to assess the substrate surface coverage, nucleation density , grain size and crystal orientation. The square facets are associated with (100) planes whereas the triangular facets are associated with (111) planes. SEM is also used to study the film thickness by scanning the film along its cross-section.

The diamond films prepared in the present work were studied by the scanning electron microscope (SEM) Leica Stereoscan 440 Model manufactured by M/s Leica Cambridge Ltd. UK. The samples were mounted on the standard specimen mounting stubs by using conducting silver paste. The samples were coated with a thin layer of gold in Polaron coating unit E5000 to prevent the charging of the specimen. The samples were scanned in the vacuum ~ 10^{-6} torr. For comparative study the electron beam parameters were kept constant while analyzing all the samples. The micrographs of the samples with 20 keV EHT and 25 pA beam current were recorded by 35 mm camera attached on the high resolution recording unit.

The block diagram of the Scanning Electron Microscope used in the present study is shown in Fig. 2.10.

2.4.4 Energy Dispersive Analysis of X-Rays (EDAX)

Analysis of X-rays emitted from a sample can be accomplished by energy dispersive spectrometers which permit analysis by discriminating among X-ray energies. This method is called energy dispersive spectroscopy. The perfect qualitative analysis by this technique permits identification of all elements present in any selected region of the sample imaged on the microscope. The heart of this system is a Lithium drifted silicon Si(Li) diode whose active area is typically 10.5 mm^2 and whose thickness is 3 mm. If this diode is reverse - biased (by typically 1000 volts) a depletion region is established . All of the normally present electrons and holes in the depletion region are removed (by the externally applied electric field) . If an X-ray photon is absorbed within the depletion

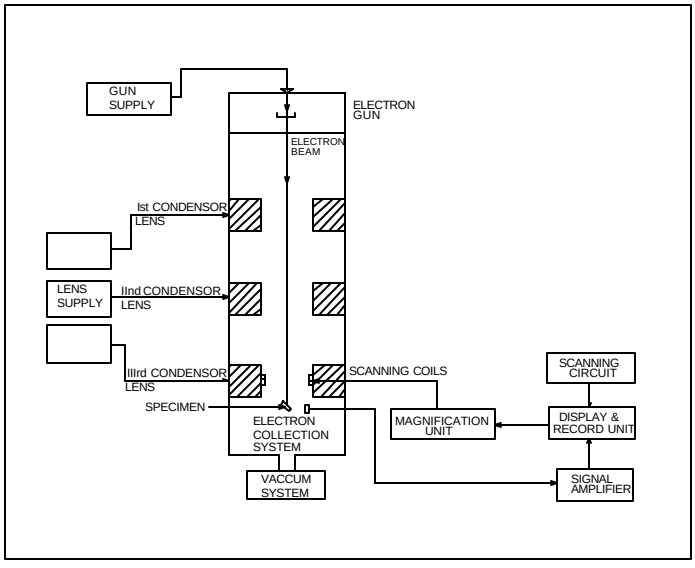

Fig. 2.10 Block Diagram and Photograph of the Scanning Electron Microscope

region, producing a number of electron-hole pairs, these charge carriers will be swept out by the electric field, and they will appear as a pulse of charge on opposite sides of the diode. This charge is converted into a voltage pulse, amplified and shaped, its amplitude is converted into a digital signal, and the resulting information is analyzed.

In the present study, the Scanning Electron Microscope (SEM) Leica Stereoscan-440 is incorporated with Energy Dispersive X- ray Spectrometer Model Phoenix purchased from M/S. EDAX Inc. , USA. We can obtain specimen images with elemental analysis of selected features and distribution of selected elements. It is a powerful analytical technique, which provides X- ray distribution images, line scans and point analysis of trace elements of micro volumes. The Si(Li) detector having 133 eV resolution measured at MnKα, 1000 CPS and time constant 100 μm, with super ultra thin window , which provides detection of light elements from Boron (At. No. 5) onwards all elements. SEM Quant ZAF software using ZAF matrix correction algorithms is used for qualitative and quantitative analysis..

2.4.5 X-Ray Diffraction Technique (XRD) [27]

X-Ray diffraction technique provides direct information on the crystal structure. The fundamental relation describing the diffraction of x-rays by crystalline material is given by the Bragg law,

$$2d\sin\theta = n\lambda$$

where d is the inter-planer spacing, θ is the diffraction angle , n is an integer and λ is the incident wavelength. The x-ray of specific wavelength would be diffracted at different angles depending upon the d values of various crystallographic planes having the Miller indices (hkl). An X-ray diffractometer usually consists of an X-ray source, a goniometer, a counter tube and counting electronics. Results are obtained in the form of chart of peak intensity vs. 2θ. This angle can then be converted to the d spacing between crystallographic planes using Bragg's law.

For CVD diamond films, XRD experiments can be used for both lattice parameter measurement and texture determination. X-ray diffraction patterns can be used to differentiate between the different phases of crystalline carbon. To obtain a pattern, characteristic of polycrystalline diamond, requires that the diamond film be sufficiently well crystallized. Due to the high symmetry of the diamond cubic crystal system, structure factor

calculations give very few allowable diffracting planes. The allowed diffracting planes are those for which (h+k+l) = 4n, where all the indices are even and n is any integer ; or else all indices are odd (alllowed diffraction planes {hkl} are: {111}, {220}, {311}, 400}, {331},etc). Furthermore, for randomly oriented diamond films, only one of these, the {111} diffraction line is relatively strong. In case of the growth of polycrystalline diamond films, XRD can be used to estimate the favored crystal orientation within the deposited film and to study the effects of various deposition parameters on the crystal orientation [28,29]. Since many of the diamond films are highly oriented, the relative intensities of these diffraction lines can be significantly distorted, and the diffraction pattern of an as-deposited film may not correlate with a randomly oriented reference pattern. For this reason, information on the growth texture in the films can be deduced from the diffraction patterns. The width of the diffraction lines depend upon the crystallite size and the size can be calculated using Scherrer's formula,

$$L = \frac{K\lambda}{B\cos\theta}$$

where, L is the average crystallite size; B is the broadening of the line expressed in units of 2θ; K is a constant ~ 1 and θ and λ have their usual meaning.

In the present study, "PHILIPS PW1830" rotating target type diffractometer with 2θ range from 0 to 120^0 was used. The monochromatic X-rays correspond to the CuKα line with wavelength 1.5418 Å, derived from a copper target bombarded with electrons. In this work , the accelerating voltage of 30 kV and the filament current 30 mA were used for recording the intensity vs. 2θ diffraction patterns. The patterns were recorded in the range 20^0 to 110^0. The analysis of XRD patterns was carried out by calculating lattice parameters using the Bragg diffraction condition.

2.5 Conclusion

In conclusion, the HFCVD system for synthesis of undoped and impurity doped diamond film was designed and fabricated. The M shaped filament is particularly found suitable as it yielded uniform large area coatings. A Π (pi) shaped filament holder was developed so that it eliminated various problems associated with the filament breakage. The substrate holder was

designed so as to obtain the required substrate temperature. This system then allowed deposition of uniform diamond films.

References

1. N. B. Colthup, L. H. Daley, and S. E. Wiberley, Introduction to Infrared and Raman Spectroscopy, Academic Press, NY (1975)
2. D. A. Long : in Raman Spectroscopy (McGraw-Hill International Book Company, 1977)

   S. T. Kshirsagar, Physics Education 4(3) (1987) 139
3. R. A. Cowley, The Theory of Raman Scattreing from Crystals, in 'The Raman Effect' Vol. I, Ed. A. Anderson, p96
4. G. Dolling and R. A. Cowley, Proc. Phys. Soc. (London) 88 (1966) 463

   K. S. Krishnan, Proc. Indian Acad. Sci. 24 (1946) 45
5. R. Shuker and R. Gammon, Phys. Rev. Lett. 25 (1970) 222
6. R. J. Nemanich, J. T. Glass, G. Lucovsky and R. E. Shroder, J. Vac. Sci. Technol. A6 (1988) 1783
7. D. S. Knight and W. B. White, J. Mater. Res. 4 (1989) 385.
8. S. A. Solin and A. K. Ramdas, Phys. Rev. B 1 (1970)1687.
9. L. G. Berry and R. M. Thompson, Geol. Soc. Amer. Mem. 85 (1962) 23.
10. F. Tuinstra and J. L. Koenig, J. Chem. Phys. 53 (1970)1126.
11. R. J. Nemarich and S. A. Solin, Phys. Rev. B 20 (1979)392.
12. N. Wada and S. A. Solin, Physica 105B (!981)353.
13. N. Wada, P. J. Solin and S. A. Solin, J. Non-cryst. Solids 35 (1980)543.
14. J. Robertson, Adv. Phys. 35 (1986) 318.
15. A. M. Stoneham, "Theory of Defects in Solids" (1975) (Oxford: Clarendon)
16. J. Walker, Rep. Prog. Phys. 42 (1979) 1605
17. R. Englman, "The Jahn-Teller Effect in Molecules and Crystals" (1971) (London: Wiley Interscience)

    M. D. Sturge, Solid State Physics 20 (1967) 91
18. A. J. Dekkar, in : Solid State Physics (Macmillan & Co. Ltd., 1962) p398.

19. D. S. Knight and W. B. White, Proceedings of SPIE on Raman Scattering, Luminescence and Spectroscopic Instrumentation in Technology 1055 (1989) 144.
20. T. Feng and B. D. Schwartz, J. Appl. Phys. 73 (1993) 1415.
21. L. Bergman, B. R. Stoner, K. F. Turner, J. T. Glass and R. J. Nemarich, J. Appl. Phys. 73 (1993) 3951.
22. L. Bergman and R. J. Nemarich, J. Appl. Phys. 78 (1995) 6709.
23. J. Walker, Rep. Prog. Phys. 42 (1979) 1605.
24. C. D. Clark, in : Physical Properties of Diamond, (R. Berman, ed.),Clarendon Press, Oxford (1965) 295.
25. C. D. Clark, E. W. J. Mitchell and B. J. Parsons, in : The Properties of Diamond, (J. E. Field, ed.) Academic Press, London (1979) 23.
26. J. I. Goldstein and H. Yakowitz, in: Practical Scanning Electron Microscopy (Plenum Press, New York, 1975).
27. B. D. Cullity, "Elements of X-ray diffraction" (Addison-Wesley Publishing Company Inc, Masachusetts, USA)
28. K. Kobashi, K. Nishimura, Y. Kawate, T. Horiuchi, Phys. Rev. B 38 (1988) 4067.
29. P. Ascarelli, E. Capelli, G. Mattei, F. Pinzari, V. Fares, C. Veroli, S. Martelii, Diam. Relat. Mater. 5 (1996) 308.

CHAPTER 3

SYNTHESIS OF DIAMOND FILMS UNDER DIFFERENT DEPOSITION CONDITIONS AND SUBSTRATE PRETREATMENTS

The first part of this chapter is devoted to the optimization of the deposition parameters for obtaining the good quality films in the system under use. In the second part, buffer layers of In-Sn-O (ITO) are employed to understand the diamond growth on scratched and unscratched silicon substrates. The possible role of ITO interlayer in the nucleation and growth of diamond films is discussed in details. The dependence of growth rate of diamond films on the thickness of the ITO interlayer is also described briefly.

3.1 Introduction

As discussed in the last chapter, the low-pressure chemical vapour deposition technique appears to be the most convenient and simplest possible technique for the production of diamond films. Majority of the properties of these CVD diamond films have been observed to depend on the microstructure of these films which is, in general, determined by the processes involved in initial phases of nucleation, growth and coalescence of grains. These processes strongly depend on the choice of deposition conditions[1-11]. Moreover, the *insitu* incorporation of impurities in diamond films is a complex process and strongly depends on the deposition conditions used [12]. In order to resolve the effects of impurities on the properties of diamond films, which is aim of this work, it is necessary to know the quality of the pure (undoped) diamond film as a function of deposition conditions for a given particular system configuration.

All the applications of the diamond films require least non-diamond carbon content and strongly interconnected crystallites while some specific applications like optical, infrared and X-ray transparent windows require, additionally, higher nucleation densities [13]. Therefore, in general, the quality of the film should be measured in terms of the non-diamond content of the film, nucleation density and the average crystallite size. The investigation of these parameters as a function of deposition condition then becomes necessary.

The CVD diamond deposition by most of the methods involves a carbon source gas (generally a hydrocarbon), diluted in hydrogen gas and the atomic hydrogen (H^0) produced in the reactor enhances the nucleation and growth. Therefore, the major deposition conditions would be the chamber pressure, hydrocarbon to H_2 ratio and total flow of the gases through the chamber. The chamber pressure strongly controls the mean free path of the source molecules reaching to the substrate surface which is supposed to play a critical role in vapor-phase deposition affecting the growth rate and quality of the film. Lee et al. [14] have grown the diamond films with reaction pressures varying between 50-800 torr and have shown that the films grow free from non-diamond content when the reaction pressure was low (< 100 torr). Kim et al. [15], on the other hand, observed that when the pressure was decreased below 30 torr, the non-diamond component was found to significantly increase. These results suggest that

there is a certain range of pressure values where the non-diamond content in the film can be minimum.

In addition to optimization of the chamber pressure, which may minimize the non-diamond content, the selective etching of the non-diamond phase present, if any, may be achieved by diluting the hydrocarbon in hydrogen (i.e. adjusting the ratio of hydrocarbon to hydrogen). The excitation source, e.g. hot filament in the present study, can decompose the molecular hydrogen into atomic hydrogen (H^0) which can react with non-diamond carbon preferentially at the prevailing temperature[15]. Additionally, the presence of atomic hydrogen helps in stabilizing the sp^3 bonded carbon leading to the nucleation sites for growth of diamond crystallites. Although the atomic hydrogen has been shown to play an important role in diamond growth, it can also have an adverse effect in suppressing diamond nucleation because the nucleation sites can also be etched out by the atomic hydrogen when it is smaller in size than a required critical size[16]. Therefore, to obtain good quality diamond film, the ratio of hydrocarbon to atomic hydrogen should be optimum.

The flow rate of the gas mixture further affects the transport of the reactive species, produced by the excitation source, towards the substrate. For lower flow rate, the steady state diffusion controlled flow would dominate the transport while for higher flow rate, the transport would be dominated by the forced flow [17]. However, higher flows also reduce the residence time of reactive species as well as of H^0 near the substrate surface. Hence, forced flow, though can increase the deposition rate, may also act adversely if it is increased beyond certain critical value where the reactive species will be driven away without deposition on the substrate [18]. Hence, it is also necessary to optimize this parameter.

Other deposition parameters that can influence the quality of the film are substrate temperature (T_s), substrate surface texture etc. Substrate temperature provides the required energy to the species condensing on the surface of the substrate to diffuse to a stable position to form the nuclei and growth of the crystal. Hence higher the substrate temperature, better the quality of the films. However, it should be noted that Debye temperature (Θ_D) of diamond is ~ 1590^0C [19] above which heat capacity becomes independent of temperature. Hence, as T_s approaches Θ_D, the sp^3 bonded carbon material would start softening and this

would set conversion of sp^3 bonded carbon to sp^2 bonded carbon. An optimum T_s is therefore expected. This optimum T_s value may also depend on other deposition parameters.

The range of growth parameters can, however, depend on the deposition technique and the system configuration used. Therefore it would be necessary to perform deposition experiments to discover the best possible set of deposition conditions to achieve the best quality film in the system under use.

In addition to the above deposition parameters, the texture of substrate surface is found to have strong influence on the nucleation density (ND) [20-22]. The diamond nucleation on perfect surfaces, e.g. mirror polished Si wafers, is known to be extremely sluggish ($ND < 10^4$ cm^{-2}) [23] whereas the imperfect surfaces obtained by scratching with diamond or other similar hard particles produces high nucleation density ($>10^7$ cm^{-2}) [24,25]. But, the scratching with diamond powder produces spectacular effects particularly for Si substrates[20-22,26]. High ND's are useful for specific applications, e.g., optical, infrared and X-ray transparent windows, and for production of highly oriented films at low substrate temperatures [27,28]. However, the scratching process can be detrimental to the fabrication of diamond thin film devices on silicon substrates which are processed for electronic device packaging. Moreover, the role of scratching is still debated heavily [29,30]. It is not yet clear whether these scratches act as traps for the abrasive particles which essentially provide the nucleation sites [24,25], or they provide sharp geometric features such as edges and apexes which can nucleate diamond by themselves [31,32].

More recently, the use of metal oxide buffer layers has been suggested as a nondestructive alternative to scratching for obtaining better NDs and improved quality diamond films on silicon [33]. The oxygen released by the oxide layer was expected to suppress the sp^2-bonded graphitic nucleation and allow faster supersaturation of the buffer layer with the metal carbide that may act as nucleation site. However, this restricts the selection of the buffer layer to oxides of carbide forming metals only. The nucleation enhancement using other metal oxide layers, e.g., carbide nonformers, is not yet attempted.

Therefore, in the present chapter, the first part is devoted to the optimization of important process parameters for obtaining good quality films in the HFCVD reactor. A range of diamond films free from any (intentionally incorporated) impurities was therefore prepared

by varying the various deposition parameters over a wide range of their magnitudes. The data collected by subjecting these films to various characterization techniques are then presented as a function of deposition conditions and analyzed for crystallizing out the optimum deposition conditions.

In the second part, we have used Indium tin oxide (In-Sn-O / ITO) buffer layers to understand the diamond growth on unscratched and scratched silicon substrates. The ITO coating is expected to work in two ways : first it would cover the scratches and surface defects and as well bury the nucleation sites generated by the scratching process; secondly, the elements In and Sn are not well-known for carbide formation, though their carbides may exist in amorphous state [34,35]. Thus, the ITO layer was expected to retard the nucleation. In contrast, in the present work, high NDs have been observed on ITO-coated Si substrates independent of the pretreatment applied to them. The effect of ITO buffer layer on the ND and growth of the diamond film grown on Si substrate scratched with other hard particles such as ceramic powder is also presented.

3.2 OPTIMIZATION OF THE DEPOSITION PARAMETERS

3.2.1 Experimental

The HFCVD set-up (described in details in chapter 2) was used to deposit the diamond films. Optically polished single crystal p-type Si<100> (340 μm in thickness and resistivity of 1-10 Ω cm^{-1}) wafers were used as the substrate. The Si substrates were subjected to a light abrasion with 1/2 μm size diamond powder and subsequently degreased in acetone and rinsed in 40% HF acid solution prior to their loading in the deposition chamber. For the deposition of the films, a mixture of the semiconductor grade gases CH_4 and H_2 was used. The ranges of different deposition parameters used are listed in Table 3.1

TABLE 3.1 : HFCVD Deposition Parameters

Deposition Parameter	Range of Variation
CH_4 percentage in H_2	1.0 - 3.0 %
Gas mixture Flow Rate	200 - 500 SCCM
Deposition Pressure	5 - 40 torr
Filament Temperature	850 ± 20°C
Substrate Temperature	1950± 50°C
Filament-substrate distance	10 mm
Deposition Period	180 min.

The film composition in terms of the proportions of sp^3 bonded carbon relative to that of the sp^2 bonded carbon was characterized with the help of Raman scattering. The Scanning Electron Microscopy (SEM) was used to study the surface morphological changes as a function of various deposition conditions.

3.2.2 Results and Discussion

3.2.2(A) Effect of Chamber Pressure

To study the effect of the chamber pressure on the growth behavior, it was varied from 5 to 40 torr and the other deposition parameters were maintained constant, i.e. (a) 2% methane concentration (b) Total flow rate = 300 SCCM (c) T_f = 1950±50°C (d) T_s = 850±20°C and (e) the deposition time period of 180 min.

The SEM photographs shown in Fig.3.1(a-d) reveal the surface morphology of the diamond films grown for the gas pressure of 40 torr, 30 torr, 20 torr and 5 torr respectively. The surface morphology of these films appears to have common features which indicate that the surface is made up of closely packed large triangular pyramidal and cubooctahedral shaped diamond particles with well developed {111} facets. Most of these particles are not single crystals but have twin structure[36]. Another observation from the surface morphology is that the particle size and the nucleation

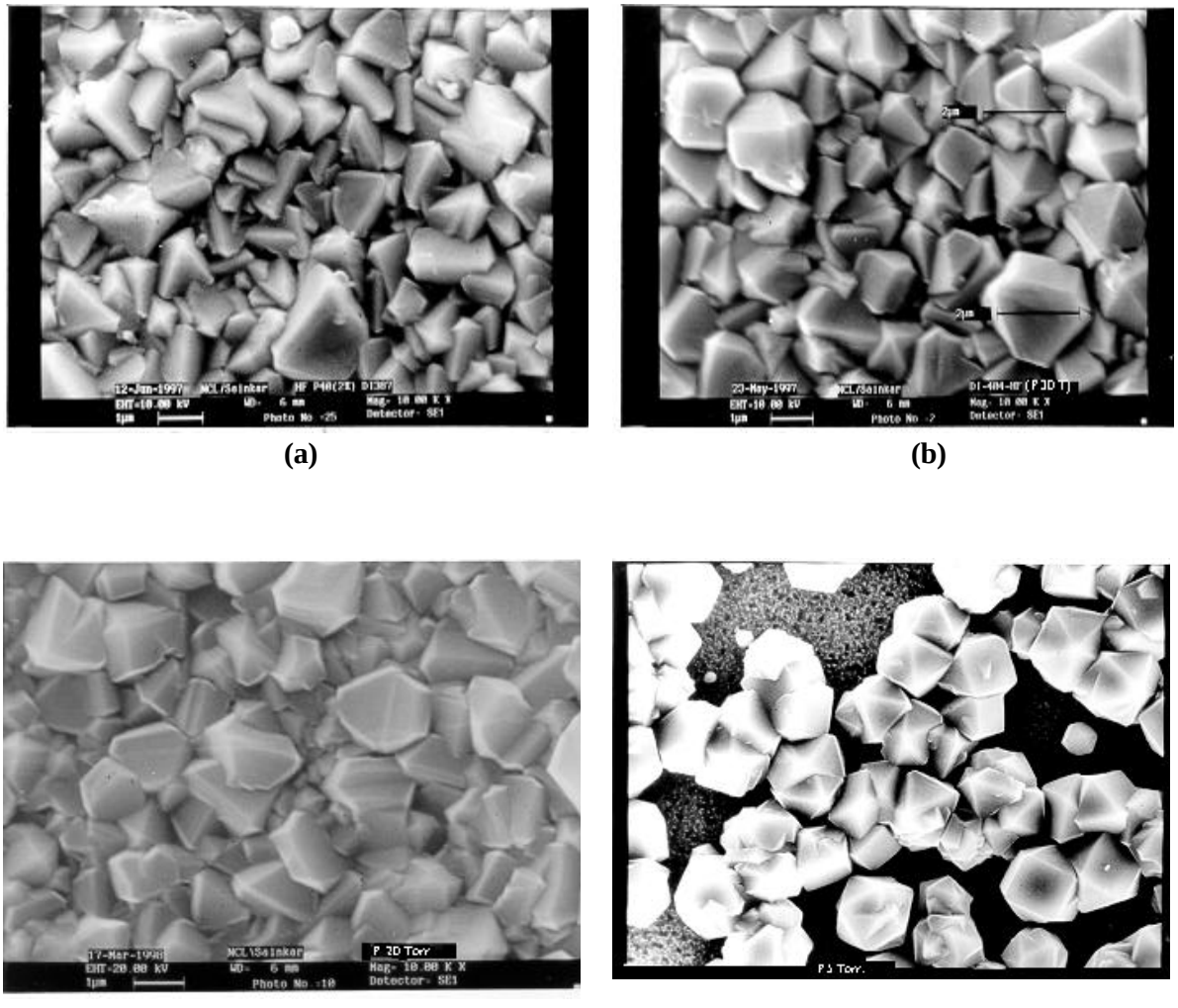

(a) **(b)**

(c) **(d)**

Fig. 3.1 SEM Photographs of the surface morphology of the diamond films deposited at the chamber pressure of (a) 40 Torr (b) 30 Torr (c) 20 Torr and (d) 5 Torr.

density is very sensitive to the chamber pressure used for deposition. The nucleation density was measured at several different sites of the sample and averaged nucleation density is presented in the following.

The nucleation density (ND) for the film grown at 40 torr (Fig. 3.1 a) is nearly 2.0×10^8 / cm ^{2} and the average particle size is found to be ~ 1.00 μm. When the pressure is decreased to 30 torr, the separation between the particles is found to increase and the ND decreases to ~ 1.6×10^8 / cm^2. The average particle size in this case increases to 1.5 μm (Fig. 3.1 b). As the pressure is further decreased to 20 torr (Fig. 3.1 c), the separation between the

particles goes on increasing. The ND in this case decreases to 1.2×10^8 / cm^2 and the average particle size increases to 1.75 μm. For the film grown at 5 torr, the surface is made up of only cubooctahedral shaped crystals (Fig. 3.1 d). From the surface morphology, it is very clear that the particles are well separated from each other. The nucleation density further decreases to 6.5×10^7/ cm^2 and the average particle size in this case is 2.0 μm. In order to optimize both, the nucleation density and the average particle size, the representative growth rate may be obtained by taking the product of the nucleation density and the average particle size. The growth rate, thus calculated, is observed to be optimum at the chamber pressure of 30 Torr (as shown in Fig. 3.2).

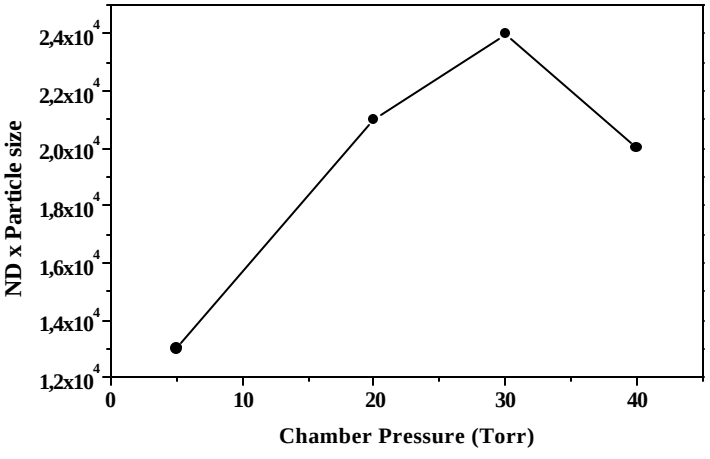

Fig. 3.2 Variation of (ND x Particle size) vs. Chamber Pressure

The Raman spectra of these films are shown in Fig. 3.3. Each spectrum shows the sharp peak at 1332 cm^{-1} which indicates the presence of diamond crystals [23,24]. The broad peak occurring at the 1550 cm^{-1} which arises from a non-diamond phase such as amorphous carbon or sp^2 bonded carbon [24] is also observed in each case with varying intensities. The intensity ratio of the non-diamond components to the diamond components is higher at low reaction pressures than at high pressures. The Raman spectrum of the film grown at 30 torr shows the intensity ratio of 1550 cm^{-1} band to 1332 cm^{-1} band (I_G/I_D) to be minimum (as shown in Fig. 3.4) which implies the minimum amount of non-diamond carbon present in this film.

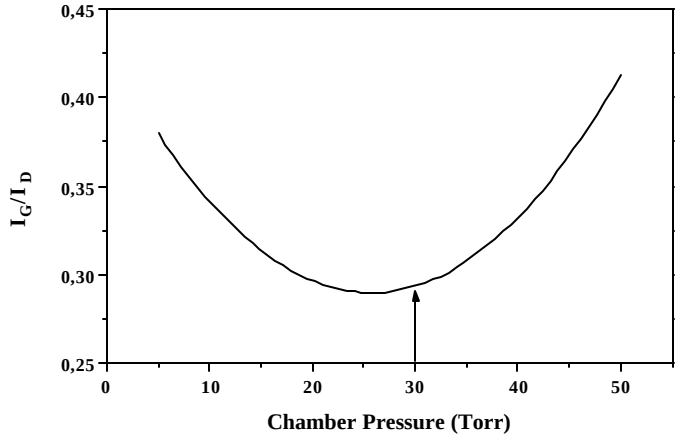

Fig. 3.4 Variation of (I_G/I_D) vs. Chamber Pressure

These observations can be attributed to the change in mean free path of the depositing species due to the change in deposition pressure. At the higher deposition pressure, the mean free path of the dissociated hydrogen atom is decreased so that the number of hydrogen atoms available for removal of carbon from the substrate surface is also reduced. As a result, the surface is quickly covered with the carbon containing species and hence nucleation density and the amount of non-diamond carbon contents in the film increases with increasing pressure. On the other hand, at the lower pressure the concentration of atomic hydrogen at the substrate surface is high as the increased mean free path reduces the chance of recombination. As a result, the nucleation is retarded and the nucleation density decreases. But, since the non-diamond carbon is removed effectively, the better quality diamond film is obtained. If the pressure is decreased beyond 30 Torr, the mean free path increases further so that there is very less probability that atomic hydrogen will reach the substrate surface. Also the flux of carbonaceous species reaching the substrate decreases. This results in the increase in non-diamond content of the film and further decrease in the nucleation density. It may however be noted that the scattering cross section of sp^2 bonded carbon is ~ 50 times greater than that of

sp^3 bonded carbon [37,38], and hence, the amount of non-diamond carbon present in all these samples is negligibly small.

Kim et al. [15] have earlier reported the effect of chamber pressure on the growth of diamond films grown on unpretreated Si <100> substrates in an HFCVD reactor. However, in that case it was claimed that more nucleation density was observed at the lower pressure (5 torr) and better quality at higher pressure (30 torr). The observation was explained in terms of the rate of SiC formation on the substrate surface. Our results are in accordance with the later observation i.e. better quality growth at comparatively higher pressure. But, at lower pressure, our results indicate exactly opposite effect. One possible reason for this discrepancy could be that, in our work, diamond-abraded substrates were used for deposition so that the role of SiC formation in diamond nucleation was of secondary importance.

Our results agree with a number of other reports [11,39,40] on the effects of the reaction pressure during HFCVD of diamond.

3.2.2(B) Effect of Hydrocarbon (CH_4)/Hydrogen Ratio

In order to optimize the methane/hydrogen ratio, methane concentration was varied from 1.0 % to 3.0 % maintaining the total gas flow and other common deposition parameters as uniform as possible for all the experiments e.g. (a) 300 SCCM of total gas flow (b) $T_f = 1950 \pm 30^oC$ (c) $T_s = 850 \pm 20^oC$ (d) deposition pressure = 30 Torr (e) the deposition time period of 180 min. These experimental conditions have generated a set of diamond films such that the changes occurring in the film composition, quality and morphology could be reliably correlated to the methane concentration alone.

Fig. 3.5 shows the Raman spectra of the diamond films grown with the source (methane) concentration from 1.0% to 3.0%. The Raman spectrum of the film with 1.0% CH_4 concentration shows a sharp peak at 1332 cm^{-1}. This 1332 cm^{-1} band indicates presence of the diamond crystals [23,24]. This spectrum also shows a very broad band centered around 1550 cm^{-1} which corresponds to a non-diamond phase of carbon[24]. The spectrum with 1.5 % CH_4 concentration also shows a sharp peak at 1332 cm^{-1} with a broad band centered at 1550 cm^{-1}. The relative strength of these bands clearly indicates that when the methane concentration is above 2%, the graphitic content in the film becomes significant (as shown in Fig. 3.6). Raman

spectrum of the film grown with 3.0 % CH_4 concentration has larger strength of 1550 cm-1 band indicating the significant

Chapter 3
Synthesis of Diamond Films Under.....

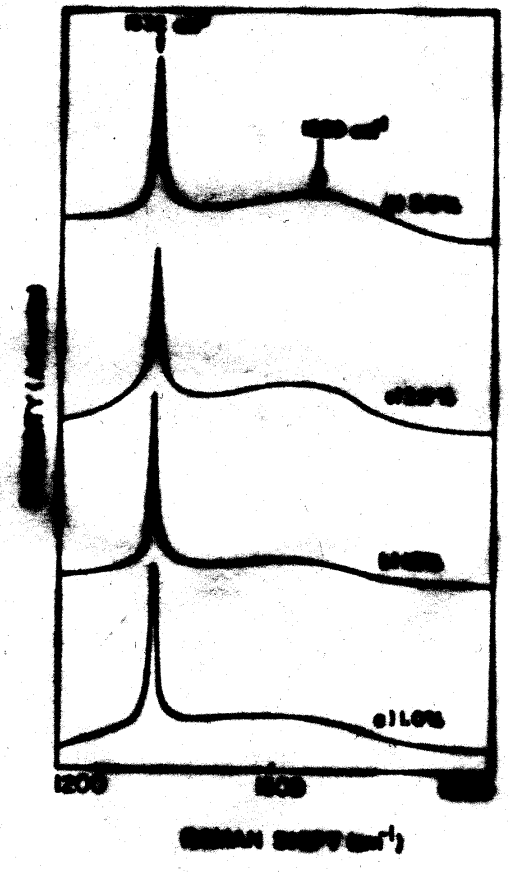

Fig. 3.5 Raman spectra (normalized for 1332 cm^{-1} band) of the diamond films grown with different relative concentrations of CH_4 with respect to H_2 (*a*) 1%, (*b*) 1.5%, (*c*) 2%, and (*d*) 3%

amount non-diamond content in the film. Mercier et al. [41] and Kweon et al.[42] have also reported the similar observations.

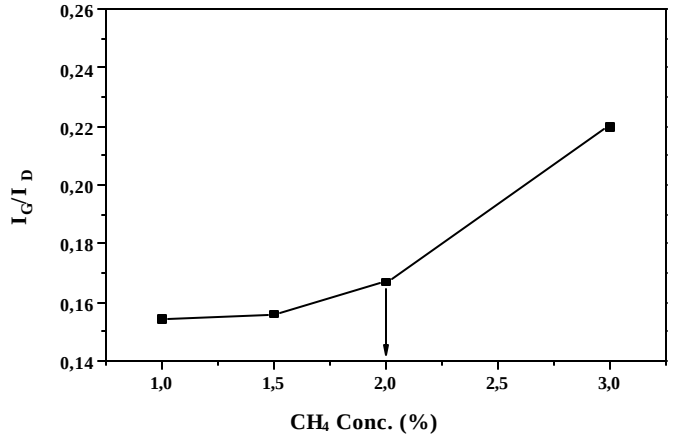

Fig. 3.6 Variattion of (I_G/I_D) vs. CH_4 Conc.

The corresponding SEM photographs of the surface morphology of these samples are shown in Fig. 3.7 (a-d). The crystallite size is seen to increases from ~ 0.5μm for 1.0 % CH_4 conc. to ~1.5μm for 2 % CH_4 conc. and then it decreases to ~ 1.0μm when the CH_4 conc. increases to 3 %. Thus, it appears that the best grain size observed is 1.5μm at 2 % CH_4 conc. The growth rate (in terms of the product of nucleation density and average grain size) is also observed to increase till 2 % CH_4 conc. and for further increase, it is observed to decrease. This decrease in the growth rate for the CH_4 conc. beyond 2% is not clearly understood. The possible reason may be that the additional carbon is deposited in the form of sp^2 bonded amorphous carbon which is not seen in the SEM photograph.. Similar observations are also reported by Matsumoto et. al [43] and Zhu et al [44].

The increase in the growth rate with the methane concentration may be due to the increase in ionized radicals available for the growth of diamond. Also as the number of carbon containing species increases in the total gas flow, relative concentration of hydrogen atoms available for removal of carbon from the substrate surface is also reduced. The surface is quickly covered with carbonaceous deposition resulting in the faster nucleation. Therefore the growth rate is high. If the concentration is increased beyond the

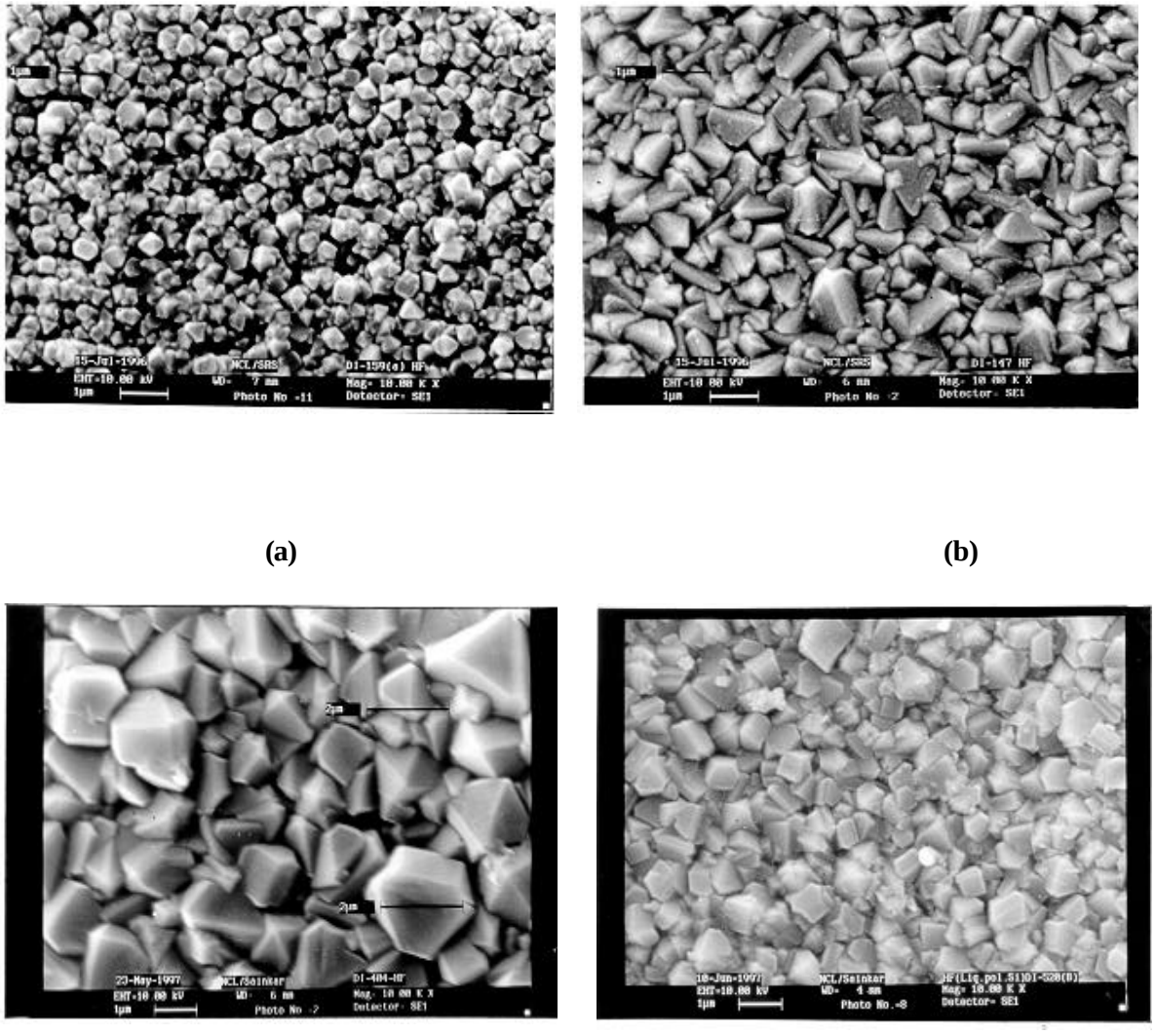

(a) **(b)**

(c) **(d)**

Fig. 3.7 SEM photographs of the surface morphology of the diamond films grown with (a) 1.0% (b) 1.5% (c) 2.0% and (d) 3.0% CH4 concentrations

critical value, again the growth rate decreases which is probably due to the dominance of non-diamond (graphitic / amorphous) carbon with a lower growth rate, because of the conditions of the reversible reactions. At the lower conc. of CH_4, as the non-diamond carbon is removed effectively, the quality of the deposit is improved [39,45].

Our results are in accordance with a number of other reports [14,46,47] on the effect of the methane concentration in HFCVD of diamond thin films.

3.2.2(c) Effect of the Flow Rate

To study the effect of the flow rate, it was varied from 200 SCCM to 500 SCCM maintaining the other deposition parameters constant for all the experiments, viz. (a) 2% methane concentration (b) $T_f = 1950 \pm 50^oC$ (c) $T_s = 850 \pm 20^oC$ (d) deposition pressure = 30 Torr and (e) the deposition time of 180 min. These experimental conditions have generated a set of diamond films such that the changes occurring in the film composition, quality and the morphology could be reliably correlated to the flow rate alone.

Fig. 3.8 shows the Raman spectra of the diamond films grown for different gas flow rates varying from 200 SCCM to 500 SCCM. Raman spectrum of the film with 200 SCCM (196 SCCM H_2 + 4 SCCM CH_4) flow rate shows a sharp peak at 1332 cm^{-1}. This spectrum also shows a broad band in the range 1500-1600 cm^{-1} centered at 1550 cm^{-1} indicating the non-diamond graphitic phase of carbon. In case of the film with the flow rate 300 SCCM (294 SCCM H_2 + 6 SCCM CH_4), the Raman spectrum shows a sharp diamond peak at 1332 cm^{-1} with minimum intensity of the broad band at around 1500-1600 cm^{-1}, i.e. the non-diamond graphitic carbon is negligible. When the flow rate is increased beyond 300 SCCM, for e.g. 400 SCCM (392 SCCM H_2 + 8 SCCM CH_4), the spectrum clearly indicates that the non-diamond graphitic phase of carbon in the film is increased (as shown in Fig. 3.9).

The SEM photographs of the surface morphology of these films are shown in Fig. 3.10 (a-d). It shows that the lower gas flow rate has led to a better quality films whereas the higher flow rate leads to a dense deposition (higher nucleation density). These observations can be attributed to the change in the velocity of the gas molecules which results in the change in the mass transport of the reactive radicals of hydrocarbon and the atomic hydrogen [40]. The reduction in the gas flow rate means a reduction of the gas incoming velocity and an increase in the gas residence time within the deposition chamber[48] and therefore it results into a better quality deposition. On the other hand, a higher flow rate would result into a smaller residence time and therefore a faster

deposition of inferior quality diamond. Higher residence time allows the carbon species to react with atomic hydrogen forming gaseous species and resulting in low deposition rate which, in turn, improves the quality of the diamond crystallites. For lower residence time,

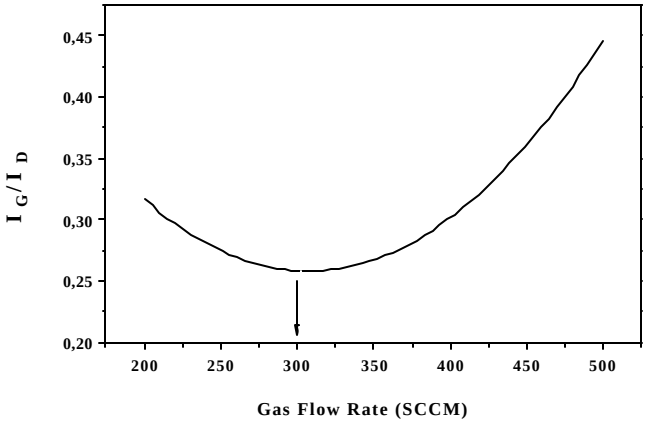

Fig. 3.9 Variation of (I_G/I_D) vs. gas flow rate

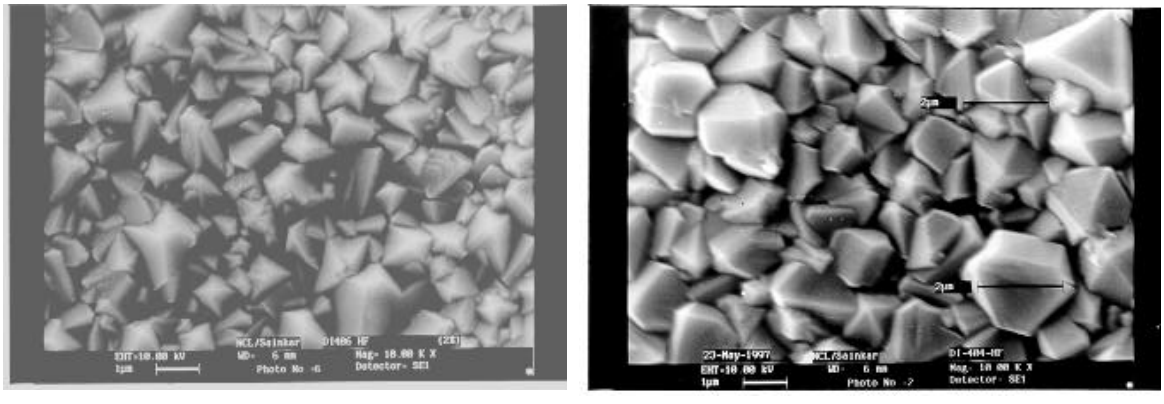

(a) **(b)**

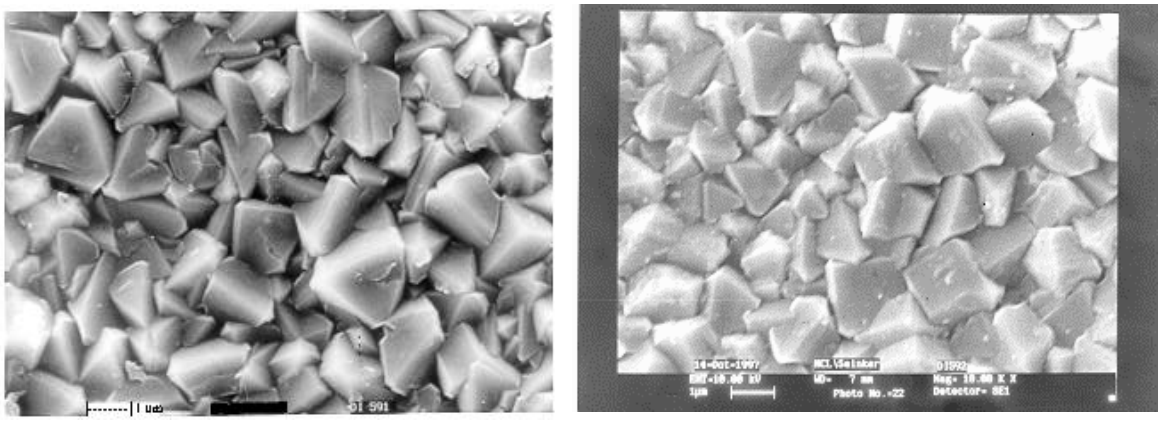

(c) **(d)**

Fig. 3.10 SEM photographs of the surface morphology of the diamond films grown as a function of total gas flow rate-
(a) 200 SCCM (b) 300 SCCM (c) 400 SCCM and (d) 500 SCCM

the removal of the hydrocarbon species from the gas phase is reduced and thereby their rate of deposition on substrate increases. This leads to low quality diamond crystallites. In our system, the flow rate of 300 SCCM appears to be optimum.

Thus, during diamond CVD, there are two competing phenomena, viz. deposition of the carbonaceous species and etching of the non-diamond carbon species by atomic hydrogen. When the flow is such that both these processes are balanced, the better quality film is obtained. The quality and the nucleation density is found to be optimum when the flow rate was 300 SCCM (294 SCCM H_2 + 6 SCCM CH_4) in the present system.

3.2.3 Conclusion

In conlusion, by using the M-shaped filament, we have optimized the deposition parameters for obtaining best quality diamond films using HF-CVD system.. Among the various deposition parameters, (A) gas pressure in the chamber (B) gas flow in the chamber and (C) the realative concentration of the hydrocarbon gas with respect to the hydrogen gas were optimized. Our system has shown that the best quality diamond films can be grown on Si substrate by employing gas pressure of 30 Torr, gas flow rate of 300 SCCM and hydrocarbon gas concentration of 2% in hydrogen. The quality of the film was assessed in terms of the crystallite size, nucleation density and lowest possible sp^2 bonded carbon. These parameter

values are therefore employed for studying the effect of other factors such as substrate temperature and incorporation of impurities on the growth and properties of diamond films.

3.3 ENHANCEMENT OF NUCLEATION AND GROWTH OF DIAMOND FILMS USING DIFFERENT SUBSTRATE PRETREATMENTS

3.3.1 Experimental

In the present study, the silicon substrates cut from a optically polished single crystal wafer (3 inch in diameter and 340 μm in thickness with p-type resistivity 1-10 Ω cm) were pretreated in different ways and classified as follows :

(A) first type were as-received mirror-polished wafers degreased in acetone and bathed in 40% HF; (B) second type were the substrates lightly abraded by hand for ~ 10 min. using 0.5 μm size diamond grit and subsequently degreased and bathed in HF; (C) the third type were selected from the first and second types but additionally subjected to heat treatment in air at ~ 950^{o}C for ~ 3 hrs to burn off the diamond particles trapped on the substrate surface during the scratching process and subsequently bathed in HF; and (D) the fourth type were selected from all the above three types but were additionally coated with ITO (Indium-Tin-Oxide) layer of different thickness in a pre-optimized rf-sputter deposition system (described in details in chapter 2) using a target having composition In_2O_3 : 9 M% SnO_2 . The ITO films so deposited were transparent and had the resistance of ~ 1-10 Ω. The HFCVD system was used for depositing the diamond films on all the substrates pretreated as above. The deposition parameters used are listed in Table 3.2.

TABLE 3.2 : HFCVD deposition Parameters.

Deposition Parameter	Value
CH_4 percentage in H2	2 %
Gas mixture Flow Rate	300 SCCM
Deposition Pressure	30 Torr
Filament Temperature	850 ± 20°C
Substrate Temperature	1950± 50°C
Filament-substrate distance	10 mm
Deposition Period	180 min.

3.3.2 Results and Discussion

In figure 3.11(a-b), SEM photographs of the surface morphology of the diamond films deposited on as-received mirror polished Si substrates pretreated as described in (C) and (D) above are shown. The as-received mirror polished + heat-treated (type C) shows (figure 3.11 a) ND ~ 10^5 cm^{-2} whereas the heat-treated + ITO coated substrate (type D) shows ND ~ 5 x 10^7 cm^{-2} (figure 3.11 b). The latter thus shows the ITO induced enhancement of ND by a factor of ~ 500. The ND for as-received mirro-polished Si (type A) was observed to be ~ 1.1 x 10^6 cm^{-2}. The lowest nucleation density on the mirror polished + heat-treated (type C) substrate may be attributed to a reduction in the number of nucleation sites due to heat treatment. We believe that the as-received Si substrate (type A) may also have fine diamond particles trapped on its surface during the polishing process, which may act as nucleation sites. However, on heating these substrates in air, the trapped diamond particles burn off and in turn reduce the nucleation density.

In figure 3.11(c-d), the SEM photographs of the surface morphology of the diamond films deposited on the scratched Si substrates (type B) pretreated as described in (C) and (D) are shown. The ND ~ 4.5 x 10^4 cm^{-2} was observed for scratched + heat-treated Si substrate (type C) as seen in figure 3.11(c) whereas scratched + heat-treated + ITO-coated Si substrate (type D) shows again increase in ND ~ 8.2 x 10^7 cm^{-2} (figure 3.11 d). The

nucleation density for the simply scratched substrate (type B) is ~ 5 x 10^7 cm^{-2} (figure 3.11 e). When the scratched substrate was additionally coated with ITO buffer layer (type D), the nucleation density is found be enhanced to ~ 2 x 10^8 cm^{-2} as shown in figure 3.11 f.

We heat treated in air at 900^0C for 3 hrs a readymade 2 μm thick diamond film deposited on scratched Si substrate. The SEM examination of this substrate did not show presence of any diamond particles. Moreover, redeposition experiments on these heat treated substrates, exhibited extremely sluggish nucleation. These results suggest that the scratches play mainly the role of traps for fine diamond particles, which serve as nucleation sites.

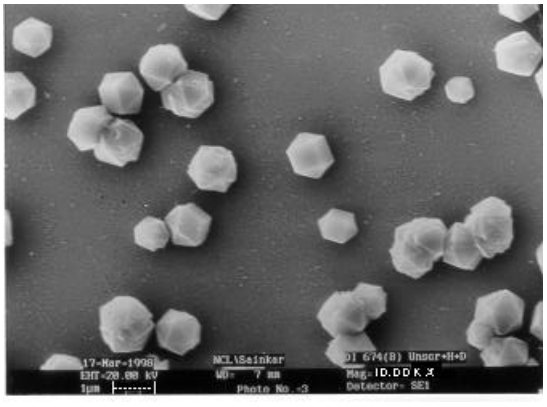

(a)

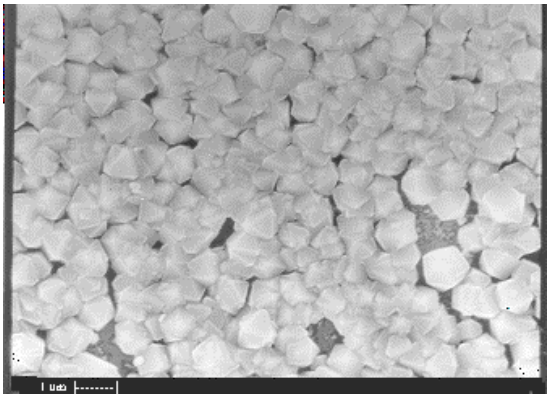

(b)

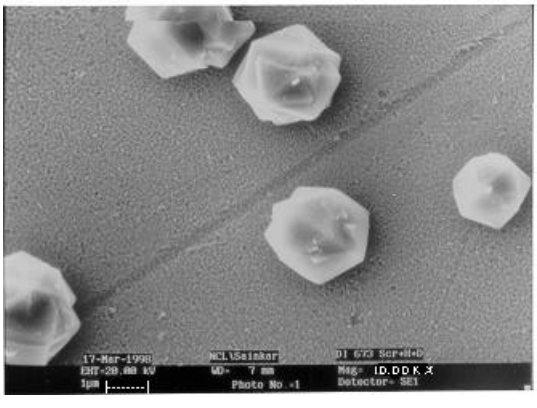

(c)

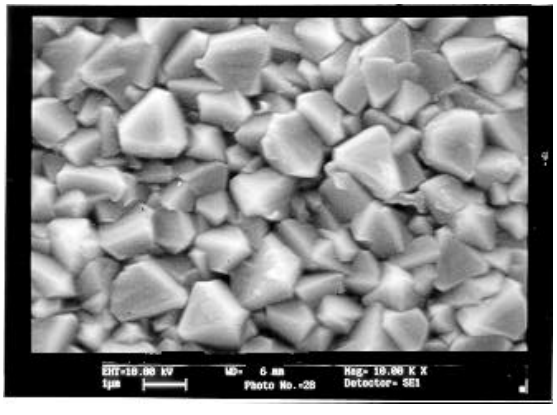

(d)

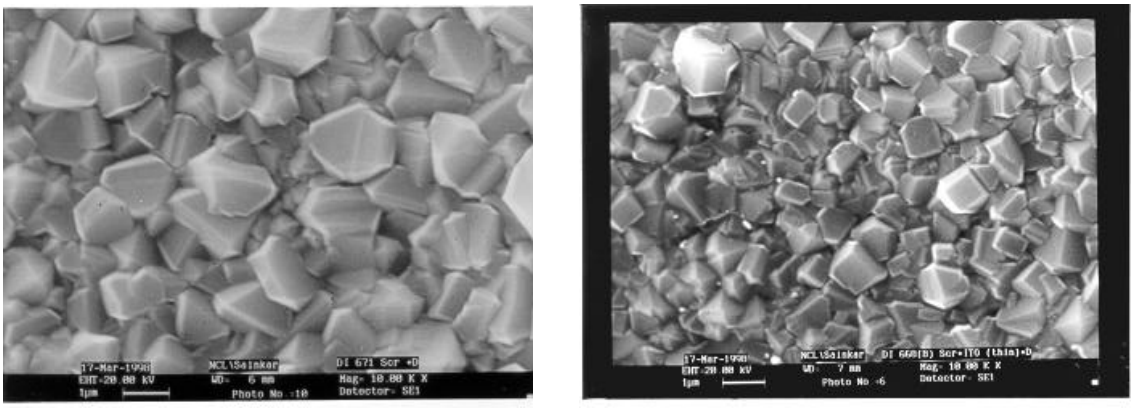

(e) **(f)**

Fig. 3.11 SEM Photographs of the surface morphology of the diamond films deposited on -
(a) mirror polished + heat treated Si (b) mirror polished + heat treated + ITO coated Si (c) scratched + heat treated Si (d) scratched + heat treated + ITO coated Si
(e) scratched Si (f) scratched + ITO coated Si substrates.

We have also repeated the series of deposition experiments on Si substrates which were scratched by using a ceramic powder containing mainly alumina and subsequently coated with ITO buffer layer. The results observed in this case are shown in the following Fig. 3.12 and are similar to those obtained for silicon substrates scratched with diamond powder.

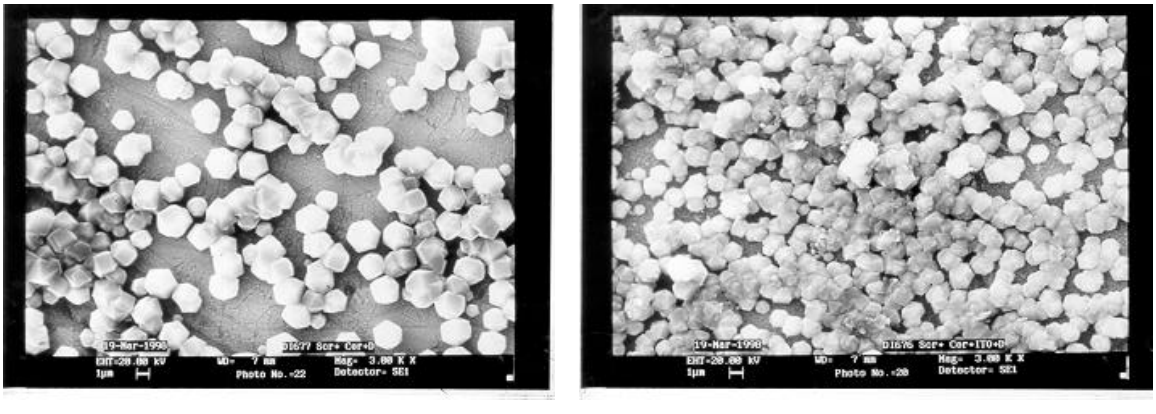

(a) **(b)**

Fig. 3.12 SEM photographs of the surface morphology of the diamond films deposited on :
(a) ceramically scratched and
(b) ceramically scratched + ITO coated Si substrates.

Interestingly, the ITO layer appears to assist the diamond film deposition on the Si substrates in at least two ways: First, it allows diamond nucleation and secondly, it improves the quality of diamond crystals. The latter refers to the improvement with respect to the symmetrical polyhedral growth of individual crystallites accompanied by reduction in graphitic carbon. The crystallite size was also found to increase with ITO buffer layer thickness. This is shown in following figure 3.13. It shows that the average crystallite size is maximum for the film in which ITO thickness is maximum.

Raman spectra of these various films are shown in figure 3.14 and 3.15. These spectra show the well-known strong band at 1332 cm^{-1} characteristic of diamond crystals with additional broad band at 1500-1580 cm^{-1}. The latter band is attributed to the sp^2-bonded carbon phase, which may have amorphous structure. It may be noted that the spectra do not show simultaneous presence of diamond and graphite crystals, the latter

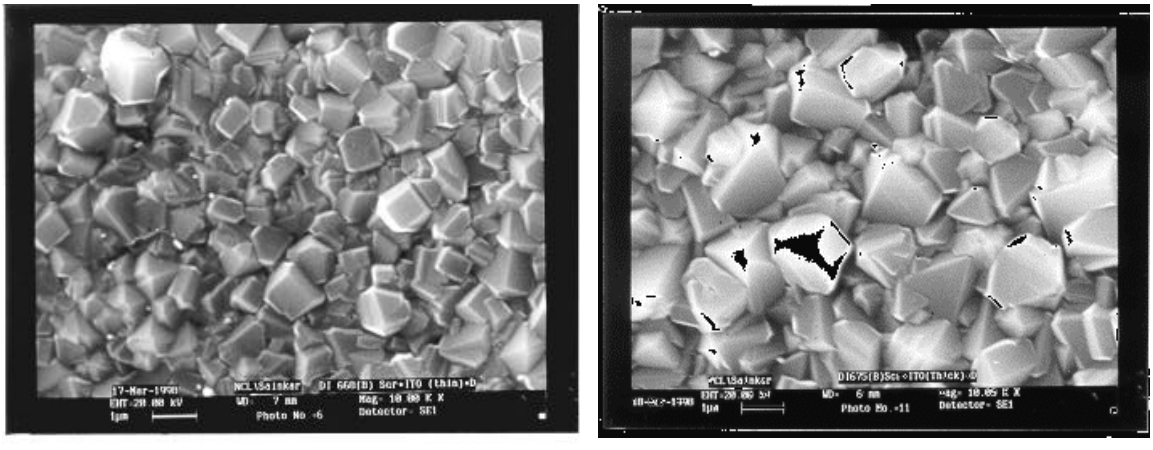

(a) **(b)**

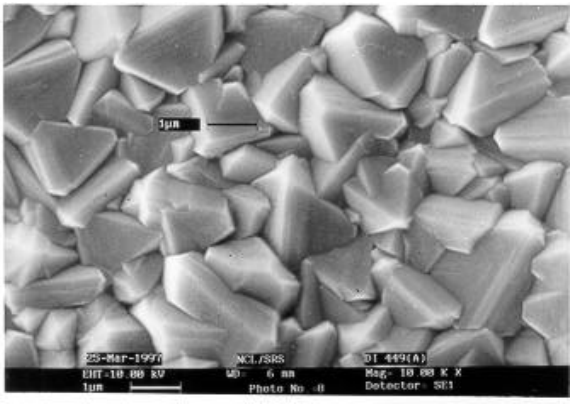

Fig. 3.13 SEM Photographs of the surface morphology of the diamond films deposited on scratched + ITO coated Si substrate as a function of ITO thickness.
ITO deposited for-
(a) 45 min.
(b) 90 min.
(c) 120 min.

(c)

Chapter 3
Synthesis of Diamond Films Under.....

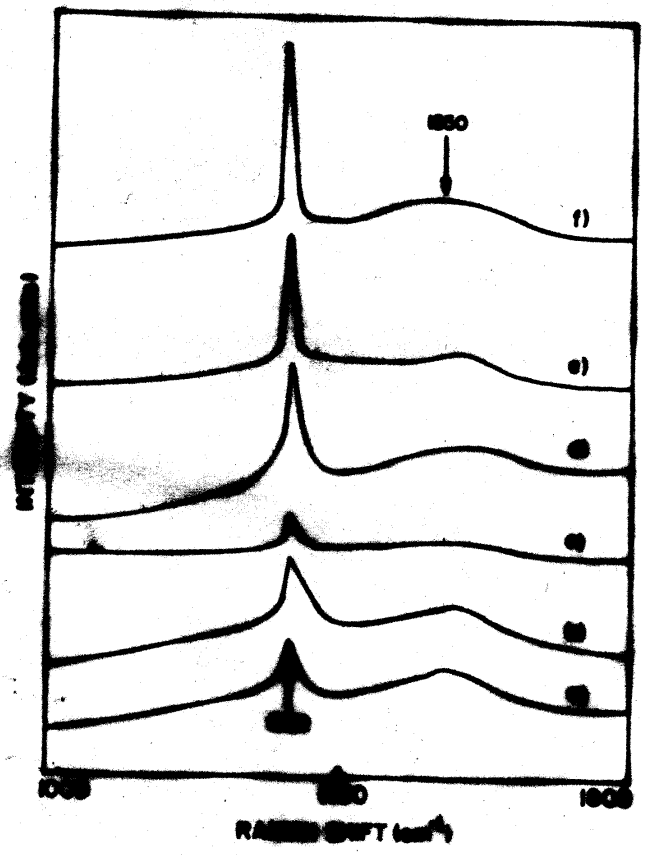

Fig. 3.14 **Raman spectra of the diamond films deposited on (*a*) mirror polished + heat treated Si, (*b*) mirror polished + heat treated + ITO coated Si, (*c*) scratched + heat treated Si, (*d*) scratched + heat treated + ITO coated Si, (*e*) scratched Si, and (*f*) scratched + ITO coated Si substrates**

Chapter 3
Synthesis of Diamond Films Under.....

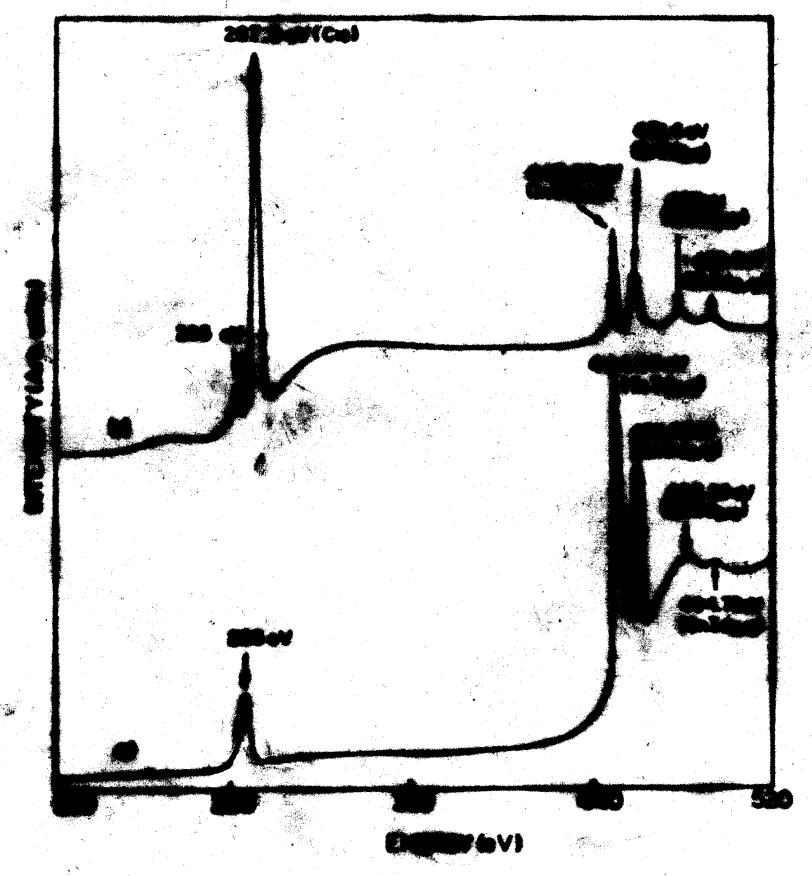

Fig. 3.16 XPS spectra of (*a*) ITO coated Si substrate, and (*b*) thin diamond film deposited on the ITO coated Si substrate

being characterized by the two well known Raman bands, one at 1580-1600 cm^{-1} (G-band) and the second at 1360 cm^{-1} (D-band) which has strength dependence on the graphite particle size [49]. The broad band centered at 1550 cm^{-1} seen in our spectra is therefore taken as representative of only the sp^2-bonded amorphous carbon phase [50]. The scattering cross-section of the G-band vibrations is ~ 50 times higher than that of sp^3-bonded carbon phase [37,38]. This suggests that the sp^2-bonded phase is in amorphous state and its content is negligibly low. The heat-treated substrates show most sluggish nucleation with least Raman signals even for G-band suggesting that the graphitic content in these films is also low. This later observation may be attributed to the higher reactivity of atomic hydrogen with the sp^2-bonded species deposited on the substrate surface.

The XPS spectra of the thin diamond film (< 0.05 μm) deposited on the ITO coated Si substrate are shown in Fig. 3.16. It indicates no appreciable changes in $3d_{5/2}$ and $3d_{3/2}$ bands for In and Sn. Thus the possibility of formation of carbides of these metals at the interface may be ruled out and hence other sources for nucleation sites on the ITO coated substrates need to be looked for. The observations from XPS spectra imply that the In and Sn might have diffused out to the surface of the diamond film by loosing their oxygen to suppress the sp^2-bonded graphitic radicals. Hence we speculate that the nucleation has occurred via gas-surface interface reactions that may stabilize the nucleation through sp^3-bonded C-H radicals.

3.3.3 Conclusion

In conclusion, in the present study, we have reported the results on nucleation and growth of diamond films deposited by hot filament CVD technique on as-received mirror-polished and scratched silicon substrates coated with In-Sn-O (ITO) buffer layers. The scratching treatment has been shown to trap the diamond seeds while the topographical features appear to have no role. In and Sn from the buffer layer are proposed to act as catalysts in the nucleation and growth of the diamond films and therefore, the nucleation density (ND) for variously pretreated substrates is found to improve by a factor greater than 500 when they are

coated with ITO layer. The oxygen from oxide buffer layer is proposed to help in enhancing the nucleation on perfect surfaces and also in reducing the graphitic content in the film.

References

1. R. E. Clausing, L. Healtherly, K. L. More & G. M. Begum, Surf. Coat. Technol. 39/40 (1989) 199.
2. P. Ascarelli, E. Cappelli, G. Mattei, F.Pinzari, V. Fares, C. Veroli & S. Martelli, Diam. Relat. Mater. 5 (1996) 308.
3. R. Rawles, W. Morris & M. D'Evelyn, Appl. Phys. Lett 69 (1996) 4032.
4. B. Spitsyn, L. Bouilov, B. Derjaguin, J. Cryst. Growth 52 (1981) 219.
5. C. Chu, R. Huage, J. Margrave & M. D'Evelyn, Appl. Phys. Lett. 61 (1992) 1393.
6. S. Jin, T. Moustakes, Appl. Phys. Lett. 65 (1994) 404.
7. N. Lee, A. Badzian, Appl. Phys. Lett. 67 (1995) 2011.
8. S. C. Sharma, M. Green, R. C. Hyer, C. A. Dark, T. D. Black, A. R. Chourasia, D. R. Chopra, and K. K. Mishra, J. Mater. Res. 5 (1990) 2424
9. R. Meilunas, M. S. Wong, K.C. Sheng, R. P. H. Chang, Appl. Phys. Lett. 54 (1989) 2204.
10. A. K. Sikder, T. Sharada, D. S. Misra, D. Chandrasekaran, and P. Selvam, Diam. Relat. Mater. 7 (1998) 1010
11. Z. Yu, A. Flodstorm, Diam. Relat. Mater. 6 (1997)81.
12. M. Werner, and R. Locher, Rep. Prog. Phys. 61 (1998) 1665
13. C. Wild, "Low Pressure Synthetic Diamond: Manufacturing and Application", ed. B. Dischler and C. Wild (1998) p.189
14. C. H. Lee, T. D. Fu & Y. F. Chen, J. Mater. Sci. 28 (1993) 170.
15. D. G. Kim, H. C. Lee & J. Y. Lee, J. Mater. Sci. 28 (1993) 6704.
16. S. S. Park & J. Y. Lee, J. Mater. Sci. 28 (1993) 1799.
17. P. E. Pehrsson, F. G. Celii, and J. E. Buttler, in "Diamond Films and Coatings" ed. R. F. Davis (1992) (Noyes Publication, Park Ridge, NJ, USA)
18. J. E. Buttler, and F.G. Celii, Electrochem. Soc. Proc. 89 (1989) 317

19. R. Berman, "The Properties of Diamond" (J. E. Field,ed.) Academic Press, London (1979)
20. E. J. Bienk & S. S. Eskildsen, Diam. Relat. Mater. 2 (1993) 432.
21. R. Rameshan & T. Roppel, J. Mater. Res. 7 (1992) 1144.
22. A. A. Morish & P. E. Pehrsson, Appl. Phys. Lett. 59 (1991) 417.
23. X. Jiang, K. Schiffmann & C. P. Klages, Phys. Rev. B 50 (1994) 8402.
24. S. Iijima, Y. Aikawa & K. Baba, Appl. Phys. Lett. 57 (1990) 2646.
25. S. Iijima, Y. Aikawa & K. Baba, J. Mater. Res. 6 (1991) 1491.
26. B. Singh, Y. Arie, A. W. Levine & O. R. Meskar, Appl. Phys. Lett. 52 (1988)451.
27. B. R. Stoner, C. T. Kao, D. M. malta & R. C. Glass, Appl. Phys. Lett. 62(1993) 2347.
28. F. Hong, J. C. Hsieh, J. J. Wu, G. T. Liang & J. H. Hwang, Diam. Relat. Mater. 2(1993)365.
29. J. C. Angus & C. C, Hayman, Science 241 (1988)1823.
30. W. A. Yarbrough & R. Messier, Science 247 (1988)688.
31. P. A. Dennig & D. A. Stevenson, Appl. Phys. Lett.59 (1991) 1562.
32. P. A. Dennig, H. Shiomni, D. A. Stevenson & N. M. Johnson, Thin Solid Films 212 (1992)63.
33. S. M. Kanetkar, A. A. Kulkarni, A. Vaidya, R. D. Vispute, S. B. Ogale, S. T. Kshirsagar & S. C. Purandare, Appl. Phys. Lett. 63 (1993) 740.
34. P. Mpawenayo & M. Nsabimana, Mater. Res. Soc. Symp. Proc. (Novel Refract. Semicond.) 97 (1987) 301.
35. R. A. Soref, J. Appl. Phys. 72 (1992) 626.
36. M. P. Pai, D. V. Musale, S. T. Kshirsagar, A. Mitra & S. R. Sainkar, Thin Solid Films 322 (1998) 167.
37. N. Wada & S. A. Solin, Physica B+C 105(1981) 353.
38. R. E. Shroder, R. J. Nemarich & J. T. Glass, Phys. Rev. B 41 (1990) 3738.
39. M. Frenklatch & H. Wang, Phys. Rev. B 43 (1991) 1520.
40. J. W. Kim, Y. J. Baik, K. Y. Eun & D. N. Yoon, Thin Solid Films 212 (1992) 104.
41. J. Merceir, A. M. Bonnot, E. Caignol, in : Diamond and Diamond-like films and

coatings (ed) R. E. Clausing, L. L. Horton, J. C. Angus & P. Koidl (New York, Plenum Press) p. 533.

42. D. Kweon, J. Lee & D. Kim, J. Appl. Phys. 69 (1991) 8329.
43. S. Matsumoto, Y. Sato, M. Tsutsumi & N. Setaka, J. Mater. Sci. 17 (1982) 3106.
44. W. Zhu, A. R. Badzian & R. Messier, Proc. of SPIE, on Diamond Optics III 1325 (1990) 187.
45. T. Sharda, A. K. Sikder, D. S. Misra, P. Selvam in : Proc. National Conf. Thin Film Characterization and Applications, Ed. S. K. Narayandas, D. Mangalraj (Allied Publishers Ltd., 1996) p.319.
46. A. K. Kulkarni, Bull. Mater. Sci. 17 (1994) 1379.
47. S. J. Harris, A. M. Weiner, S. Prawer & K. Nugent, J. Appl. Phys. 80 (1996) 2187.
48. Y. F. Zhang, D. Dunn-Rankin & P. Taborek, J. Appl. Phys. 74 (1993) 6941.
49. P. Lespade, A. Mrchand, M. Couzi & F. Cruege, Carbon 22 (1984) 375.
50. M. Yoshikawa, G. Katagiri, H. Ishida & A. Ishitani, Solid State Commun. 66 (1988) 1177.

CHAPTER 4

Si INCORPORATION IN DIAMOND FILMS

This chapter is devoted to the studies on the effect of Si incorporation on the growth behavior and properties of the diamond films. Raman and photoluminescence spectra of these films are discussed in details. The dependence of 1.683 eV line in PL spectrum of the CVD diamond films on the substrate temperature is studied and discussed. The films grown on non-silicon substrates such as Alumina and Copper are also analysed for the possibility of emission of PL at 1.683 eV in absence of Si contamination which generally comes from Si substrate. Some results on co-doping of Boron along with Si in diamond films are also discussed briefly in the present work.

4.1 Introduction

As seen in the last chapter, the inexpensive polycrystalline diamond films grown by HF–CVD technique have intrinsic properties nearly same as those of natural or synthetic diamond crystals and offer great promise for their use as a substitute for the expensive natural or synthetic diamond in a variety of diamond based optical and electronic device applications [1]. As a result of this high potential, a large progress has already been made in production and growth of these films on diamond as well as inexpensive non-diamond substrates such as Si, Cu, Al_2O_3 and Mo [2,3]. However, the diamond films grown on non-diamond substrates by CVD are polycrystalline and highly defective [4]. Some of these defects such as dislocations, line defects, self-interstitials, point defects, stacking faults etc. may be intrinsic in nature and can be minimized by controlling the deposition conditions [4]. On the other hand the undesired impurities which may come from non-diamond substrate or other sources in the deposition chamber, can diffuse during the CVD growth into diamond film and can give rise to extrinsic defects [3]. A small amount of such an undesired impurity may have pronounced adverse or advantageous effects on the nucleation, growth and properties of the CVD films. In order to make the diamond films grown on non–diamond substrates more attractive for device applications, investigations of these defects are mandatory. There are very few studies reported in literature on impurity incorporations in diamond films.

Among the various impurities observed in natural and synthetic diamonds, Si is the most commonly observed but in most of the cases, it is unintentionally incorporated impurity. The natural diamonds can pick up the Si contamination from Si containing ores on the earth crust while in synthetic crystals, it may come from the materials constituting the growth apparatus. However, this unintentional incorporation of Si in CVD diamond deposited on Si substrates is expected to result mainly from the interface diffusion of substrate Si atoms during the nucleation and growth [5]. On one hand, Si has strong tendency to bond in tetrahedral (sp^3) configuration and is also expected to bond with the surface carbon atoms to form SiC which can provide nucleation sites for continuous growth [6] and, therefore, Si should enhance the nucleation and growth. On the other hand, as the covalent radius of Si (r_{si}~1.11Å) is much

larger than that of carbon (r_c ~0.77Å) the diffusion of Si atoms into the diamond lattice would be extremely slow. This implies that the substrate Si atoms should be localized in principle, at the diamond/Si substrate interface [7]. Alternatively, the Si atoms may also get incorporated non-substitutionally and hence induce strains and stresses in the film leading to a variety of defects and vacancies in the diamond film [2]. Such defects can be completely new or may be similar to intrinsic defects associated with the diamond lattice. The studies reported so far have been performed mainly on the unintentionally doped Si impurity and are reviewed in the following section. This is then followed by the motivation and objectives of the present work.

4.2 Background Literature on Si Impurity in Diamond

Most of the earlier work in this field was concentrated on the production of thin polycrystalline films and the reviews of progress made in this area have been reported by many researchers [8-12]. Relatively little characterization has been done of lattice defects and chemical impurities in such CVD diamond. The defects and impurities, which have a strong influence on the optical and electronic properties of these diamond films are primarily characterized by their electronic energy levels within the forbidden gap of the perfect crystal [4]. Many such states have been observed and characterized in natural diamond by optical spectroscopies such as optical absorption, luminescence [13,14] and photoconductivity [15]. These techniques have been applied recently for investigation of the defect states in CVD grown diamond films. Particularly the cathodoluminescence (CL), where the optical emission arises from electronic recombination following excitation by an energetic electron beam [16] has been one of the most successful technique for characterization of defects and impurities in diamond. Photoluminescene (PL), though is more selective method for excitation than CL, has also been used popularly to characterize the defects and impurities in diamond films [14]. The incorporation of Si impurity and the defect levels introduced in the forbidden gap have been studied by the CL as well as PL techniques while there exists no other experimental data or report on the incorporation of Si in the diamond film.

The earliest CL measurement were carried out by Vavilov et al. [17] using CVD diamond produced by thermal decomposition of gaseous carbon compounds in a closed system. They observed a number of sharp lines characteristic of nitrogen + vacancy or nitrogen

+ interstitial optical centers. They also observed a sharp emission line at 1.684 eV which was guessed to be associated with Si. In order to understand the origin of this latter line, vavilov et al. [17] also performed CL measurements on various ion-implanted diamond crystals. The Si implanted natural diamond crystals displayed the emission near 1.684 eV and therefore they correlated the origin of 1.684 eV line to the presence of Si. This was the first report on the incorporation of Si in the diamond crystals.

Most of the optical centers detected by vavilov et al. [17] have been observed subsequently in polycrystalline diamond produced both by thermal [4] and microwave CVD techniques[18]. When CVD diamond specimens are excited by visible light, a broad featureless band is generally observed. This PL begins at photon energy close to that of the excitation and extends throughout the carbon vibrational Raman region (1100-1800 cm^{-1} from 514.5 nm laser line) [19]. In Raman spectroscopy, this broad PL is often correlated to the PL background or fluorescence background. Robins et al.[19] have reported Raman spectra of 48 diamond specimens grown by filament assisted CVD technique, where they observed strong correlation between the intensity of the PL background and the intensity of sp^2 bonded carbon Raman band positioned at a wave number shift of ~1525 cm^{-1} and has a full width at half maximum (FWHM) of ~200 cm^{-1}. The one-to-one correlation between these two parameters led Robins et al.[19] to conclude that the PL background arises from sp^2- bonded carbon atoms clustered within the majority of sp^3 bonded diamond grains in similar way to that of the PL in amorphous hydrogenated carbon (a-C:H) or in polynuclear aromatic molecules.

Robins et al.[4] have reported the studies on luminescent defects in CVD diamond films deposited as a function of deposition temperature. They compared the CL spectra in these films to the spectra of known defects in natural and synthetic diamond and identified several types of defects present in the films which were attributed to nitrogen-vacancy complex, interstitial nitrogen and dislocation line defects. Though these samples were deposited on crystalline Si substrates , they did not observe the 1.681 eV line. Among the various CL lines observed for samples deposited at substrate temperature of about 800^0C, an intense narrow line with peak energy 1.675 ± 0.002 eV and FWHM 0.025 eV was observed. This line was assigned to the neutral atomic vacancy, generally referred to as 'zero phonon line' and denoted by general radiation (GR1 center) [14]. These centers may be viewed as an

localized state due to an optically active electron essentially confined within one or two atomic spacings of a small crystallite imperfection such as vacancies. In case of diamond, the simplest possible model of the neutral vacancy V^0 may be understood from the following picture: In this picture[20], the atoms of the perfect diamond crystal form sp^3 hybrids, which give directed bonds. When an atom is removed, four bonds are broken. The electrons in the four sp^3 hybrid orbitals on the neighbours to the vacancy, and which previously participated in bonds to the removed atom, rearrange themselves forming what may be called as the "Defect-Molecule Model". The behavior of these four defect electrons in the 'dangling bonds' determines the properties of the center. Such an electron confined to be within two atomic spacings of the defect will then give electronic transition between its two lowest states and in the mid-gap-region [21]. The properties of these transition then arise mainly from the electron-lattice interaction. The pair of ZPL at 1.665 eV and 1.673 eV (744.5 and 741.0 nm), a broad vibronic band peaking at 2 eV form the GR1 band. The lines have been observed mainly in diamond irradiated with high energy electrons [22].

Irradiation of type IIb diamonds has shown that the GR1 center is a donor and compensates the acceptor [23] and implies that positively charged and paramagnetic vacancies are present in such crystal. However, contrary to this, there is evidence that GR1 center is ionized by emitting hole [24], i.e. acceptor like behavior. Hence, the picture is somewhat ambiguous at present and it may be that the defect can be either a donor or a acceptor, depending on the fermi level [25]. These GR1 bands can shift depending upon the stress present around the center. Moreover, GR1 ground state is degenerate, and therefore, a Jahn-Teller effect is expected to splitt the ground state level [14].

The peak shift relative to the value reported for GR1 center (1.673 eV) and the large FWHM of the line were thought to be arising from internal stress effects in the film. The morphology and crystal growth habit of these samples showed transition from predominant cubic and cubo-octahedral at T_s=600^{0}C to an octahedral growth at T_s > 800^{0}C, where the crystalline diamond morphology was most poorly defined because of the secondary nucleation. Such morphology may be an indication of large stress in the film. This stress has been suggested to shift and broaden the GRI line. The PL of these samples (T_s >800^{0}C) was observed to show a sharp line at 1.680 eV, but they did not observe the line at 1.685 eV which vavilov et al.[17]

have observed. It was argued that the line with energy 1.675 eV, 1.685 eV were not from optical transition of Si center, as the position and width of the Si related lines are more likely to be unaffected by the uniaxial stress and strain in the film.

Yokata et al.[26] studied the emission at 1.675 eV as a function of nitrogen impurity in the diamond films where the relative intensity of the 1.675 eV line has found first to increase upto a certain increase of the concentration of nitrogen in the starting gas mixture and subsequently decreased for the additional increase in the nitrogen concentration. They attributed the origin of this line again to the presence of GR1 center rather than the silicon center. Collins et al.[27] have also investigated the effect of nitrogen on the 1.681 eV center and suggested that the center probably involves Si as originally found by Vavilov et al.[17], but with additional speculations that it necessarily involves some crystal disorder. Their measurements have suggested that nitrogen nearest neighbour pairs may be present in the material deposited above T_s=800^{0}C and suggested that the formation of the 1.681 eV center needs additionally some crystal disorder. The line shape and position of 1.681 eV line in diamond films deposited on substrate material (Si, Mo, Ni) with T_s= 875^{0}C (for all samples) have been studied by Freitas et al.[2]. The occurence of 1.681eV emission for films deposited on Ni and Mo substrates was interpreted in terms of the stress shifted and broadened neutral atomic vacancy emission which otherwise occurs at 1.675 eV. They observed broader 1.680 eV line for films deposited on Si substrates and suggested that the broadening of this line may indicate the additional effects of Si on the diamond film. For example, a significantly broader Raman line width was observed for these films which is indicative of additional stress induced due to Si absorption in the diamond film.

The 1.680 eV center, a common feature observed in PL spectra of CVD diamond films has been assigned to the neutral vacancy center (v^0, whose zero phonon line ZPL is at 1.673 eV), and which is induced in all natural and synthetic diamond by irradiation [2]. The comparison of the 1.682 eV center with v^o shows that the former is blue shifted by 5 to 8 meV and has line width of 4 to 10 times broader than the latter. Therefore it was suggested that the line 1.680 eV may be associated with the centers such as the defect with ZPL at 1.685 eV observed in homo and hetero epitaxial CVD films intentionally doped with Si [17] or Si-implanted and annealed natural diamond [28]. The 1.680 eV system in the undoped diamond

films shows about 5 meV redshift from Si center. Moreover, the energy position and line width of the Si center seems to be independent of the substrate, deposition technique or crystalline grain size and such behavior was not observed with 1.68 eV line in their study. It was proposed that the residual stress of the order of 1 to 2 GPa parallel to <100> could be enough to induce a shift of 6 to 7 meV blueshift if one assumes that the 1.680 eV system is the neutral vacancy [13]. This stress can vary from sample to sample. Therefore, the need of careful experiments on well controlled samples to achieve a definite identification of 1.680 eV center was suggested. Ruan et.al. [29], therefore studied CL as a function of annealing at temperatures $500^0C<T<1350^0C$. The annealing studies are useful because they provide information on the motion of defect or impurity centers. The neutral vacancies in natural diamond become mobile at temperatures around 800^0C and therefore annealing at $T>800^0C$ can result in disappearance of the GR1 band (ZPL at 1.673 eV). The 1.681 eV line did not show reduction in its intensity even at 1300^0C and hence they ruled out the possible connection between the GR1 center and 1.681 eV peak. When the excitation electron energy was changed from 5 to 10 KeV, the intensity of 1.681 eV peak was observed to increase linearly and thus they concluded that the Si from the substrate diffuses into the film at the interface and its concentration decreases towards the film surface. These results, they attributed to the Si center at the interface.

Graham et al.[30] have also analyzed the defects and impurities in diamond films grown by CVD. They attributed the broad CL bands observed at 2.90 ± 0.001eV. and 2.25 ± 0.004 eV to the recombination of electrons and holes at closely spaced and widely separated donor acceptor pairs respectively. The donor was thought to be an aggregate of nitrogen [31] and the acceptor was boron [32,33]. They attributed the narrow peak observed at 1.679 ± 0.001 eV to interstitial silicon impurities. Shing et al.[34] argued that the Si diffusion from Si substrate into the diamond film would depend on the substrate or deposition temperature. They deposited the films in the temperature range 400 to 750^0C and reported the PL dependence on deposition temperature. They found the intensity of 1.681 eV line to increase with increase in deposition temperature and supported that the 1.681 eV line is due to Si center.

Feng et al.[35] studied the dependence of 1.681 eV emission line parameter as a function of temperature , excitation energy and even the CH_4/H_2 ratio. They also obtained the

data supporting the hypothesis that the 1.681 eV line is not the stress shifted GR1 line. They however, do not support the Si center hypothesis. According to them, the Si impurity model is though convincing it is not conclusive on the basis of previous results. Their studies show quenching of intensity of 1.681 eV line with increase in stress and hence it is only seen in high quality films. Hence they also recommended more investigations on this topic. Gorokhovski et al.[36] investigated the low temperature PL of the Si impurity center in diamond films grown by CVD. Laser excitation at 514.5 nm and resonant with the ZPL absorption line at 737 nm (1.6823 eV) were used. The PL lines were seen to narrow at resonant excitation which revealed vibrational structure of Si center at 515 cm^{-1} and supported the diatomic quasimolecular Si_2 center. The line width of 767 nm was found to increase with increase in measurement temperature, which is also true for vibrational diatomic Si center. Clark et al.[37] studied the Si impurity in synthetic diamond grown from metal melts containing Si. The PL spectra measured in the temperature range 1.8-77K revealed a 12-line fine structure close to 1.682 eV. These lines were then correlated to existence of ^{28}Si, ^{29}Si and ^{30}Si, which supported that 1.682 eV line originates from Si center. However this spectral fine structure was not observed for CVD diamond films, which they argued to disappear due to the stress in the CVD film which broadens the fine structure and allows the merging of the structure. They, therefore, studied the PL in samples heat treated from 1100 to 2200^0C, but the fine structure was not observed which they argued that even the heat treated film contains stress. They suggested that the center involves Si, but it should also be accompanied by vacancies at the neighbouring lattice sites.

There are contradicting reports regarding the diffusion of Si in the bulk of diamond film. In this regard, Bergman et al.[7] have reported that the 1.68 eV defects are created at early stages of diamond nucleation and growth resulting in higher concentrations of this type of defect in the vicinity of Si substrate. They observed that the relative PL intensity of 1.680 eV band decreases with increasing deposition time which has also been found by Robins et al.[19]. This indicates that Si diffusion in the bulk of the diamond film decreases with increasing thickness if this band is due to Si center. On the other hand , Lannon et al.[38] observed that a silicon adlayer is always present on the surface of the growing film after studying the surfactant mediated nucleation and growth of diamond films.

Bergamann and Nemanich [5], therefore, undertook the Raman and photoluminescence analysis of the stress state and impurity distribution in the diamond. They detected three types of impurities, namely N, Si and sp^2 bonded graphitic phase. After compensating the thermal interfacial stress and the stress due to grain boundary, they found that the internal stress was of compressive nature, which was supported by their Raman line shape analysis. The line shape of 1.681ev showed that the Si centers are related with Si/diamond interfacial stress. The Si band exhibited narrower line width compared to that of N which was argued to support that Si band contains less internal stress than the N center. They proposed that these two centers are probably related to different types of stress sources. Gross et al.[39] investigated the energy eigen values obtained from *ab initio* cluster calculations with the Si vacancy on the center. Their structure supported the twelve line optical band to vacancy-Si complex which has a very unusual, possibly unique structure with a Si atom at the center of a split vacancy.

Dannefaer et al.[40] have studied the photoluminescence of CVD diamond films and made very interesting observations. ***In the undoped diamond film with {111} faceting, a broad PL band centered at 1.720 eV was observed. They suggested these films to be more defective and associated this band to vacancy clusters observed by positron lifetime measurements. The film with {100} faceting showed a broad PL spectrum centered around 1.830 eV which was assigned to divacancies. In case of the randomly oriented film, a sharp PL band at 1.680 eV was observed. This band was attributed to monovacancies. In the boron doped ($10^{20}/cm^3$) diamond film, no PL was observed and*** it was suggested that the boron interstitials might have reduced the concentration of vacancies. Hertnett [41] has also suggested that B atoms incorporated in the diamond lattice effectively passivate the defects responsible for the 1.680 eV PL peak. However, it is yet not clear whether the B bond with Si is terminating the dangling bonds due to vacancies or it acts as compensator for Si induced defects states.

4.3 Objectives of the Present Work

From the above literature review, it is clear that there are two schools of thoughts regarding the origin of photoluminescence bands (particularly 1.681 eV band) in CVD diamond films. According to the one school, the 1.681 eV band is stress shifted GR1 band, i.e.

it arises from neutral vacancy centers. According to the second school, the 1.681 eV band in CVD diamond films is different from GRI band and it is related to Si impurity in diamond. Here, it must be mentioned that, though many research groups have reported the luminescence spectra in CVD diamond films, the origin of the different luminescence lines is not well understood. ***In particular, the interpretation of the emission line at around 1.681 eV has been the subject of controversy.*** This also has left unanswered the question as to how the Si impurity behaves when incorporated in diamond.

The appearance of a sharp band at 1.681 eV in the photoluminescence and cathodoluminescence spectra of several of CVD samples has been so far considered as the only evidence for the unintentional incorporation of Si in CVD diamond films. However some samples so deposited have either shown complete absence of 1.681 eV or excessive enhancement in intensity of the same band for samples prepared by others. ***These conflicting experimental results suggest that the topic is still open for further systematic investigations involving intentional insitu doping of the Si impurity in CVD diamond films prepared under various controlled deposition conditions.*** The only attempt to dope Si intentionally has been the ion implantation of Si in diamond. But it can result in additional disorder induced defects [42]. Therefore the only alternative to dope Si atoms in CVD diamond films is the intentional *insitu* incorporation of Si during the growth of the film. Therefore, in the present chapter, the studies on synthesis and structural characteristics of *insitu* Si doped diamond films grown on different substrates (Si, Al_2O_3, Cu) are reported. Also, it has been suggested that Boron atoms incorporated in diamond lattice can effectively passivate the defects (or vacancies) responsible for 1.681 eV band [41]. As the covalent radius of boron (r_{Bi} ~0.46 Å) is much smaller than that of carbon (r_c~0.77Å), boron interstitials may reduce the concentration of vacancies [40]. Thus, boron incorporation in the diamond films is expected to change the growth behavior and properties of the diamond films. Therefore, in this chapter, some results on co-doping of boron along with Si in diamond films are also discussed briefly. The films were characterized by Scanning Electron Microscopy (SEM) and X-ray diffraction (XRD) techniques to understand the possible role of Silicon in the growth mechanism which is discussed in details. The Raman and associated photoluminescence measurements are also reported in order to understand the effect of Si on various emission lines in photoluminescence

spectra of these films. The elemental analysis of the films was carried out by using the Energy Dispersive Analysis of X-rays (EDAX).

4.4 Experimental

In the present work, the diamond films were grown by HF-CVD technique (described in details in chapter 2). The optically polished p-type Silicon (Si) <100> (resistivity ~ 10Ω-cm, 300 μm thick), Alumina (Al_2O_3) (500 μm thick) and Copper (Cu) (500 μm thick) were used as substrates for supporting the diamond films. The substrates were held at a distance of 10 mm below the plane of M-shaped filament. The substrate holder was made to rest on a heat sink of variable heat capacity which could be achieved by varying the size, mass and configurations of the heat sink. Using this heat sink, it was possible to vary the substrate temperature by keeping the substrate surface to filament distance constant. The different heat sinks used were configured of copper, graphite and ceramic so as to get the substrate temperatures (T_s) about 750^0C, 850^0C and 950^0C respectively. The substrates were lightly scratched by using diamond powder (~ 0.5 μm) and were ultrasonically cleaned in acetone and rinsed in 40% HF acid solution prior to their loading in the deposition chamber. For the deposition of the films, a mixture of the semiconductor grade gases CH_4 , SiH_4 , B_2H_6 and H_2 was used. The methane fraction (X) and the silane fraction (Y) in the source gas are defined as :

$$X = \frac{[CH_4]}{[CH_4] + [SiH_4]} \quad \text{and} \quad Y = \frac{[SiH_4]}{[CH_4] + [SiH_4]}$$

The deposition parameters used are listed in Table- 4.1

TABLE 4.1: HFCVD Deposition Parameters

Deposition Parameter	**Value**
CH_4 percentage in H_2	2%
Gas mixture flow rate	300 SCCM
Deposition Pressure	30 Torr
Filament Temperature (T_F)	$1950 \pm 50\ ^0$C
Substrate temperature (T_S)	750-950 ^{0}C
Deposition Period	3-6 hrs.

4.5 Results and Discussion

In order to study the effect of Si concentration on the growth and properties of HF-CVD diamond films, SiH_4 gas was introduced in the mixing unit prior to the entry of precursor gas mixture in the deposition chamber. To introduce different concentration levels of Si in the growing diamond films, SiH_4 gas proportion with respect to methane gas flow was varied from 0% to 2.44% of volume. This set of films was deposited on Si <100> substrates keeping all other deposition parameters identical as listed in the table 4.2 and therefore the variation in any property as a result of Si impurity introduced in the film may be correlated to the gas phase concentration of SiH_4 alone. The Si concentration introduced in the film is taken to be proportional to the SiH_4 gas concentration as given in the table 4.2.

Table 4.2 Deposition conditions and the concentration of different gases used for the growth of Si doped diamond Films

Sample Title	H_2 Gas Flow (SCCM)	CH_4 Gas Flow (SCCM)	SiH_4 Gas Flow (SCCM)	Percent SiH_4 Conc.	Filament Temp. (T_F) (^{0}C) ± 50	Substrate Temp.(T_S) (^{0}C) ± 20	Deposition Time (T) (hrs)
DS#727	300	6.0	0.0	0.0	1950	950	6.0
DS#724	300	6.0	0.005	0.08	1950	950	6.0
DS#723	300	6.0	0.01	0.17	1950	950	6.0
DS#722	300	6.0	0.025	0.42	1950	950	6.0
DS#721	300	6.0	0.050	0.83	1950	950	6.0
DS#716	300	6.0	0.075	1.23	1950	950	6.0
DS#714	300	6.0	0.10	1.64	1950	950	6.0
DS#718	300	6.0	0.15	2.44	1950	950	6.0

The filament temperature (T_f) is selected as ~ 2000^0C because at this temperature sufficient amount of H_2 can undergo dissociation whereas the other gases, viz. CH_4 and SiH_4 undergo almost 100% dissociation in the viscinity of the hot filament. Similarly, the substrate temperature (T_s) is selected to be ~ 950^0C because at this temperature, additional SiH_4 and CH_4 can be decomposed at the substrate surface. Other important aspect for selecting this T_s is that the morphology would not undergo any transformation unless it is caused only due

to the presence of Si in the grains. The results obtained on doped films are compared with those of undoped film and are presented in the following.

4.5.1 Si doped diamond films vs. SiH_4 Concentration

4.5.1(a) Morphology of the Si-doped films vs. SiH_4 concentration

The SEM photographs of the surface morphology of the films grown in CH_4/H_2 system at various Si concentrations are shown in Fig. 4.1 (a-h). Fig. 4.1(a) is the SEM photograph of the nominally pure diamond film supported on Si substrate and has no Si introduced externally. If any Si is present in this film, then it must be only from the supporting Si substrate. With no intentionally added Si, {111} faceted crystals with well-defined crystal habit are obtained. Their growth appears to be determined by the re-entrant corner nucleation [43]. Some of these crystals have crystalline configuration with parallel re-entrant corners, which have their twin planes approximately parallel to the growth direction, i.e. {112} oriented crystals [43] while some of the crystals have the {111} facets angled with respect to substrate plane and there are empty dark spaces between these crystals. On addition of Si to diamond films, the morphology is seen to remain more or less same upto the SiH_4 concentration of 0.83%, but the dark spaces are seen to get filled with additional growth and the twinning effect is seen to increase tremendously till SiH_4 concentration reaches 2.44% in gas phase. For higher concentration of SiH_4, crystal size is seen to increase almost to double of the crystals in the nominally pure diamond film, for e.g., sample prepared using SiH_4 concentration of 0.05 SCCM (0.83%). For further addition of SiH_4, crystallite size appears to increase but the ditches formed between adjacent crystals are seen to accumulate some fine grained material. The sample prepared by using 0.15 cc of SiH_4 has large concentration of the fine grained material accumulated in the troughs formed by the large pyramidal shaped {111) faceted crystals.

The additional growth of grain size without any overgrowth appears to be due to catalytic role of Si. For higher concentration of Si (> 0.075 SCCM) , there is transition to pyramidal morphology with {111} faceted crystals having the growth direction of these pyramid along {100}. The ditches between the grains show accumulation of fine needle shaped crystalline material. This material is likely to be different from

sp^3 bonded carbon, and may be attributed to the presence of either undissolved excess Si seperated out from the diamond phase or SiC phase.

Thus, it appears that the Si does play a role in enhancing the grain size as well as the sharpness of the crystal edges. The average crystallite size for nominally pure film is ~ 1.5 μm whereas the sample with 2.44 % SiH_4 concentration shows the average crystallite size to be ~ 2.5 μm. The increased size of crystallite indicates possible growth process via Si catalytic activity at the surface. The Si being larger in size, is likely to be agitated outward where it forms a sp^3 bonds with the carbon atom underneath and addatom process seperates out Si leaving it seperated from diamond crystal. For very high concentration of SiH_4, Si naturally accumulates outside the grains and enhances the pyramidal growth.

4.5.1(b) XRD Spectra of Si-doped films vs. SiH_4 concentration

The XRD spectra of the nominally pure and Si doped samples are shown in the Fig. 4.2. The sample prepared without SiH_4 addition appears to have no extra diffraction lines in the 2θ range from 20^0 to 110^0. The different diffracting planes of diamond are denoted as D{hkl} henceforth. The huge peak at $2\theta=69.0^o$ that corresponds to d value=1.3599 Å, is attributed to Si {400} planes of the substrate Si which has {100} orientation. The shoulder at $2\theta = 71.62^0$ (d=1.3164 Å) may be attributed to {202} planes of SiC which may be formed at the interface. The samples prepared with Si incorporation shows additional bands from SiC while SiC{202} band becomes well resolved and intensive. For SiH_4 concentrations beyond 0.075 SCCM (1.23%), new bands on both the sides of D{111} line are observed with additional bands from SiC in the 2θ range of $20\text{-}40^0$. Particularly, the band at $2\theta=42.80^0$ (d=2.1110 Å) corresponding to SiC {104} becomes comparable in intensity for the film grown with 0.1 SCCM (1.64%) and 0.15 SCCM (2.44%) SiH_4. These results imply that the formation of SiC is possible at higher concentration of SiH_4. As seen from SEM photograph (figure 4.1 (g) & (h)), the needle-like accumulated material may be identified as polycrystalline SiC. Most of the additional lines may be corresponding to the SiC hexagonal needle.

The ratio of intensity I[D{111}]/I[SiC{202}] is plotted in Fig. 4.3 as a function of gas phase SiH_4 concentration. The variation appears to be slow, but linear

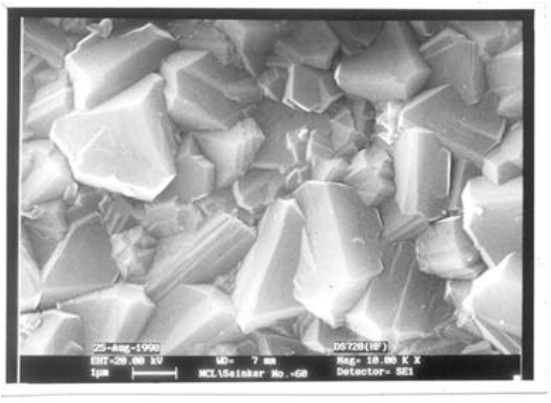
25-Aug-1998
EHT=20.00 kV
WD= 7 mm
DS728(0%)
Mag= 10.00 K X
1µm
NCL\Sainkar No.=60
Detector= SE1

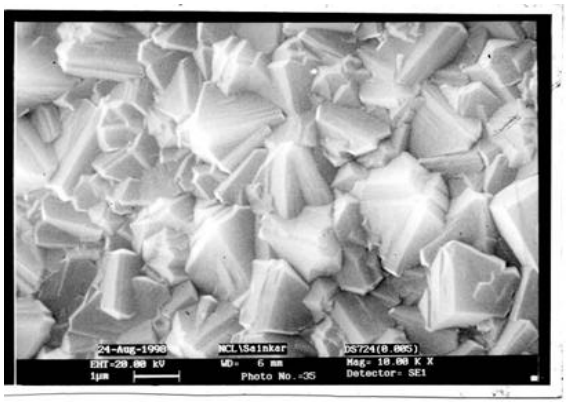
24-Aug-1998
NCL\Sainkar
DS724(0.005)
EHT=20.00 kV
WD= 6 mm
Mag= 10.00 K X
1µm
Photo No.=35
Detector= SE1

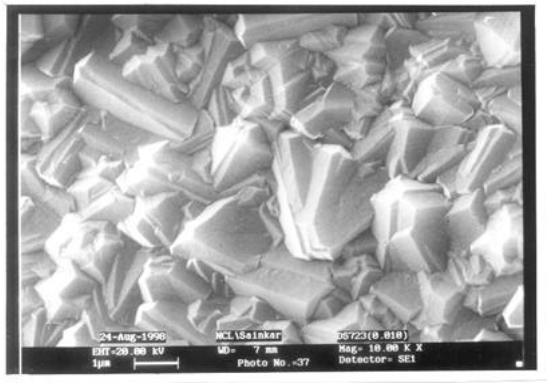
24-Aug-1998
NCL\Sainkar
DS723(0.010)
EHT=20.00 kV
WD= 7 mm
Mag= 10.00 K X
1µm
Photo No.=37
Detector= SE1

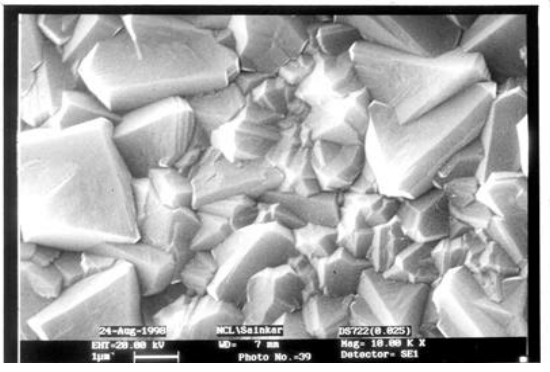
24-Aug-1998
NCL\Sainkar
DS722(0.025)
EHT=20.00 kV
WD= 7 mm
Mag= 10.00 K X
1µm
Photo No.=39
Detector= SE1

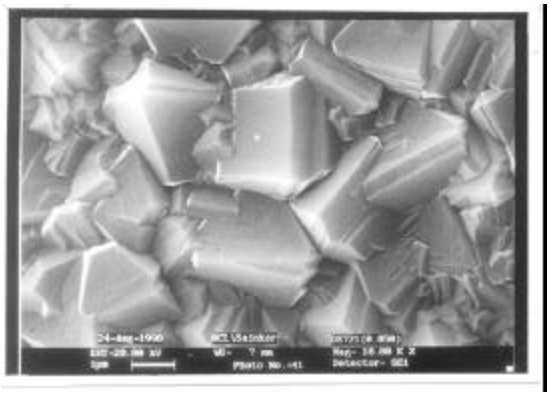
24-Aug-1998
NCL\Sainkar
EHT=20.00 kV
WD= 7 mm
Mag= 10.00 K X
1µm
Photo No.=41
Detector= SE1

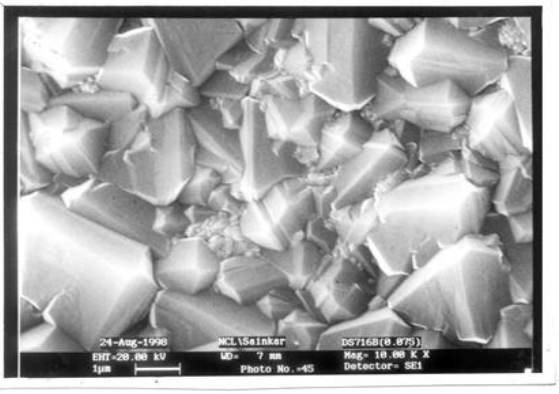
24-Aug-1998
NCL\Sainkar
DS716B(0.075)
EHT=20.00 kV
WD= 7 mm
Mag= 10.00 K X
1µm
Photo No.=45
Detector= SE1

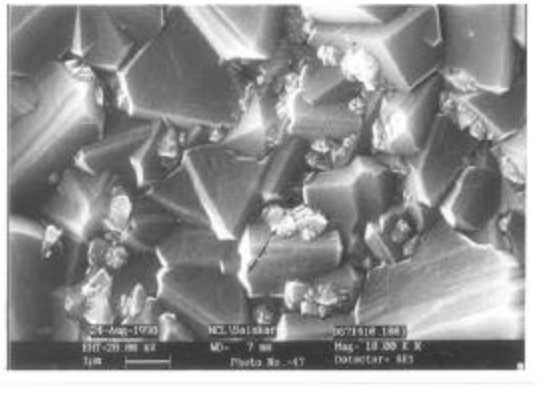
24-Aug-1998
NCL\Sainkar
EHT=20.00 kV
WD= 7 mm
Mag= 10.00 K X
1µm
Photo No.=47
Detector= SE1

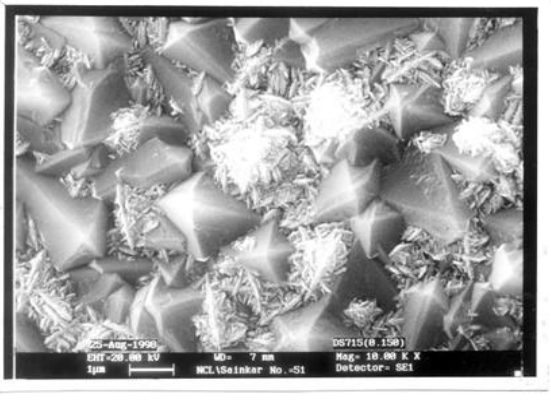
25-Aug-1998
EHT=20.00 kV
WD= 7 mm
DS715(0.150)
Mag= 10.00 K X
1µm
NCL\Sainkar No.=51
Detector= SE1

Fig. 4.1 SEM photographs of the surface morphology of the diamond films grown on Si substrate with different SiH4 concentartions (a) 0% (b) 0.08% (c) 0.17% (d) 0.42% (e) 0.83% (f) 1.23% (g)1.64% & (h) 2.44%.

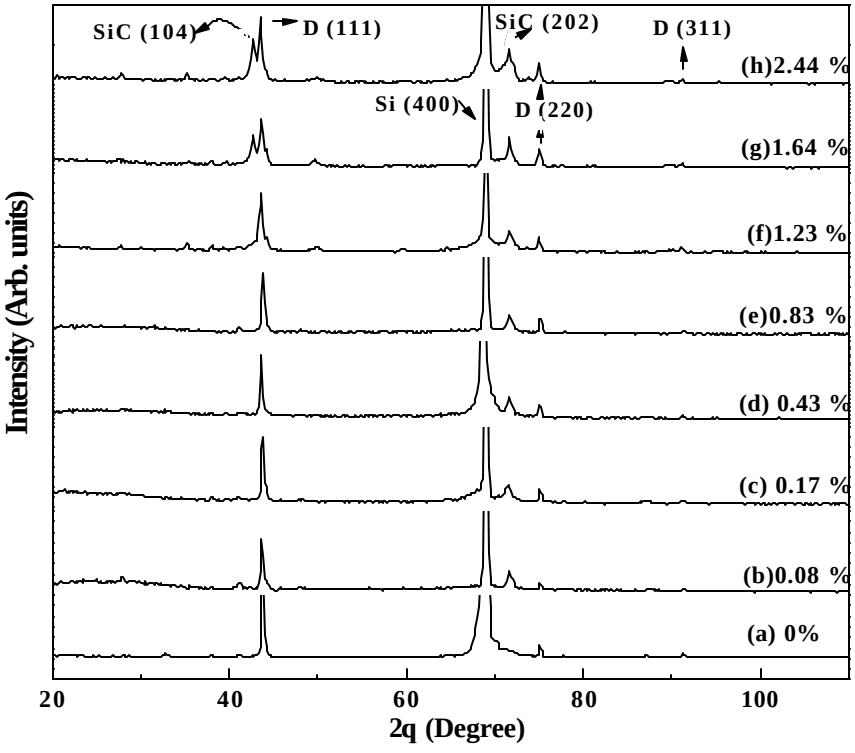

Fig. 4.2 XRD patterns of the diamond films grown on Si substrate with different SiH_4 fractions in CH_4

which implies that the [D]/[SiC] ratio is more or less constant. Such possibility may be attributed to the presence of SiC only at the substrate-film interface. The line width (FWHM) of D{111} band is plotted against the gas phase SiH_4 concentartion (Fig. 4.4) which shows no change in the line width. This may be attributed to the possible segregation of Si atoms to grain boundary rather than its incorporation in the diamond crystals. This segregated Si may be in the form of hexagonal needle shaped SiC as seen before.

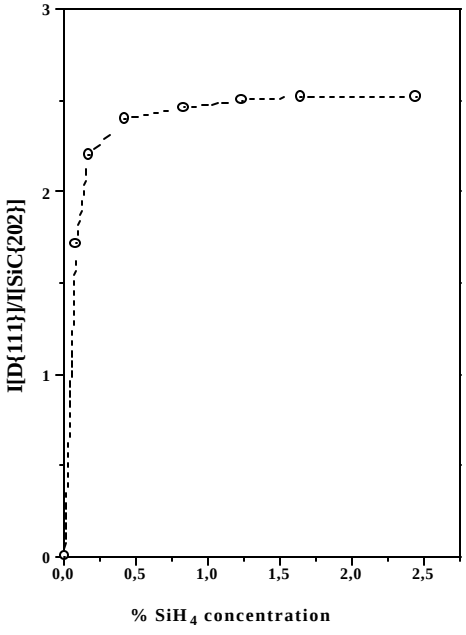

Fig. 4.3 I[D(111)]/I[SiC(202)] as a function of SiH_4 concentration

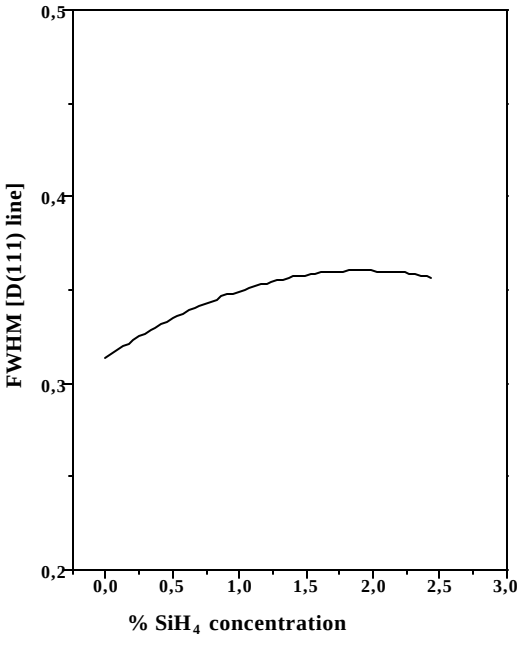

Fig. 4.4 FWHM [D(111) line] as a function of SiH_4 concentration

4.5.1(c) Raman Spectra of Si-doped films vs. SiH_4 concentration

The Raman spectra of the films under this study are shown in Fig. 4.5 where the C-C vibrational bands are expected to show up in the frequency range 1000 to 1800 cm^{-1}. The band corresponding to the sp^3-bonded carbon is present at 1332 cm^{-1} in the spectra of all the films while bands corresponding to sp^2 bonded carbon are almost not seen at 1550 cm^{-1}. In fact, the scattering cross section of the sp^2 bonded carbon is 50 times larger than that of sp^3 bonded carbon [44,45]. Hence, it is possible to conclude that the film shows purely sp^3 bonded structure, and the sp^2 bonded species are almost absent. It is likely that the sp^2 bonded carbon which is generally present at the grain boundary is consumed by segregating Si and forming the seperated SiC phase. The FWHM of the 1332 cm^{-1} band plotted as a function of gas phase SiH_4 concentration (Fig. 4.6) shows almost linear increase for lower concentration and saturates for higher concentrations of SiH_4. This implies that, as the Si solubility in diamond is low, the

diamond lattice gets saturated with Si impurity for [SiH_4]< 0.83%. This causes dilation of the diamond lattice

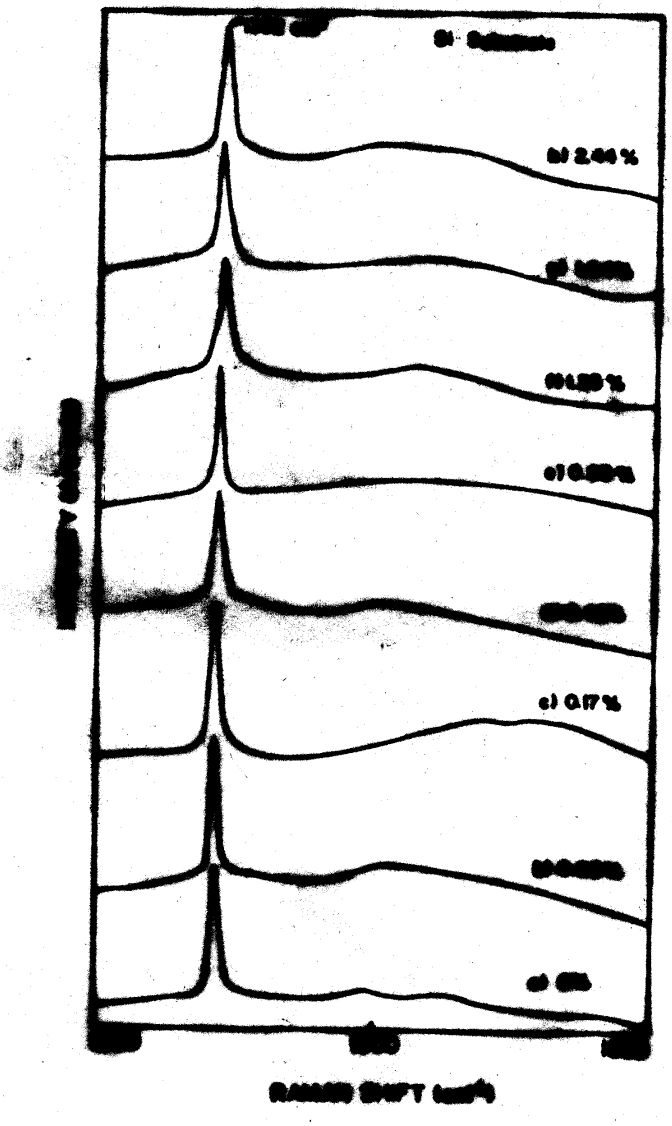

Fig. 4.5 Raman spectra (normalized for 1332 cm^{-1} band) of the Si-doped diamond films grown on Si substrate as a function of Silane concentration

and increases the FWHM of the 1332 cm^{-1} Raman band. Since the atomic size of Si is almost 50% larger than the size of carbon atom, its accomodation at a regular diamond lattice site is likely to distort the lattice locally. As Si has strong tendency for forming sp^3 bonds, its accomodation may require displacement of two carbon atoms [36] and this may result in Si-vacancy structure. Moreover, Si-C bond is more stronger than Si-Si bond and therefore accommodation of pair of Si atoms at one site is unlikely [36]. Though, the pair of Si atoms may be bonded to one carbon atom which may lead to larger distortion. The samples prepared with larger concentration of SiH_4, however, do not show such behavior in XRD. The enhancement of a sp^3 bonding resulted due to Si is seen through the growth of larger crystallite for higher SiH_4 concentration. The segregation of Si to the surface of the grain is therefore, likely to act as catalyst for adding carbon atoms to the growing crystallite.

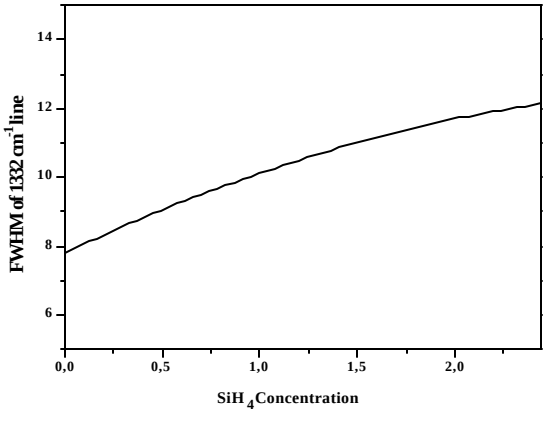

Fig. 4.6 FWHM of the 1332 cm^{-1} Raman line as a function of SiH_4 concentration

4.5.1(d) Photoluminescence Spectra of Si-doped films vs Si concentration

The photoluminescence spectra of some of these films were excited by using the Ar^+ ion laser lines at 514.5 nm and 488.0 nm and are plotted as PL intensity as a function of shifted frequency from the excitation radiation frequency. The PL spectra of the nominally pure (undoped) diamond film excited with both the lines are shown in Fig.4.7. There are two sharp bands unshifted with respect to the excitation radiation frequency, positioned at 520 cm^{-1} and 1332 cm^{-1}. These are vibrational Raman bands which are well-known to originate from the

excitation of transverse optical modes of Si and diamond crystals respectively. The 520 cm^{-1} band is attributed to the single crystal Si

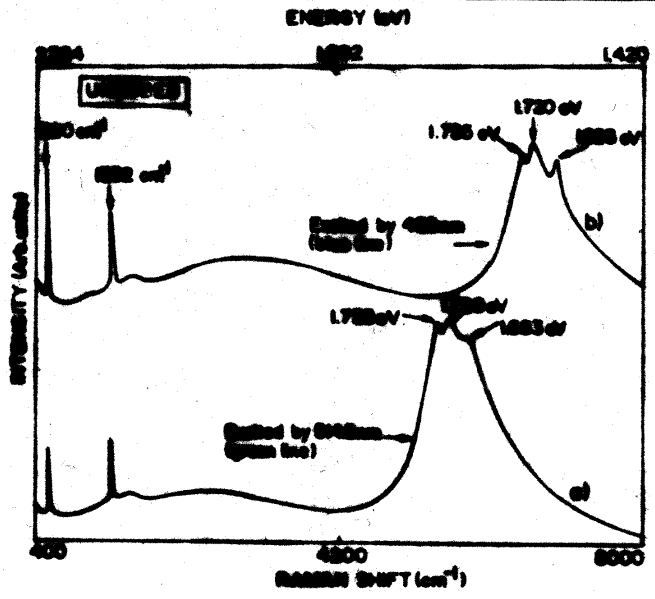

Fig.4.7

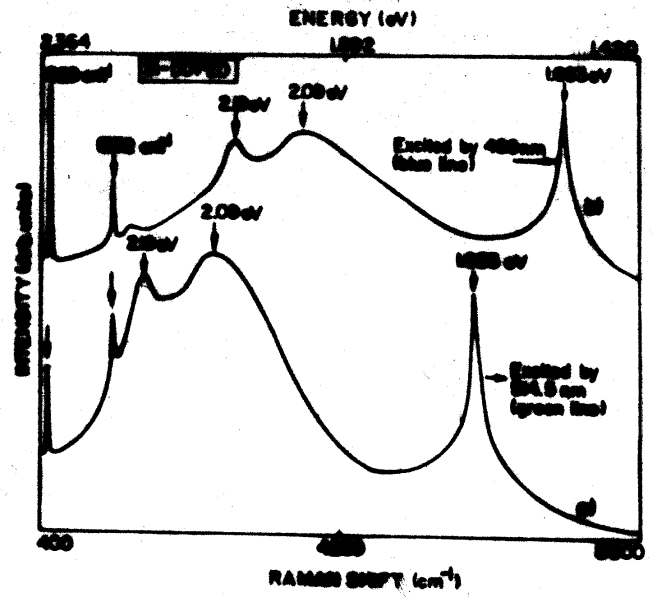

Fig.4.8 The PL Spectra of the Si-doped diamond film corresponding to a) 514.5 nm and b) 488 nm excitation radiation.

substrate. As the optical band gap of diamond is ~ 5.5 eV, the diamond film deposited on Si substrate is transparent to both the excitation radiations, viz. 2.41 eV and 2.54 eV. Hence, these excitation radiations can easily reach to the supporting Si substrate. Moreover, Si has optical band gap of ~ 1.1 eV, and therefore, for the given excitation radiation frequency, it gives rise to resonant Raman scattering at 520 cm^{-1} which is attributed to single phonon scattering from TO-vibrational modes with K=0. This Raman scattered radiation has photon energy of 2.2 eV and hence can travel backward with less absorption through the diamond films. Hence, the sharp band at 520 cm^{-1} can only come from the Si-substrate [46].

Similarly, the 1332 cm^{-1} band is attributed to the excitation of transverse optical mode of the single crystal diamonds deposited on the Si substrate [47]. Since the band gap of diamond is 5.5 eV, the excitation radiation with photon energy < 5 eV can only produce normal Raman scattering with low scattering (cross section)efficiency. Additional unshifted (with respect to excitation radiation) weak but considerably broad band is also seen to be centered at ~ 1550 cm^{-1} which can be attributed to the vibrational Raman band from the amorphous sp^2 bonded graphitic carbon [48]. In fact, the scattering cross section for sp^2 bonded non-transparent graphitic material is almost 50 times larger than the sp^3 bonded transparent diamond material. This implies that for the comparison of proportion of such sp^2 bonded amorphous carbon with respect to sp^3 bonded crystalline diamond phase, the intensity of the 1550 cm^{-1} bands needs to be reduced by a factor of ~1/50 (0.02). On doing the reduction, the amorphous phase would appear to be negligibly small in concentration. The possible location of the graphitic amorphous phase, if any present, would be only at the surface of the diamond film or trapped between the diamond crystallite boundaries.

The shifted frequency range 2000 cm^{-1} to 8000 cm^{-1} in the spectra excited by 514.5 nm and 488.0 nm are seen to have corresponding bands similar in shape and size but shifted from each other by the frequency difference of the excited frequency. Hencce, these bands may be attributed to a possible PL emission. The shifted PL bands and unshifted Raman bands with the excitation by 514.5 nm (19432 cm^{-1}) and 488 nm (20492 cm^{-1}) laser lines are summarized in Table-4.3.

Table-4.3 Positions of various bands with different excitation laser lines

Band Position when the excitation laser line is 514.5nm (19432 cm^{-1})	**Band Position when the excitation laser line is 488nm (20492 cm^{-1})**	**Identification of the band (Raman/PL)**
520 cm^{-1}	520 cm^{-1}	Raman
1332 cm^{-1}	1332 cm^{-1}	Raman
1748 cm^{-1} (2.19 eV)	2808 cm^{-1} (2.19 eV)	PL
2612 cm^{-1} (2.09 eV)	3672 cm^{-1} (2.09 eV)	PL
5456 cm^{-1} (1.735 eV)	6516 cm^{-1} (1.735 eV)	PL
5580 cm^{-1} (1.720 eV)	6640 cm^{-1} (1.720 eV)	PL
5880 cm^{-1} (1.683 eV)	6940 cm^{-1} (1.683 eV)	PL

For nominally pure diamond film, the weak but very broad band centered at ~2700 cm^{-1} is generally known to come from PL emission by sp^2 bonded carbon species. Since these species are small in concentration, the band intensity is also low. On the other hand, there are intense broad bands centered at 5580 cm^{-1} and 6640 cm^{-1} respectively from 514.5 nm and 488 nm excitation. Since the excitation frequency is shifted by ~1060 cm^{-1}, the 5580 cm^{-1} band is also shifted by ~1060 cm^{-1} to 6640 cm^{-1} for 488.0 nm. This clearly indicates that the band near 5580 cm^{-1} or 6640 cm^{-1} is an photoluminescence band. This band is composed atleast of three bands peaking at 1.735 eV, 1.720 eV and 1.683 eV. These bands have been reported in literature to originate from what is known as General Radiation (GR1) [14] emitted by defect centers formed by general carbon vacancies in the crystal lattice. Multi-component nature of this band may be attributed to various possible strain shifted defect energy levels from where the transitions may take place.

The PL spectra of the Si doped diamond film corresponding to excitation radiation 514.5 nm and 488.0 nm from the Ar^+ ion laser are shown in Fig. 4.8. The vibrational bands corresponding to single crystal silicon substrate and the deposited diamond crystals are seen to be positioned at 520 cm^{-1} and 1332 cm^{-1} respectively. The vibrational spectrum excited by 514.5 nm radiation is seen to have strong background from PL bands peaking at 1748 cm^{-1} (2.19 eV) and 2612 cm^{-1} (2.09 eV), whereas the same PL bands are seen to shift to higher wavenumber positions at 2808 cm^{-1} (2.19 eV) and 3672 cm^{-1} (2.09 eV) respectively when excited by the high frequency radiation 488.0 nm. In the latter case, the broad weak band corresponding to graphitic sp^2 bonded carbon is seen to emerge at 1550 cm^{-1}. The strength of

this band is so weak that it only accounts for the negligibly small amount of this phase which may only be present at the film surface or in the space between the crystallites. The origin of the PL emission broad band positioned at 1748 cm^{-1} (2.19 eV) and 2612 cm^{-1} (2.09 eV) is still not clear. Bergman et. al [7] have proposed that this emission may be the result of amorphous sp^3 bonded carbon phase which produces defect state distribution in the band gap. These broad band PL spectra are similar to those formed in the amorphous hydrogenated carbon material which possesses sp^2 and sp^3 bonding configuration [49,50].

The photoluminescence spectra of the diamond films grown on Si substrate as a function of silane fraction in the feed gas are shown in Fig.4.9. The broad bands observed in the PL spectra of our samples are similar to those observed in many studies of the amorphous hydrogenated carbon material (a-C:H) which possess a random network of sp^2 and sp^3 bonding configuration [49,50]. The line shape and the peak position of these spectra is reported to vary from sample to sample depending on the growth condition which affect the atomic distribution and short range order (SRO) in these films. The variation in the SRO can produce variation in the band tail states and therefore the broad PL (a-C:H) has been assumed to originate from the transitions in the exponential distribution of tail states which extend into the forbidden gap. Inclusion of sp^2 bonded material is also probable in our samples.

The GR1 band observed at 1.720 eV for the undoped diamond film seems to be suppressed drastically in Si doped diamond films and relatively sharp band at 1.683 eV is observed. Since the band is sharp and observed after incorporating Si in the film, it may be obvious to correlate to ZPL transition from Si impurity in the diamond lattice. The origin of this line has been investigated by many researchers [19,29,36,51,52]. The possible source for the origin of this Si-related line in the PL spectra is discussed as follows. The PL broad band centered at 1.720 eV has been observed in the diamond films prepared by hot filament CVD [40]. The origin of this band is in general attributed to clustered vacancies in diamond crystals. Inclusion of such clusters of upto six vacancies, a size which is thought to be a particularly stable cluster, are possible in diamond crystal structure [40]. These vacancy clusters in the diamond films have been detected by positron-lifetime spectroscopy. However, these studies indicated completely inhomogeneous distribution of these vacancies in various crystallites depending upon the deposition technique as well as deposition parameters. The disappearance of the 1.720 eV

band in the Si doped sample indicates that the Si can dramatically reduce such clustered vacancy content in diamond films. Similar results are also observed by Dannefaer et al.

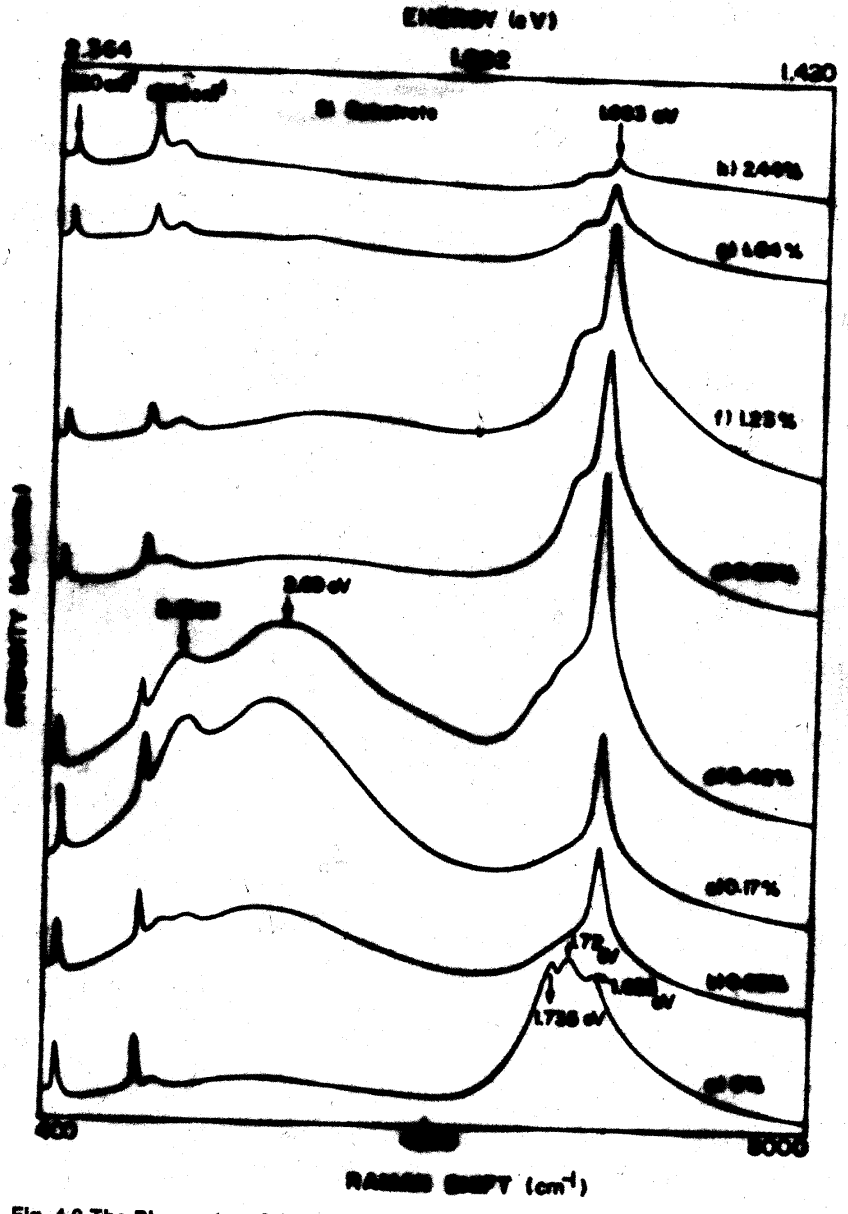

Fig. 4.9 The PL spectra of the Si-doped diamond films grown on Si substrate as a function of Silane concentration (excitation radiation = 514.5 nm laser line)

[40] and their positron life time measurements have indicated presence of monovacancies in large fractions compared to the other clustered vacancies. It is likely that Si atoms doped in diamond may get trapped at these clustered vacancies which may eventually get converted into monovacancies. The increase in concentration of incorporated Si further decreases the intensity of 1.720 eV band and increases the intensity of 1.683 eV band. These results suggest the possibility of Si-monovacancy complexes in the Si doped diamond films [40].

Thus, the intensity of the 1.683 eV line ($I_{1.683}$) is observed to strongly depend on the SiH_4 concentration. $I_{1.683}$ first increases with SiH_4 concentration, reaches a maximum at 0.42% of SiH_4 and then decreases for further increase in SiH_4 concentration. The dependence of $I_{1.683}$ on silane concentration is plotted in Fig. 4.10. This dependence of PL intensity on the SiH_4 concentration can be explained using the concept of luminescence efficiency which is defined as the number of photons emitted per incident photon absorbed by the material. An excited activator center, which has absorbed an incident photon, returns to the ground state with emission of a photon only if there is no other activator center within a sphere of radius R around a central activator atom[53]. In other words, the activators interact with each other in such a way that if the distance between them is < R, they can quench each other. Therefore, for small concentrations of the activators, the luminescence efficiency increases proportionally with the concentration whereas for high concentrations, the mutual quenching takes over leading to a decrease in the luminescence efficiency and therefore of PL intensity.

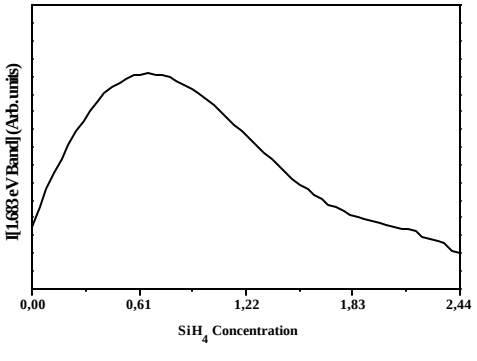

Fig.4.10 Photoluminescence Intensity of 1.683 eV band as a function of SiH_4 concentration

4.5.2 Effect of Substrate Temperature (T_s) on Si incorporation in diamond films

In order to study the growth behavior and properties of diamond films as a function of substrate temperature (T_s), the films were grown with and without SiH_4 in the source gas mixture for 3 hours at temperatures varying from 750^0C to 950^0C keeping all other deposition parameters identical, i.e. (a) gas flow rate=300 SCCM, (b)CH_4 conc.=2 %, (c) SiH_4 fraction in methane=0.83%, (d) chamber pressure=30 Torr (e) T_f=1950^0C,and (f) deposition period=180 min.

4.5.2(a) Surface Morphology of the Si doped Films vs. Substrate Temperature

Fig. 4.11(a-f) shows SEM photographs of the surface morphology of the nominally pure (undoped) and Si-doped films deposited at substrate temperatures of 750, 850 and 950 ^{0}C. The morphology of the undoped films (Fig. 4.11 a,c,e) shows single crystals or twinned diamond particles with the {111} planes of these particles lying parallel to the substrate. The morphology changes from crystallites having {111} facets parallel to substrate, to pyramidal crystals at 950^0C. The average crystallite size is seen to increase with increase in deposition temperature. For the film grown at T_S=750^0C, the average grain size is ~0.75 μm which is seen to increase to ~1.0 μm and ~1.5 μm for the films grown at T_s = 850 and 950^0C respectively. The increased T_s provides higher creep velocities to the deposited species on the substrate which allows the particles to grow in bigger size. The films grown with fixed silane fraction (0.83%) and at varied substrate temperatures (T_s) also showed similar trend in the variation of surface morphology (Fig.4.11 b,d,f). In case of the films grown at higher substrate temperature ($T_s > 850^0$C), the incorporated Si is observed to segregate and get accumulated at the grain boundaries in the form of fine needle shaped crystalline material. In case of the films grown at lower T_s, Si is not observed to separate out from the diamond phase, and it may, therefore, be assumed to get trapped in the vacancies in the crystals .

4.5.2(b) XRD Spectra of Si doped films vs. Substrate temperature

The XRD patterns of the undoped diamond films grown at T_s=750, 850 and 950^0C are shown in Fig. 4.12. They show prominent diamond signatures and the overall film crystal orientation is observed to be {111}. With the increasing substrate

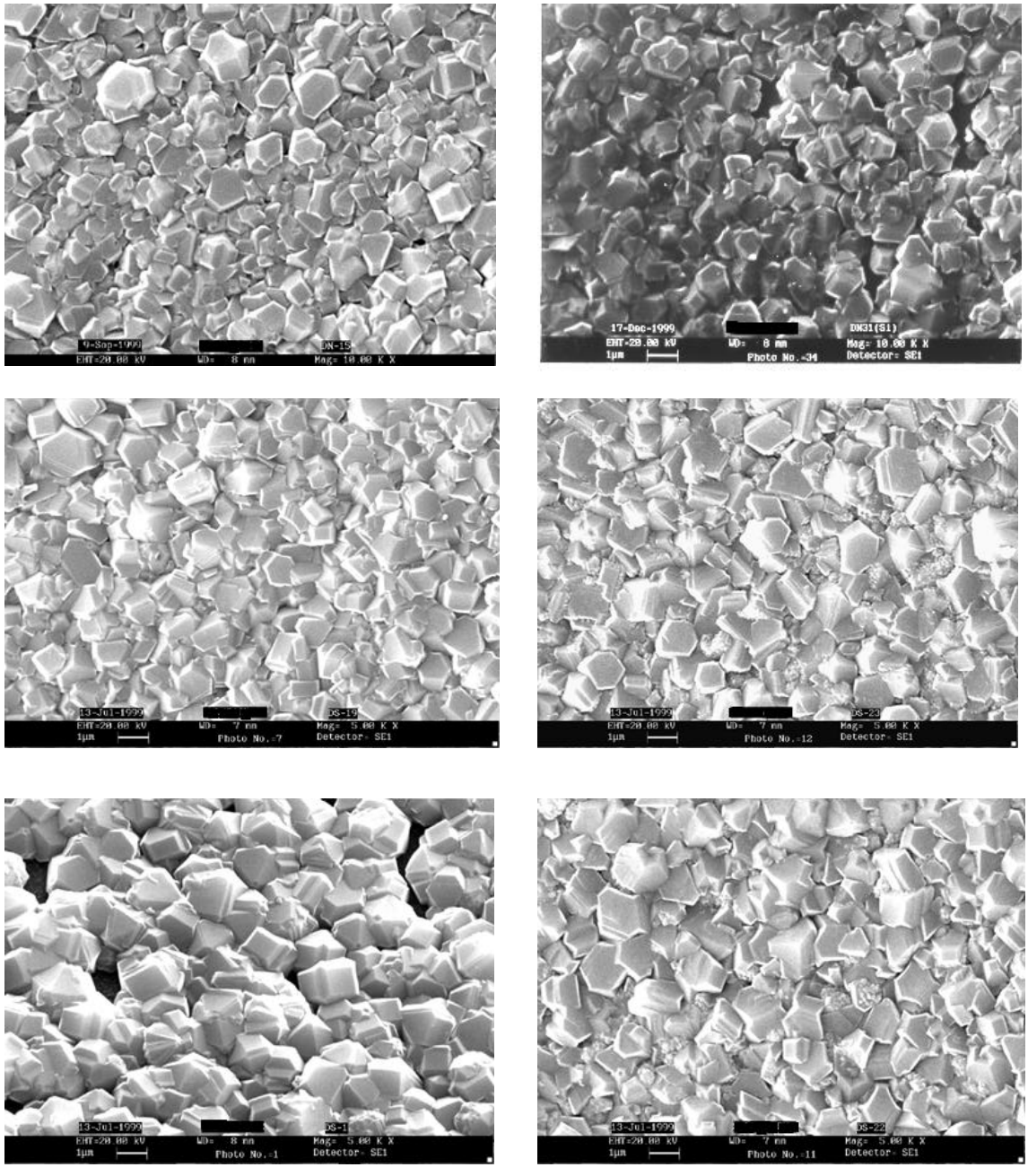

Fig. 4.11 SEM photographs of the surface morphology of the undoped and Si-doped (0.83%) diamond films grown on Si substrate as a function of T_s. (a), (b), (c) : undoped diamond films and (d), (e), (f): corresponding Si-doped diamond films grown at T_s=750,850 and 950^{0}C respectively.

temperature, the intensity of D(111) line is observed to increase indicating the increase in the number of crystallites having {111} orientation. This implies that the growth rate is increased with increase in substrate temperature. As the substrate temperature is increased, additional lines at $2\theta=42.925^0$ (d=2.1052 Å) and 71.525^0 (d= 1.3180 Å) corresponding to SiC{104} and SiC{202} are observed. This SiC may be formed at the diamond-Si substrate interface during the high temperature growth of the film. The Si-doped diamond films also exhibit similar spectra as shown in Fig. 4.13. In this case, additional line at $2\theta= 32.80^0$ (d=2.728 Å) corresponding to SiC(100) is observed which may be due to the *insitu* incorporation of Si during growth.

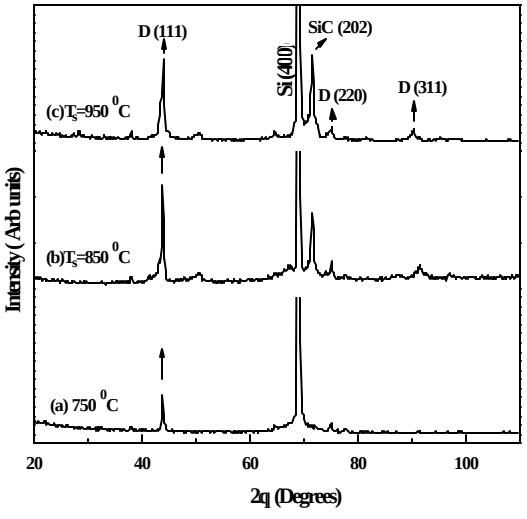

Fig. 4.12 XRD patterns of the undoped doped diamond films as a function of T_s

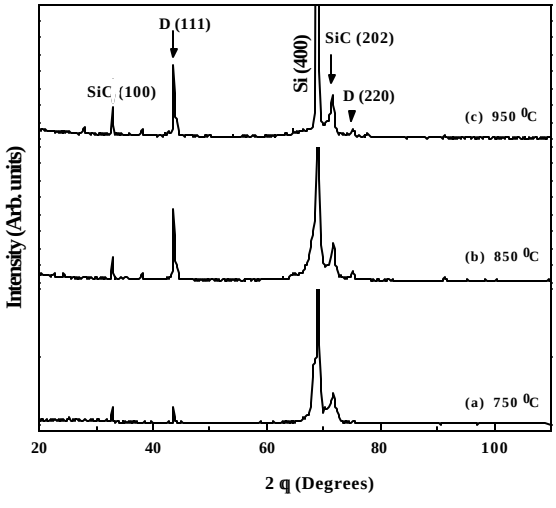

Fig. 4.13 XRD patterns of the (0.83% SiH_4) diamond films as a function of T_s

4.5.2(c) Raman Spectra of Si doped films vs. Substrate temperature

The Raman spectra of the undoped films grown at T_s=750, 850 and 950^{0}C are shown in Fig. 4.14. They exhibited a sharp band at 1332 cm^{-1} which indicates the presence of diamond crystals. With the substrate temperature, the intensity of the 1332 cm^{-1} band is found to increase as a result of increase in particle size of the crystallites in the film. These results clearly indicate increase in the growth rate of the film. Since there are no signals due to sp^2 bonded graphitic carbon, it may be understood that these films contain purely diamond crystals and graphitic carbon is almost absent in these films. The Raman spectra of the Si-doped (0.83%) diamond films grown at the above substrate temperatures also exhibited similar behavior as shown in Fig. 4.15.

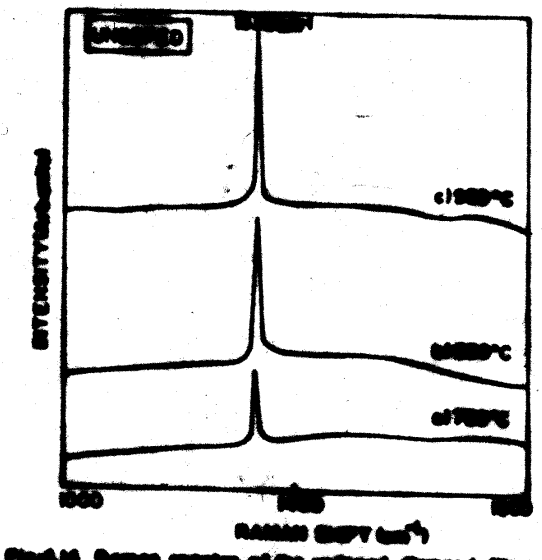

Fig:4.44 Raman spectra of the undoped diamond films grown on Si substrate vs substrate temperature.

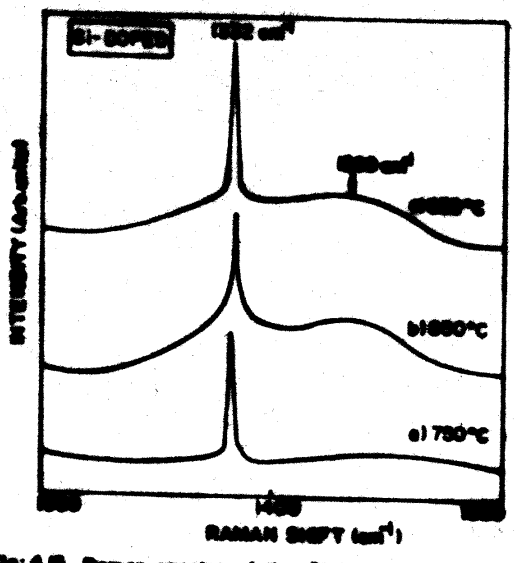

Fig: 4.45 Raman spectra of the Si-doped diamond films grown on Si substrate vs substrate temperature.

4.5.2(d) Photoluminescence Spectra of Si doped films vs. substrate temperature

Fig. 4.16 shows variations in PL spectra of undoped diamond films grown on Si<100> substrate as a function of substrate temperature. Each of these PL spectra shows the presence of bands at 1.72 eV and 1.68 eV. Their relative intensity ($I_{1.72}/I_{1.68}$) is seen to increase with the substrate temperature (T_s). In case of the film grown at T_s=750^{0}C, ($I_{1.72}/I_{1.68}$) is minimum whereas this ratio is found to increase with the substrate temperature. The presence of 1.68 eV line in the PL spectra of the film, at first sight, apparently needs to be attributed to Si incorporation in the film, where the Si being assumed to come from the Si-substrate surface. As the substrate temperature is increased, the growth rate is almost doubled (as seen from Fig. 4.11). In case of Si, its size being bigger as compared to carbon, it may not get diffused into the bulk of the film but may remain at the film-substrate interface only or may form SiC. This may be the reason of getting additional lines due to SiC in the XRD spectra of the films grown at higher substrate temperatures of 850 and 950^{0}C. With increasing substrate temperature, the intensity of the band at 1.72 eV is found to increase. This implies that the number of multiple vacancies formed during the growth has now increased. At higher substrate temperature, the mobility of the depositing species on the the substrate may be higher resulting in the fast nucleation and enhanced growth rate. During the fast growth, more number of vacancies remain unoccupied and give rise to multiple vacancies. Thus, the increase in growth rate can be responsible for the formation of increased number of clustered vacancies. As a result, density of the defects induced by Si atom decreases and therefore, for higher temperature T_s = 950^{0}C, the band at 1.68 eV is weak (Fig. 4.16 c). At T_s = 750^{0}C, the growth rate is low and Si impurity may get enough time to diffuse into the bulk of film and enter into the clustered vacancies converting them to the monovacancies and hence the band at 1.68 eV is prominent (Fig. 4.16 a) in the PL spectra of the film grown at 750^{0}C [40].

In case of the Si doped films grown with lower T_s , Si is not observed to separate out from the diamond phase (as seen from surface morphology in Fig. 4.11), but may be getting diffused in the diamond crystals or trapped in the vacancies in the crystals. Therefore, as observed in the case of undoped films grown at different T_s, the PL

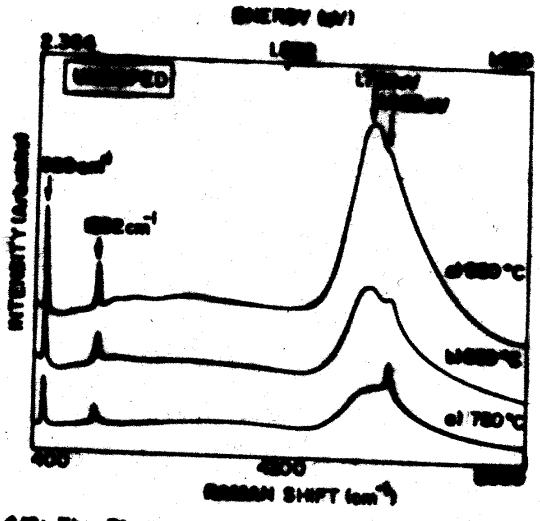

Fig. 4.16: The PL spectra of the undoped diamond films grown on Si substrate vs. substrate temperature.

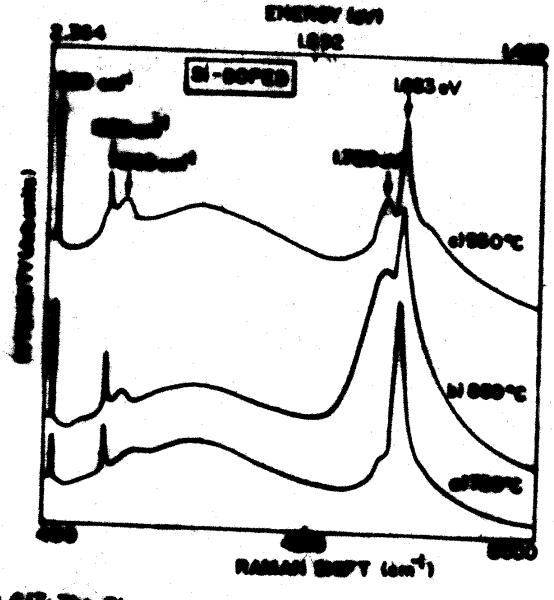

Fig. 4.17: The PL spectra of the Si-doped diamond films grown on Si substrate vs. substrate temperature.

spectrum in this case also shows the sharp and intense 1.68 eV line in the film grown at 750^0C (Fig. 4.17). As the deposition temperature is increased, the excess Si is seen to segregate out

and to get accumulated at the grain boundaries and thus the PL intensity of 1.68 eV line is also observed to decrease with increase in T_s .

4.5.3 Diamond Films deposited on Non-silicon Substrates vs. Si doping

In the previous section, we have presented the results on the effect of incorporation of Si on the growth and properties of diamond films grown on Si substrate. However, the use of Si substrate is likely to interfere with the correlation of results to the externally incorporated Si. To resolve the possible substrate interference to Si doping, the films were grown on electronic grade alumina (Al_2O_3) and copper (Cu) substrates. The films were grown at T_s=750^{0}C for 3 hours, keeping other parameters identical as mentioned in Table-4.1.

4.5.3(a) Diamond films on Alumina Substrate

Fig. 4.18 shows the representative SEM photographs of the surface morphology of the films grown with 0% and 0.83% SiH_4 fractions in CH_4 and corresponding EDAX spectra. From the SEM photographs, it is observed that the surface of the undoped (0% SiH_4) film is made up of cubo-octahedral shaped diamond particles with well developed {111} facets. Growth rate as estimated from SEM measurements of the cross section was ~1.3 μm/hr. The high nucleation density ~ 1.2 x 10^8 cm^{-2} is characteristic of the abrading of the alumina substrate with diamond powder. On the other hand, the Si doped film shows low nucleation density with degradation in the overall quality of the film. The EDAX spectrum of the undoped film (Fig. 4.18 b) shows the presence of C $K_á$ (at energy value 0.277 keV) peak. The spectrum shows some more peaks belonging to (i) Al $K_á$ (1.486 keV) and O $K_á$ (0.525keV) attributed to the alumina substrate, (ii) Au$M_á$ (2.122 keV) attributed to the gold deposited on the sample surface for avoiding charging of the sample. Alongwith these peaks, additional peak at 1.739 keV belonging to Si$K_á$ is observed in the EDAX spectrum of Si-doped diamond films (Fig. 4.18 d-f) and thus, confirmed the presence of Si in the films. Fig. 4.19 shows the PL spectra of the films grown on Al_2O_3 substrate. In the PL spectrum of the undoped film grown on Al_2O_3 substrate, the band at 1.681 eV is absent whereas the Si doped films clearly show a sharp band at 1.681 eV. The intensity of this band was found to be dependent on SiH_4

concentration as observed earlier (in case of Si substrate). Fig. 4.20 shows the Raman spectra of these films. These spectra exhibited the band at 1332 cm^{-1}, indicating the presence of diamond crystallites. In this case also, the line width of the diamond line is observed to increase with the SiH_4 concentration. The XRD patterns of the nominally pure and the Si doped (0.83%) diamond films grown on Al_2O_3 substrate were recorded in 2θ range from 40^0 to 48^0 and are shown in Fig. 4.21. These patterns show the overall orientation of crystallites in the film to be {111}. Thus, the results are consistent with the results observed in case of Si substrate.

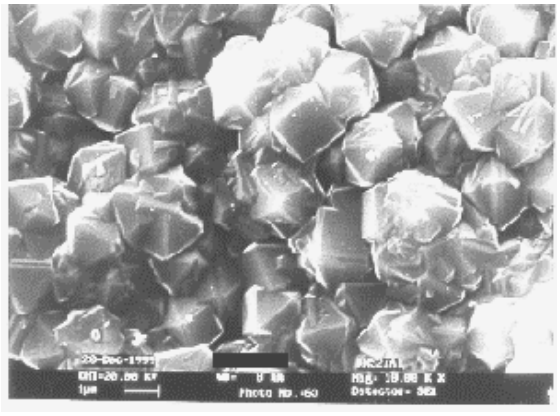

(a)

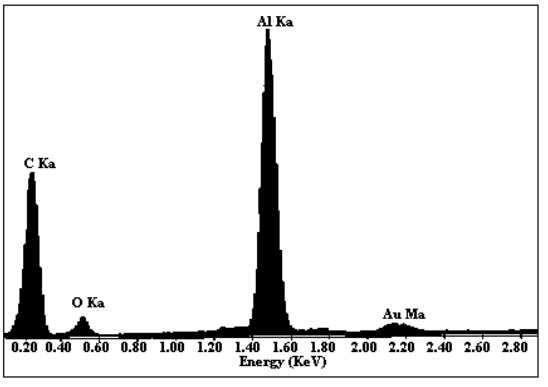

(b)

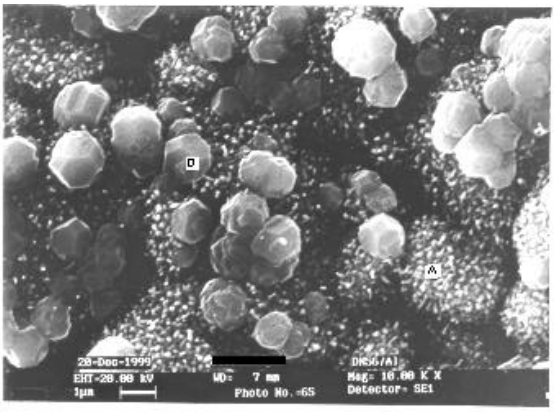

(c)

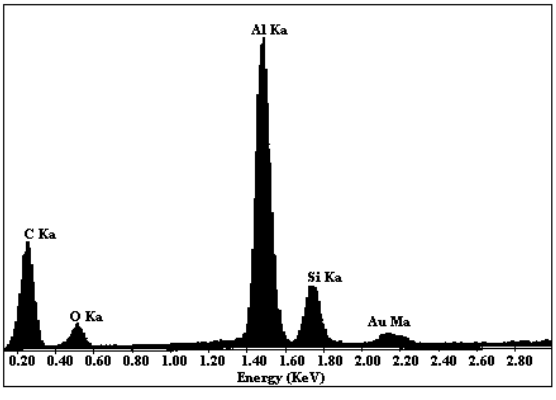

(d)

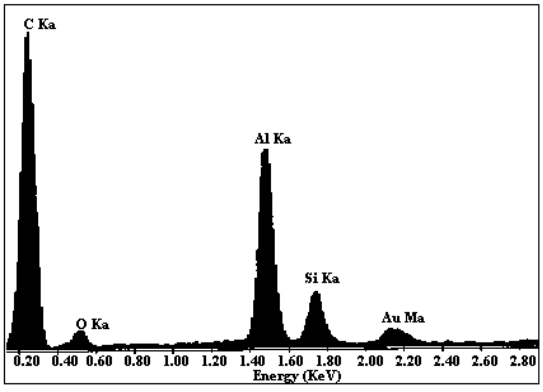

(e)

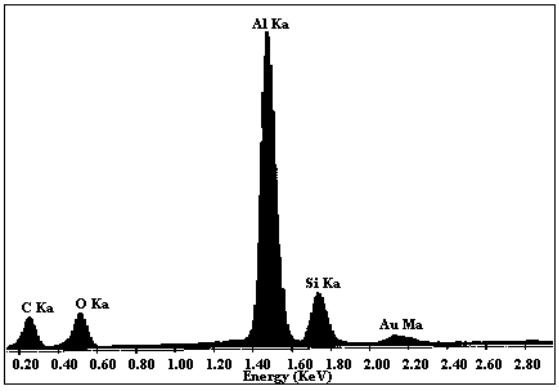

(f)

Fig. 4.18 (a) SEM photograph and (b) EDAX spectrum of the pure diamond film grown on Al_2O_3 substrate (c) SEM photograph of the film grown on Al2O3 substrate with 0.83% SiH_4 concentration(d) EDAX spectrum of the film when electron probe covers entire area of fig. c (e) EDAX spectrum when the probe is on the area marked D in fig. c, and (f) EDAX spectrum when the probe is on the area marked A in fig. C

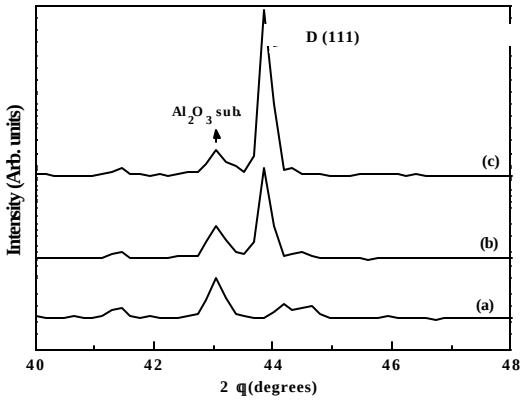

Fig. 4.21 XRD patterns of the diamond films grown on Al_2O_3 substrate
(a) Al_2O_3 substrate only
(b) pure diamond film and
(c) film grown with 0.83% SiH_4 fraction in CH_4

Chapter 4
Si incorporation in Diamond Films

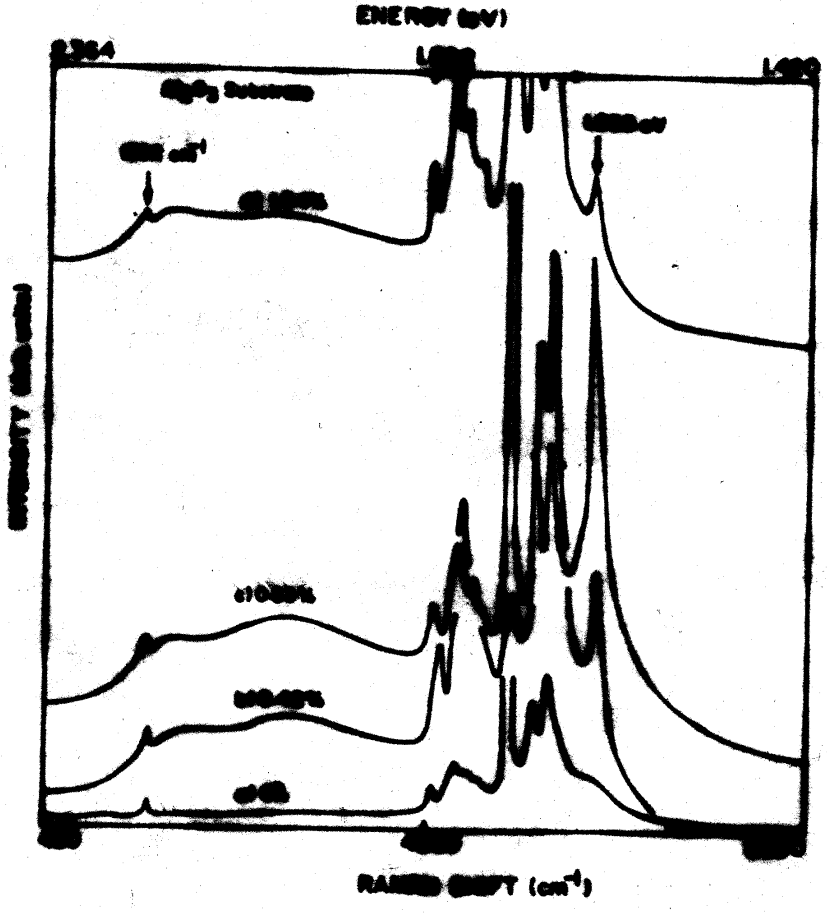

Fig. 4.19 The PL spectra of the Si-doped diamond films grown on Al_2O_3 substrate as a function of Silane concentration (the bands between 1.89 eV and 1.74 eV are due to the PL emission from Al_2O_3 substrate)

4.5.3(b) Diamond films on Copper Substrate

The surface morphology and the corresponding EDAX spectra of the nominally pure (0% SiH_4) and Si-doped (0.83% SiH_4) films grown on Cu substrate are shown in Fig. 4.22. The $CK_á$ (0.277 keV) peak is clearly observed in the spectra of undoped diamond film. The spectrum showed some more peaks belonging to (i) $CuL_á$ (0.93 keV), Cu $K_á$ (8.040 keV) and Cu $K_ß$(8.904 keV) attributed to copper substrate and (ii) $AuM_á$ (2.122 keV) attributed to the gold deposited on the sample surface. Alongwith these peaks, additional peak at 1.739 keV belonging to $SiK_á$ is observed in the EDAX spectrum of Si-doped diamond film. The XRD patterns of the diamond films grown on Cu substrate with and without SiH_4 are shown in Fig. 4.23. The overall orientation of the crystallites in the film is observed to be {111}. In the XRD pattern of the film grown with 0.83% SiH_4 fraction in CH_4, additional line at $2\theta=42.70^0$ (d= 2.1152 Å) is observed which is assigned to SiC (104). The Raman spectra of these films exhibited the sharp band at 1332 cm^{-1}, indicating the presence of diamond crystallites (as shown in Fig. 4.24). Fig. 4.25 shows the PL spectra of the undoped and Si doped diamond films grown on Cu substrate. In the PL spectrum of the undoped diamond film grown on Cu substrate, a broad band centered at about 1.716 eV with a small humps at 1.683 eV and 1.736 eV is observed while for the Si doped film, a sharp band at 1.683 eV is observed.

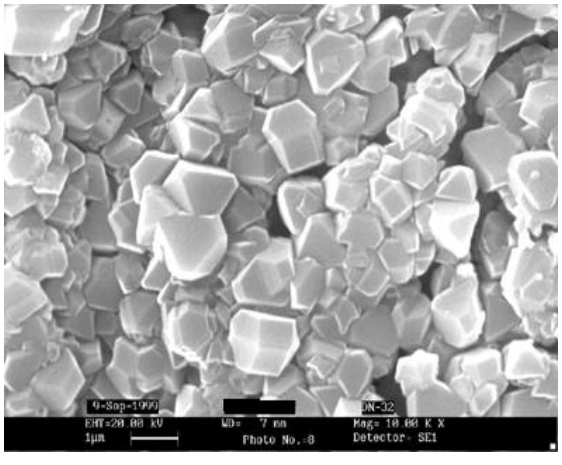

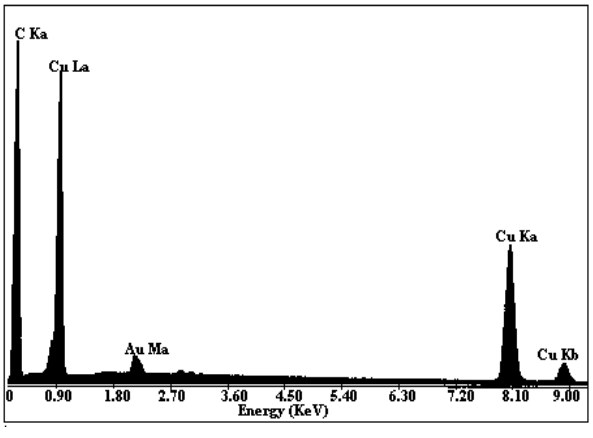

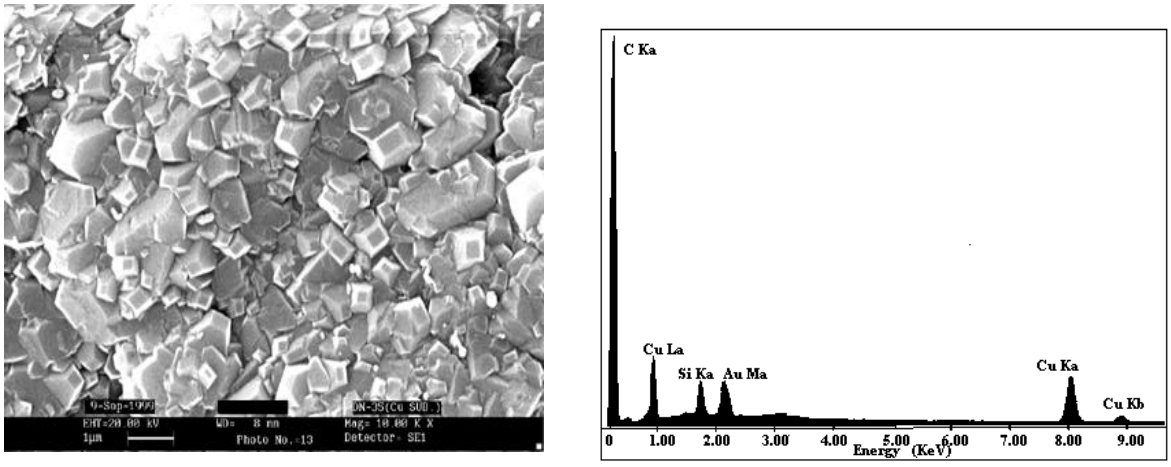

Fig. 4.22 (a) & (b) SEM and EDAX spectrum of the pure diamond film, (c) & (d) SEM and EDAX of Si-doped (0.83%) diamond film grown on Cu substrate.

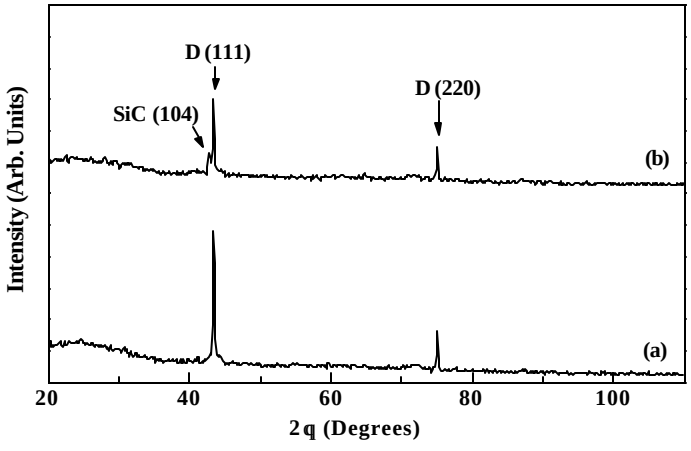

Fig. 4.23 XRD patterns of the diamond films grown on Cu substrate with- (a) 0% and (b) 0.83% SiH_4 concentration.

Thus, the changes produced in the growth characteristics and properties of the diamond films grown with SiH_4 on copper substrate are consistent with those observed in case of silicon and alumina substrates which confirms the reproducibility of the results on different substrates.

4.5.4 Effect of co-doping of Boron along with Si in diamond films

In order to study the effect of *insitu* incorporation of Boron on the growth behavior and properties of nominally pure as well as Si-doped diamond films, B_2H_6 gas was introduced in the mixing unit prior to the entry of precursor gas mixture in the deposition chamber. The different deposition parameters used are listed in Table 4.3.

Table 4.3. Deposition Parameter used for Boron Incorporation

Deposition Parameter	**Value**
Total Gas Flow Rate	300 SCCM
CH_4 Concentration	2 % (6 SCCM)
SiH_4 Flow Rate	0.025 SCCM
B_2H_6 Flow Rate	0.1 SCCM
Filament Temp. (T_f)	1950 ± 50^0C
Substrate Temp. (T_s)	950 ± 20^0C
Deposition Period	4 hrs.

The four types of samples deposited using the above parameters are as follows: (a) nominally pure (undoped) diamond film, (b) the film grown with 0.1 SCCM B_2H_6, (c) the film grown with 0.025 SCCM SiH_4 and (d) the film grown with 0.025 SCCM SiH_4 and 0.1 SCCM B_2H_6 (dual doped).

Fig. 4.26 shows the SEM photographs of the surface morphology of the above films. The surface morphology of all the films is seen to remain more or less same showing {111} faceted, pyramidal shaped crystals with well defined crystal habits. Raman spectra of these films (Fig. 4.27) also do not show any appreciable variation. All the spectra show the sharp 1332 cm^{-1} band indicating the presence of diamond crystallites.

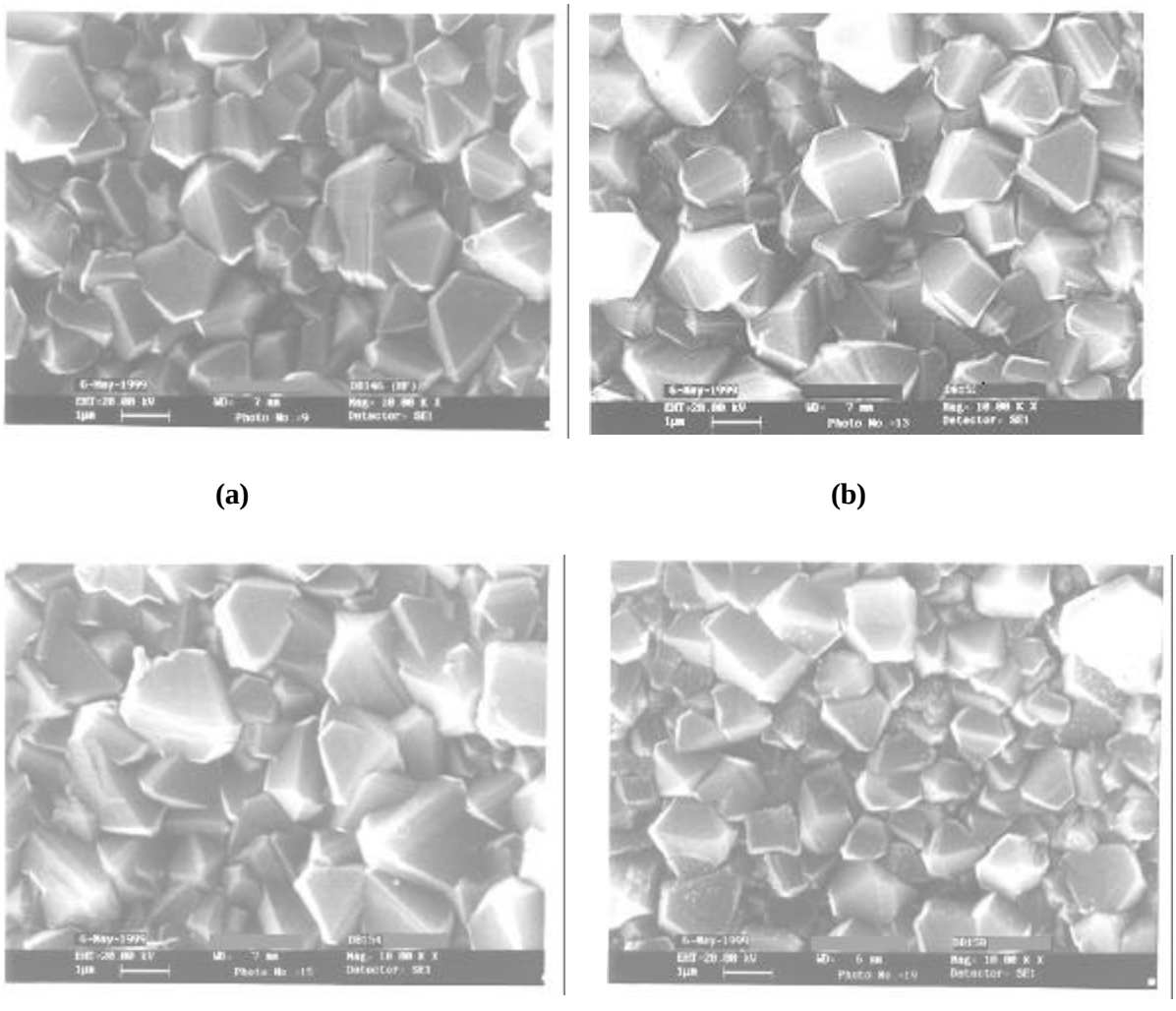

(a) **(b)**

(c) **(d)**

Fig. 4.26 SEM photographs of the surface morphology of the diamond films grown on Si substrate (a) nominally pure (undoped), and with (b) 0.1 SCCM B_2H_6, (c) 0.025 SCCM SiH_4, and (d) 0.025 SCCM SiH_4 + 0.1 SCCM B_2H_6 (co-doped).

The photoluminescence spectra of these films are shown in Fig. 4.28. As discussed in the previous section (4.5.I), the nominally pure (undoped) diamond film shows the broad band at 1.720 eV with a small shoulder at 1.683 eV (Fig. 4.28a) and the film grown with 0.025 SCCM SiH_4 shows a sharp band at 1.683 eV (Fig. 4.28c). The film grown with 0.1 SCCM boron also shows a broad band at 1.720 eV(Fig.4.28b). The PL spectrum of the dual doped film (grown with 0.025 SCCM SiH_4 and 0.1 SCCM B_2H_6) (Fig. 4.28d) shows complete absence of the PL band at 1.683 eV. This observation may

Chapter 4 *Si incorporation in Diamond Films*

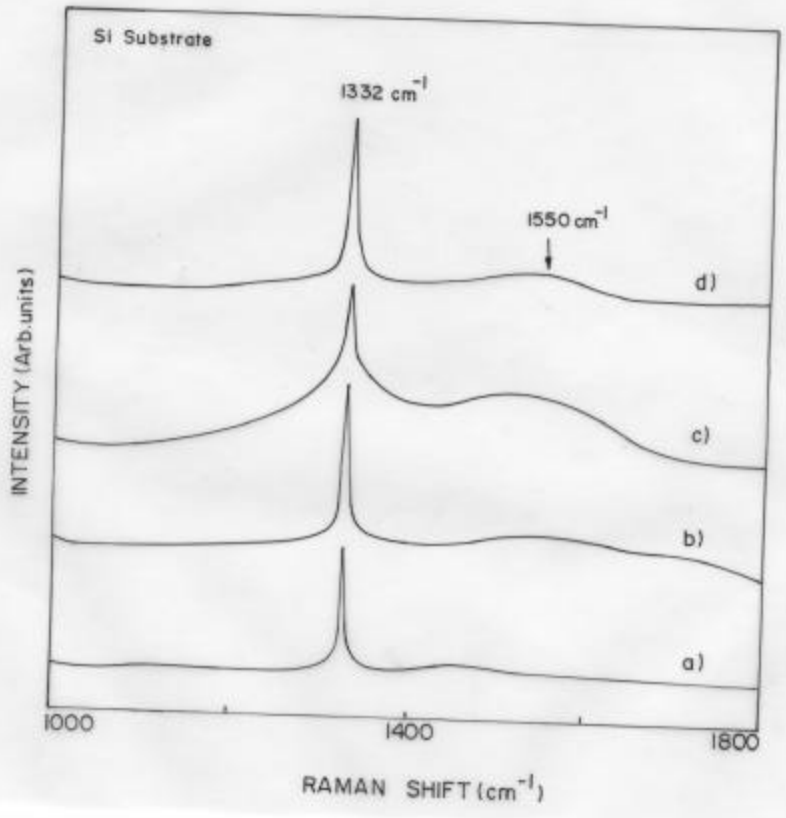

Fig. 4.27 Raman spectra (normalized for 1332 cm^{-1} band) of the diamond films grown on Si substrate (*a*) without SiH_4 & B_2H_6, and with (*b*) 0.1 SCCM B_2H_6, (*c*) 0.025 SCCM SiH_4 , and (*d*) 0.025 SCCM SiH_4 + 0.1 SCCM B_2H_6 (co-doped)

be attributed to the reduction in the concentration of monovacancies present in the Si-doped film due to the boron interstitials as suggested by Dannefaer et al. [40]. Hertnett [41] has also reported the similar observation and suggested that B atoms incorporated in the diamond lattice may effectively passivate the defects responsible for the 1.683 eV PL

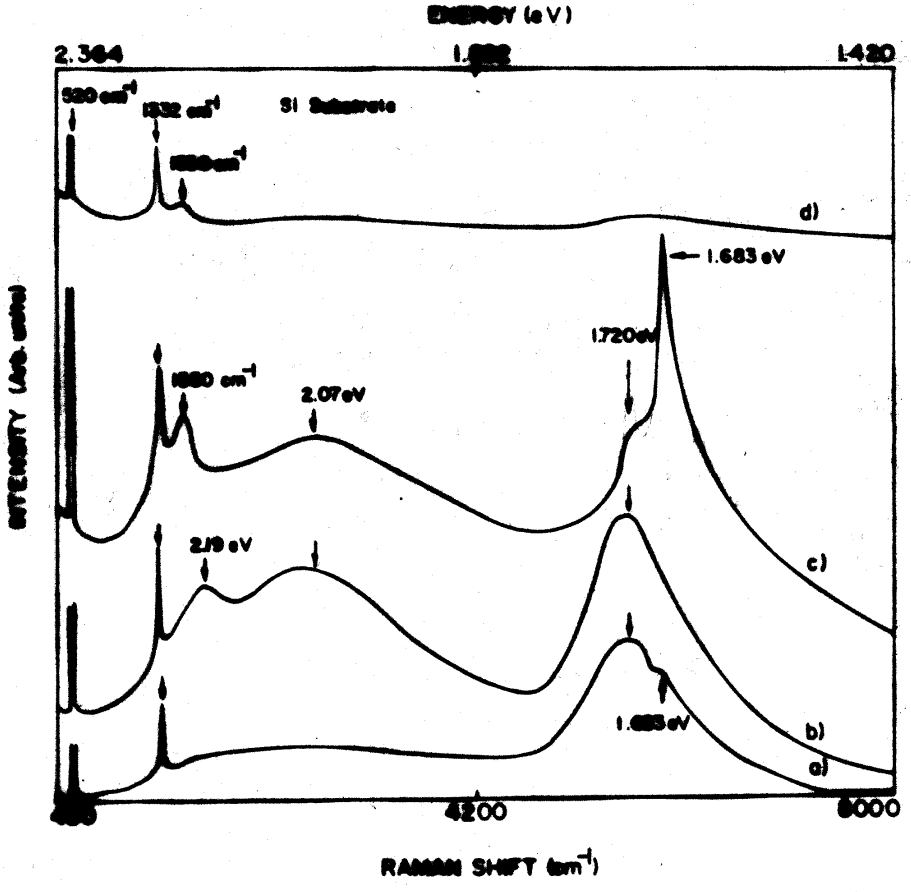

Fig. 4.28 The PL spectra of the diamond films grown on Si substrate (*a*) without SiH_4 & B_2H_6, and with (*b*) 0.1 SCCM B_2H_6, (*c*) 0.025 SCCM SiH_4 , and (*d*) 0.025 SCCM SiH_4 + 0.1 SCCM B_2H_6 (co-doped)

band. However, it is not yet clear whether the B bond with Si is terminating the dangling bonds due to vacancies or it acts as compensator for Si induced defect states.

4.6 Conclusion

We have investigated the effect of *in situ* incorporation of Si impurity on the structure and properties of diamond films. It appears that Si plays a role in enhancing the crystallite size as well as the sharpness of the crystal edges. This increase in crystallite size indicates posssible growth process via Si catalytic activity at the surface. The increased FWHM of the 1332 cm^{-1} Raman band is attributed to dilation of diamond lattice caused by large size Si atoms.

The Si incorporation in diamond films grown on Si, Alumina and Copper substrates results in the sharp and intense 1.683 eV photoluminescence line. This PL line was attributed by the earlier workers to Si vacancy centers whereas the Si was proposed to come from the substrate. Therefore, as was proposed by earlier workers, the origin of 1.683 eV band may be related to Si vacancy centers. However, this band is also observed when other impurities (N, P etc.) were also incorporated (which is discussed in next chapter). Therefore, we have proposed that the band at 1.683 eV is related to the structural defects produced in the film due to the impurity incorporation. The PL at 1.683 eV is also shown to have substrate temperature dependence and thereby on the morphology. The latter appears to have effect through the quality of diamond crystals. The sharpness of the band at 1.683 eV is attributed to the presence of the monovacancies whereas the broad band at ~1.72 eV is attributed to the clustered vacancies.

The *insitu* co-doping of Boron and Silicon in the diamond film results in the disappearance of the PL emission at 1.683 eV which may be due to the reduction in the concentration of monovacancies present in the Si-doped films. However, it is not yet clear whether the B bond with Si is terminating the dangling bonds due to vacancies or it acts as compensator for Si induced defect states.

References

1. M. Werner and R. Locher, Rep. Prog. Phys. 61 (1998) 1665.
2. J. A. Freitas, J. E. Buttler and U. strom, J. Mater. Res. 5 (1990) 2502.
3. J. Ruan, W. J. Choyke and W. D. Partlow, Appl. Phys. Lett. 58 (1991) 295.

4. L. H. Robins, L. P. Cook, E. N. Farabaugh and A. Feldman, Phys. Rev. B 39 (1989)13367.
5. L. Bergman and R. J. Nemarich, J. Appl. Phys 78 (1995) 6709.
6. R. F. Davis, ed. "Diamond Films and Coatings, development, properties, and applications", Noyes Publications, Park Ridge, NJ,USA (1992).
7. L. Bergman, B. R. Stoner, K. F. Turner, J. T. Glass and R. J. Nemarich, J. Apl. Phys. 73 (1993) 3951.
8. J. E. Buttler and H. Windischmann, MRS Bulletin 23 (9) (1998) 22.
9. M. Werner and R. Locher, Rep. Prog. Phys. 61 (1998) 1665.
10. P. K. Bachmann, D. Leers and H. Lydtin, Diamond and Relat. Mater. 1 (1991)1.
11. J. C. Angus, Thin Solid Films 216 (1992) 126.
12. P. K. Bachmann, D. Leers and D. U. Wiechert, J. De Physique IV, Colloque C2, suppl. au Journal de Physique II, vol 1 (1991) C2-907.
13. C. D. Clark, E. W. J. Mitchell and B. J. Parsons, in "The Properyies of Diamond" edited by J. E. Field (Academic, London, 1979) p. 23.
14. J. Walker, Rep. Prog. Phys. 42 (1979) 1605.
15. V. K. Bazhenov, I. M. Vikulin, and A. G. Gontar, Sov. Phys. Semicond. 19 (1985) 829.
16. B. G. Yacobi and D. B. Holt, J. Appl. Phys. 59 (1986) R1.
17. V. S. Vavilov, A. A. Gippius, A. M. Zaitsev, B. V. Deryaguin, B. V. Spitsyn and A. E. Aleksenko, Sov. Phys. Semicond. 14 (1980) 1078.
18. A. T. Collins, M. Kamo, and Y. Sato, J. Phys. D 22 (1989) 1402.
19. L. H. Robins, E. N. Farabaugh A. Feldman, and L. P. Cook, Phys. Rev. B 43 (1991) 9102.
20. A. M. Stoneham in "Theory of Defects in Solids" (Clarendon Press, Oxford, 1975).
21. M. D. Styrge, Solid State Physics 20 (1967) 91.
22. C. D. Clark, P. J. Kemmey, and E. W. J. Mitchell, Disc. Faraday Soc. 31 (1961)96
23. H. B. Dyer, and P. Ferdinando, J. Appl. Phys., 17 (1966) 419
24. L. A. Vemeulen, C. D. Clark, and J. Walker, "Lattice Defects in Semiconductors" Inst. Phys. Conf. Ser. No. 23 (Bristol: The Institute of Physics) (1974) 294.

25. G. D. Watkins, " Radiation Damage in Semiconductors", (Paris: Dunod) (1965) 97.
26. Y. Yokota, H. Kawarada and A. Hiraki, in "Diamond, Boron Nitride, Silicon Carbide and Related Wide Bandgap Semiconductors", edited by J. T. Glass, R. F. Messier, and N. Fujimori (Mater. Res. Soc. Symp. Proc.162, Pittsburgh, PA, 1990).
27. A. T. Collins, M. Kamo, and Y. Sato, J. Mater. Res. 5 (1990) 2507.
28. A. M. Zaitsev, V. S. Vavilov, and A. A. Gippius, Sov. Phys. Leb. Inst. 10 (1981) 15.
29. J. Ruan, W. J. Choyke and W. D. Partlow, J. Appl. Phys. 69 (1991) 6632.
30. R. J. Graham, T. D. Moustakas, and M. M. Disko, J. Appl. Phys. 69 (1991) 3212.
31. G. Davis, Chem. Phys. Carbon 13 (1977) 1.
32. R. M. Chrenko, Phys. Rev. B 7 (1973) 4560.
33. E. C. Lightowlers and A. T. Collins, J. Phys. D 9 (1976) 951.
34. Y. H. Shing, D. H. Rich and F. S. Pool, J. Appl. Phys. 71 (1992) 6036.
35. T. Feng and B. D. Schwartz, J. Appl. Phys. 73 (1993) 1415.
36. A. A. Gorokhovosky, A. V. Turukhin, R. R. Alfano and W. Phillips, Appl. Phys. Lett. 66 (1995) 43.
37. C. D. Clark, H. Kanda, I. Kiflawi and G. Sittas, Phys. Rev. B 51 (1995) 16681.
38. J. M. Lannon and J. S. Gold, Appl. Phys. Lett. 73 (1998) 226.
39. J. P. Goss, R. Jones, S. J. Breuer, P. R. Briddon and S. Oberg, Phys. Rev. B 77 (1996) 3041.
40. S. Dannefaer, W. Zhu, T. Bretagon and D. Kerr, Phys. Rev. B 53 (1996) 53.
41. T. M. Hertnett, "Characterization of diamond deposited in a microwave plasma", M.S. thesis in Solid State Science, The Pensylvania State University, University Park, PA (1988).
42. J. S. Williams, Rep. Prog. Phys. 49 (1986) 491.
43. J. Michler, J. Stiegler, Y. Von. Kaenel, P. Moeckli, W. Dorsch, D. Stenkamp, and E. Blank, J. Cryst. Growth 170 (1997) 404.
44. N. Wada, and S. A. Solin, Physica B+C 105 (1981) 353.
45. R. E. Shroder, R. J. Nemanich, and J. T. Glass, Phys. Rev. B 41 (1990) 3738.
46. D. M. Bhusari, A. S. Kumbhar, S. T. Kshirsagar, Phys. Rev. B 47 (1993) 6460.

47. R. J. Nemanich, J. T. Glass, G. Lucovsky, and R. E. Shroder, J. Vac. Sci. Technol. A6 (1988) 1783.
48. R. J. Nemanich, and S. A. Solin, Phys. Rev. B 20 (1979) 392.
49. S. Lin, and B. J. Feldman, Phys. Rev. Lett. 48 (1982) 829.
50. J. Wagner, and P. Lautenschlager, J. Appl. Phys. 59 (1986) 2044.
51. A. V. Turukhin, C-H Liu, A. A. Gorokhovsky, R. R. Alfano, and W. Philips, Phys. Rev. B 54 (1996) 16448.
52. T. Sharda, A. K. Sikder, D. S. Misra, A. T. Collins, S. Bhargava, H. D. Bist, P. Veluchamy, H. Minoura, D. Kabiraj, D. K. Awasthi, and P. Selvam, Diam. Relat. Mater. 7 (1998) 250.
53. A. J. Dekker, in "Solid State Physics" (Macmillan & Co. Ltd, London, 1962) p398.

CHAPTER 5

INFLUENCE OF NITROGEN ON THE GROWTH OF DIAMOND FILMS

In this chapter, the effect of nitrogen on the quality and growth of CVD diamond films is discussed. The films are grown on different substrates such as Si, Alumina and Copper. The films thus deposited are characterized by different characterization techniques such as SEM, Raman scattering, XRD and phtoluminescence spectroscopy and the results are presented in details. N-doped diamond films, irrespective of the substrate used, exhibited PL emission at 1.683 eV. This emission band in absence of Si impurity appears to contradict earlier results. A monovacancy center which may take part in this emission is briefly discussed.

5.1 Introduction

In the previous chapter, it is seen that unintentional or intentional incorporation of Si impurity in the CVD diamond films influences the structural and optical properties of the material. The observed changes in the physical properties of these films have been attributed to the significant increase in mechanical stress as well as increase in the number of vacancy defects created due to the distortion of diamond lattice caused by the large size of Si atoms compared to that of the surrounding carbon atoms. However, this should not be mistaken as if other impurities which may have similar or smaller size compared to carbon atom, shall have no effect on the growth, structure and physical properties of diamond films. Such other impurity that can get unintentionally incorporated into the diamond film is the gaseous nitrogen which may enter the deposition chamber through the minor atmospheric leaks or the contaminants present in the reaction gases. Nitrogen has covalent radius comparable to that of carbon atom ($r_C \sim 0.77$ Å and $r_N \sim 0.75$ Å) and it can occupy diamond lattice site easily, leading to high solubility of N in the material. Since N lies next to C in the periodic table, it has an extra electron which upon substitution at lattice sites can produce n-type conducting material. Since diamond possesses optical band gap of 5.5 eV and it has highest thermal conductivity, the semiconducting devices produced by using the n-type diamond can operate efficiently at high ambient temperature. Moreover, its excellent thermal conductivity suggests that the CVD diamond films would be most useful as substrate for high power electronics.

The theoretical investigations show that N as a donor has much lower formation energy than the phosphorous [1,2]. However, contrary to expectations, experiments with synthetic and natural diamond show that, in addition to the deep donor level at 1.7 eV [3] below conduction band, a variety of N-related defects are created that dominates transport and recombination of carriers in diamond and degrades not only the electronic properties of the material but also the thermal conductivity. Therefore, for a successful production of electronic grade material, exploration of N-related effects is important. The literature available on this subject is therefore reviewed in the following section which is then followed by the motivation and objective of the present work.

5.2 Background Literature on Nitrogen Impurity in CVD Diamond Films

Both the natural and synthetic diamond crystals have been observed to contain a variety of impurities which strongly influence the physical properties of the material. The minor elemental contents in natural diamond had been determined by a number of spectroscopic studies [4-6]. Si, Ca, Mg, Al, Fe, Ti, Cu and B have generally found to be the most abundant non-gaseous impurities. Considerable amount of gaseous impurities have also been found in natural diamond [7,8]. Among these, nitrogen is the predominant gaseous impurity and its concentration ranges as large as 0.1%. Infrared absorption at 7.8 μm showed its proportionality to the amount of N present in the natural diamond. This implies that N has high solubility in diamond and may be found either concentrated in small aggregates or dispersed as single N in substitutional sites of diamond lattice. This allows classification of natural diamond crystals as type-Ia (i.e. high percentage of N) or type-Ib (i.e. low percentage of N). Most natural diamonds are of type-Ia with N concentration ~ 0.1% ($>10^{20}$ cm^{-3}) while synthetic diamonds are of type Ib with N concentration varying from 10^{14} to 10^{20} cm^{-3} [9]. The type Ia diamond show IR absorption bands in the 7-13 μm range while type Ib are transparent in this range. The UV-visible absorption cut-off frequency for type Ia is approximately 3000 Å (4.15 eV) while for type Ib, it is at 2250 Å (5.5 eV). Moreover, the paramagnetic resonance spectra show that the N is paramagnetic impurity with g=2.0024, which indicates possibility of a unpaired electron at N site. This implies that the N can act as a donor impurity when it is present in small concentration. Theoretical calculations have shown that N donor level may be lying at 2.05 eV below the conduction band [10].

The optical absorption spectra of the natural diamond show continuum of absorption starting at about 1.7 eV and rising rapidly with sharp peak at ~ 4 eV until it merges with the fundamental absorption edge at 5.5 eV. The peak at 1.7 eV is related to transmission from N-donor level at 1.7 eV into the conduction band while the transition from valence band to the localized donor level corresponds to ~ 4.0 eV band [11]. The location of the donor orbital is confirmed from EPR studies to closely localize around the {111} C-N bond with distortion elongation of C-N bond by 10 to 20% over the normal C-C distance [12]. The deep donor

level implies that a large fraction of donor electron is likely to be in bound state at room temperature [13]. This eliminates nitrogen as a viable dopant to achieve n-type diamond with any measurable conductivity. On the other hand, with the help of the studies on the selected natural diamonds with variable nitrogen content, it has been determined that the N is associated with a wide assortment of states localized within the band gap which are responsible for a host of defect induced phenomena [3,14]. The incorporation of N in natural semiconducting IIb diamond has shown, on the contrary, decrease in conductivity which has been attributed to a possible role of N as a compensating center for acceptor states [15].

The emergence of the low pressure CVD techniques has now allowed the incorporation of the dopants in the diamond lattice in a controlled manner. The correlation of changes produced by nitrogen in variety of diamond films has provided the powerful tool for studies of the important band gap states. First such study is carried out by Mort et. al.[15] who have reported the electrical conductivity measurements of the nominally undoped HFCVD diamond film and the one doped with nitrogen (4×10^{19} atoms/cm^3). It was observed that the electrical conductivity decreased by several orders of magnitude (for temperatures above room temperature). Qualitatively, this decrease, as expected, may be due to the compensation of existing acceptor states in nominally undoped diamond thin film by substitutional nitrogen that introduces a deep lying donor level. The vacancies in undoped diamond film migrate during annealing while in nitrogen-rich diamond, the vacancies are predominantly trapped during annealing at the nitrogen sites [16].

Jin and Moustakas [17] studied the electrical conductivity in diamond films and found strong correlation between growth habit and the electrical conductivity activation energy. Their results suggest that B impurities incorporate more efficiently in substitutional sites when the growth habit is {111}while N impurities incorporate more efficiently when the growth habit is {100}. The required activation energies were found to be 0.3-0.4 eV for B and 1.5 eV for N which are consistent with the ionization energies of the respective dopants. Further studies on N incorporation in CVD diamond films carried out by Jin and Moustakas [18] showed the N-doping efficiency in diamond to be very low while the growth habit was observed to change from {111} to {100} with the increase of nitrogen in the microwave discharge from N/C = 0.1% to 10%. The low doping efficiency was attributed to the proposal that the growth mode

involves simultaneous deposition and etching of N-species while change of morphology is attributed to the possible distortion of the diamond lattice along the {111}direction upon substitutional incorporation of nitrogen. Some researchers have attributed this distortion to Jahn-Teller effect [19] and predicted that the C-N bond along the {111} direction should be 10-14% longer than the C-C bond. However, EPR and related studies indicate that even higher distortion (36%) is possible [20]. Kajihara et al. [10] attributed the large distortion to Pauli electrostatic repulsion with the N moving towards the {î î î} direction and the carbon towards {111} direction.

Other important observation was the increase in the growth rate from 0.4 to 1.0 μm/hr with N/C change from 0.1 to 40% and the sharpening of the diamond Raman peak with the amount of nitrogen in the gas phase. This provided the evidence for defect induced stabilization of CVD diamond suggested by Bar-Yam and Moustakas [21]. In their model, they suggested that the n or p type doping in diamond should lead to reduction in point defects, i.e. carbon vacancies. This is because doping shifts the Fermi level at the growing surface towards the conduction or valence bands and thus, charges the vacancies negatively or positively, respectively, which, in turn, causes reduction in formation energy. This reverses the thermodynamic stability between diamond and graphite at much lower N concentration [22].

Most synthetic diamonds grown at high temperatures and high pressures contain paramagnetic single substitutional N atoms as ($[N\text{-}C]^0$) often referred to as P_1 centers [19,23] concentrations of which can be as high as 500 ppm. Similar is also the case with diamond grown by CVD with $[N\text{-}C]^0$ concentrations as high as 300 ppm [24]. For the single substitutional N center, approximately 24% of the unpaired electron population is on the nitrogen and 67% on one carbon neighbor [19,23]. It is this unique carbon neighbor which is indicated in the notation $[N\text{-}C]^0$. The defect is thus neutral. However, natural or CVD diamonds can contain several thousands ppm of N and in such case, N is incorporated in aggregates rather than in $[N\text{-}C]^0$ centers [25]. As seen before, these diamonds are known as type Ia. Two different forms of these aggregates have been recognized, viz. the A and B centers. The A center involves two N atoms [26], for e.g. $[N\text{-}N]^0$, i.e. a pair of adjucent substitutional atoms which gives rise to IR absorption at 1282, 1203, 1093, and 480 cm^{-1} [27,28]. The B center may be formed by four N atoms around a vacancy [25], which is not yet well understood. Both

A and B centers are not paramagnetic. However, contrary to this expectation, Vay Wyk and Loubser [29] observed EPR from the A center when they illuminated it with ultraviolet light. They proposed that the illumination created $[N\text{-}N]^+$ center which became paramagnetic. However, these centers were not observed to act as electron traps or donors. The theoretical estimates based on EPR results indicated that the N-C bond length in the $[N\text{-}C]^0$ center is similar to the N-N bond length in the $[N\text{-}N]^+$ center. It appears that the $[N\text{-}N]^+$ can be created via electron capture by $[N\text{-}N]^{2+}$ or by ionization of $[N\text{-}N]^0$ or possibly by both depending on the traps and donors available [25].

With so much understanding about the N incorporation, the enormous influence of N admixtures to the reactant gas during CVD of diamond has become the subject of recent investigation, particularly as one of the most important deposition parameter. It has been shown that small quantities of N in the gas phase can lead to a change of growth rates [30], to a change of texture and morphology [18,30,31] to the suppression of twinning of particular growth sector [32]. These investigations indicated that admixing of N to reaction gases in CVD of diamond by various techniques is an important parameter for development of high quality diamond films. Polycrystalline diamond films are known to grow from cubo-octahedral nuclei consisting of {100} and {111} faces. But, the incorporation of nitrogen in reactant gases has been successfully used to grow homoepitaxial {111} diamond film where the growth of {100} faces is suppressed. On the other hand, growth of {100} textured diamond films by addition of N has also been achieved when the N gas was in 20-200 ppm range [18,30,33]. The results demonstrate that the nature of the substrate used for growth has no appreciable influence on the {100} texture which implies that interaction of N with the growing {100} surface is highly important factor in gas phase chemistry which influences the surface kinetics at the diamond nuclei and the twin formation on {111}. The possible role that N plays in gas phase chemistry has been speculated to be the enhancement of products of sp^3 bonded $-CH_3$ species on the growth surface [33]. ***This speculation, however, needs to be verified since 20-200 ppm concentration of nitrogen in the gas phase is unlikely to change the gas phase chemistry enormously. In this context, the possible contribution to growth chemistry from the species such as NH_x and CNH_x needs to be examined because compared to C-***

C bond, the C-N bond is stronger [34] and NH_x, CNH_x radicals have lower desorption rates [33].

The contamination of N during CVD deposition is thus seen to influence enormously the electrical [15,35] and thermal [36] properties of diamond layers as well as their morphology, phase purity and crystal orientation [37]. Small additions of N in MW-CVD have shown increase in crystal quality as revealed by Raman spectra [18,30] while some researchers found only negligible or deteriorating effects [35,36]. However, it needs to be noted that the nitrogen concentrations which caused particular effects depended upon the CH_4 concentration [30,36]. On the other hand, CVD diamond films have also been synthesized using pure CH_4/N_2 gas mixtures without additional H_2 [31]. This implies that the atomic N and CN could support or imitate the usual role of atomic hydrogen in diamond CVD due to the reaction with adsorbed C and H at the growing diamond surface. Some preliminary work supporting similar speculations has been reported by Bohr et. al. [37]. They attributed the effects of N_2 additions to a reduction of carbon supersaturation due to the abstraction of adsorbed H atoms caused by CN and HCN.

Diamond has a negative electron affinity (NEA) [38-41] which is useful for electron junction diode emitters [42,43]. For this emission to occur, a source of electrons must be present either in the conduction band or in a subband near the vacuum energy level [44]. Such source can be made available by nitrogen as it forms a deep donor level at ~ 1.7 eV below the diamond conduction band [45]. The nitrogen doped diamond has exhibited enhanced electron emission due to higher resistivity of the N-doped samples compared to B-doped samples and require fields of 0-1 $V\mu m^{-1}$. N doped samples have also shown emission of beamlets. ***It is not yet clear as to whether the electrons are accelerated to these energies in the bulk of the diamond or at high electric fields near the emitting surface [46].***

The electronic structure of the N-V center in diamond has been studied by *ab initio* calculations [47]. It is proposed that the center is a neutral rather than a negatively charged nitrogen-vacancy center with properties dominated by its two unpaired nitrogen electrons which in ground state are permitted to be unpaired because of the presence of vacancy. Optical excitations on the zero phonon line at 1.945 eV are well described by transitions of these electrons [47]. Li et al. [48] have measured the substitutional nitrogen

activation energy in diamond films by temperature dependence of conductivity in the range 300-673 K. The deep donor ionization energy was found to be ~ 1.62 ± 0.02 eV which suggest that this is due to a single N atoms that occupy substitutional lattice sites in diamond, a result consistent with an electrical donor effect occurring in the bulk of the diamond films. Talbot-Ponsonby et al.[49] have reported the EPR imaging studies of the distribution of single substitutional nitrogen impurity through the polycrystalline diamond films grown by CVD.

The investigation of defect formation in chemical vapor deposition of diamond films is critical in understanding the basic mechanisms of electronic transport and optical interactions which underline the applications in developing electronic and optical devices. It is well known that luminescence spectroscopy is very sensitive probe for studying defects in solids. It has been observed by various researchers that the photoluminescence spectra of diamond films grown by various chemical vapor deposition methods shows a broadband extending from approximately 1.5 to 2.5 eV and centered at ~ 2 eV [50-54]. In many instances, this broadband PL appears as the strongest feature in the spectrum. However, a complete model explaining the origin of this broadband PL is not yet formulated. Collins et. al. [55] have reported the studies on CL of crystal diamonds of type Ia and type Ib in which it is shown that this broadband luminescence has its origin in the electron-lattice coupling (vibronic interaction) of nitrogen related centers with ZPL at 1.945 and 2.154 eV. The other group of researchers [56-58] have suggested that the presence of graphitic carbon (sp^2-bonded carbon) can give rise to the broadband PL in CVD diamond films. The amorphous carbon films exhibit PL emission centered at 1.8 - 2.0 eve [59-62]. The PL spectra of undoped diamond film exhibits the 1.681 eV band which has been attributed to an optical transition in a Si complex center [56, 63-67]. Bergman et al. [68] investigated the role of N-doping on the optical spectra of CVD diamond films and proposed the origin of the characteristic broadband luminescence positioned in the range 1.5-2.5 eV centered at 2.0 eV. The sharp PL lines at 1.945 eV and 2.154 eV are attributed to ZPL of N-centers in diamond lattice. Their results provided support for origin of the broadband luminescence as the optical transition of an in-gap state distribution in CVD diamond film attributed to the disordered forms of the sp^2 bonded carbon rather than the electron-lattice interaction of the nitrogen center as was thought by earlier workers [69]. The model of in-gap state distribution resembles to the models previously developed for amorphous

materials [70,71]. ***In addition to this they observed that 1.681 eV band is enhanced abruptly after nitrogen incorporation in diamond films. This change in the band is not yet clearly understood***

In this context, it is important to note the observation by Jin and Moustakas [18] that the doping efficiency of nitrogen in the diamond films is below the detection limit of X-ray photoelectron spectroscopy, 0.5 % (8.5×10^{20} cm^{-3}) even for the films in which the ratio of N/C in the gas phase is 40 %. Therefore it is suggested that the strong dependence of nitrogen on the film morphology is not a result of nitrogen incorporation , but is instead directly caused by nitrogen-related surface processes and surface kinetics [33].

Nitrogen incorporation into diamond is being examined since this element is usually present as a contaminant in at least μg/g amounts and its presence alters the growth process and the film morphology, composition and structure [72-74]. Moreover, the deliberate incorporation of nitrogen as an n-type dopant is potentially of great interest in electronic applications [75,76]. This contamination in low concentrations is more effective in producing enormous changes in growth and properties of diamond films, particularly, when the gas dissociation agency involves MW or RF plasmas. Some studies have also been made by involving HF-CVD for synthesis and post deposition plasma treatment of these films [77]. Despite these investigations, a host of fundamental problems remains unresolved, particularly, the n-type doping and the role of nitrogen in gas phase and growth chemistry. ***Most of the work published so far on nitrogen incorporation has been carried out on samples synthesized by MW-CVD while the HF-CVD is used very sparingly.*** Since nitrogen can ionize more efficiently in plasma surrounding, the plasma assisted techniques can be more effective to N contamination and its effect on the diamond growth can be enormous. Whether such impurity incorporation would be viable by using HF-CVD, needs to be verified. Moreover, the effect of nitrogen impurity on the properties of diamond films also depends upon other deposition conditions, e.g. methane concentration, substrate temperature, etc. Since nitrogen can act as compensator in B-doped and other defects containing samples, its role in stabilizing other defects needs to be explained. Similarly, despite the fact that nitrogen is a deep donor, it has been argued that intrinsic diamond which contains typically 10-80 ppm nitrogen, is p-type. Hence, the mechanism of nitrogen incorporation in CVD diamond is still an open

question. This is because of the complexity of the N-incorporation processes involved which depend not only on the experimental parameters but also on the diamond crystal orientations and its surface termination.

From this scenario, it is clear that very little is known about nitrogen in CVD diamond films and the data available in the literature is not consistent. Therefore the systematic and detailed studies on the effect of incorporating nitrogen on the growth behavior, its role in growth mechanism and properties of CVD diamond films is needed. In the present chapter, the results on nitrogen incorporation in diamond films are reported and discussed in detail.

5.3 Experimental

The films were synthesized by the method of hot filament assisted chemical vapor deposition (HFCVD) in a vapor deposition system especially designed for diamond deposition. Various substrates such as c-Si <100> , copper and alumina (Al_2O_3) were used for depositing the films. All the substrates were subjected to a light abrasion with 1/2 μm size diamond powder and subsequently cleaned ultrasonically in acetone and rinsed in 40% HF acid solution before loading them in the deposition chamber. The substrates were held at a distance of 10 mm below the plane of M-shaped filament. The substrate holder was made to rest on a heat sink of variable heat capacity which could be achieved by varying the volume and configurations of the heat sink. Using this heat sink, it was possible to vary the substrate temperature by keeping the substrate surface to filament distance constant. The different heat sinks used were configured of copper, graphite and ceramic so as to get the substrate temperatures (T_s) about 750^0C, 850^0C and 950^0C respectively. The deposition chamber was evacuated to the pressure of less than 10^{-2} torr prior to the introduction of the feed gases. For the deposition of the films, a mixture of the semiconductor grade gases CH_4 , N_2 and H_2 was used. The nitrogen fraction (X0 and methane fraction (Y) in the source gas are defined as:

$$X = \frac{[N_2]}{[CH_4] + [N_2]} \quad \text{and} \quad Y = \frac{[CH_4]}{[CH_4] + [N_2]}$$

The deposition parameters used are listed in table 5.1

Table 5.1 : HFCVD Deposition Parameters

Deposition Parameter	Value
Total Gas Flow Rate	300 SCCM
Methane Concentration	2%
Nitrogen concentration	0.1 - 3.0 SCCM
Filament Temperature (T_f)	$1900 \pm 50\ ^0C$
Substrate Temperature (T_s)	750, 850, 950 ($\pm$ 20) ^0C.
Deposition Pressure	30 Torr.
Deposition Period	3 hrs.

5.4 Results and Discussion

The effect of nitrogen on the growth and properties of diamond films was studied by adding nitrogen into the feed gas mixture prior to its entry in the deposition chamber. To introduce different concentration levels of nitrogen in the growing diamond films, N_2 gas proportion with respect to methane gas flow was varied from 0% to 50% of volume. This set of films was deposited on Si <100> substrates keeping all other deposition parameters identical as listed in the Table 5.2 and therefore the variation in any property as a result of nitrogen impurity introduced in the film may be correlated to the gas phase concentration of N_2 alone.

Table 5.2. Deposition conditions and the concentration of different gases used for the growth of N doped diamond films

Sample Identification	H2 Flow Rate (SCCM)	CH4 Flow Rate (SCCM)	N2 Flow Rate (SCCM)	Percentage N_2 Conc.	Sub. Temp. (^0C)
DN # 15	300	6.0	0.0	0.00	750
DN # 12	300	6.0	1.0	14.00	750
DN # 20	300	6.0	1.5	20.00	750
DN # 21	300	6.0	1.8	23.00	750
DN # 22	300	6.0	2.0	25.00	750
DN # 29	300	6.0	2.5	29.50	750
DN # 37	300	6.0	3.0	33.00	750
DN # 38	300	3.0	3.0	50.00	750

5.4.1 N dpoed diamond films vs Nitrogen Concentration

5.4.1(a)Morphology of N doped films vs. N_2 concentration

The SEM photographs of the surface morphology of the diamond films grown as listed in Table 5.2 are shown in Fig. 5.1 (a-h). It is seen that the morphology of the investigated diamond films is strongly dependent on the ratio N/C. The surface of the film, in which nitrogen was not introduced during the growth, is observed to consist of crystallites having randomly oriented {111} facets lying parallel to the substrate plane (Fig. 5.1a). However, the morphology is seen to change from {111} faceted platelets to pyramidal shaped crystals. The low concentration of nitrogen (N/C ≤ 20%), crystals have well defined edges and crystallite size enhances from 0.6 mm for 0% N to 2.0 mm for 20% N. The film grown with 14% N is seen to have crystals with a square top edge whereas for high concentration, the square converges to a point. This pointed pyramidal growth is mainly characteristic of the N-controlled growth. The increase of the size of the crystallites indicate enhancement of growth rate due to N-chemistry at the substrate. For large nitrogen concentration, i.e. > 30%, the morphology is seen to have secondary nucleation which increases immensely for ~50% nitrogen concentration and the crystallite with multiple nucleation and overgrowth are seen. This multiple nucleation may be related to enormous growth rate where the atomic species do not find enough time to creep around to add to well defined crystallite site and hence form secondary crystallites on the surface of the bigger crystals. This is likely to reduce the sharpness of the edges of crystallites, in a similar way as it happens in case of dendritic growth [31]. The overgrowth is likely to be sp^2 bonded graphitic carbon which is evidenced by Raman spectra as discussed in the following section. This transition in growth habit with the incorporation of higher nitrogen concentration in the films may be related to the unique large distortion along the (111) direction of the C-N bond. Qualitatively, it can be argued that in the presence of a large distortion along the (111) direction , it is difficult to grow along the same direction, because it is energetically favourable for the growth to proceed along another crystallographic direction.[18]. Similar morphological changes have been reported by other researchers [33,37].

Fig. 5.2 shows the dependence of diamond growth rate on the nitrogen concentraton in the feed. The growth is seen to increase from ~ 1.1 μm/hr for a

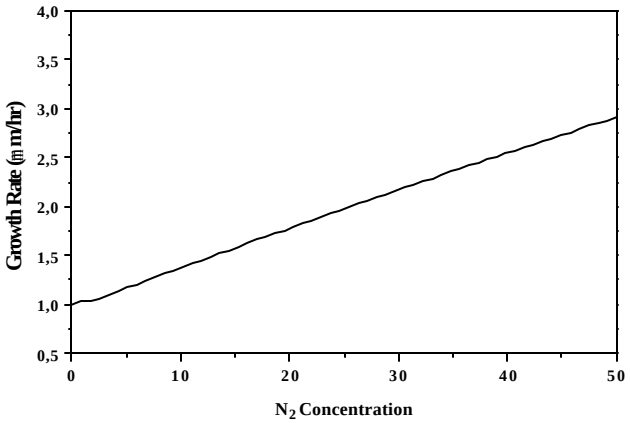

Fig. 5.2 Growth rate as a function of N_2 concentration

deposition without nitrogen to ~ 2.8 µm/hr for a deposition with 50 % nitrogen in the feed gas. The growth rate was measured by the SEM measurements of the cut cross section of the film.

5.4.1 (b) XRD Spectra of N-doped films vs. N_2 concentration

The X-ray diffraction patterns of these films are shown in the Fig. 5.3.

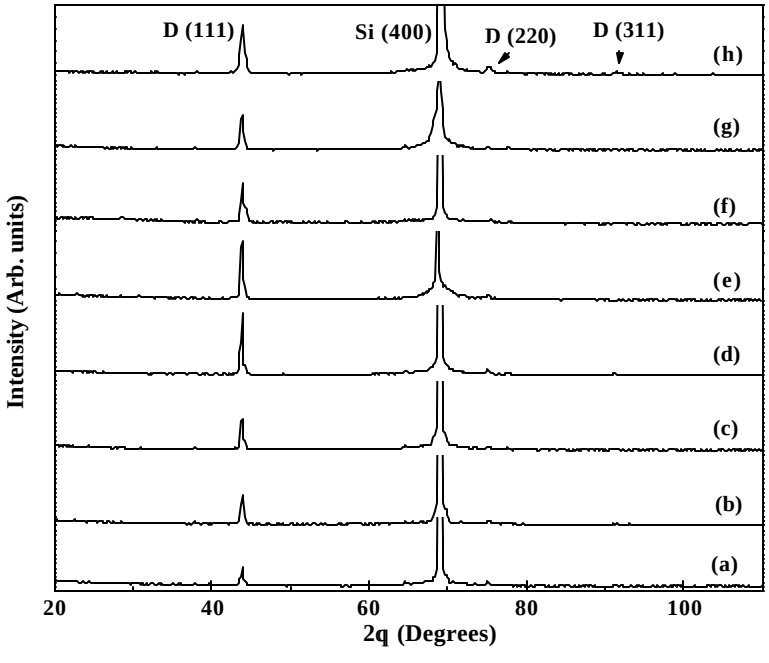

Fig. 5.3 XRD patterns of the diamond films grown at different N_2 concentrations - (a) 0% (b) 14% (c) 20% (d) 23% (e) 25% (f) 29.5% (g) 33% (h) 50%

These patterns show the enhancement in the intensity of D(111) line with nitrogen concentrations which implies increase in {111} texture of the film. Also, for the nitrogen concentrations > 25%, intensity of lines due to D(220) and D(311) is slightly enhanced.

5.4.1(c) Raman Spectra of N-doped diamond films vs. N_2 concentration

The structural properties and the composition of the films in terms of the proportions of sp^3 bonded carbon to that of sp^2 bonded carbon were studied with the help of Raman scattering studies. The Raman spectra of the diamond films prepared from N_2-H_2-CH_4 mixtures for various N_2/CH_4 concentrations are shown in Fig. 5.4. It is clear from these spectra that at low N_2 concentrations, the Raman spectra show rather good quality CVD diamond with a predominant and very sharp 1332 cm^{-1} Raman line, a characteristic of sp^3 bonded carbon. It is observed that the Raman spectra of the films grown with high nitrogen concentration (> 25%) show the additional broad sp^2 feature at around 1500-1560 cm^{-1} introduced by nondiamond carbon phase. With the increase in nitrogen concentration, the intensity of this broad sp^2 feature is found to increase and the width is found to decrease.The increased presence of the non-diamond carbon phases is a result of the deterioration of the crystallites, most probably by nitrogen-induced multiple nucleation and overgrowth which finally leads to the deposition of layers with an amorphous appearance [33]. For the diamond film grown without nitrogen, the 1332 cm^{-1} Raman line was observed to be very sharp i.e. the full width at half maximum (FWHM) was minimum and with the nitrogen concentration, it was found to increase. The variation of FWHM with nitrogen concentration is plotted in Fig. 5.5. This increase of FWHM may be attributed to the nitrogen dependent strain introduced in the crystallites[78].

The increase in the growth rate and crystallite size with increasing nitrogen concentration may be due to two possible mechanisms:

(1) The growth characteristics are improved and hence, in addition to the atomic hydrogen (H^0), there may be atomin nitrogen (N^0) species playing same role of atomin hydrogen [31]. The N^0 may be formed at the filament surface and diffused towards substrate surface. The N^0 may react with sp^2 carbon by forming CN at the substrate

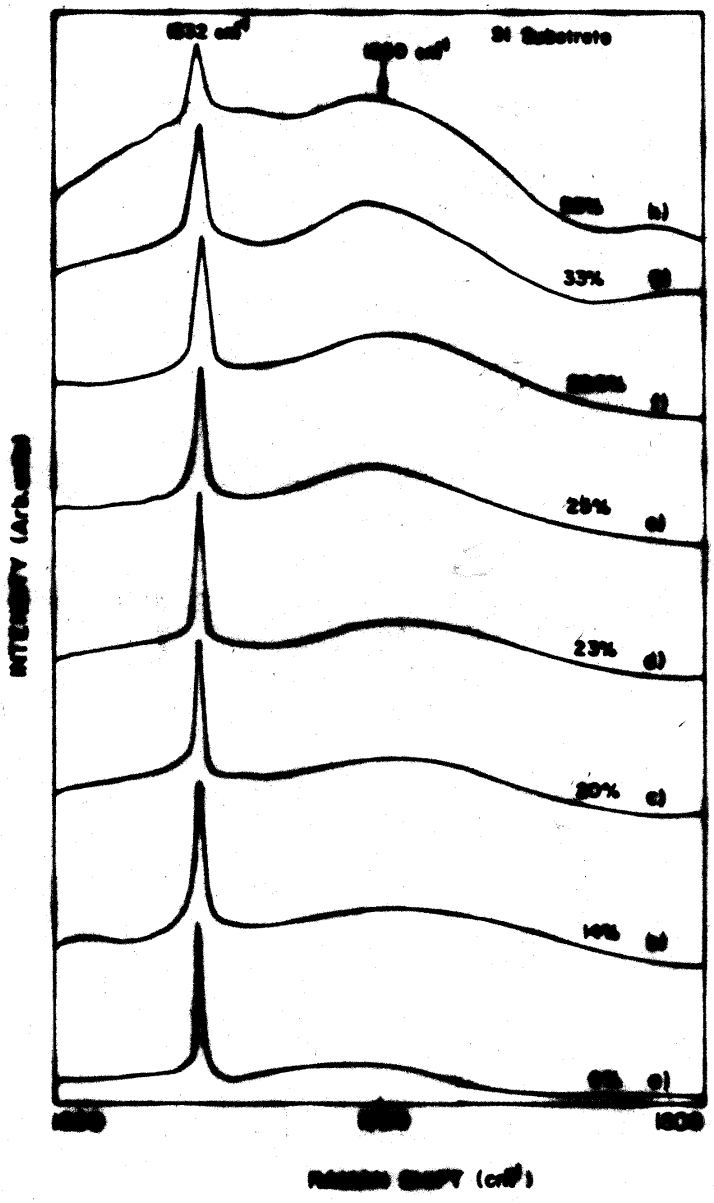

Fig. 5.4 Raman spectra (normalized for 1332 cm^{-1} band) of the N-doped diamond films grown on Si substrate as a function of nitrogen concentration

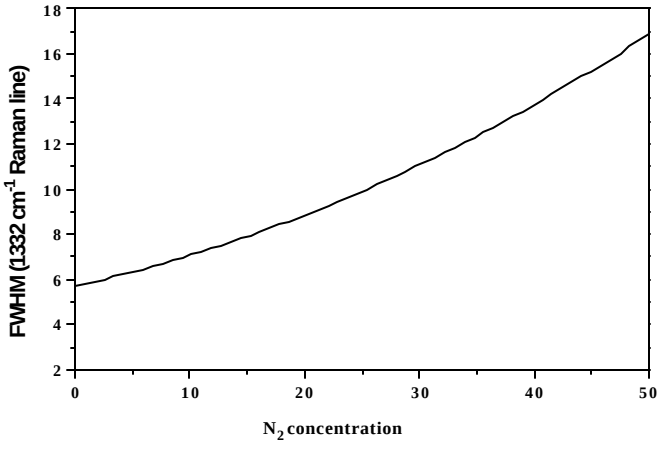

Fig. 5. FWHM of 1332 cm^{-1} diamond line as a function of N_2 concentration

surface. However, -CN (cyanogen) radicals are generally known to decompose to carbon elements at the prevailing substrate temperature [79]. Abstraction of hydrogen from the growing surface can also occur via formation of HCN [31] by interaction of CN with hydrogen terminals. These two reactions can enhance the growth rate as well as the crystallite size. However, these processes do not seem to be as efficient as of H^0 since the sp^2 bonded carbon is seen to increase with nitrogen concentration (> 20%).

(2) For the mixture of $CH_4+N_2(>20\%)+H_2$, the role of atomic hydrogen may be diminished as during deposition, it is partly removed by its reaction with N^0. The reduction in H^0 may lead to increase in sp^2 bonded carbon as seen in Raman spectra.

5.4.1(d) Photoluminescence studies of N-doped diamond films

Fig. 5.6 shows the PL spectra of nitrogen doped and undoped diamond films as a function of nitrogen concentration. The spectra were recorded utilizing the 514.5 nm (2.41eV) green line of the argon ion laser. From these spectra, the nitrogen related PL bands are identified and the influence of the nitrogen on the broadband PL is examined. The PL spectra of undoped diamond film (Fig. 5.6a) exhibits sharp 1.683 eV band alongwith a broad shoulder at 1.720 eV. Many of the researchers have attributed the 1.683 eV band to optical transition in a Si complex centre [80-82] and the 1.72 eV band to vacancy clusters [83]. With the nitrogen incorporation, the broad band centered at 1.72 eV is observed to disappear and

the sharp 1.683 eV band is observed. Bergmann et. al. [68] have also reported the similar observations. It is observed that the 1.683 eV band is

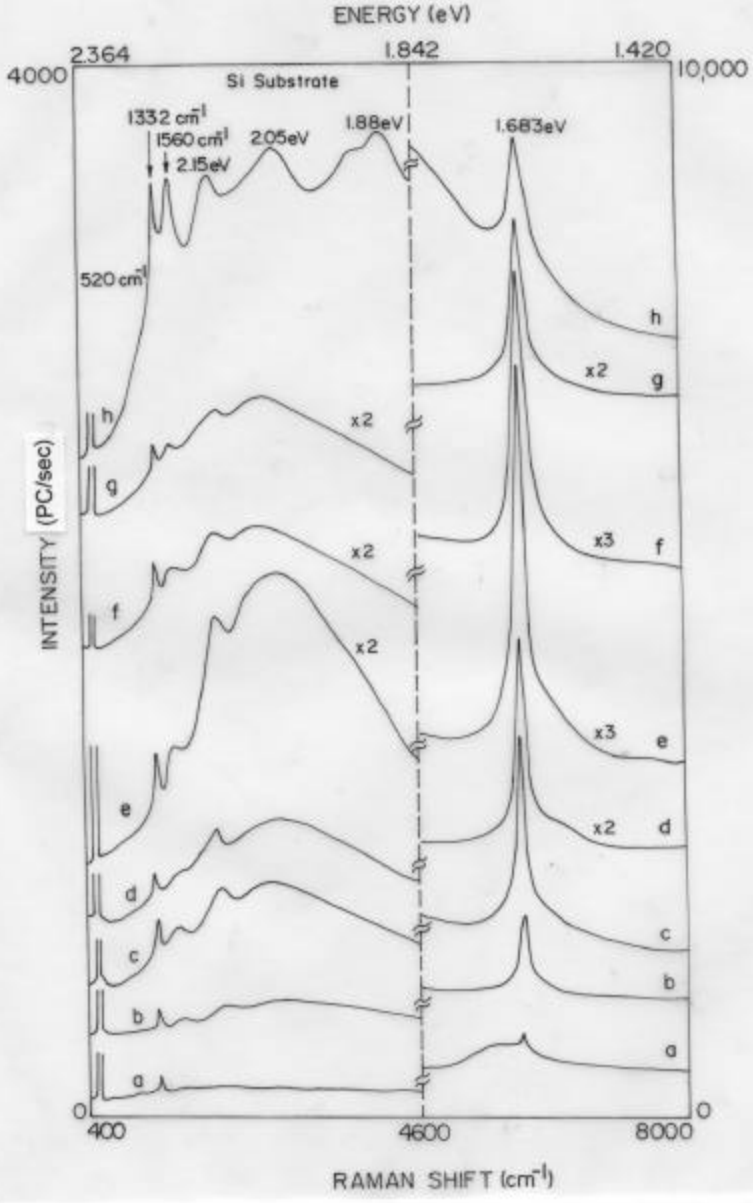

Fig. 5.6 The PL spectra of the N-doped diamond films grown on Si substrate as a function of nitrogen concentration

strongly dependent on nitrogen concentration. The dependence of this band on nitrogen concentration is shown in Fig. 5.7. The behavior of the 1.683 eV line with nitrogen concentration is same as observed in the silicon doped films. In this case also, this behavior can be attributed to the change in the luminescence efficiency of the centers with the impurity (nitrogen) concentration (as discussed in the previous chapter).

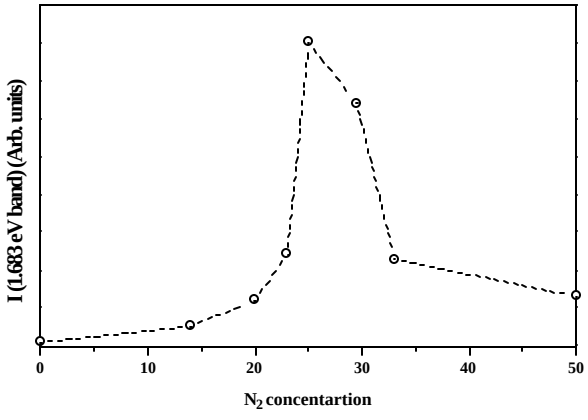

Fig. 5.7 Intensity of 1.683 eV PL band as a function of N_2 concentration

In addition to the band at 1.683 eV, nitrogen-related bands at ~ 2.15 eV and 2.05 eV are also observed in the PL spectra of the nitrogen incorporated films. The 2.15 eV and 2.05 eV bands are proposed to be due to a transition in a center consisting of a single substitutional nitrogen atom with one or more vacancies [68]. In the PL spectrum of the film grown with 50% nitrogen concentration, these both the bands are comparable to the 1.683 eV band.

5.4.2 Substrate Temperature Dependence on N-doped diamond films

In order to study the growth behavior and properties of the nitrogen doped diamond films as a function of substrate temperature, the films were grown with 20% N_2 fraction in CH_4 for 3 hours at the substrate temperatures varying from 750^0C to 950^0C keeping all other deposition parameters identical. Fig. 5.8 shows the SEM photographs of the surface

morphology of the films deposited at the substrate temperatures of 750^0C, 850^0C and 950^0C. The surface morphology of these films appears to have common

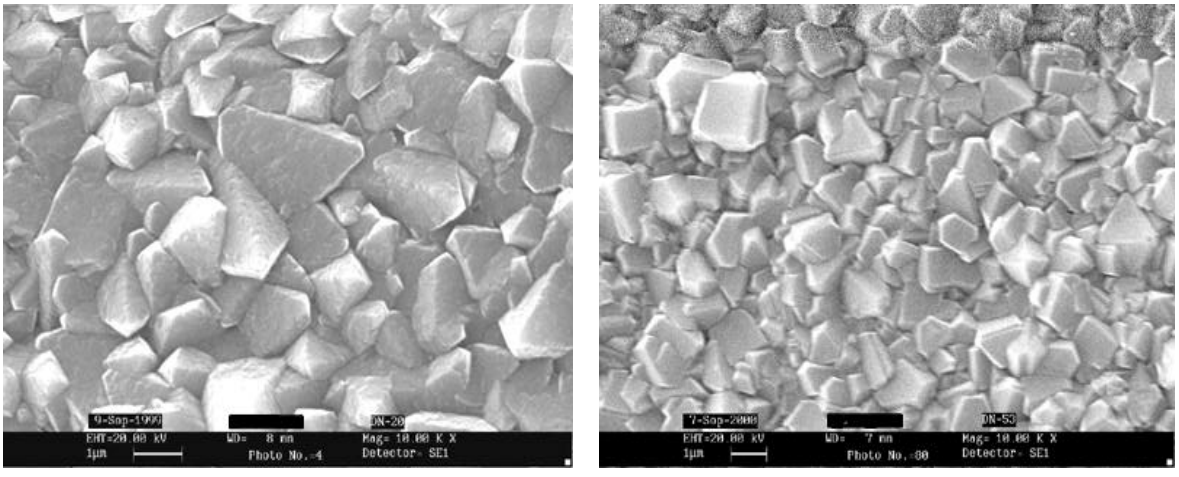

(a) **(b)**

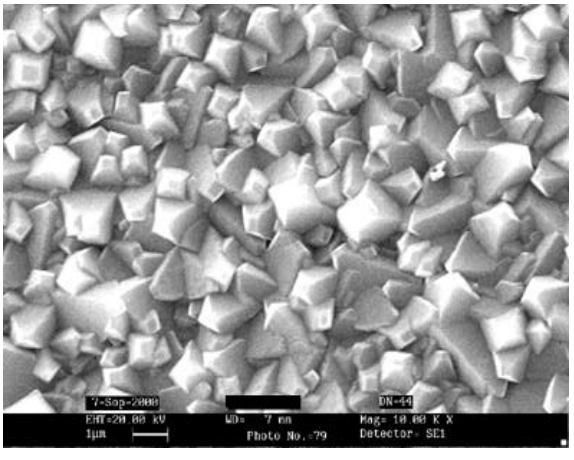

(c)

Fig. 5.8 SEM photograph of the surface morphology of the diamond films grown with 20% N_2 fraction in CH_4 at the substrate temperatures of-

(a) 750^0C (b) 850^0C and (c) 950^0C (Please note the change in magnifacation)

features which indicate that the surface is made up of pyramidal shaped diamond particles with well developed {111} facets. The pyramidals are seen to have square like faces at the top which implies that the crystal orientation is likely to change to {100}. The average crystallite size is observed to increase from 1.25µm to 1.50µm and 1.75µm when the substrate temperature is increased from 750^0C to 850^0C and 950^0C respectively.

The X-ray diffraction patterns of the films grown with 20% N_2 fraction in CH_4 at different substrate temperatures are shown in Fig. 5.9. These XRD patterns show the texture of the film to be {111). The XRD patterns of the films grown at higher substrate temperatures show additional line at 2θ=49.80 0 (d=1.83) which is assigned to SiC (106). At higher substrate temperatures, the growth rate is relatively high. Therefore,
the Si from the substrate may not diffuse into the bulk of the film, but it may form the carbide and will remain at the film/substarte surface boundary.

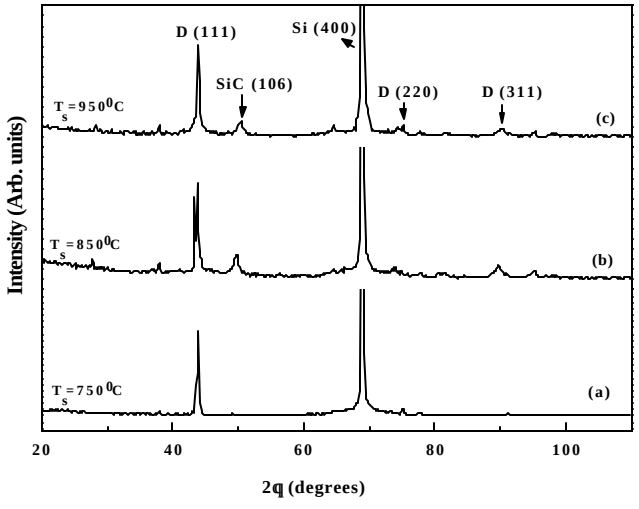

Fig. 5.9 XRD patterns of the diamond films grown with 20% N_2 fraction in CH_4 at the substrate temperatures of - (a) 750 ^{0}C (b) 850 ^{0}C (c) 950 ^{0}C

These films were also characterized by photoluminescence spectroscopy so as to study the defect distribution in the film. Fig. 5.10 shows the photoluminescence spectra of these films. It shows two sharp bands positioned at Raman shift of 520 cm^{-1} and 1332 cm^{-1}. These are vibrational Raman bands which are well known to originate from the excitation of transverse optical modes of Si and diamond crystals [84]. The 520 cm^{-1} band is attributed to the single crystal Si substrate while the 1332 cm^{-1} band is attributed to the polycrystalline diamond film deposited on Si substrate. In addition to these bands, the spectra also show the broad photoluminescence bands positioned at 2.15 eV and 2.05 eV and a sharp band at 1.683 eV. The bands at 2.15 eV and 2.05 eV are related to nitrogen and are proposed to be due to a

transition in a center consisting of a single substitutional nitrogen atom with one or more vacancies [68]. As seen in the previous chapter, the 1.683 eV band is attributed to the monovacancies formed in the film during the growth. The intensity of this band is found to increase with the substrate temperature. This observation can be explained as follows: With the substrate

Chapter 5 *Influence of Nitrogen on the Growth of Diamond Films*

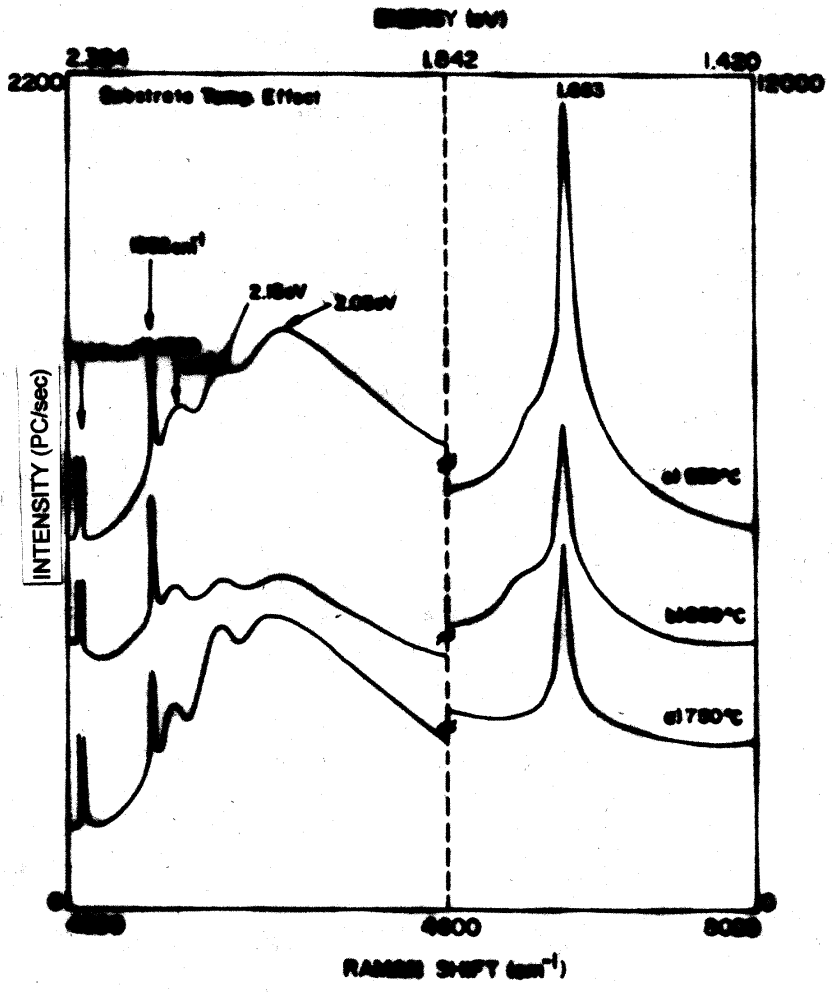

Fig. 5.10 The PL spectra of the N-doped diamond films grown on Si substrate vs. substrate temperature

temperature, the growth rate increases and as the covalent radius of nitrogen (r_N ~ 0.75 Å) is comparable to the covalent radius of carbon (r_C ~ 0.77 Å), nitrogen may get trapped in the vacancies. It may result in the conversion of large number of clustered vacancies into monovacancies or N-V centers. Therefore, the intensity of the 1.683 eV band which is attributed to the presence of monovacancies [83], increases with the substrate temperature.

5.4.3 Nitrogen Incorporated Diamond Films on Non-Silicon Substrates

In order to verify the role of nitrogen on the growth and properties of diamond films grown on Si substrate, the films were also grown on alumina (Al_2O_3) and copper (Cu) substrates. The deposition parameters used were same as listed in Table 5.2.

5.4.3 (a) N-doped diamond films on Alumina Substrate

The representative SEM photographs of the surface morphology of the diamond films grown on alumina substrate with 0% and 20% nitrogen fraction in CH_4 are shown in Fig. 5.11.

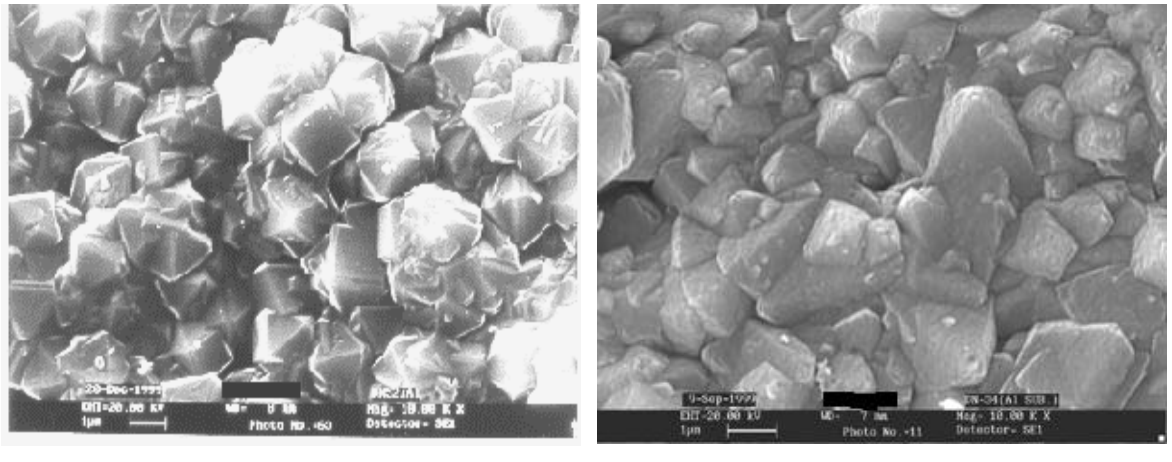

(a) **(b)**

Fig. 5.11 SEM photograph of the diamond films grown on Al_2O_3 substrate with (a) 0% and (b) 20% N_2 fractions in CH_4

The morphology of the film grown without nitrogen addition shows large, well-defined cubo-octahedral crystallite facets. The top surface shows a predominance of {111} growth habit, with a average grain size of around 1.5 μm, which is characteristic of high quality diamond samples grown by HFCVD. Dramatic morphological changes are observed in the film grown with nitrogen incorporation. It shows the presence of multinucleation and overgrowth. The average grain size is found to increase upto 2.0 μm which was ~ 1.5 μm for the film grown without nitrogen. The overall surface morphology appeared to be{111} faceted.

The quality of the CVD diamond films grown on alumina substrate was evaluated by Raman spectroscopy. The spectra were recorded for Raman shifts between 1000 and 1800 cm^{-1} and are shown in Fig. 5.12. In this case, we have considered two spectral features: the line width (FWHM) of 1332 cm^{-1} diamond band, and the intensity of the broad bands in the spectral region around 1550-1580 cm^{-1} (I_G) which are commonly ascribed to sp^2-bonded carbon, normalized with respect to the peak intensity of the diamond band (I_D). It was observed that the ratio I_G/I_D increased by a factor of about 2 for nitrogen additions between 0% to 50% (shown in Table 5.3). At higher concentrations of nitrogen, significant increase was observed in the diamond line width which increased from 6.6 cm^{-1} at 0% N_2 concentartion to almost 13.2 cm^{-1} at 50% N_2 concentration of nitrogen. The corresponding Raman spectra revealed an improvement of the diamond phase quality for the films grown with low nitrogen concentrations as evidenced from the higher peak intensity of the 1332 cm^{-1} diamond band while for higher nitrogen concentration, the diamond quality was observed to decrease as the non-diamond content in the film becomes more pronounced.

Table 5.3 : Characteristic Raman features of the films grown on Al_2O_3 substarte in CH_4-H_2-N_2 system.

N_2 Conc. (%)	FWHM (cm^{-1})	I_G/I_D
0.0	6.6	0.46
14.0	7.3	0.62
20.0	9.0	0.80
23.0	9.9	0.82
25.0	9.2	0.83
29.5	10.8	0.91
33.0	12.5	0.84
50.0	13.2	0.65

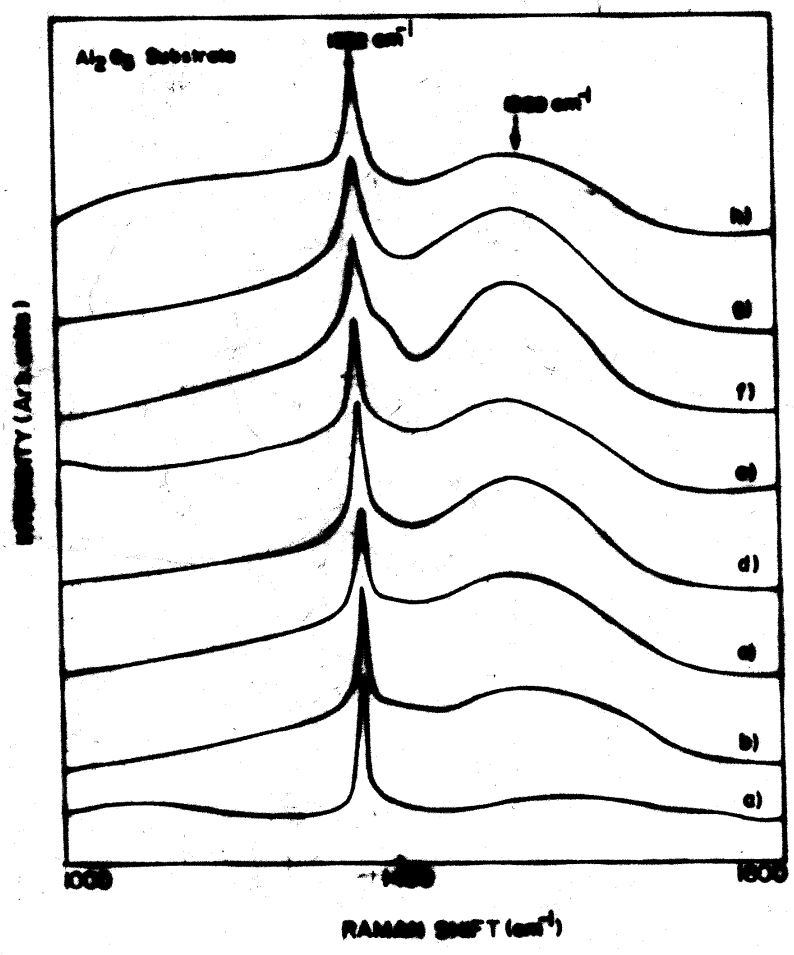

Fig. 5.12 Raman spectra (normalized for 1332 cm^{-1} band) of the N-doped diamond films grown on Al_2O_3 substrate as a function of nitrogen concentration (*a*) 0%, (*b*) 14%, (*c*) 20%, (*d*) 23%, (*e*) 25%, (*f*) 29.5%, (*g*) 33%, and (*h*) 50%

Another impotant aspect of concern is the evolution of defects and impurities in the film with increasing nitrogen concentration in the feed gas. This aspect was studied by the photoluminescence (PL) measurements of the films. The PL spectra of the films grown on alumina substrate as a function of nitrogen concentartion are shown in Fig. 5.13 (representative full range spectra from 2.364 eV to 1.917 eV), Fig. 5.14 (energy range 2.364 eV to 1.917 eV) and Fig. 5.15 (energy range 1.730 eV to 1.420 eV). The spectra in the range 2.364 to 1.917 show the nitrogen related bands positioned at 2.15 eV and 2.05 eV (similar to those observed in case of Si substrate). The PL spectra recorded in the range 1.730 eV to 1.420 eV show the sharp band at 1.683 eV in the films grown with nitrogen and is found to be strongly dependent on the nitrogen concentration. ***The dependence of this band on N_2 concentration is observed to be similar to that observed in case of Si substrate.*** The films were also characterized by X-ray diffraction technique to confirm the presence of diamond crystallites. The representative XRD patterns of the diamond films grown with 0% and 20% N_2 fractions in CH_4 are shown in Fig. 5.16. The film texture is observed to be {111} dominant.

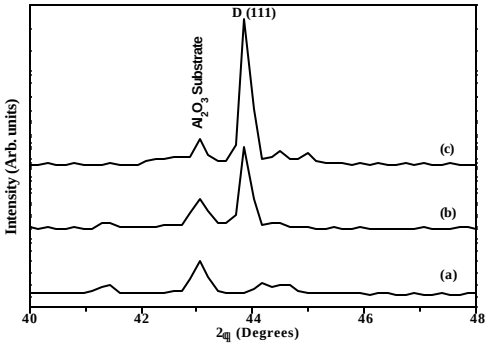

Fig. 5.16 XRD patterns of (a) Al_2O_3 substrate and the diamond films grown on Al2O3 substrate with- (b) 0% and (c) 20% N_2 fractions in CH_4.

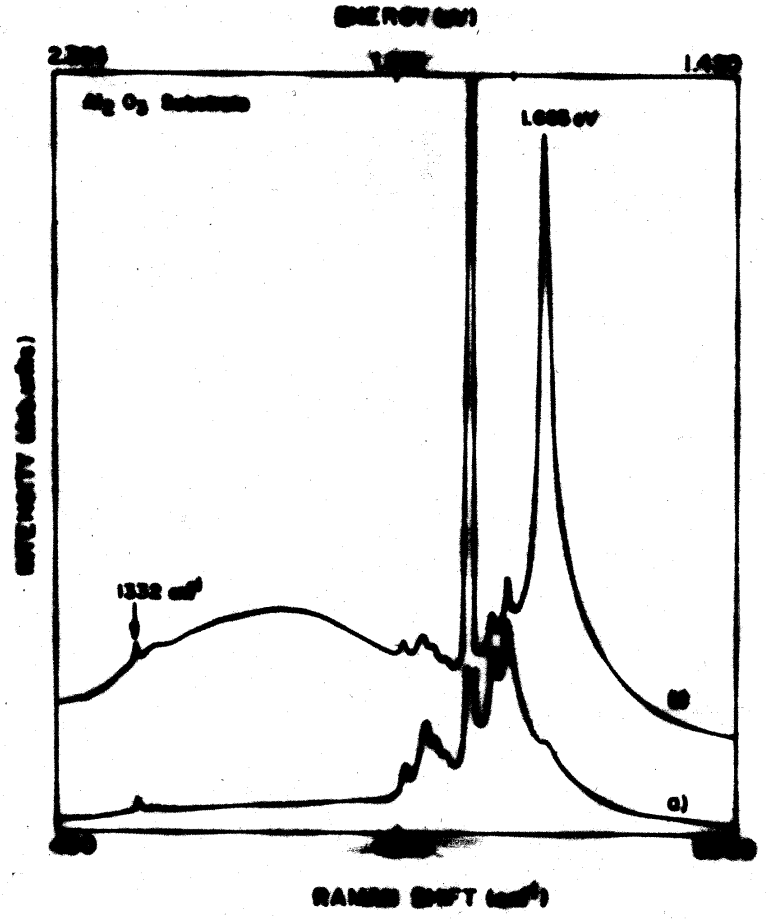

Fig. 5.13 Representative full range (2.364 eV to 1.420 eV) PL spectra of the diamond films grown on Al_2O_3 substrate with (*a*) 0%, and (*b*) 20% nitrogen concentration (the bands between 1.89 eV and 1.74 eV are due to the PL emission from Al_2O_3 substrate)

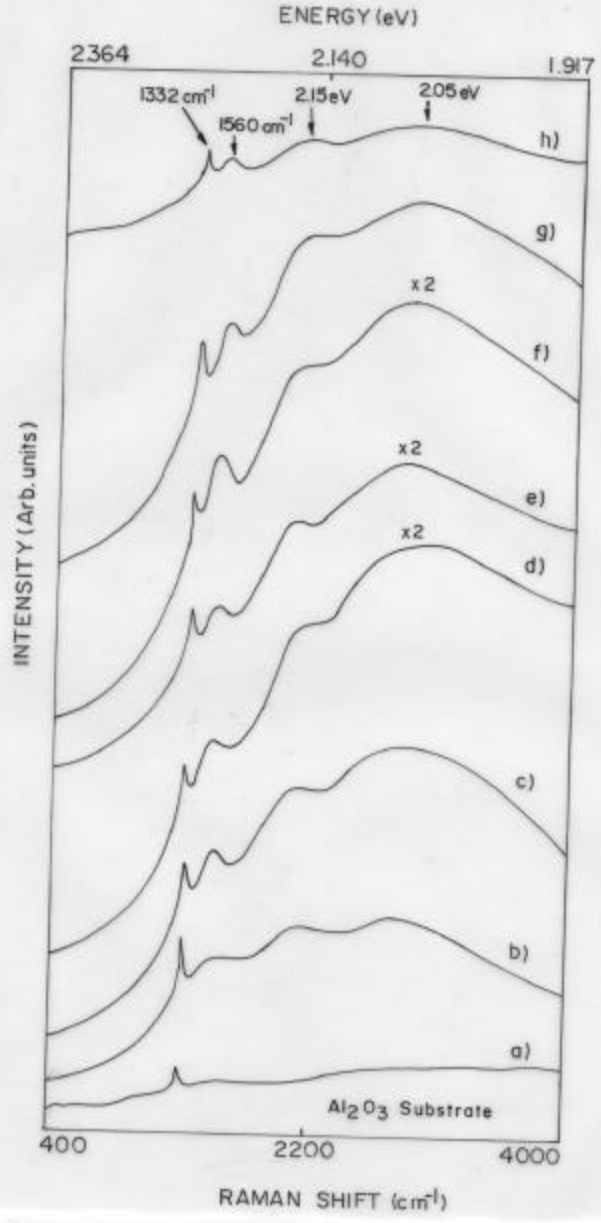

Fig. 5.14 The PL spectra (in the range of 2.364 eV to 1.917 eV) of the diamond films grown on Al_2O_3 substrate as a function of nitrogen concentration (*a*) 0%, (*b*) 14%, (*c*) 20%, (*d*) 23%, (*e*) 25%, (f) 29.5%, (*g*) 33%, and (*h*) 50%

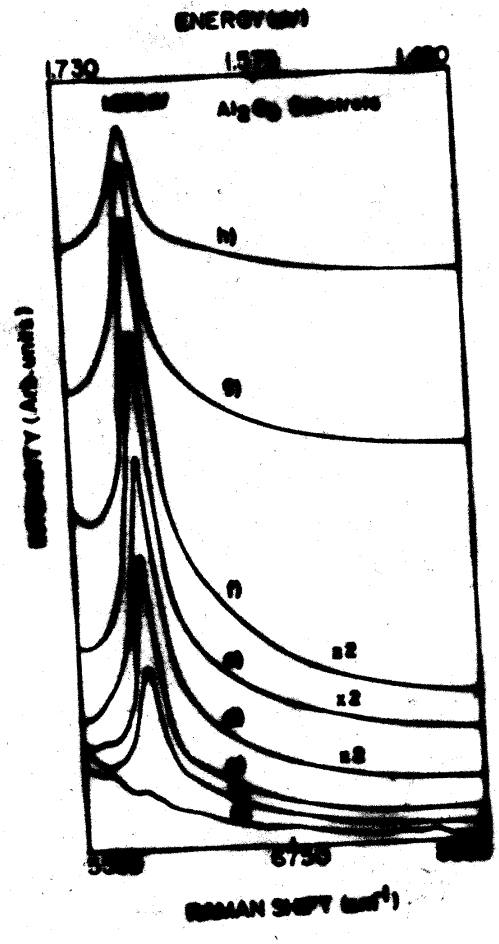

Fig. 5.15 The PL spectra (in the range of 1.730 eV to 1.420 eV) of the diamond films grown on Al_2O_3 substrate as a function of nitrogen concentration (*a*) 0%, (*b*) 14%, (*c*) 20%, (*d*) 23%, (*e*) 25%, (*f*) 29.5%, (*g*) 33%, and (*h*) 50%

5.4.3(b) N-doped diamond films grown on Copper Substrate

Similarly, the films were grown on copper substrate. The representative SEM photographs of the surface morphology of the nominally pure film and the film grown with 20% nitrogen concentration are shown in Fig. 5.17. The morphology of the film grown without nitrogen addition shows large, well-defined cubo-octahedral crystallite facets. The top surface shows a predominance of {111} growth habit, with a average grain size of around 1μm. The film grown with nitrogen incorporation shows the pyramidal shaped diamond particles with the square like faces on the top of the pyramid. The average grain size is found to increase upto 1.5μm.

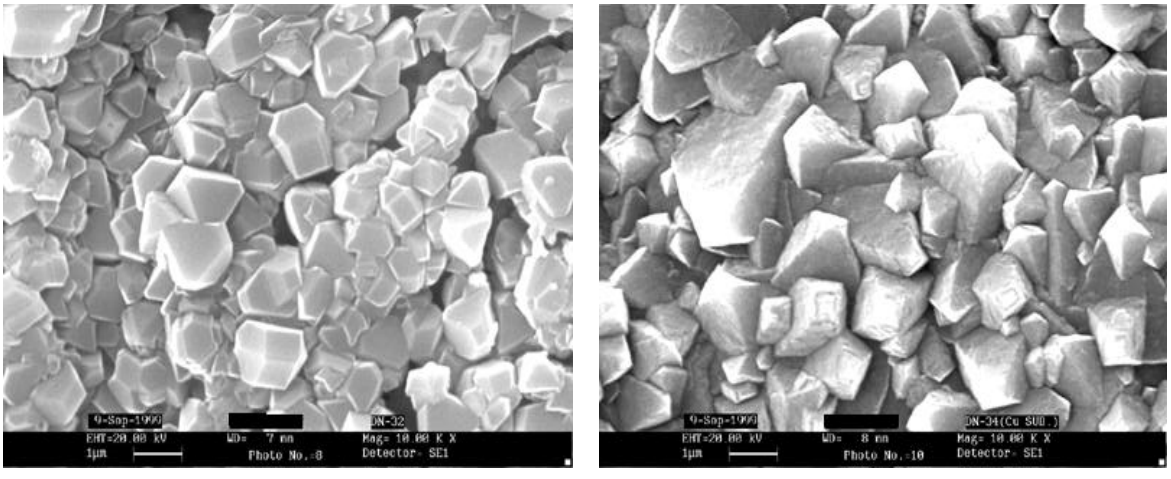

(a) **(b)**

Fig. 5.17 SEM photographs of the diamond films grown on Cu substrate with- (a) 0% and (b) 20% N_2 fractions in CH_4

The Raman spectra of these films are shown in Fig. 5.18. The spectrum of nominally pure diamond film exhibits a sharp band at 1332 cm^{-1} with FWHM of 7.1 cm^{-1}. The spectrum also shows the additional broad feature between 1500-1600 centered at 1560 cm^{-1} which is very small as compared to 1332 cm^{-1} band. This broad feature is assigned to the sp^2 bonded non-diamond content in the film. The Raman spectrum of the film grown with nitrogen revealed the poorer diamond phase purity , which is illustrated by an increase of non-diamond carbon features around 1560 cm^{-1} and decrease in the intensity of the diamond band at 1332 cm^{-1} with higher FWHM (9.0 cm^{-1}). The X-ray diffraction patterns of the films grown on Cu substarte are shown in Fig. 5.19. The intensity of the diffraction line corresponding to 2θ=

43.85^0 (d=2.0629 Å) which is assigned to D(111) is found to increase after nitrogen addition. This suggests that the growth rate is improved in the film grown with nitrogen. The spectra also show the other diffraction line at $2\theta = 75.21^0$ (d= 1.2623 Å) which is assigned to D(220) confirming the presence of diamond crystallites.

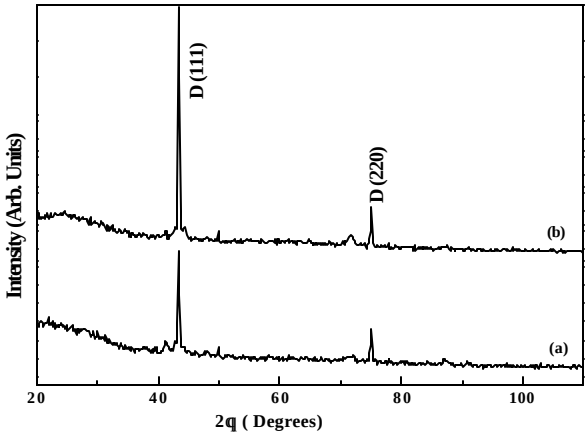

Fig. 5.19 XRD patterns of the diamond films grown on Cu substarte with-
(a) 0% and
(b) 20% N_2 fractions in CH_4

Fig. 5.20 shows the PL spectra of the undoped and nitrogen doped (20%) diamond films grown on Cu substrate. In the PL spectrum of the undoped diamond film grown on Cu substrate, a broad band centered at about 1.72 eV with a small hump at 1.683 eV was observed while for the nitrogen doped film, a sharp band at 1.683 eV was observed. In addition to these bands, the nitrogen related bands at 2.15 eV and 2.05 eV are also observed in the film grown with nitrogen. These results are similar to the results observed in case of the films grown on Si and Al_2O_3 substrates.

5.5 Conclusion

SEM, Raman and photoluminescence measurements were employed in the present study to investigate the role of nitrogen incorporation on the growth, structure and properties of diamond films. Upon N incorporation, the surface morphology of the films is

observed to change from {111} facets to pyramidal shaped crystallites while the growth rate is observed to enhance from 1.1 μm/hr to 2.8 μm/hr. The higher concentration of nitrogen leads to the multinucleation and overgrowth. The latter is likely to be sp^2 bonded graphitic carbon as evidenced from the Raman spectra.

Our results on the photoluminescence measurements lead to the following conclusions:

(a) The PL spectra of the nitrogen-doped CVD diamond films indicate that the incorporation of nitrogen into the diamond lattice introduces the optical centers at 2.15 eV and 2.05 eV which are attributed to N-vacancy centers.

(b) The occurrence of 1.683 eV band in diamond so far was attributed by earlier workers to Si impurity (contamination) introduced by the Si substrate. However, contrary to this, the films deposited on Al_2O_3 and Cu substrates (electronic grade) where direct Si impurity contamination was unlikely, have also exhibited this band line at 1.683eV after nitrogen incorporation and its intensity showed the concentration dependence similar to that observed for Si impurity incorporation. ***This raises doubt about the earlier correlation of the origin of the 1.683 eV line to Si-vacancy centers in diamond.*** The PL in the present case therefore needs to be attributed to nitrogen induced defects, in general, the monovacancies similar to those proposed for Si doped films. Thus we speculate that the 1.683 eV related centers may have common origin for films deposited on all type of substrates.

References

1. A. B. Anderson and S. P. Mehandra, Phys. Rev. B 48 (1993) 4423.
2. S. A. Kujihara, A. Antonelli and J. Bernhole, Physica B 185 (1993)144.
3. J. Walker, Rep. Prog. Phys. 42 (1979) 1605.
4. F. G. Chesley, Am. Mineralogist 27 (1942) 20.
5. F. A. Raal, Am. Mineralogist 42 (1957) 354.
6. E. N. Bunting and A. V. Valkenburg, Am. Mineralogist 43 (1958) 102.
7. W. K. Kaiser, W. L. Bond and Tanenbaum, Bull. Am. Phys. Soc. Ser. II (4) (1959) 27.

8. W. K. Kaiser and W. L. Bond, Phys. Rev. 115 (1959) 857.
9. J. E. Field, The properties of Diamond (Academic, London, 1979).
10. S. A. Kajihara, A. Antonelli, J. Bernhole and R. Car, Phys. Rev. Lett. 66 (1991)2010.
11. A. Mainwood, J. Phys. C: Solid State Phys. 12 (1979) 2543.
12. J. Loubser and J. A. Van-Wyk, Rep. Prog. Phys. 41 (1978) 1202.
13. K. Jackson, M. R. Pederson and J. G. Harrison, Phys. Rev. B 41 (1990) 12641.
14. A. T. Collins, M. Kamo and Y. Sato, J. Phys.: Condensed Matter 1 (1989) 4029.
15. J. Mort, M. A. Machonkin and K. Okumura, Appl. Phys. Lett. 59 (1991) 3148.
16. G. Davies, S. C. Lawson, A. T. Collins, A. Mainwood and S. J. Sharp, Phys. Rev. B 46 (1992) 13157.
17. S. Jin and T. D. Moustakas, Appl. Phys. Lett. 63 (1993) 2354.
18. S. Jin and T. D. Moustakas, Appl. Phys. Lett. 65 (1994) 403.
19. W. V. Smith, P. P. Sorokin, I. L. Gelles and G. J. Lasher, Phys. Rev. 115 (1959) 1546.
20. C. J. Ammerlaan, Inst. Phys. Conf. Ser. 59 (1981) 81.
21. Y. Bar-Yam and T. D. Moustakas, Nature 342 (1989) 786.
22. Y. Bar-Yam and T. D. Moustakas, Mater. Res. Soc. Symp. Proc. 162 (1990) 201.
23. A. Cox, M. E. Newton and J. M. Baker, J. Phys.: Condensed Matter 6 (1994) 551.
24. A. Cox, Ph. D. Thesis, University of Oxford, 1993.
25. O. D. Tucker, M. E. Newton and J. M. Baker, Phys. Rev. B 50 (1994) 15586.
26. T. Evans and Z. Qi, Proc. Royal Soc. London Ser. A 381 (1982) 159.
27. G. B. B. M. Sutherland, D. E. Blackwell and W. G. Simeral, Nature 174 (1954) 901.
28. P. R. Briddon and R. Jones, Physica B 185 (1993) 179.
29. J. A. Van-Wyk and J. Loubser, J. Phys. C 16 (1983) 1501.
30. R. Locher, C. Wild, N. Herres, D. Behr and P. Koidl, Appl. Phys. Lett. 65 (1994)34.
31. A. Badzian, T. Badzian and S. Tong Lee, Appl. Phys. Lett. 62 (1993) 3432.
32. C. Wild, R. Kohl, N. Herres, W. Miller-Schert and P. Koidl, Diam. Relat. Mater. 3 (1994) 373.
33. G. Z. Cao, J.J. Schermer, W. J. P. Van Enckevort, W. A. L. M. Elst, and L. J. Gilling, J. Appl. Phys. 79 (1996) 1357.

34. Handbook of Chemistry and Physics, 70 th ed., edited by R. C. Weast, D. R. Lide, M. J. Astle, and W. H. Beyer (CRC Boca Raton, FL, 1989), p. F-198.
35. E. Boettger, A. Bluhm, X. Jiang, L. Schafer, and C.-P. Klages, J. Appl. Phys. 77 (1995) 6332.
36. N. Fujimori, A. Ikegaya, T. Imai, N. Ota, and T. Shabata, Sumitomo Electric Industries, European Patent No. EP 0,469,626,A2 (1992).
37. S. Bohr, R. Haubner, and B. Lux, Appl. Phys. Lett. 68 (1996) 1075.
38. F. J. Himpsel, J. A. Knapp, J. A. Van Vechten, and D. E. Eastman, Phys. Rev. B 20 (1979) 625.
39. B. B. Pate, B. J. Waclawaski, P. H. Stefan, C. Binns, T. Ohte, M. H. Hecht, P. J. Jupiter, M. L. Shek, D. T. Pierce, N. Swanson, R. J. Celotta, I. Liundau and W. E. Spicer, Physica B 117/118 (1983)783.
40. M. W. Geis, J. A. Gregory, and B. B. Pate, IEEE Trans. Electron devices 38 (1991) 619.
41. J. Van der Weider and R. J. Nemarich, Phys. Rev. B 45 (1994)13629.
42. M. W. Geis, N. N. Efremow, J. D. Woodhouse, M. D. McAleese, M. Marchywka, D. C. Socker, and J. F. Hochedez, IEEE Electron Device Lett. 12 (1991) 456.
43. G. R. Brandes, C. P. Beetz, C. A. Feger, and R. L. Wright, Diam. Relat. Mater. 4 (1995) 586.
44. M. W. Geis, J. C. Twichell, J. Macaulay, and K. Okano, Appl. Phys. Lett. 67 (1995)1328.
45. H. B. Dyer, and L. du Preez, J. Chem. Phys. 42 (1965) 1898.
46. M. W. Geis, J. C. Twichell, N. N. Efremow, K. Krohn, and T. M. Lyszczarz, Appl. Phys. Lett. 68 (1996) 2294.
47. A. Lenef, and S.C. Rand, Phys. Rev. B 53 (1996) 13441.
48. B. B. Li, M. C. Tosin, A. C. Peterlevitz, and V. Baranauskas, Appl. Phys. Lett. 73 (1998) 812.
49. D. F. Talbot-Ponsonby, M. E. Newton, and J. M. Baker, J. Appl. Phys. 82 (1997) 1201.
50. J. A. Freitas, Jr., J. E. Buttler, S. G. Bishop, W. A. Carrington, and U. Storm, Matter.

Res. Soc. Symp. Proc. 162 (1990) 237.

51. D. S. Knight, and W. B. White, Proc. SPIE 1055 (1989) 144.
52. E. S. Etz, E. N. Farabaugh, A. Feldman, and L. H. Robins, Proc. SPIE 969 (1988) 86.
53. J. A. Freitas, Jr., J. E. Buttler, and U. Storm, J. Mater. Res. 5 (1990) 2502.
54. L. H. Robins, E. N. Farabaugh and A. Feldman, Proc. SPIE 1325 (1990) 130.
55. A. T. Collins and S. C. Lawson, J. Phys.: Condensed Matter 1 (1989) 6929.
56. A. Badzian, T. Badzian, R. Roy, R. Meisser and K. E. Spear, Mater. Res. Bull. 23 (1988) 531.
57. R. J. Nemarich, J. T. Glass, G. Lucovsky, and R. E. Shroder, J. Vac. Sci. Technol. A6 (1988) 1783.
58. Y. Sato and M. Kamo, Surf. Coat. Technol. 39/40 (1989) 183.
59. J. Robertson, Adv. Phys. 35 (1986) 317.
60. J. Wagner, and P. Lautenschlager, J. Appl. Phys. 59 (1986) 2044.
61. I. Watanabe, S. Hasegawa, and Y. Korate, Jpn. J. Appl. Phys. 21 (1982) 856.
62. S. H. Lin, and B. J. Feldman, Philos. Mag. B 47 (1983) 113.
63. L. Bergman, B. R. Stoner, K. F. Turner, J. T. Glass and R. J. Nemarich, J. Appl. Phys. 73 (1993) 3951.
64. V. S. Vavilov, A. A. Gippius, A.M. Zaltsev, B. V. Deryagin, B. V> Spitsyn and A. E. Aleksenko, Sov. Phys. Semocond. 14 (1980) 1078.
65. J. Ruan, W. J. Choyke, and W. D. Partlow, Appl. Phys. Lett. 58 (1991) 295.
66. J. Ruan, W. J. Choyke, and W. D. Partlow, J. Appl. Phys. 69 (1991) 6632.
67. T. Feng, and B. D. Schwartz, J. Appl. Phys. 73 (1993)1415.
68. L. Bergman, M. T. McClure, J. T. Glass and R. J. Nemarich, J. Appl. Phys. 76 (1994) 3020.
69. M. E. Pereira, M. I. B. Jorg, and M. E. Thomaz, J. Phys. C 19 (1986) 1009.
70. N. E. Mott, and E. A. Davis, Electronic Process in Non-Crystalline Materials (Clarendon, Oxford, 1979).
71. J. M. marshall and R. A. Street, Solid Statae Commun. 50 (1984) 91.
72. T. M. Hong, S. H. Chen, Y. S. Hou, and C. F. Chen, Thin Solid Films 270 (1995)

148.

73. R. S. Tsang, C. A. Rego, P. W. May, M. N. R. Ashfold and K. N. Rosser, Diam. Relat. Mater. 6 (1997) 247.
74. K. Kamo, S. Koizumi, S. R. P. Silva and G. A. L. Amaratunga, Nature 381 (1996) 140.
75. P. Lerner, N. M. Miskovsky, and P. H. Cutler, J. Vac. Sci. Technol. B 16 (1998) 900.
76. I. T. Han, N. Lee, S. H. Kim, and D. Jeon, J. Vac. Sci. Technol. B 16 (1998) 2052.
77. S. F. Durrant, V. Baranauskas, A. Peterlevitz, B. B. Li, M. C. Tosin, E. C. Rangel, J. Wang, S. G. Castro, and M. A. B. de Moraes, Thin Solid Films 355-356 (1999) 184.
78. R. J. Buckley, T. D. Moustakas, L. Ye, and J. Varon, J. Appl. Phys. 66 (1989)3595.
79. N. V. Sidgwick, "The Organic Chemistry of Nitrogen (Clarendon, Oxford, 1942) p 301.
80. J. A. Freitas, J. E. Buttler, and U. Storm, J. Mater. Res. 5 (1990) 2502.
81. J. Ruan, W. J. Choyke, and W. D. Partlow, Appl. Phys. Lett. 58 (1991) 295.
82. T. Feng and B. D. Schwartz, J. Appl. Phys. 73 (1993) 1415.
83. S. Dannefaer, W. Zhu, T. Bretagnon, and D. Kerr, Phys. Rev. B. 53 (1996) 1979.
84. S. A. Solin, and A. K. Ramdas, Phys. Rev. B 1 (1970) 1687.

CHAPTER 6

GROWTH OF FLUORINATED DIAMOND FILMS

In this work, tetrafluoromethane (CF_4) is added to standard CH_4/H_2 mixtures for diamond growth in hot-filament assisted CVD reactor. The films are grown for various concentrations of CF_4. The changes produced in the surface morphology, Raman scattering amd the photoluminescence properties are discussed in details in this chapter.

6.1 Introduction:

The growth of polycrystalline diamond films by chemical vapour deposition (CVD) has used most commonly dilute concentrations of hydrocarbon gas (e.g. CH_4) mixed with hydrogen. The activation of such a source gas mixture results in the production of radical species, principally atomic hydrogen (H^0) and methyl radicals (CH_3) which impinge upon a heated substrate. It has been, in general, accepted that the methyl radicals are the primary species responsible for diamond growth under a variety of conditions [1]. However, the CH_3 radical is a plane molecule and has an unpaired electron in p-like atomic orbital of carbon in an isolated system [2]. On the other hand, a CF_3 radical is a trigonal pyramidal molecule and has an unpaired electron in sp^3 like hybrid orbital of carbon in an isolated system. Moreover, graphite can be fluorinated easily where the bonding orbitals of carbon change from sp^2-like to sp^3-like hybrid orbitals [2]. Therefore, the use of a fluorine-based carbon system should result in diamond growth with better growth rates as well as quality which may exceed the results achieved with conventional hydrocarbon system [3,4]. Fluorinated precursors may produce gas-phase diamond growth species other than the methyl radical which could facilitate diamond growth. Additionally, fluorocarbon precursors may enable the use of fluorine-hydrogen abstraction reaction to sustain diamond growth [5]. These suggestions are based on a thermodynamic consideration that halogen-based reactions will produce hydrogen-halogen molecules instead of the less stable hydrogen molecules which are produced in conventional CVD diamond systems[3].

Thermochemistry studies [6] have shown that, in the absence of hydrogen and hydrocarbons, halogenated surfaces are stable enough to avoid the diamond growth, but if hydrogen and hydrocarbons are added, the growth is quite favorable. It has also been depicted that typical gas-phase reactions of hydrocarbons and fluorine have higher rate coefficients with much lower activation energy than their counterparts with hydrogen [7]. This is very likely to happen also for surface reactions. The abstraction of hydrogen atoms from the diamond surface has been widely accepted as a limiting step for diamond growth at low temperatures. In case of purely H-based system, the H-abstraction involves H-H bond formation resulting in molecular

H_2 which is stable at the substrate temperature involved. The rate of H-abstraction can be enhanced by fluorine interaction which has more affinity towards hydrogen [8].

However, relatively few experimental studies have been reported on diamond synthesis from fluorinated gas mixtures. Rudder et al. [9] have reported the fluorinated growth of diamond films on Si substrates by using RF-plasma CVD method. They deposited the films at 5 Torr and 850 ^{0}C on as-received mirror polished silicon wafers and observed dense nucleation and well-defined facets. From x-ray photoelectron spectroscopy, fluorine was observed to be bound to the surface carbon atoms. It showed C1s electron shifted to 285 eV and 288 eV corresponding to C-C bonding and C-F bonding respectively. The fluorine bonding to diamond surface was thought to arise from residual contamination of the surface upon termination of the RF discharge. At the growth temperature of about 850 ^{0}C, it has been shown that fluorine can not reside on a diamond surface in the atomic hydrogen environment produced by the high-power RF disharge as any surface fluorine would likely be extracted from the surface during growth via the formation of HF [10]. Fox et al.[5] have also reported the similar observations. They used the fluorinated gas mixtures and deposited the diamond films at various substrate temperatures in the range of 600-900 ^{0}C at constant microwave power, carbon mole fraction and pressure. From XPS studies, they estimated the amount of fluorine detected to be ~1% of the near-surface region composition. The films thus grown were then subjected to argon ion bombardment for 10 minutes using 5000 V potential. In these ion bombarded films, no fluorine was detected. Thus, they showed that although residual fluorine was detected on the surface after deposition, fluorine was not incorporated into the film. According to few researchers , it may be due to very short lifetime of fluoro (hydro) carbon species which makes their participation in the growth process very unlikely, unless formed very close to the substrate [8,11]. Kadono et al.[2] have also reported the growth of diamond films using fluorinated carbon source. They deposited the diamond films from CF_4-H_2 mixture using microwave plasma CVD and found that the better quality diamond films were grown even upto 40% concentration of CF_4,. For higher concentrations, the ratio of peak intensity of non-diamond material of carbon at around 1500 cm^{-1} to that of the diamond peak at 1333 cm^{-1} was

found to be more than one. This observation suggestes that, using fluorinated source gases, better quality films can be grown at lower concentration of fluorinated source (e.g. CF_4).

The most likely gas phase and surface reaction in C-H-F system is the formation of HF by atomic fluorine with the gas phase hydrocarbons, atomic and molecular hydrogen and surface bonded hydrogen [12]. This suggests that atomic fluorine enhances the formation of gas phase hydrocarbon radicals, such as CH_3, and atomic hydrogen when reacting with molecular hydrogen in the gas phase. Further, it was suggested that, HF may preferentially etch graphite and amorphous carbon rather than sp^3 bonded diamond [12]. Shimada et al. [13] found that CF_4 RF plasma etching of diamond films resulted in the selective removal of amorphous carbon and graphite structures from the diamond surface which supports the above suggestion.

Work of some researchers have shown that the fluorination of the C-H diamond CVD system can enhance the deposition at low substrate temperature without simultaneous deterioration in quality or growth rate of the deposition [14-18]. Trava-Airoldi et al.[19,20] found that by adding CF_4 to a CH_4-H_2 HFCVD system, substrate temperature could be decreased from 950 ^{0}C to 580 ^{0}C, producing smoother films when deposited on WC. Corat et al.[8,21] were also able to bring the substrate temperature down to 390 ^{0}C in a similar system. A comparative study of HFCVD CH_4-H_2 and CHF_3-H_2 systems, by Schmidt et al.[22], showed the later to produce films even at 400 ^{0}C, while no films were obtained with the former at the same substrate temperature. However, Schmidt et al. [22] were unable to obtain diamond with a CF_4-H_2 precursor mixture in the same system at this temperature, probably due to the high activation energy required by the CF_4.

Grannen et. al [23] have reported that the addition of fluorinated species to the diamond CVD system increases growth rates. They found that the diamond films deposited using a gas mixture of CF_4-H_2-O_2 by microwave plasma CVD yielded four times the growth rate, and three times the adhesion at the same substrate temperature as compared to the growth in a CH_4-H_2-O_2 system. Corat et al.[24] have observed growth rates 40% higher when adding CF4 to a CH_4-H_2 HFCVD system. Asmann et al.[25] have proposed that the increase in the growth rate may be due to increased hydrogen abstraction from the diamond surface by gas

phase fluorine. As a result of this hydrogen abstraction, active sites on the growing surface may increase. If this same abstraction was facilitated at lower temperature, it would also account for the enhancement of low temperature growth of diamond in the fluorinated system. This would depend on the ability of gas phase fluorine to reach the substrate at these lower temperatures and availability of the required energy for hydrogen abstraction by fluorine. However, while fluorine stabilizes the surface, the C-F bond is difficult to break and has a higher bond strength (552 kJ/mole) than H-H bond (436 kJ/mole). Therefore, at lower substrate temperature, formation of sp^3 bonded carbon may be limited by the availability of sites and the growth process will be restricted.

Thus, the above background literature indicates that the growth of diamond films with the fluorine-based system has been shown to be very encouraging. However, most of the studies reported so far have been concentrated on the lowering of the growth temperature and growth rate enhancement. Also, it is seen that the lifetime of the fluorohydrocarbon species is very short which makes their participation in the low temperature (~400 ^{0}C) growth process unlikely, unless formed very close to the substrate. If these species are formed very close to the substrate at comparatively high temperature, then the species may take part in the growth process. Also, the F atom is larger in size (0.72 Å) than that of H (0.32 Å) and hence has low surface mobility during the growth of diamond films. However, its size is comparable to that of carbon (0.77 Å). Therefore, if the fluorinated species participate in the growth process, it is also probable that fluorine may get incorporated as an impurity into the diamond lattice. It may occupy the substitutional sites or may get trapped in the vacancies formed during the growth process. Accordingly, the defect distribution, growth habits and structural properties of the diamond films may change. However, there are scanty reports on this aspect of the diamond films grown in C-H-F system.

Therefore, in the present chapter, tetrafluoromethane (CF_4) is added to standard CH_4/H_2 mixture for diamond growth in HFCVD system and its effect on the growth habits, structural properties and defect formation is studied in details. Investigations on structural properties and the growth habits of the film are carried out by laser Raman spectroscopy, x-ray

diffraction, x-ray photoelectron spectroscopy (XPS) and scanning electron microscopy whereas the defect distribution in the film is studied by photoluminescence spectroscopy.

6.2 Experimental:

The polycrystalline diamond films were grown by Hot-Filament CVD technique. The optically polished p-type Si <100> (resistivity ~10 Ù cm, 300 µm thick) was used as the substrate material for supporting the diamond films. The substrates were lightly scratched by using 0.5 µm diamond powder and were ultrasonically cleaned in acetone and rinsed in 40% HF acid solution prior to their loading in the deposition chamber. The substrates were held at a distance of 10mm below the plane of the M-shaped filament. For the deposition of the films, a mixture of the semiconducting grade gases CH_4, CF_4, and H_2 was used. The CH4 fraction (X) and the CF4 fraction (Y) in the source gas are defined as:

$$X = \frac{[CH4]}{[CH4] + [CF4]};$$

$$Y = \frac{[CF4]}{[CH4] + [CF4]}.$$

The CF4 fraction in the toatal flow of (CH4+CF4) was varied from 0% to 100%.

The important deposition conditions under which the films were grown are listed in table 6.1.

Table 6.1: HFCVD Deposition Conditions:

(CH_4+CF_4) percentage in H_2	2%

Gas mixture flow rate (H2+CH4+CF4)	300 SCCM
Deposition Pressure	30 Torr
Filament Temperature (T_F)	1900 ± 50 ^{0}C
Substrate Temperature (T_S)	750 ± 20 ^{0}C
Deposition Period	3 hrs.

6.3 Results and Discussion:

In order to study the effect of fluorine incorporation on the growth and properties of diamond films, the films were grown for different CF_4 fractions in CH_4 keeping the total flow of (CF_4+CH_4) in H_2 constant (2% in 300 SCCM of the total flow).

Figure 6.1 shows the SEM photographs of the surface morphology of the films grown on Si substrate with the increasing tetrafluoromethane (CF_4) fraction (0-100%) and decreasing methane (CH_4) fraction (100-0%) in the mixture of (CH_4+CF_4). The surface morphology shows that the surface, in general, is made up of well developed {111}facets of predominantly octahedral form with dense nucleation. The average grain size for the film grown with 0% CF4 fraction is ~ 0.5 μm which is observed to increase gradually with CF4 fraction. For 83% CF4 fraction, it is observed to be ~1.25 μm. When the CF4 fraction was 100% (i.e. 0% CH4), diamond crystallites are not observed to grow suggesting that certain minimum amount of CH4 is must for the growth of diamond film. These features of the surface morpholy suggest that the fluorinated methane-hydrogen gas mixtures have a larger nucleation rate than the methane-hydrogen gas mixture and tend to grow diamond with a high crystallinity [3].

The Raman spectra of the diamond films at various CF_4 concentrations are shown in figure 6.2. They show the strong band at 1332 cm^{-1}, characteristic of diamond crystals, except when the concentration of CF_4 in CH_4 was 100%, i.e., when there is no

methane in the feed gas mixture, diamond growth is not observed. The Raman spectrum of the film grown with 50% CF_4 in CH_4 shows the band at 1332 cm^{-1} to be more sharp and intense suggesting the better diamond growth for this proportion of CF_4 and CH_4. When the CF_4 fraction in methane was increased beyond 50%, the Raman intensity of the 1332 cm^{-1} band was observed to reduce and when this fraction was made 100%, no diamond band was observed. Our results are in accordance with a number of other reports (e.g. 2,3,8) on the growth of diamond films in C-H-F system.

The most likely gas phase and surface reaction in C-H-F system is the formation of HF by atomic fluorine with gas phase hydrocarbons and atomic and molecular hydrogen. This HF may preferentially etch graphite and amorphous carbon when compared to diamond [12] resulting in the reduction in non-diamond content of the film. For higher concentration of CF_4 , most of the growth surface may get terminated by the fluorine atoms and therefore the etching rate may reduce resulting in the increase in non-diamond content of the film. In the absence of methane, the entire surface of the growing film may get fluorinated. The fluorinated surfaces are stable enough to avoid the diamond growth, but if hydrocarbons are added, the growth is quite favourable [8]. It has also been depicted by Frenklach et al. [7] that typical gas-phase reactions of hydrocarbons and fluorine have higher rate coefficients with much

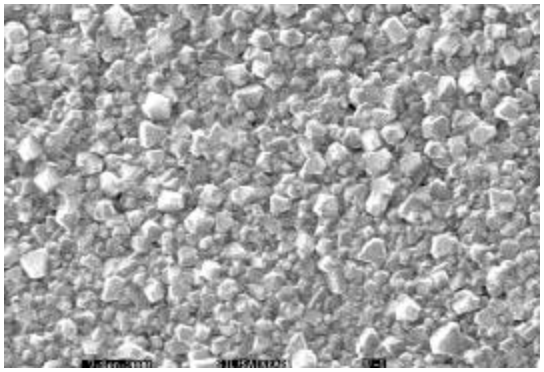

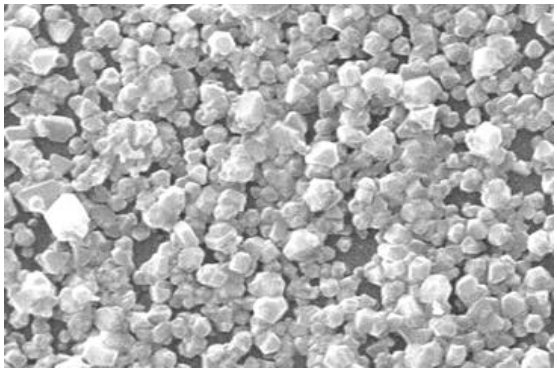

lower activation energy than their

(a) **(b)**

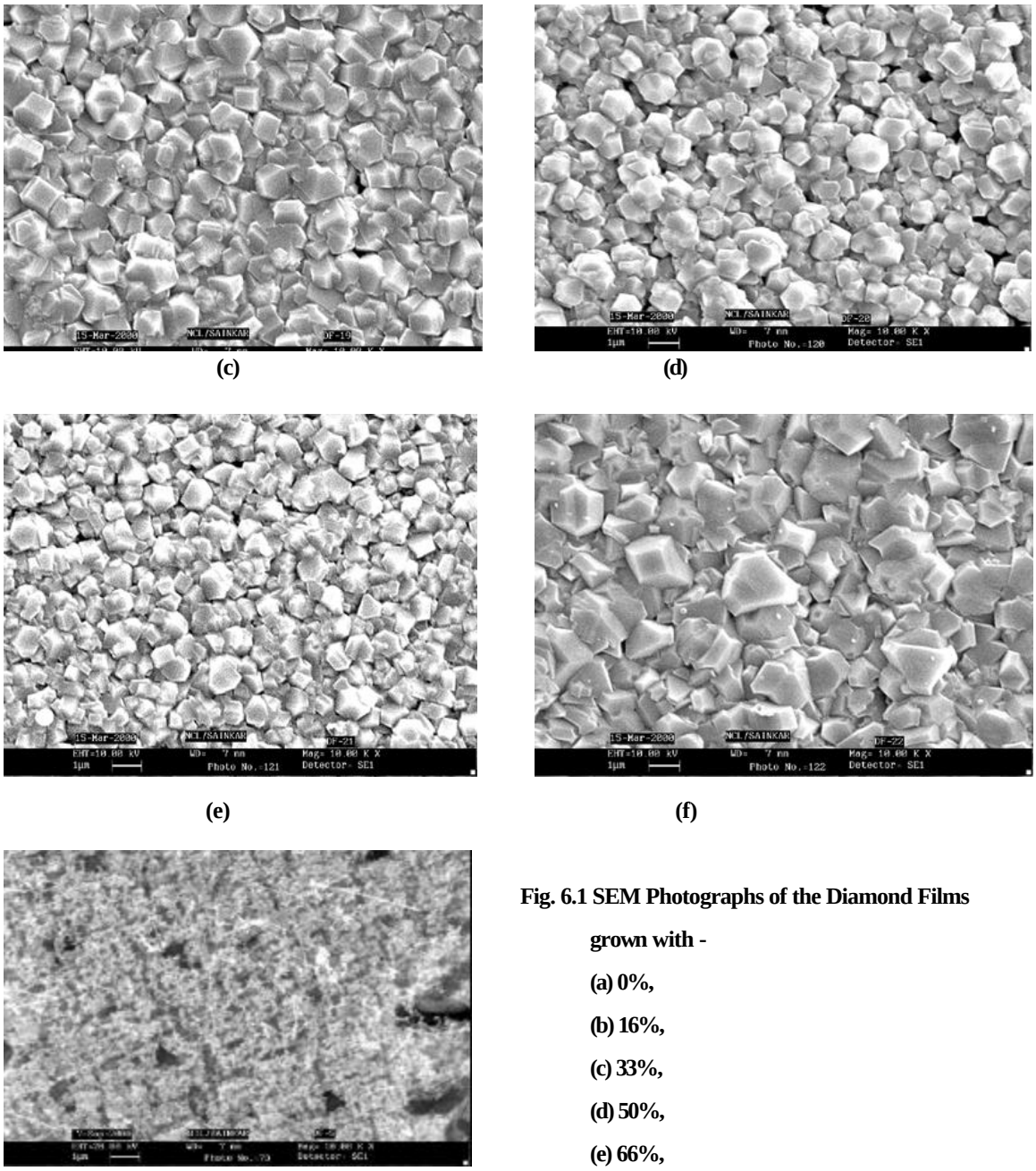

(c) **(d)**

(e) **(f)**

(g) 100% CF_4 Fractions in CH_4

Fig. 6.1 SEM Photographs of the Diamond Films grown with -

(a) 0%,

(b) 16%,

(c) 33%,

(d) 50%,

(e) 66%,

(f) 83% and

(g)

counterparts with hydrogen. Therefore, certain minimum amount of CH_4 is a must for the growth of diamond films.

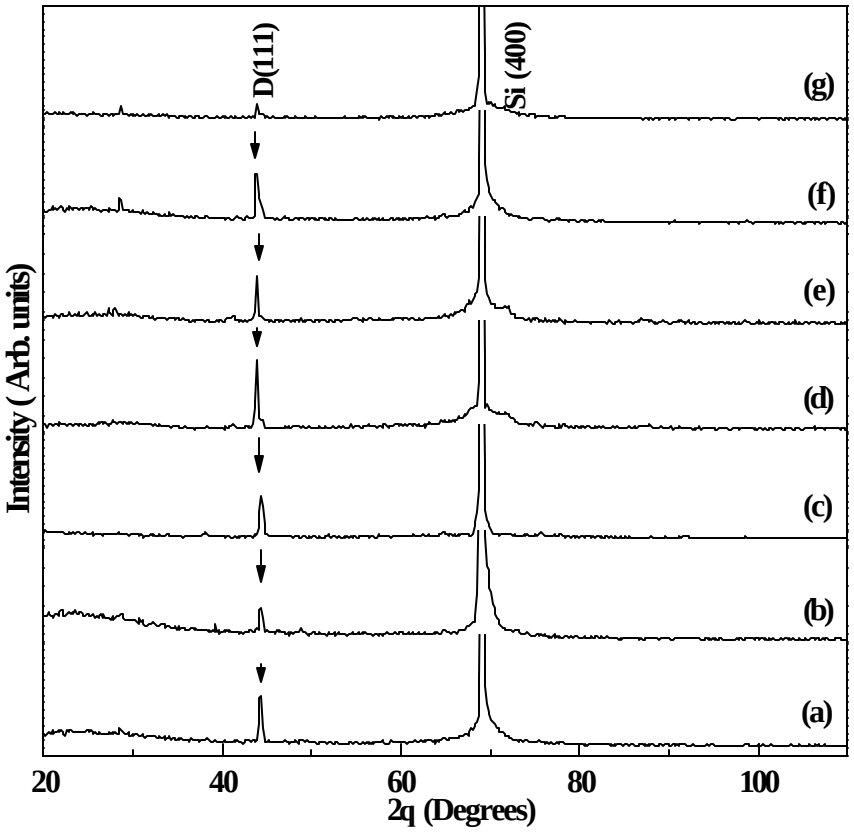

The XRD patterns of these films cofirmed the presence of diamond crystals. These patterns are shown in figure 6.3. It was observed that all the films exhibited {111} texture.

Figure 6.3 XRD patterns of the diamond films grown with-
(a) 0% (b) 16% (c) 33% (d) 50% (e) 66%
(f) 83% and (g) 100% CF_4 fractions in CH_4

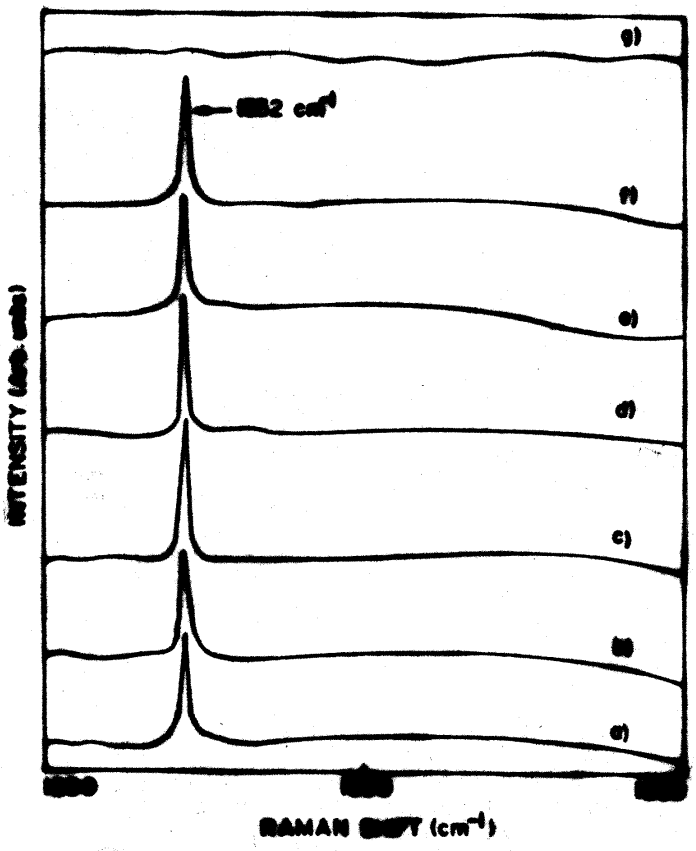

Fig. 6.2 Raman spectra (normalized for 1332 cm^{-1} band) of the diamond films grown on Si substrate with (*a*) 0%, (*b*) 16%, (*c*) 33%, (*d*) 50%, (*e*) 66%, (*f*) 83%, and (*g*) 100% CF_4 fractions in CH_4

Chapter 6 *Growth of Fluorinated Diamond Films*

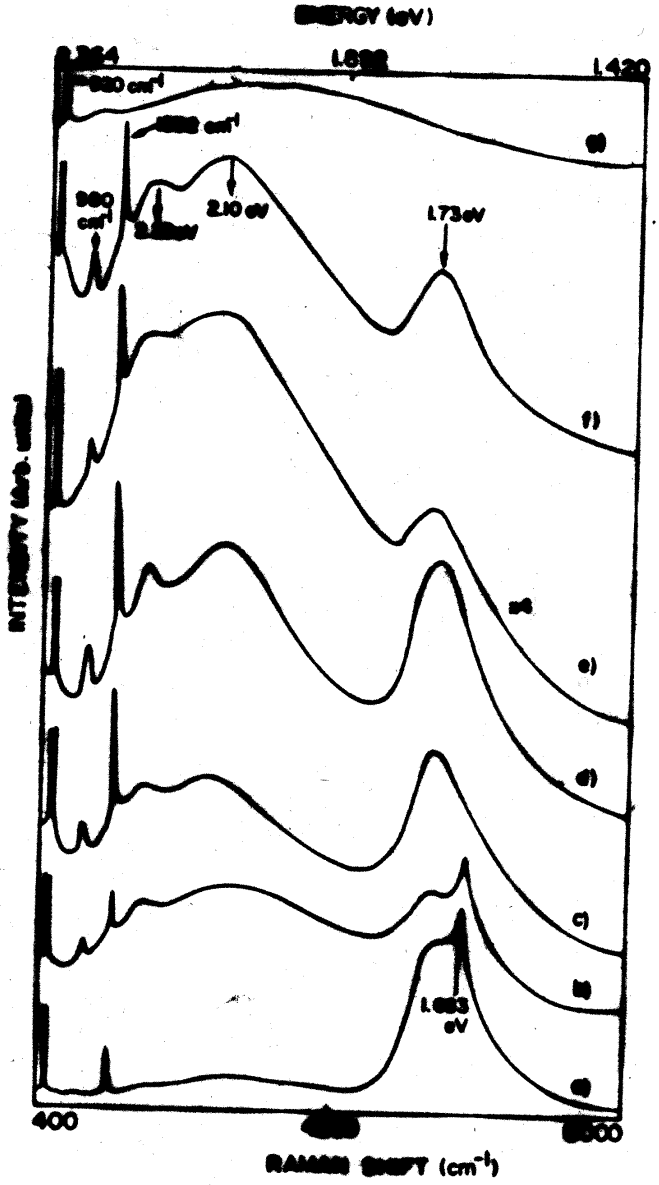

Fig. 6.5 The PL spectra of the diamond films grown on Si substrate with (*a*) 0%, (*b*) 16%, (*c*) 33%, (*d*) 50%, (*e*) 66%, (*f*) 83%, and (*g*) 100% CF_4 fractions in CH_4

Energy dispersive X-ray analysis (EDAX) was also used to study the diamond films produced in a C-H-F system. But no fluorine signal was observed in the diamond films produced in this system. Our observation is in agreement with the observation reported by Corat et al. [24]. They also carried out the EDAX measurements and did not found fluorine signal in the fluorinated diamond films. Althogh, fluorine was not detected in EDAX measurements, it was detected on the surface of the films by the chemical analysis with X-ray photoelectron spectroscopy. The C1s and F1s core level XPS spectra of the diamond films grown with 50%, 66% and 83% CF4 in CH4 are shown in figure 6.4. The C1s peak in each spectra is observed at 288 eV. The C1s peak for sp^3 bonded carbon is expected to be at 284.6 eV. This increase in the binding energy of C1s electron may be due to the formation of species like C_nF_n [26] which suggests the presence of fluorine on the surface of the film. This supports the observation reported by Rudder et al. [9]. They also observed the C1s line of fluorinated diamond films at 288 eV and they assigned it to fluorine bonding. The fluorine bonding to the diamond may be present during growth or it may arise from residual contamination of the surface upon termination of the growth process. The same observation is also reported by Fox et al. [5] who estimated the amount of fluorine to be ~1% of the near surface region composition. Similarly, the F1s peak in each spectra is observed at 690 eV. This peak is thought to be due to the formation of CF_n [26] or $(CF_2)_n$ [27] species on the surface. Thus, the XPS measurements of the films suggested that fluorine may be present on the surface of the film.

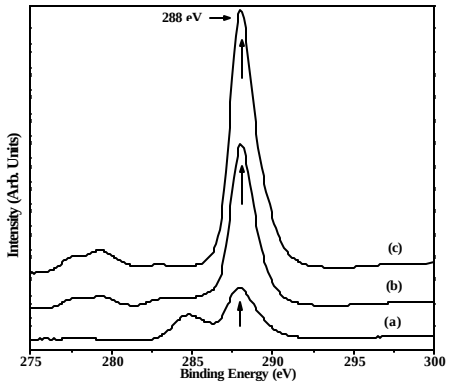

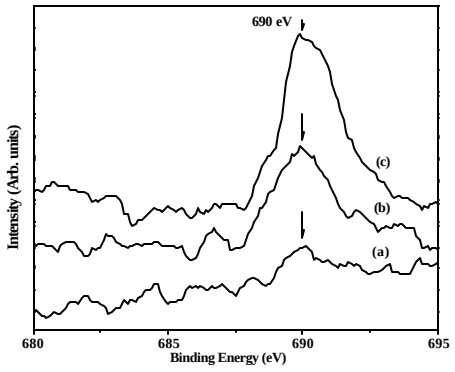

C1s **F1s**

Fig. 6.4 C1s and F1s core level XPS spectra of diamond films grown with- (a) 50% (b) 66% and (c) 83% CF_4 fractions in CH_4

Figure 6.5 shows the PL spectra of these films grown on Si substrate as a function of CF_4 fraction in CH_4. These spectra are recorded by the same spectrometer used for the Raman scattering measurements. The PL spectrum of the film grown without CF_4 incorporation (figure 6.5a) shows a sharp band at 1.683 eV with a broad shoulder centered at 1.730 eV. However, in the spectra of the films grown in C-H-F system, the band at 1.730 eV is observed to be dominent. For higher fraction of CF_4 in CH_4 (33%), only the broad band at 1.730 eV is observed and the band at 1.683 eV is found to disappear. Neither of these bands are observed for the film grown without CH_4.

The band at 1.683 eV is related to the monovacancies formed during the growth of the film [28]. These monovacancies may be formed due to the diffusion of silicon from the substrate into the film. Therefore, in the PL spectrum of the film grown without CF4 incorporation, the sharp band at 1.683 eV is observed. When CF_4 is introduced in the gas mixture, fluorine may form the bond with carbon on the growing surface of the film. As the covalent radius of F (0.72 Å) is comparable to the covalent radius of carbon (0.77 Å), it may get incorporated in the film. But, being monovalent, it can form the bond with one carbon atom only and no further bonding can take place with fluorine. It can give rise to the formation of voids (vacancy clusters) and hence the appreaciable amount of stress around the fluorine atom. The broad band at 1.730 eV may be attributed to the formation of these vacancy clusters. Dannefaer et al.[28] have attributed the 1.720 eV line to vacancy clusters. The shift of about 0.010 eV observed in our case may be due the stress creared in the film around the fluorine atom. As the fluorine concentration is increased, the band at 1.730 eV is observed to increase

which may be due to the increase in the voids formed. After certain concentration of fluorine, as most of the growing surface is terminated by fluorine atoms, growth rate is deterioted

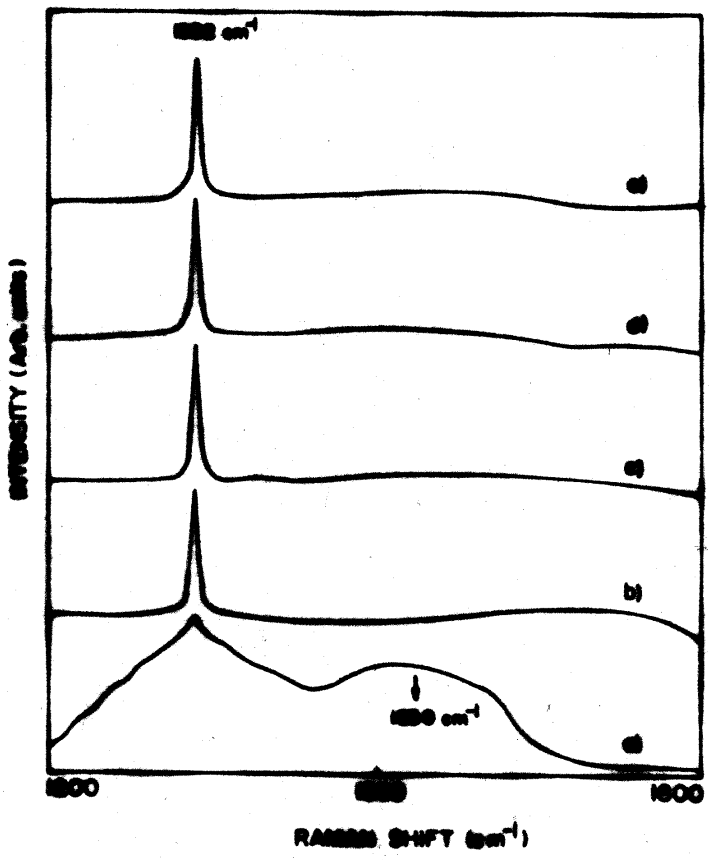

Fig. 6.7 Raman spectra (normalized for 1332 cm^{-1} band) of the diamond films grown on Si substrate with fixed CF_4 fraction in CH_4 (33%) at various gas flow rates (*a*) 100 SCCM, (*b*) 200 SCCM, (*c*) 300 SCCM, (*d*) 400 SCCM, and (*e*) 500 SCCM

Chapter 6 Growth of Fluorinated Diamond Films

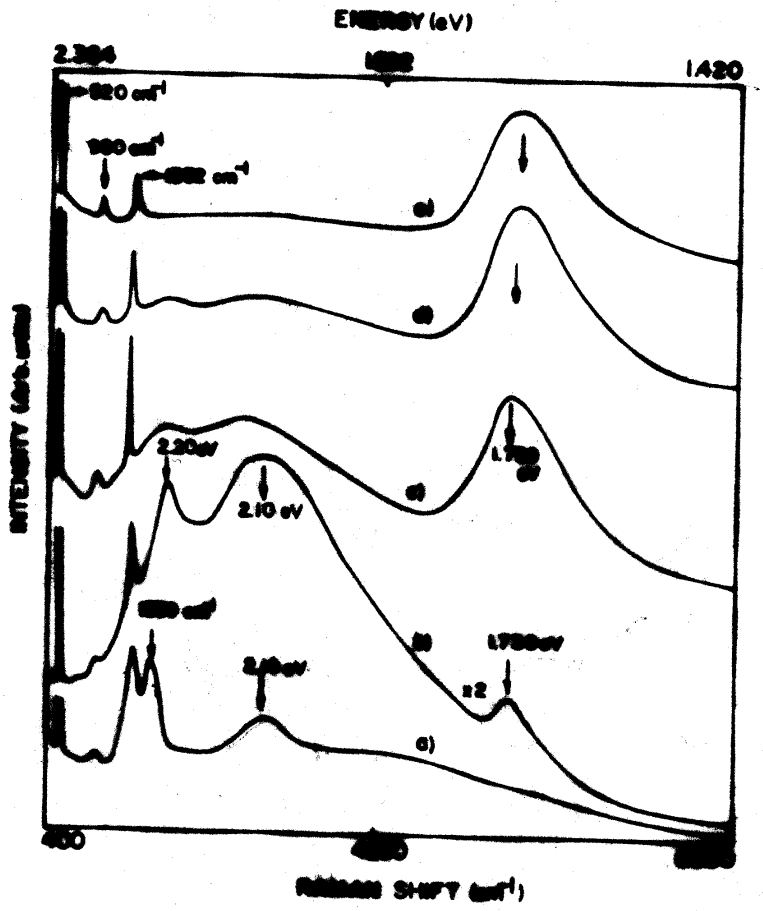

Fig. 6.9 The PL spectra of the diamond films grown on Si substrate with fixed CF_4 fraction in CH_4 (33%) at various gas flow rates (*a*) 100 SCCM, (*b*) 200 SCCM, (*c*) 300 SCCM, (*d*) 400 SCCM, and (*e*) 500 SCCM

resulting in less number of voids and therefore, the intensity of the band at 1.730 eV may be reducing. As certain minimum amount of CH_4 is a must for the growth of diamond films, diamond film could not be grown with CF_4 alone. Hence, no PL band was observed in the film grown without CH_4.

In addition to the above bands, the PL spectra of the films also show the broad bands at ~2.20 eV and 2.10 eV. The origin of these bands is still not clear. Nemanich et al [R] have proposed that this emission may be the result of amorphous sp^3 bonded carbon phase which produces defect state distribution in the band gap.

In order to study the effect of total gas flow on the growth and properties of the diamond films grown in C-H-F system, the films were grown for the different gas flows varying from 100 SCCM to 500 SCCM, keeping the fraction of CF_4 in CH_4 fixed..Figure 6.6 shows the SEM photographs of the surface morphology of the films grown with 33% CF_4 in CH_4, (i.e.2 SCCM CF_4 in 4 SCCM CH_4) but with varied gas flow rate. From the surface morhology of these films, it is observed that the nucleation density is minimum whereas the average grain size is maximum (~2.5 μm) for the film grown with minimum gas flow rate (figure 6.6a). As the flow rate is increased, the nucleation density is observed to increase while the average grain size is observed to decrease. The average grain size decreases to ~0.75 μm for the film grown with maximum flow rate of 500 SCCM (figure 6.6e).

The Raman spectra of these films are shown in figure 6.7. From these spectra, it is seen that the sharp diamond peak at 1332 cm^{-1} is observed in the Raman spectra of each film. The spectrum of the film deposited with the total flow of 100 SCCM shows a broad feature centered at ~ 1550 cm^{-1}. This broad feature is associated with non-diamond material that is perhaps residing between the grains. For the films grown with higher flow rates, this feature is found to disappear, i.e. for the total flow rate higher than 200 SCCM, non-diamond content of the film is found to be negligibly small.

For the film grown with low H_2 flow, the hydrogen flow may not be sufficient to etch out the non-diamond carbon of the film. Therefore, the non-diamond content in the film is maximum in this case. For the higher H_2 flows, the HF formed in the gas phase as well as

enough H_2 is available for the removal of non-diamond carbon. Therefore, in this case, the non-diamond content in the film is negligible.

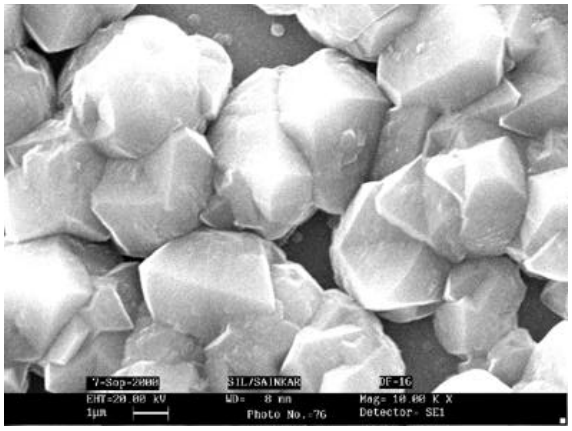

(a)

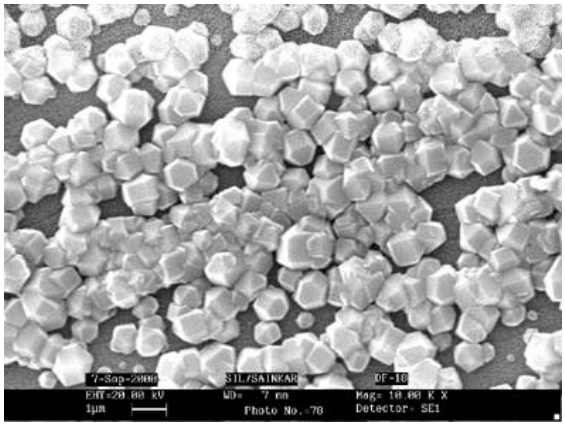

(b)

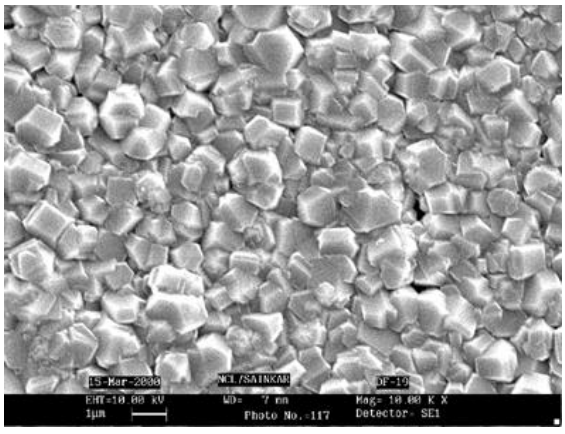

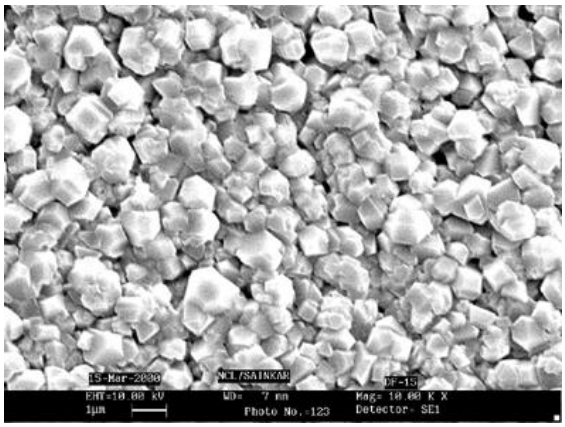

(c) **(d)**

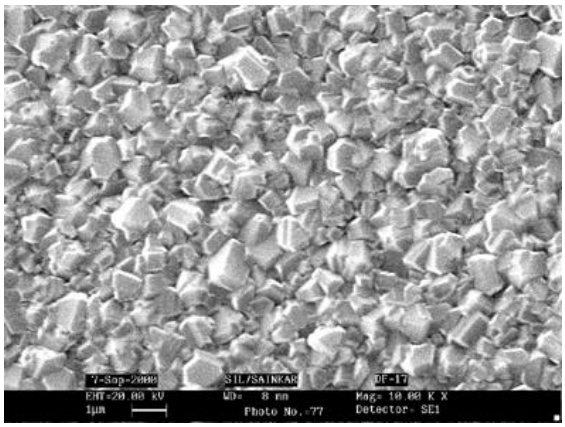

Fig. 6.6 SEM Photographs of the diamond films grown with fixed CF4 fraction in CH4 (33%) but with differnent gas flow rates-
(a) 100 SCCM
(b) 200 SCCM
(c) 300 SCCM
(d) 400 SCCM
(e) 500 SCCM

(e)

The XRD patterns of the films grown with different gas flow rates are shown in the following figure 6.8.

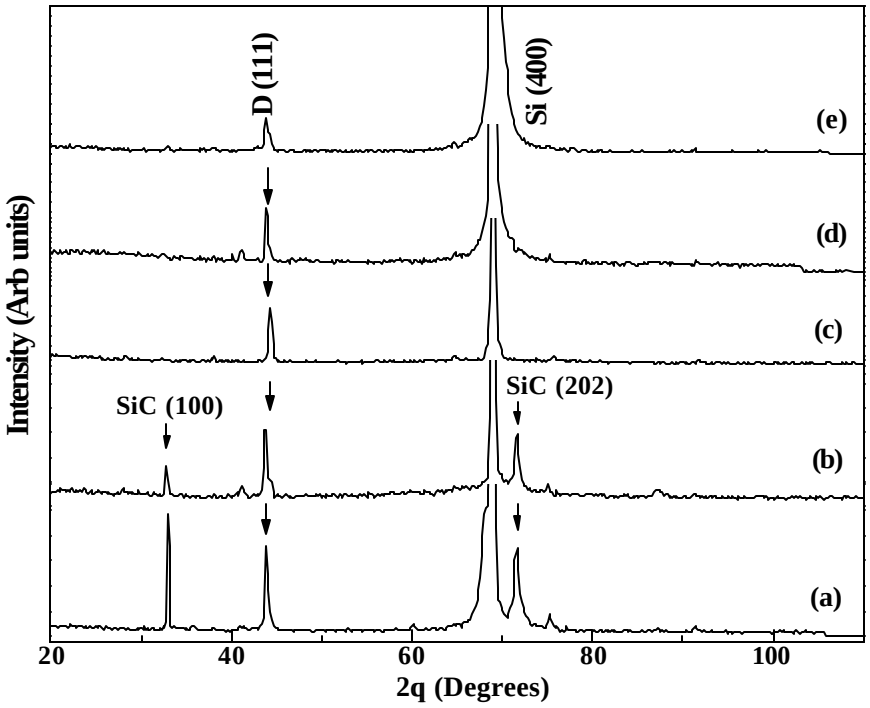

Fig. 6.8 XRD patterns of the diamond films grown with fixed CF4 fraction in CH4 (33%) but with differnent gas flow rates- (a) 100 SCCM (b) 200 SCCM (c) 300 SCCM (d) 400 SCCM (e) 500 SCCM

They show prominent diamond signatures for all the samples and the overall texture of the film is observed to be {111}. Additional lines are observed at 2θ=32.80 ^{o} (d=2.730 Å) and 71.70 ^{o} (d=1.316 Å) in the XRD patterns of the films grown with the flow rates of 100 SCCM and 200 SCCM. These lines are assigned to SiC (100) and SiC (202) respectively. At these lower flow rates, amount of hydrogen is less as compared to carbon which results in the decrease in diamond growth rate. It may cause the additional carbon to diffuse into the substrate silicon forming the carbode. Therefore, the additional lines due to SiC are observed in the XRD patterns of the films grown with lower flow rates.

The PL spectra of these films are shown in figure 6.9. No photoluminescence is observed in the film grown with the total flow of 100 SCCM while the PL spectrum of the film grown with total flow of 200 SCCM shows small but sharp band at 1.683 eV. In addition to this, the bands at 2.19 eVand 2.06 eV are also observed in the PL spectrum of this film. For the flow rates higher than 200 SCCM, the band at 1.730 eV is dominant as compared to the other bands.

For the films grown at higher flow rates, nucleation density is found to be more than that of the films grown at lower flow rates. During the growth of the films with higher nucleation density, some fluorine atoms may get incorporated as an impurity in the diamond lattice and may create voids (vacancy clusters) and the stress may be generated in the film as discussed previously. Therefore, the strong broad band at 1.730 eV is attributed to the vacancy clusters formed during the growth [28].

References:

1. S. J. Harris and L. R. Martin, J. Mater. Res. 5 (1990) 2313.
2. M. Kadono, T. Inoue, A. Miyanaga and S. Yamazaki, Appl. Phys. Lett. 61 (1992)772.
3. C. H. Chu and M. H. Hon, Diam. and Relat. Mater. 2 (1993)311.
4. M. Frenklach, R. Kematick, D. Huang, W. Howard, K. E. Spear, A. W. Phelips and R. Koba, J. Appl. Phys. 66 (1989) 395.
5. C. A. Fox, M. C. McMaster and W. L. Hsu, Appl. Phys. Lett. 67 (1995)2379.
6. S. J. Harris and D. N. Belton, Appl. Phys. Lett. 59 (1991) 1949.
7. M. Frenklach, in “Proceedings of 2nd International Symposium on Diamond

Materials", edited by A. J. Purdes, B. M. Meyerson, J. C. Angus, K. E. Spear, R. F. Davis and M. Yoder (The Electrochemical Society, Washington, DC,1991) p. 142.

8. E. J. Corat, V. J. Trava-Airoldi, N. F. Leite, M. C. A. Nono and V. Baranauskas, J. Mater. Sci 32 (1997) 941.
9. R. A. Rudder, G. C. Hudson, J. B. Posthill, R. E. Thomas and R. J. Markunas, Appl. Phys. Lett. 59 (1991) 791.
10. A. D. Freedman and C. D. Steinspring, Appl. Phys. Lett. 57 (1990) 1194.
11. N. G. Ferreira, E. J. Corat, V. J. Trava-Airoldi, N. F. Leite and E. D. Bosco, Diamond Relat. Mater. 7 (1998) 81.
12. F. Hentschel, I. Schimdt and C. Bennodorf, Thin Solid Films 290 (1996) 196.
13. Y. Shimada, N. Mutsukura and Y. Machi, J. Appl. Phys. 71 (1992) 4019.
14. D. E. patterson, C. J. Chu, B. J. Bai, Z. L. Xiao, N. J. Komplin, R. H. Hauge and J. L. Margrave, Diamond Relat. Mater. 1 (1992) 2313.
15. C. Pan, C. J. Chu, J. L. Margrave and R. H. Hauge, J. Electrochem. Soc. 141 (1994) 3246.
16. M. S. Wong and C. H. Wu, Diamond Relat. Mater. 1 (1992) 369.
17. R. Rameshan, R. F. Askew and B. h. Loo, in : Proc. of 3rd Inter. Symp. on Diamond Materials, Honolulu (Electrochemical Society, Pennington, 1993) p.394.
18. R. Gat, T. I. Hukka, M. P. D'Evelyn, in : Proc. of 3rd Inter. Symp. on Diamond Materials, Honolulu (Electrochemical Society, Pennington, 1993) p.516.
19. V. J. Trava-Airoldi, B. N. Nobrega, E. J. Corat, E. D. Bosco, N. F. Leite and V. Baranauskas, in : 2nd Inter. Conf. on the Applications of Diamond Films and Related Materials, Tokyo, 1993, p.539.
20. V. J. TRava-Airoldi, B. N. Nobrega, E. J. Corat, E. D. Bosco, N. F. Leite and V. Baranauskas, Vacuum 46 (1995) 5.
21. E. J. Corat, V. J. TRava-Airoldi, N. F. Leite A. F. V. Pena and V. Baranauskas, in: Novel Forms of Carbon II, San francisco (Materials Research society, 1994) p. 421.
22. I. Schimdt, F. Hentschel and C. Bendorf, Diamond Relat. Mater. 5 (1996) 1318.
23. K. J. Grannen, F. Xiong and R. P. H. Chang, Surf. Coat. Technol. 57 (1993) 155.

24. E. J. Corat, D. G. Goodwin and V. J. TRava-Airoldi, in: 2nd Int. Conf. on the Application of Diamond Films and Related Materials , Tokyo,1993, p. 697.
25. M. Asmann, J. Heberlein and E. Pfender, Diamond Relat. Mater. 8 (1999) 1.
26. D. T. Clark, W. J. Feast, D. Kilcast, and W. K. R. Musgrave, J. Polym. Sci. 11 (1973) 389.
27. C. D. Wagner, chapter 7 , " Handbook of X-ray and ultra-violet photoelectron spectroscopy", ed. D. Briggs (Heyden and Sons, London, 1977)
28. S. dannefaer, W. Zhu, T. Bretagnon and D. Kerr, Phys. Rev. B 53 (1996) 1979
29. L. Bergman, B. R. Stoner, K. F. Turner, J. T. Glass and R. J. nemarich. J. Appl. Phys. 73 (1993) 3951.

CHAPTER 7

IMPLANTATION OF IMPURITIES IN DIAMOND FILMS

This chapter presents the study of Li, N, and P ion implanted diamond films. Structural proterties of these implanted films are carried out by laser Raman spectroscopy and XRD, surface morphology by SEM while the distribution of defects is studied by photoluminescence spectroscopy. These results are discussed in details in the present chapter.

7.1 Introduction

In general, incorporation of impurities or dopant atoms in CVD diamond films is experienced in two ways, viz. 1) *in situ* or 2) *ex situ* process. The *in situ* incorporation involves introduction of the impurity atoms during the growth process itself while the *ex situ* incorporation is achieved either by diffusion or ion-implantation. The structural changes and their implications caused by *in situ* incorporation of impurities such as Si, N and F in diamond films during the deposition have been studied in the previous chapters. However, in this method, there is hardly any control over the concentration and depth profile of the impurities within the film. In case of *ex situ* incorporation of impurities, particularly, by diffusion, extremely high temperatures are required because of the low diffusion coefficient of impurities in diamond at moderate temperatures. To overcome these shortcomings, ion implantation may be a better choice to incorporate the desired impure atoms in diamond films. Using this latter technique, it is possible to control the concentration and depth profile of the implanted dopants whereas by suitable masking, spatially selective doping is possible. Because ion implantation involves forcing energetic ions to penetrate into a solid, it is possible to produce metastable alloys and desired dopant distribution which are not achievable by normal equilibrium diffusion techniques. However, it is important to note that as the ion gets decelerated on its way in the solid, a great deal of damage is caused which must be annealed before effective doping can be realized [1].

In order to understand the *in situ* incorporation of impurities in CVD diamond, it is thought that the ion implantation studies of the impurities may be useful in resolving the problems which may have obscured the various phenomena by the slow diffusion process in diamond. The following section describes the ion implantation process and subsequently provides a brief review of the literature available on this subject in relation to CVD diamond doping. The results observed in case of the ion implanted films are discussed in details.

7.1.1 Ion Implantation Technique

The ion-implantation technique is the most widely applied doping technique in modern semiconductor technology as it allows vertically as well as laterally well defined dopant profiles. In principle, ion implantation is a surface modification technique based on the bombardment of solid surfaces with selected energetic ionic species having energy in the range of a few tens to few hundreds of keV [2,3]. In this technique, ionized dopant atoms are accelerated through an electrostatic field and are allowed to strike the surface of the material undertaken for doping, called target. Depending upon their energy, the ionized dopant atoms penetrate to various depths in the target. The ion current that flows between the electrodes, presents the ion dose. Hence it is possible to control the ion dose whereas the penetration depth can be controlled by ion energy, target temperature, orientation of the target surface with reference to the ion direction, etc. [4].

Since ion-energies used in most ion implantation experiments are in keV range, the atoms of the solid which are displaced from their sites by the incoming ions acquire substantial energy to atomically displace other atoms in their track. Such sequential scattering events generate a zone in the neighborhood of incoming ions which contains a large concentration of defects. This zone, which is often refered to as "collision cascade region," generally has a high vacancy concentration and surrounding the cascade region one finds many randomly distributed interstitials. This cascade formation occurs over a time scale of only 10^{-13} - 10^{-11} sec and hence makes implantation a highly non-equilibrium process. The extent of the structural disorder produced by the ion and hence the process of cascade formation is also dependent on the ion energy. This is because the cross section of ion-target atom collision processes contribute with different strengths over different energy regimes. The process of collision is statistical in nature and is reproduced by computer codes such as transport of ions in matter (TRIM) which are based on Monte-Carlo simulation programme[5]. This programme follows the trajectory of each ion and of the target atoms displaced as a result of high momentum transfer collisions. The successive collisions of ion with target atoms slows down the ion on its way into the solid. The general way of treating the slowing down of an ion in matter is through the stopping power, dE/dx, defined as the energy dE lost by an ion traversing the distance dx[4]. Stopping power is usually divided into two major independent components, (i) collisions with electrons in the solid which slow down the moving ions and is known as

electronic stopping, $(dE/dx)_e$, (ii) The moving ions undergo inelastic collisions with the atoms of the target material, called nuclear stopping and denoted as $(dE/dx)_n$. The typical penetration depths for ions below the surface are of the order of a few hundreds of angstroms. However, the range and depth distribution are also affected by the structural status of the sample, i.e. single crystal with its orientation along crystallographic axis, polycrystalline or amorphous, etc.

For implanted samples, a subsequent thermal processing is necessary, basically for two reasons: firstly, the implanted dopant atoms partly reside on interstitial sites inside the crystal lattice and are thus electrically inactive. Secondly, the implanted ions displace target atoms and thereby cause implantation damage, typically vacancies, interstitials, dislocations, etc [4]. Since each ion produces a large number of defects, the effect of the damage tends to mask the chemical effects of the implant. Therefore, a subsequent thermal annealing treatment is necessary to heal the implantation damage and activate the dopants by moving them into substitutional lattice sites. Rapid thermal annealing [6] at very high temperature allows removal of the damage with minimal dopant movement. In the following section, the literature reviews on the ion implantation experiments of various impurities in natural, synthetic and CVD diamond are discussed briefly.

7.1.2 Ion Implantation of Impurities in Diamond

The use of ion implantation to modify the electrical, mechanical and chemical properties of the solid surface is well established [4]. In case of silicon based electronics, this approach with the desired dopant species has been successfully exploited. But as far as diamond is concerned, it has not proved as successful as in the case of silicon and other semiconducting materials. This is due to the fact that diamond is metastable with respect to graphite and hence the implanted diamond has a tendency to revert to graphite either upon annealing or in reponse to a sufficiently high ion dose. In addition, the very high atomic density of diamond and the very short C-C bond length inhibit effective substitutional doping of diamond with the exception of p-type doping achievable using boron implantation [1]. However, similar efforts to obtain n-type diamond using phosphorus as the dopant during CVD as well as by implantation have generally failed possibly because the phosphorus atom is too large to be substitutionally incorporated into the diamond lattice [7].

For the realization of high-temperature and radiation hard electronic devices and detectors, effective n- and p-type doping of diamond is required [8]. Though the ion implantation is a practical means to incorporate dopants into the diamond lattice in a controlled way, for the successful doping, it is necessary to devise implantation and annealing schemes such that (i) the radiation damage induced by ion implantation will be repaired without the formation of graphite, and (ii) the dopants will be electrically activated.

The doping of crystalline diamond by this technique with the implantation energies from few tens to few hundreds of keV has been scarcely studied [9]. For this energy range, the penetration of energetic ions in the diamond lattice creates mainly vacancies and interstitials. In the case of experiments on Sb implantation in natural single crystal diamond, Branustein et al.[10] observed that the relative disorder created in the diamond lattice increased linearly with the ion dose and saturated for doses higher than $1.5x10^{14}$ ions/cm^2. The saturation of the disorder above the threshold dose was interpreted in terms of the relative amount of the amorphous phase in the damaged region. Fontain et al.[11] investigated the effect of the implantation dose on atomic structure by the Raman spectra of the implanted films. For doses below threshold, the Raman spectra were dominated by the single narrow diamond peak at 1332 cm^{-1}. For doses above the threshold, the narrow diamond peak disappeared and the spectra were dominated by broad bands at 1350 and 1520-1550 cm^{-1} commonly attributed to the presence of amorphous or disordered carbon. Moreover, the electrical resistivity of the implanted samples exhibited a sharp drop for doses above the threshold confirming that a phase transition has occurred. The formation of a continuous crystalline graphite phase was observed after annealing above 400^0C for the samples in which amorphization was observed after implantation. When the temperature of the samples during implantation was significantly increased, the amorphization threshold was found to shift towards the higher implantation doses [12].

For p-type doping in diamond, boron implantation is a well established technique. It has been shown[7] that cold implantation followed by rapid annealing (CIRA) is the best scheme for boron implantation. Cold implantation “freezes in” the implant as well as the damage so that the interstitials and vacancies are kept in close proximity. The high temperature anneal is assumed to take advantage from the close proximity of vacancies and interstitials and

enhances the possibility of interstitial-vacancy recombination. Thus, implanted ions can occupy electrically active sites. It has also been possible to introduce a high level of activated boron dopants by using a multiple step CIRA technique [13], i.e. multiple CIRA cycles with a small dose at each step. It has been reported that boron implanted diamond films if annealed at sufficiently high temperature, show a transition from p to n-type conductivity and also that the n-type conductivity is induced on boron implantation above room temperature. It has, therefore, been proposed that the isolated point defects in diamond act as acceptors whereas the more complex agglomerated defect structures which are probably produced during high temperature implantation as well as high temperature annealing, behave like donors.

The n-type doping has also been tried by implanting group-V impurities into diamond[14]. It has been observed that implantation of group-V impurities in diamond results in high levels of damage and graphitization. The extent of damage and the degree to which it can be annealed out depends on the various factors such as ion type, fluence (i.e. ion dose), implantation and annealing temperatures. Among these parameters, fluence has a strong influence on the implantation damage. For implantation at any temperature, there exists a critical dose, beyond which the damage cannot be recovered by annealing. For example, Braunstein et al.[10] have found that room temperature implantation of Sb into diamond at 350 keV and low fluence ($< 0.9 \times 10^{14}$ /cm^2) causes damage which can be almost completely annealed out at 1150^0C. However, for higher fluence ($>2 \times 10^{14}$/cm^2), annealing at temperatures even upto 1600^0C (where graphitization occurs) has no effect on the damage reduction. At intermediate fluences, annealing at 1150^0C following the implantation results in a only partial reduction of the damage. The range of fluences available for implantation can be extended without extensive damage and graphite formation, by the implantation at high target temperatures [15,16].

Gorbatkin et al.[14] have studied the implantation of 250 keV $^{75}As^{++}$ into diamond at room temperature and at 600^0C. They observed the implantation at temperature of 600^0C to result in a substantial decrease in lattice damage compared to room temperature implantation. Also the implantation at 600^0C was observed to result in a significant increase in the substitutionality of the As compared to room temperature implantation. Recently, Hofsass et al.[17] have reported the room temperature implantation of phosphorus into type IIa diamond with its subsequent annealing at 1200^0C. They observed majority of the P atoms to incorporate

in substitutional sites. Similar observations are reported for implantation of other group elements in diamond. For example, the room temperature implantation of 60 keV ^{73}Se ion into type IIa diamond and the subsequent annealing at 1100^0K allows incorporation of 50% of the implanted ions into substitutional lattice sites [18]. Braunstein et al.[15] have studied the implantation of Li^+ into heated diamond and observed that graphitization can be avoided by implantation at higher temperature. They found appreciable fraction of Li^+ ions to get incorporated into interstitial sites where they are expected to be electrically active donors.

From the above review, it is clear that most of the ion implantation studies have been performed on single crystal natural diamonds. However, it is conceivable that in order to fully implement the potential of diamond based electronic devices, these will eventually be realized in polycrystalline CVD diamond films and ion implantation will most likely, be the part of the diamond device manufacture process. The CVD diamond films differ from single crystal diamonds in that they are polycrystalline in nature with many grain boundaries, defects and often some graphitic or amorphous carbon impurities. These differences may result in important deviations of many properties of the film from those of natural single crystal diamond and may well lead to basic differences in the response of the polycrystalline films to ion implantation and annealing treatments. While considerable amount of work has been done on ion implantation of natural single crystal diamond, there are very few reports [19,20] on the ion implantation of polycrystalline diamond film. For application feasibility, it is necessary to study the response of these polycrystalline films to post deposition treatments.

It is to be noted that the research on ion implantation of diamond (single crystal as well as polycrystalline) is focused mainly on p- and n-type doping. However, the basic studies on structural properties and defect formation after implantation and annealing are lacking. In the present chapter, we therefore, present the studies on different impurities, namely Li, N and P, incorporated in polycrystalline diamond film via ion implantation and studied implications on structural properties and defect formation. Structural investigations are carried out by laser Raman spectroscopy, x-ray diffraction and scanning electron microscopy and the distribution of defects is studied by photoluminescence spectroscopy. The changes produced in the structural and luminescent properties of the implanted films are also studied as a function of annealing temperature.

7.2 Experimental

The polycrystalline diamond films were grown on Si(100) substrates by hot filament chemical vapour deposition technique. The substrates were pretreated in the same way as described in the previous chapter. The deposition parameters are listed in the Table 7.1. Most of the films were fairly uniform and approximately of the same thickness (~ 3.5 to 4 μm). Out of these, one was kept unimplanted and the others were used for implantation.

Table 7.1: HFCVD Deposition Parameters

Deposition Parameter	Value
CH_4 Flow Rate	2%
Total Flow Rate	300 SCCM
Deposition Pressure	30 Torr
Filament Temperature	1900 ± 50 ^{0}C
Substrate Temperature (T_s)	750 ± 10 ^{0}C
Filament-Substrate Distance	10 mm
Deposition Period	3 hrs.

The films were implanted with Li^+, N_2^+ and P^+ ions at ambient temperature and the pressure of $1x10^{-6}$ Torr. The implantation experiments were carried out at the implanter facility at Tata Institute of Fundamental Research, Mumbai. In all the ion types, the ion energy was so chosen that the projected range, i.e. the penetration depth (R_P) of these ions was nearly the same. The implantation dose chosen was $1x10^{14}$ ions/cm^2 in all the cases. The implanted films were subjected to annealing treatment in an inert atmosphere. The annealing temperature was varied from 200 ^{0}C to 600 ^{0}C.

7.3 Results and Discussion

7.3.1 The TRIM Data

The ion energy, vacancies per ion and the energy loss (electronic and nuclear) data for the different ions (Li^+, N_2^+, P^+) with nearly same projected range implanted in polycrystalline diamond film were computed using TRIM simulation [5]. The results are summarized in table 7.2.

Table 7.2: TRIM Data for different ions implanted in Diamond film

Ion Type	Ion Energy	Projected Range	Vacancies/Ion	$(dE/dx)_{Elec}$	$(dE/dx)_{Nucl}$
Li^+	40 keV	1469 Å	157	26.5 eV/ Å	3.09 eV/ Å
N_2^+	120 keV	1414 Å	521	68.74 eV/ Å	18.03 eV/ Å
P^+	220 keV	1450 Å	1035	102.4 eV/ Å	43.53 eV/ Å

From the above TRIM data, it is observed that the implantation of different ions into the polycrystalline diamond film results into the formation of vacancies in the film. The Li^+ ion implantation leads to minimum vacancies per ion while they are maximum for the film implanted with P^+ ions. The vacancies are generated when a recoil (target) atom moves from its original site. The number of vacancies produced per ion is different for different ions as it is the combined effect of the ion energy and ion mass. In this case, ion mass of phosphorus is 30.974 amu whereas that of Li is 7.016 amu. Therefore, the ion energy required by Li^+ ions to penetrate the target material (diamond film) upto certain projected range (R_P) is much smaller than the energy required by P^+ ions to penetrate into the film upto the same projected range. From the above table, it is also seen that the average electronic loss per unit distance (dX) traversed by the ion is dominant as compared to the nuclear energy loss on the surface of the film. This is typical feature of the particular ion and the ion energy used.

Fig. 7.1 indicates the variation of energy loss (dE/dX) with the thickness (X) of the diamond film as obtained from TRIM simulation. It indicates that, for lighter ion (Li^+), as it progresses through the film, the electronic energy loss goes on decreasing while the nuclear energy loss goes on increasing. In case of N_2^+ and P^+ ions which are

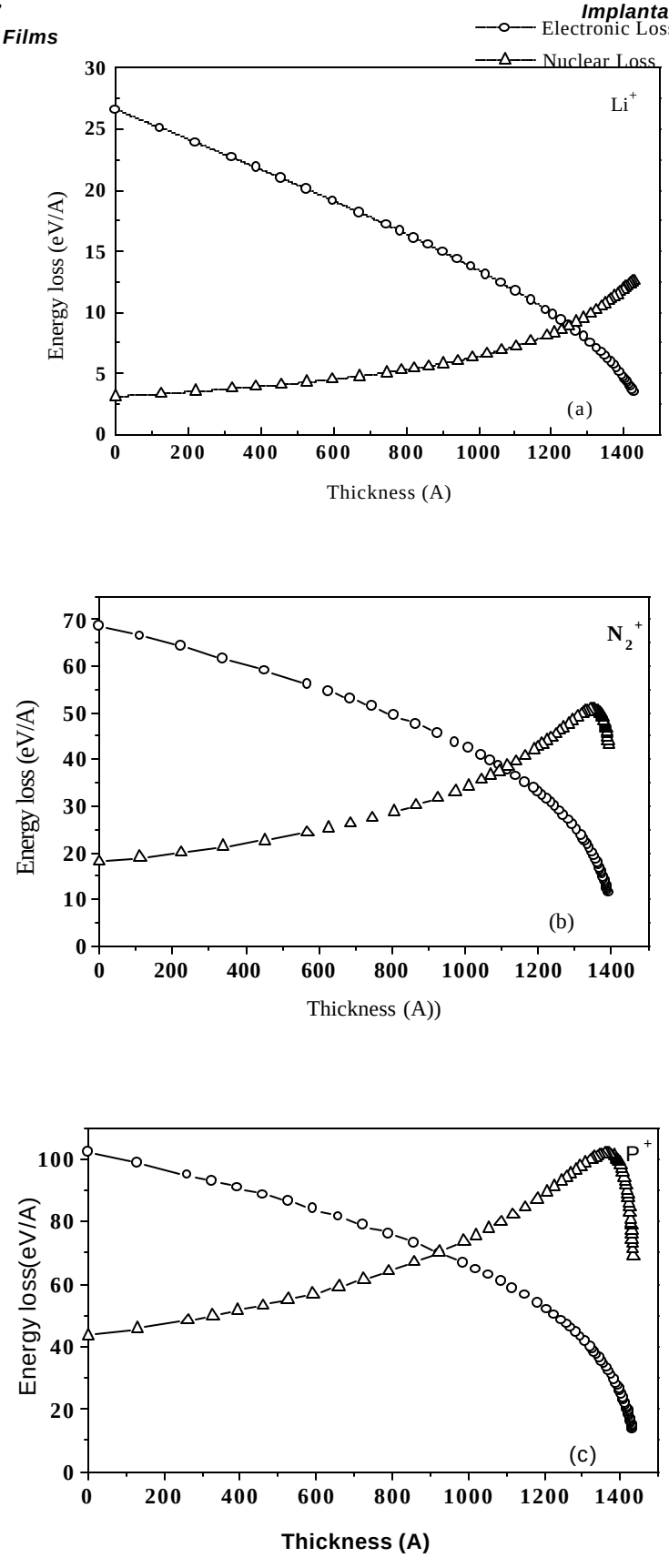

Fig. 7.1 Energy Loss (dE/dX) Vs. Depth (X) data obtained from TRIM simulation

comparatively heavy, electronic energy loss shows the same behavior, but the nuclear energy loss goes on increasing, reaches a maximum and then starts decreasing just before the ions stop within the film.

In the present ion implantation process, initially the electronic stopping is dominant, but as the ion approaches the end of its range, the nuclear stopping becomes dominant. As electronic stopping involves ionization and the displacement of target atoms, it leads to structural damage in the film. Also, the ions implanted into the film are expected to create different amount of stress depending upon their ionic radii. These features, as interpreted from TRIM data are verified by subjecting these films to different characterization techniques such as laser Raman spectroscopy, photoluminescence spectroscopy, X-ray diffraction and scanning electron microscopy.

7.3.2 Comparison of Unimplanted and Implanted Diamond Films

Fig. 7.2 shows the Raman spectra of the unimplanted and Li^+, N_2^+ and P^+ implanted diamond films. In this case, Raman spectroscopy has been used to study the effect of ion implantation on the structure of diamond films. The Raman spectrum of the unimplanted diamond film shows the sharp band at 1332 cm^{-1}, characteristic of diamond crystals. The absence of the broad band in the 1500-1600 cm^{-1} range indicates that the non-diamond content in the unimplanted film is negligible. Similarly, the films implanted with different ions do not show the non-diamond content since the ion dose selected ($1X10^{14}$ ions/cm^2) is well below the critical dose for amorphization of the diamond film. The intensity of the 1332 cm^{-1} band is found to be nearly same for Li^+ implanted film while it reduces for the N_2^+ and P^+ implanted films. The bandwidth (FWHM) of this band for implanted films is observed to increase with increasing ion mass as shown in Table 7.3. The increase in FWHM is minimum for the Li^+ implanted film whereas it is maximum for P^+ implanted film.

Table 7.3 FWHM of 1332 cm^{-1} Diamond Band for Unimplanted and Implanted films

Sample	FWHM of 1332 cm^{-1} band
Unimplanted Film	5.5 cm^{-1}
Li^+ implanted Film.	7.5 cm^{-1}
$N2^+$ implanted Film	8.1 cm^{-1}
P^+ implanted Film	10.2 cm^{-1}

The stress and the defects created in the film are the possible factors contributing to the increase in FWHM [21]. As phosphorous is heavy and large (~1.25 Å) as compared to the other ions, the stress produced and the defect density will be maximum. This is reflected in the maximum broadening of 1332 cm^{-1} band in the Raman spectrum. Similarly, lithium being the lightest and the smallest (0.60 Å) of all the ions used in the present study, the stress produced and defect density will be minimum which results in minimum broadening of the 1332 cm^{-1} band. Also, there are various other effects that the passage of energetic ion through the diamond film can produce. As the electronic stopping is much more dominant in the present case (refer to TRIM data), the passage of ion may leave the carbon electrons in a highly agitated state, creating a positively charged sheath in the path of the next ion, finally leading to Coulomb explosion [22,23]. The charge rearrangement can then give rise to a defect region and hence some amount of stress in the film [22]

The ion implanted films were also characterized by photoluminescence spectroscopy, a well established technique to characterize the defects in semiconductors. Fig. 7.3 shows the photoluminescence spectra of the unimplanted and implanted diamond films. These spectra were recorded in the range 400-8000 cm^{-1}. The PL spectrum of the unimplanted film shows the broad band near 1.720 eV. This band may be considered to be formed by superimposition of the bands centered at 1.720 eV and 1.681 eV. In case of the films implanted with Li^+ and N_2^+ ions, the PL spectra show the sharp band at 1.681 eV with a small shoulder at 1.720 eV whereas the PL spectrum of the film implanted with P^+ ion shows the sharp and

intense band at 1.681 eV with complete disappearance of the band at 1.720 eV. The band at 1.720 eV is correlated with the

Chapter 7 Implantation of Impurities in Diamond Films

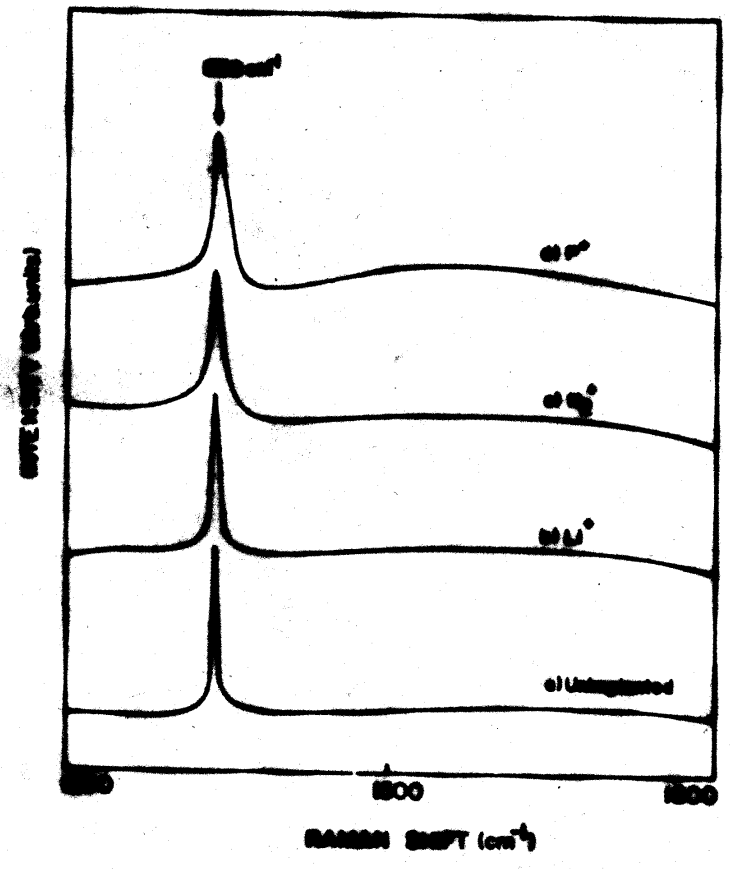

Fig. 7.2 Raman spectra (normalized for 1332 cm^{-1} band) of the (*a*) unimplanted, (*b*) Li^+-implanted, (*c*) N_2^+-implanted, and (*d*) P^+-implanted diamond films grown on Si substrate

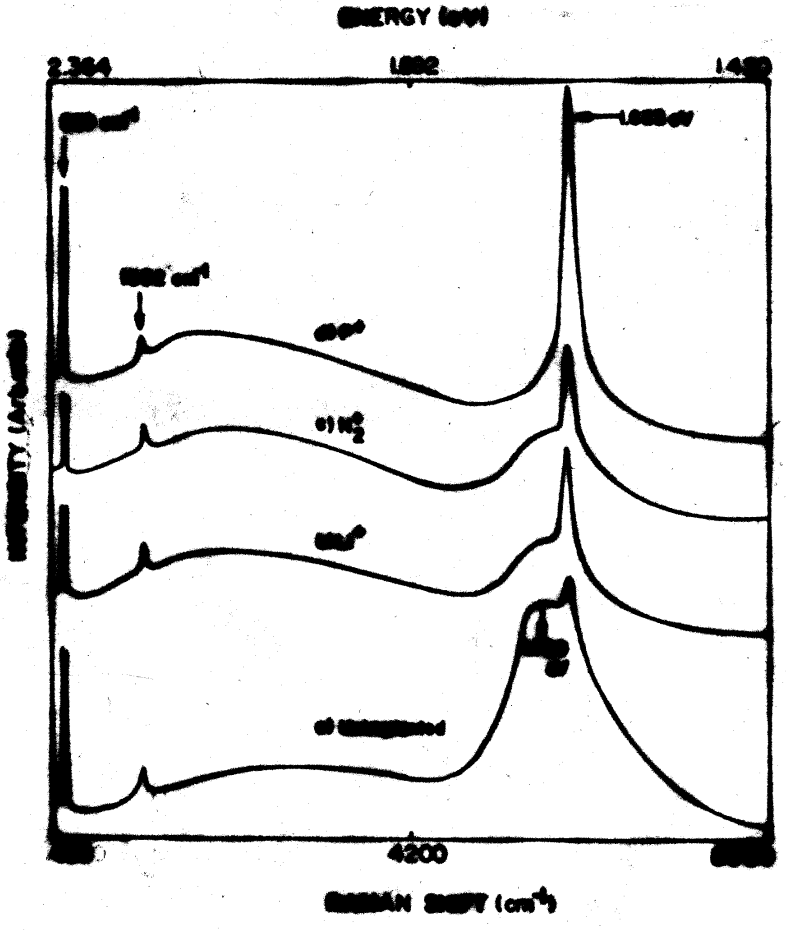

Fig. 7.3 The PL spectra of the (*a*) unimplanted, (*b*) Li^+-implanted, (*c*) N_2^+-implanted, and (*d*) P^+-implanted diamond films grown on Si substrate

vacancy clusters while the band at 1.681 eV is associated with the monovacancies formed by the impurity atoms [24]. The changes observed in the PL spectra of the implanted films can be explained with the help of the ion mass and ion energy used for the implantation. The ion mass of P^+ is much larger as compared to Li^+ and N_2^+ and hence the ion energy required to penetrate upto certain projected range is maximum while as the ion mass of Li^+ is minimum, the ion energy required to penetrate upto approximately the same projected range is also minimum. As seen from the TRIM data, for the corresponding ion energies used, the number of vacancies produced per ion is maximum for P^+ ion implanted film whereas it is minimum for Li^+ ion implanted film. As the number of vacancies formed is increasing, the impurity atoms may combine with the vacancies and as a result the luminescence due to vacancy clusters reduces. Phosphorus being larger in size, may get trapped in the vacancies and form the luminescence center in the film. As a result, the sharp and intense luminescence band is observed at 1.681 eV. On the other hand, as the number of vacancies produced in Li^+ implanted film is very small, less number of impurity atoms may combine with vacancies leading to small but sharp band at 1.681 eV. Thus, P^+ implanted film is more defective whereas Li^+ implanted film is less defective. These observations are in agreement with the results predicted from TRIM simulation.

Fig. 7.4 reveals the surface of the unimplanted and implanted diamond films. The surface morphology of these films does not change considerably after ion implantation and appears to have common features. It is observed that, in all the cases, the surface is made up of closely packed large cubo-octahederal shaped diamond particles with well developed {111} facets. It indicates that the surface morphology is relatively insensitive to the low energy ion implantation.

The XRD patterns of the unimplanted and Li^+, N_2^+ and P^+ implanted flms are shown in Fig. 7.5. The XRD patterns of the implanted films do not vary as compared to the unimplanted film. They show prominent diamond signatures for all the samples confirming the presence of diamond crystallites.

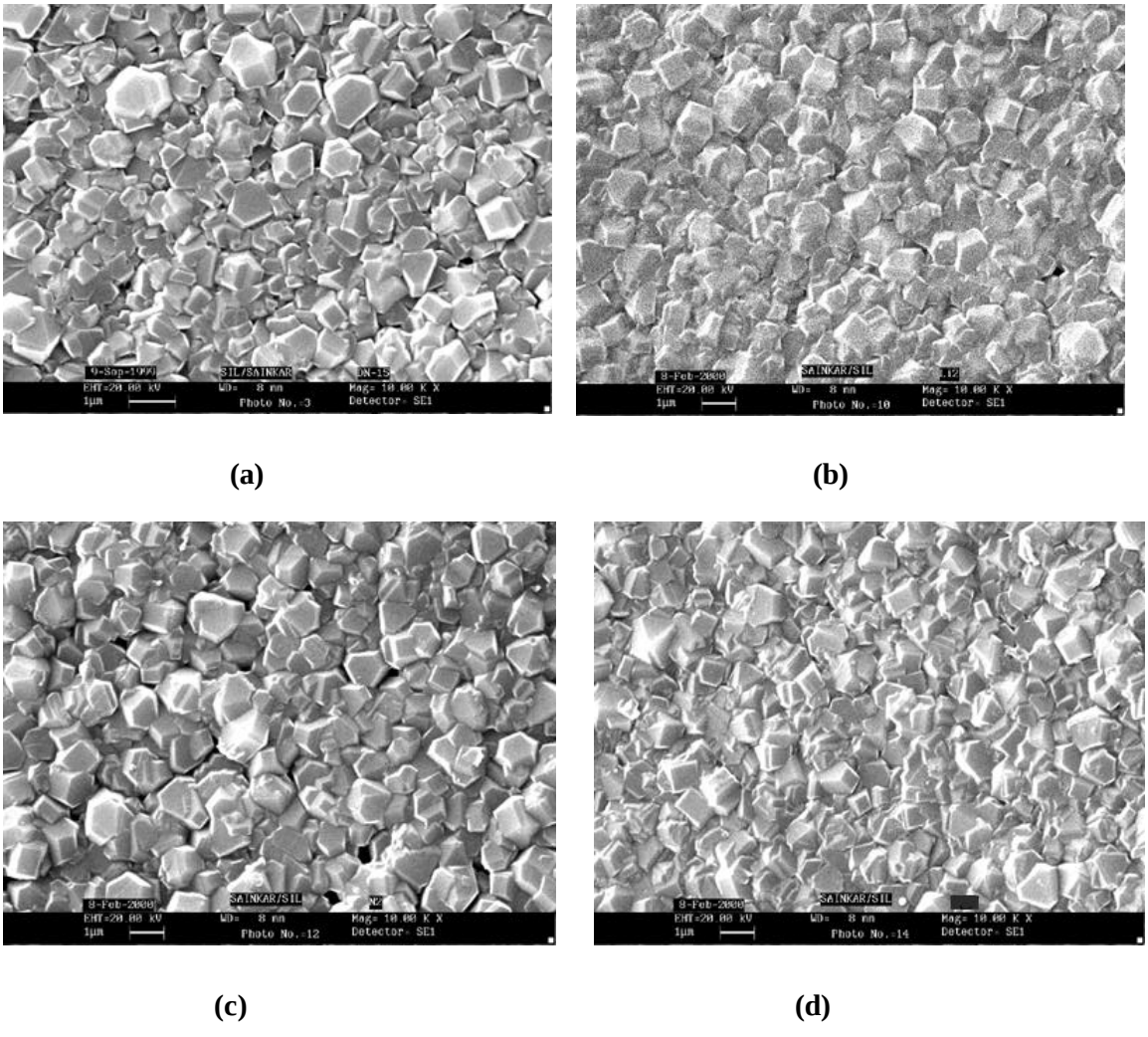

(a) **(b)**

(c) **(d)**

Fig. 7.4 SEM Photographs of the diamond films: (a) unimplanted (b) Li^+ implanted
(c) N_2^+ implanted and (d) P^+ implanted

7.3.3 Annealing Studies of Unimplanted and Implanted Diamond Films

In ion implanted films, the implanted dopant atoms displace the target atoms and thereby cause implantation damage, typically, vacancies, interstitials, dislocations etc. as discussed earlier. Therefore, if the implanted films are subsequently subjected to annealing treatment, it is expected to heal as much as possible of the implantation damage and to activate the dopants by moving them to substitutional lattice sites. Therefore, in the present work, the implanted films were annealed in an inert atmosphere at the annealing temperature ranging from 200 ^{0}C to 600 ^{0}C and the structural changes produced in the films were studied.

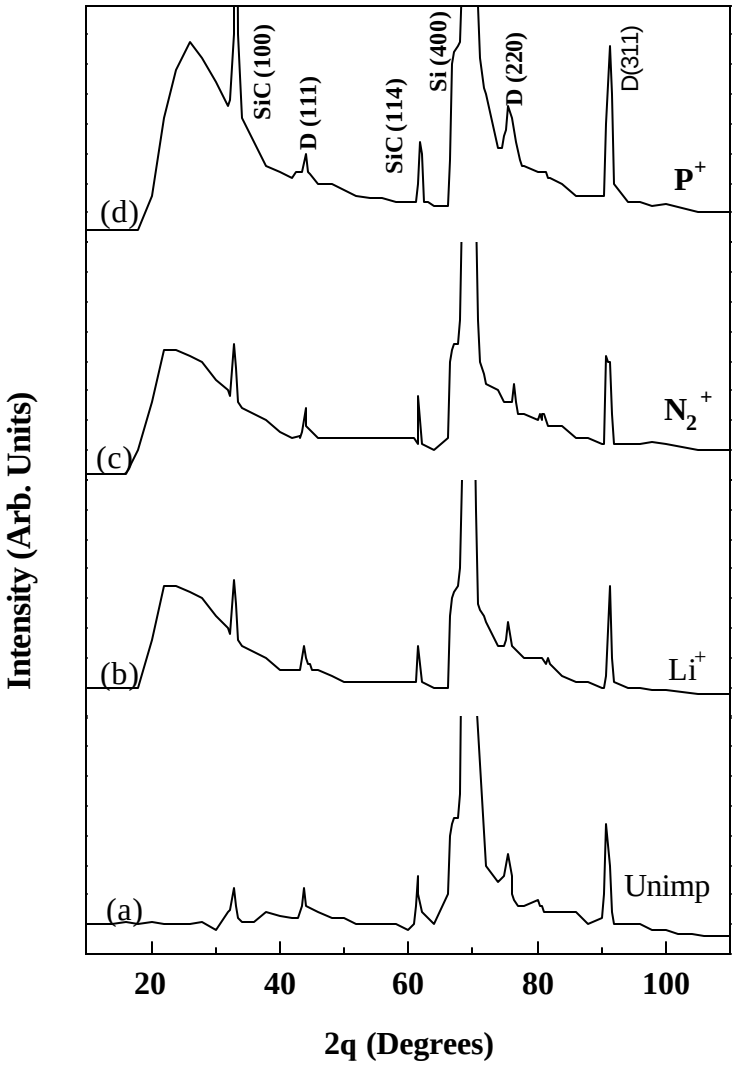

Fig. 7.5 XRD patterns of the (a) unimplnted (b) Li+ implanted (c) N2+ implanted and (d) P+ implanted diamond films.

The Raman spectra of the unimplanted and Li^+, N_2^+ and P^+ implanted diamond films after annealing treatment (T_A=600^{0}C) are shown in Fig. 7.6. All the spectra show the characteristic signature of diamond at 1332 cm^{-1}. Comparison of these spectra with the spectra of the films before annealing treatment clearly indicates that the annealing of the implanted samples resulted in the sharp 1332 cm^{-1} diamond band with decreased FWHM whereas the

annealing of unimplaned sample did not show any appreciable change in the FWHM of the same band. The values of FWHM for the different samples are shown in Table 7.4

Chapter 7
Implantation of Impurities in Diamond Films

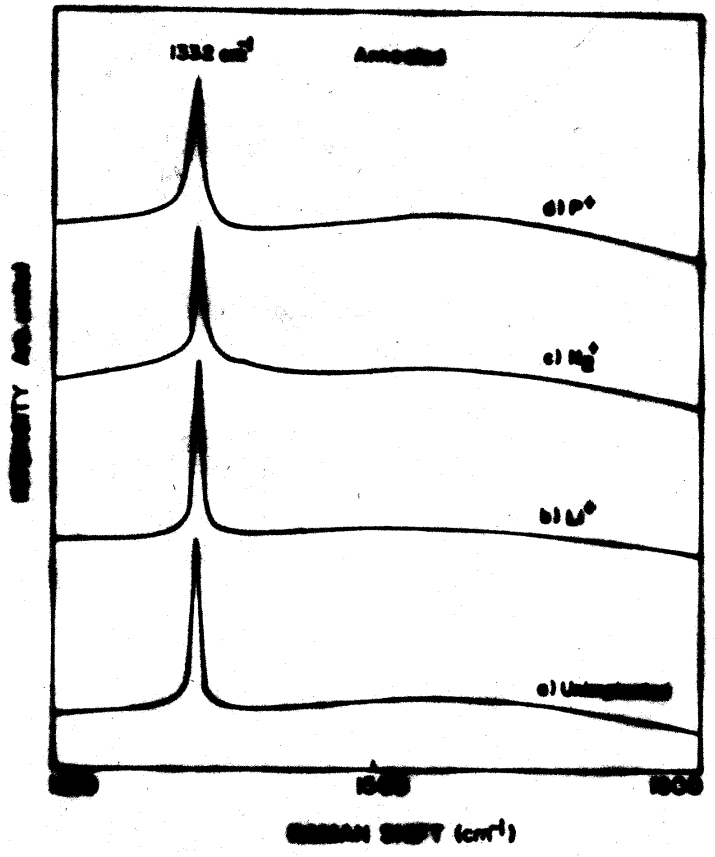

Fig. 7.6 Raman spectra (normalized for 1332 cm^{-1} band) of the (*a*) umimplanted, (*b*) Li^+-implanted, (*c*) N_2^+-implanted, and (*d*) P^+-implanted diamond films grown on Si substrate after annealing treatment

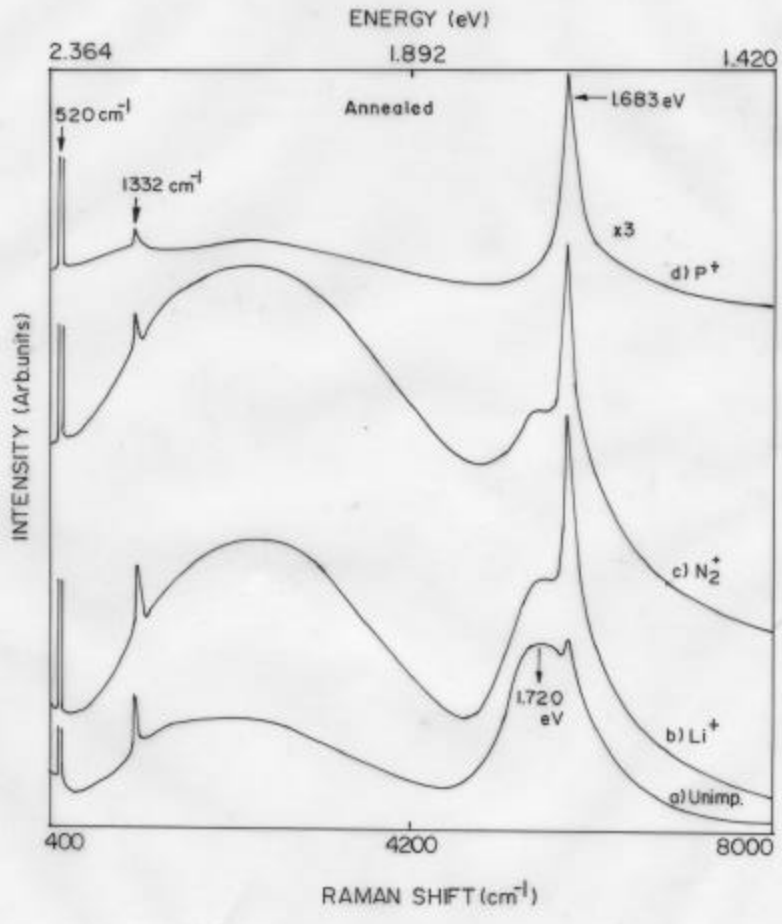

Fig. 7.7 The PL spectra of the (*a*) umimplanted, (*b*) Li^+-implanted, (*c*) N_2^+-implanted, and (*d*) P^+-implanted diamond films grown on Si substrate after annealing treatment

Table 7.4: FWHM (in cm^{-1}) of the 1332 cm^{-1} Diamond band for annealed Films

Annealing Temp. (^{0}C)	Unimplanted Film	Li^+ Implanted Film	N_2^+ Implanted Film	P^+ Implanted Film

Unannealed	5.5	7.5	8.1	10.2
200 ^{0}C	5.6	6.9	7.2	9.9
400 ^{0}C	5.6	6.5	6.9	9.2
600 ^{0}C	5.7	6.0	6.6	7.2

The decrease in FWHM of the 1332 cm^{-1} peak indicates that the stress distribution within the films has altered after annealing [25]. This observation can be attributed to the movement of the dopant atoms to the nearest substitutional lattice sites as a result of annealing. This movement may have released the stress developed in the film due to implantation and hence the annealing treatment of the implanted films may have resulted in sharp 1332 cm^{-1} band with decreased FWHM.

The PL spectra of the unimplanted and Li^+, N_2^+ and P^+ implanted films after annealing treatment are shown in Fig.s 7.7 (the representative PL spectrum of each film annealed at 600 ^{0}C is shown). The comparison of these PL spectra with the PL spectra of the films before annealing treatment clearly reveals that the peak at 1.683 eV is more pronounced in case of the implanted samples after annealing whereas the PL spectra of the unimplanted sample did not show any appreciable change after annealing. It may be due to the fact [26] that the annealing temperature used in this work is not high enough to anneal out the inherent defects and vacancies present in the unimplanted film. Therefore, the broad band centered at 1.720 eV (attributed to vacancy clusters) and the sharp band at 1.683 eV do not vary appreciably after annealing. However, in case of implanted films, there are two possible phenomena for the enhancement of 1.683 eV peak and disappearance of 1.720 eV peak. Firstly, the impurity atoms may occupy vacancies thereby reducing the contribution to 1.720 eV. Secondly, as the impurity atoms are occupying the vacancies, the multivacancies (vacancy clusters) may be getting converted to monovacancies. As the band at 1.683 eV is attributed to the monovacancies [24], the enhancement of this band in the annealed films may be due to the conversion of large number of vacancy clusters to the monovacancies. Phosphorous being larger in size as compared lithium and nitrogen, the enhancement of the band at 1.683 eV is maximum in case of the phosphorous implanted annealed film (as shown in Fig. 7.7).

The SEM photographs of the surface morphology of the unimplanted and implanted diamond films after annealing treatment are shown in the following Fig. 7.8. In this case also, the annealing treatment of Li^+ and N_2^+ implanted diamond films do not change the surface morphology of the films. But, the morphology of the P+ implanted film is observed to change after annealing treatment. It may be due to the disorder produced in the diamond lattice and the formation of a continuous graphite phase after annealing. Fontain et. al [11] have also reported the formation of a continuous crystalline graphite phase after annealing the implanted films.

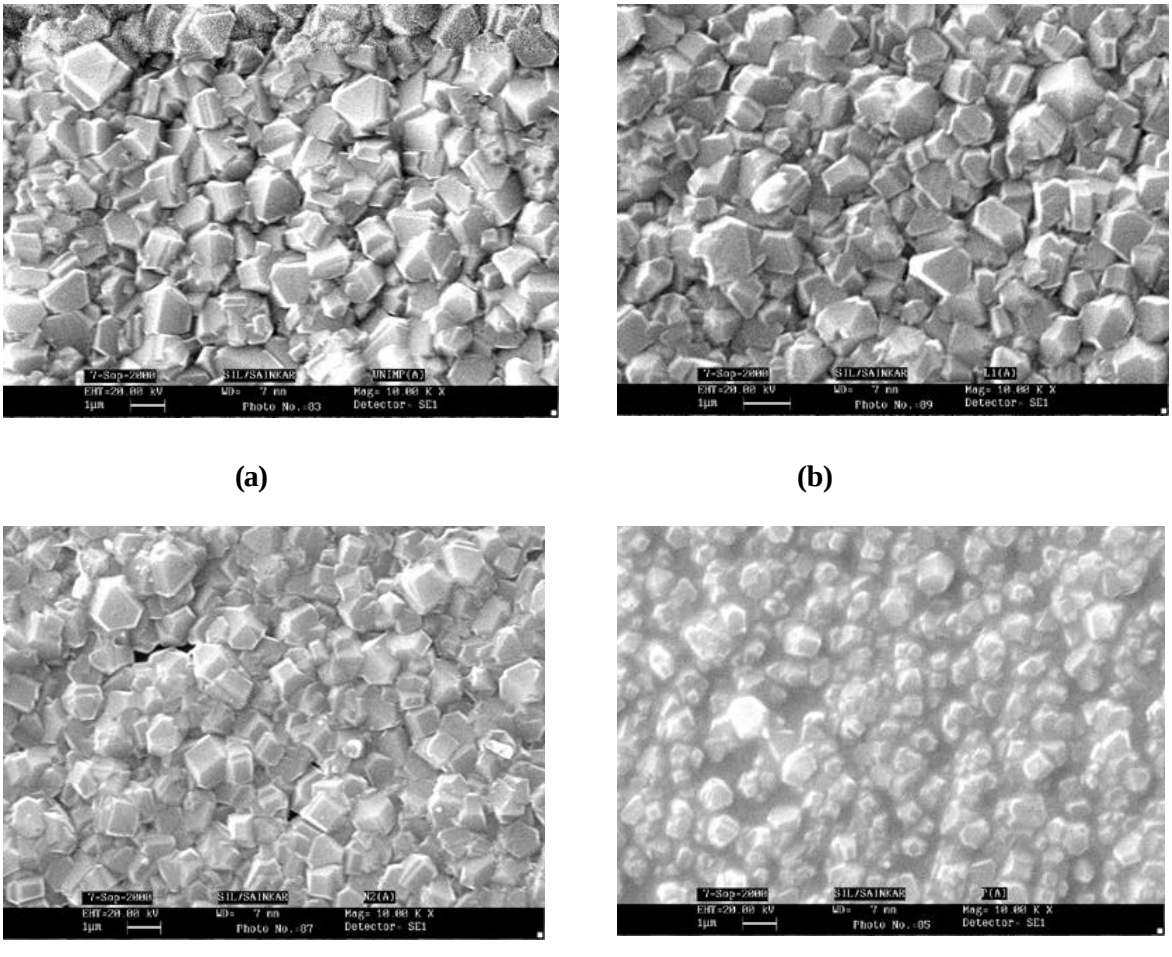

(a) **(b)**

(c) **(d)**

Fig. 7.8 SEM photographs of the (a) unimplanted (b) Li^+ implanted (c) N_2^+ implanted and (c) P^+ implanted diamond films after annealing treatment.

The XRD patterns of the unimplanted and Li^+, N_2^+ and P^+ implanted flms after annealing treatment are shown in Fig. 7.5. The comparison of these XRD patterns with the XRD patterns of the films before annealing (Fig. 7.5) shows that the additional line at $2\theta = 71.62^0$ (d=1.3165 Å), which is due to SiC (202), is observed in case of the annealed films. Another observation is that the line due to diamond (311) at $2\theta = 91.15^0$ (d=1.0786 Å) is absent in the annealed films.

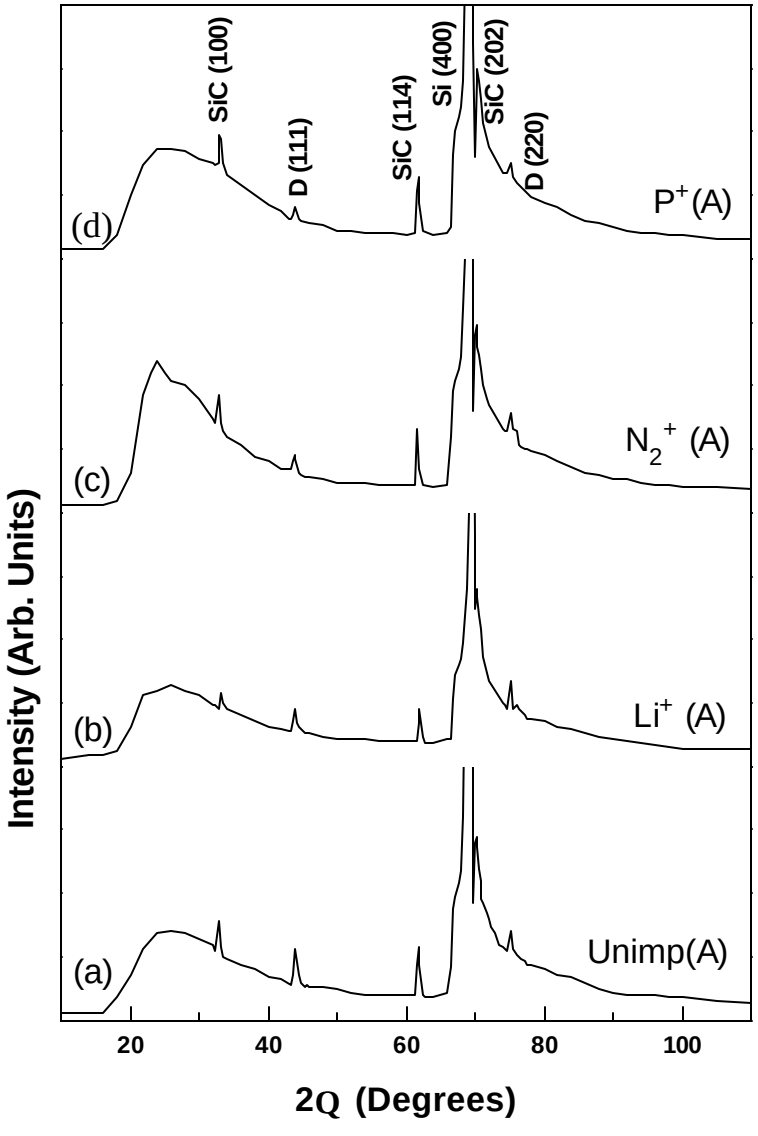

Fig. 7.9 XRD patterns of the (a) unimplnted (b) Li+ implanted (c) N2+ implanted and (d) P+ implanted diamond films after annealing.

7.4 Conclusion

In conclusion, the study of ion implanted diamond films has shown that the ion implantation in CVD diamond films leads to strain and defect related effects such as broadening of the diamond Raman line, enhancement in the intensity of 1.683 eV photoluminescence line. Also, the vacancy distribution in the film is changed depending upon the ion chosen for implantation. This, in turn, changes the broad photoluminescence band centered at around 1.72 eV. The annealing of the implanted samples releases the strain developed in the film due to implantation and alters the defect distribution in the film. The surface morphology is observed to be relatively insensitive to the low energy ion implantation.

References

1. S. Prawer, Diam. Relat. Mater. 4 (1995) 862.
2. "Ion implantation in semiconductor and other materials", edited by B. L. Crowder (Plenum Press, New York, London (1973).
3. John Melgailis, J. Vac. Sci. Technol. B 5 (1987) 469.
4. J. S. Williams, Rep. Prog. Phys., 49 (1986) 491.
5. J. Zeigler, J. P. Biersack and U. Littmark, "The stopping and range of ions in solids" Pergamon, New York (1985).
6. M. W. Thompson, "Defects and radiation damage in metals", Cambridge University Press (1969).
7. J. F. Prins, Mater. Sc. Reports 7 (1992) 271.
8. M. G. Allen, S. Prawer, D. N. Jamieson and R. Kalish, Appl. Phys. Lett. 63 (1993) 2062.
9. M. Werner and R. Locher, Rep. Prog. Phys. 61 (1998) 1665.
10. G. Braunstein, A. Talmi and R. Kalish, Radiat. eff. 48 (1980) 139.
11. F. Fontaine, a. Deneuville and L. Abello, Diam. Relat. Mater. 3 (1994) 623.
12. S. Prawer and R. Kalish, Phys. Rev. B 51 (1995) 15711.

13. J. F. Prins, Nucl. Instrum. Methods B 80/81 (1993) 1473.
14. S. M. Gorbatkin, R. A. Zuhr, J. Roth and H. Naramoto, J. Appl. Phys. 70 (1991) 2986.
15. G. Braunstein and R. kalish, Appl. Phys. Lett. 38 (1981) 416.
16. G. Braunstein and R. kalish, Nucl. Instrum. Methods 182/183 (1981) 691.
17. H. Hofsass, M. Dalmer, M. Restle, C. Ronning and H. Hofsass, J. Appl. Phys 81 (1997) 2566.
18. K. Bharuth-Ram, H. Quintel, M. Restle, C. Ronning and H. Hofsass, J. Appl. Phys 78 (1995) 5180.
19. R. Kalish, C. Uzan-Saguy, A. Somoiloff, R. Locher and P. Koidl, Appl. Phys. Lett. 64 (1994) 2532.
20. S. Prawer, A. Hoffman and R. Kalish, Appl. Phys. Lett. 57 (1990) 2187.
21. H. Windischmann, and K. J. Gray, Diam. Relat. Mater. 4 (1995) 837 and references therein.
22. A. Dunlop, D. Lesuer, N. Lorenzelli, A. Adouard, C. Dimitrov, J. M. Ramillon and L. Thome, J. Phys. D 2 (1990) 1733.
23. R. L. Fleischer, P. B. Price, and R. M. Walker, J. Appl. Phys. 36 (1975) 3645.
24. S. Dannefaer, W. Zhu, T. Bretagnon and D. Kerr, Phys. Rev. B 53 (1996) 1979.
25. J. W. Ager, D. K. Veirs and G. M. Rosenblatt, Phys. Rev. B 43 (1991) 6491.
26. J. Nakata, Phys. Rev. B 60 (1999) 2747.

Chapter 7 *Implantation of Impurities in Diamond Films*

CHAPTER 8

SUMMARY AND CONCLUSIONS

This section summarizes the results of entire work. The results obtained in different problems are correlated for arriving at a plausible conclusions.

It is shown that the hot-filament CVD system, developed in the present study can be used for the deposition of diamond films doped with different impurities. The M shaped filament mounted on a specially designed Π shaped filament holder is found to be appropriate for growing large area as well as maximum possible uniform diamond films. The substrate holder was also designed with different heat sinks so as to obtain the desired substrate temperature. The heat sinks used are made of copper, graphite and ceramic which enabled to obtain the substrate temperatures of 750, 850, 950^0C respectively.

By using the specially designed M shaped filament, we have optimized the deposition parameters, viz. (a) gas pressure in the chamber (b) total gas flow in the chamber and (c) the methane concentration with respect to hydrogen. Our system has shown that the best quality films can be grown on Si substrate by employing gas pressure of 30 Torr, gas flow rate of 300 SCCM and 2% CH_4 concentration. Keeping these parameters constant, the different substrate pretreatments have found to play the important role in enhancing the nucleation density. The films grown on ITO coated scratched Si substrate have shown In and Sn to play the catalytic role whereas the nucleation density is found to improve by a factor greater than 500. The oxide buffer layer is proposed to help in enhancing the nucleation on perfect surfaces and also in reducing the graphitic content in the film.

Studies on the effect of insitu incorporation of the impurities such as Si, N, F in the diamond films have shown to change the growth behavior and properties of the films. Si is observed to play a important role in enhancing the grain size as well as sharpness of the crystal edges whereas nitrogen incorporation in the diamond films results in the change in the surface morphology from {111} facets to pyramidal shaped crystallites with {100} facets at the top.

The growth rate of the N-doped films is observed to enhance from ~1.1 μm/hr to ~ 2.8 μm/hr. The higher concentration of nitrogen leads to the multinucleation and high growth rate. The surface morphology of the fluorinated diamond films show the films to be formed of isolated cubo-octahedral crystals and the gaps between the grains are observed to be unfilled with any other material like amorphous carbon.

Raman scattering measurements of these films show that incorporation of Si, being larger in size than carbon, causes dilation of the diamond lattice and results in the increased FWHM of the 1332 cm^{-1} Raman band. The nitrogen incorporation leads to the

increase in sp^2 bonded carbon in the form of overgrowth while it is found to be negligibly small in the fluorinated diamond films.

The photoluminescence studies of these films have shown very interesting results. In nominally pure diamond film, the band at 1.72 eV is observed to be dominant. Upon incorporation of Si, or N, this band disappears and the sharp band at 1.683 eV is observed. The former band is attributed to the clustered multiple vacancies while the latter is attributed to monovacancies. As the band at 1.683 eV is observed to be present irrespective of the impurity, either Si or N, it is suggested that these bands are not related to the impurities but are due to the defects alone (mainly vacancies) trapped by these impurities. The experiments on different substrates have suggested that the 1.683 eV related centers may have common origin in all types of substrates and it needs more experimental as well as theorotical research, as it may not be related only to Si centers. These impuruties may act as vacancy traps and therefore, monovacancy center may be created which are thought to give rise to the sharp band at 1.683 eV. In the dual doped films with boron and Si, the band at 1.683 eV is found to get suppressed completely. The boron incorporation may lead to the termination of the dangling bonds due to vacancies or it may act as compensator for Si induced defect centers. Fluorine being monovalent, is expected to act as lattice terminator and may give rise to the voids. Its incorporation enhances the intensity of the band at 1.72 eV which may be attributed to the multivacancy related centers in the film.

The ion implantation (Li^+, N_2^+, P^+) of the diamond films leads to the strain and defect related effects such as broadening of the diamond Raman line, enhancement in the intensity of 1.683 eV PL band. The vacancy distribution in the film is changed depending upon the ion chosen for implantation which, in turn, changes the broad photoluminescence band centered at around 1.72 eV. The annealing of implanted films releases the strain developed in the film due to implantation and alters the defect/vacancy distribution in the film. These results again stress the need for theorotical understanding of the origin of the 1.683 eV line which, as our results show, are probably only monovacancy centers.